THE HONG KONG POLYTECHNIC UNIVERSITY

DEPARTMENT OF CIVIL AND STRUCTURAL ENGINEERING

STUDY ON TIME-DEPENDENT STRESS-STRAIN BEHAVIORS OF CLAYEY SOILS

Fei TONG

A THESIS

SUBMITTED

IN PARTIAL FULFILMENT OF THE REQUIREMENTS FOR

THE DEGREE OF DOCTOR OF PHILOSOPHY

November 2011

CERTIFICATE OF ORIGINALITY

I hereby declare that this thesis is my own work and that, to the best of my knowledge and belief, it reproduces no material previously published or written, nor material that has been accepted for the award of any other degree or diploma, except where due acknowledgement has been made in the text.

Signature: _____

Name: Fei TONG

Abstract of thesis entitled

STUDY ON TIME-DEPENDENT

STRESS-STRAIN BEHAVIORS OF CLAYEY SOILS

The stress-strain behaviors of saturated clays are time-dependent. Thus it is essential to take into account the viscous properties of soils in geotechnical engineering practice. This thesis mainly focuses on both experimental and constitutive modeling studies of the time-dependent stress-strain behaviors of two clayey soils.

In the experimental study, the time-dependent stress-strain characteristics including creep, swelling, strain rate effects, and relaxation behaviors of Hong Kong Marine Deposits (HKMD) and Sand Mixed Bentonite (SMB) samples are investigated. In this thesis, "creep" means viscous deformation under constant effective stress; while "swelling" means viscous expansion under constant effective stress and is a reverse behavior of "creep", for saturated expansive soils.

Firstly, the time-dependent behaviors of the SMB soils are examined by Multi-Stage Loading (MSL) oedometer tests, Constant Rate of Strain (CRSN) oedometer tests, and step-changed undrained triaxial CRSN tests. From the test data, creep, swelling and strain rate effects are observed and discussed. In MSL oedometer tests, it is found that SMB soils exhibit considerable viscous behaviors which are stronger time-dependent under lower stress level, but less obvious under higher stress condition. The sand content exerts an indispensible impact on soil behaviors in terms of compression and time (or strain rate)-dependency. In CRSN tests, the strain rate effect is examined by step-changed strain rate, in both oedometer and undrained triaxial conditions. At a given rate in a CRSN oedometer test, the higher the strain rate, the higher the effective stress. In addition, results of step-changed undrained triaxial CRSN tests indicate both the deviator stress and excess porewater pressure are influenced by

strain rate. The impacts of sand content on the effective stress and porewater pressure are also discussed. At a given axial strain and a given confining pressure, the CRSN curves of SMB specimens with higher sand content have higher deviator stress and porewater pressure.

Secondly, the time-dependent behaviors of the HKMD soils are examined using MSL oedometer tests, 1D relaxation tests (in both loading and unloading stages) and settling column tests. In MSL oedometer tests, both the creep and swelling behaviors of HKMDs are less obvious compared with SMBs. In 1D relaxation tests, the viscosities of HKMDs are observed in both creep and swelling regions. Different responses in effective stress under relaxation are found in loading and unloading process and these prove that both creep and swelling are related to the viscous behaviors of HKMD soils. The time-dependent large-strain behavior is studied by settling column tests of HKMDs. By normalizing parameter in settling stage, a unique complete relationship between effective stress and strain is established. Test results reveal that the settling curve and settling rate are significantly affected by the solid phase in self-weight consolidation. After the primary self-weight consolidation, the settling rate is reduced in the "secondary self-weight consolidation".

In the constitutive modeling of the time-dependent stress-strain behaviors, based on the concept of "reference time line" and "equivalent time", the previous Elastic Visco-Plastic (EVP) model by Yin and Graham (1989, 1994 and 1999) is extended to a new Elastic Visco-Plastic model considering swelling (EVPS model). The swelling here denotes the volume expansion under constant load for saturated soils. The model considers the contribution of swelling strain rate to the total strain rate, so that the unloading/reloading loop can be simulated.

The 1D EVPS model is calibrated by the oedometer test in 1D straining, and then

the model is verified by simulating the stress-strain behaviors of SMBs in CRSN oedometer tests and 1D relaxation tests. Simulated results agree well with the test data. The 1D EVPS model is also valid in predicting all the time-dependent (or strain-dependent) behaviors of a soil element under any loading condition in 1D straining, such as constant rate of stress (CRSS) loading, unloading/reloading, swelling pressure, etc.

Based on the classical plasticity and the framework proposed in Yin and Graham (1999), a 3D EVPS model is developed. Eight parameters are needed to construct the model for a specific soil. Once all the parameters are determined by isotropic consolidation tests, this model can predict the time-dependent soil behaviors. Proper estimations of viscous parameters for both creep and swelling are essential to the 3D EVPS model. The 3D EVPS model has been adopted to simulate triaxial undrained CRSN tests on different SMB specimens. The simulated results generally agree well with the test data. The unloading/reloading loop can be reproduced. This 3D EVPS model is valid in describing all the viscous soil behaviors in 3D stress condition.

LIST OF PUBLICATIONS

Journal Papers

[1] **TONG Fei** and YIN Jianhua (2011). Nonlinear creep and swelling behavior of bentonite mixed with different sand contents under oedometric condition. Marine Georesources & Geotechnology, Vol. 29(4), pp. 346-363.

[2] **TONG Fei** and YIN Jianhua (2011). Experimental study on complete consolidation behavior of Hong Kong marine deposits. Marine Georesources & Geotechnology, accepted in Sep. 13 2011.

[3] **TONG Fei** YIN Jianhua and ZHU Guofu (2011). Experimental investigation on settling behaviour of Hong Kong marine deposits in settling column condition. Geotechnical Engineering Journal of the SEAGS & AGSSEA, Vol. 24(4), pp. 53-57.

[4] YIN Jianhua and **TONG Fei** (2011). Constitutive modeling of the time-dependent stress-strain behaviour of saturated soils exhibiting both creep and swelling. Canadian Geotechnical Journal, Vol. 48(12), pp. 1870-1885.

[5] **TONG Fei** and YIN Jianhua (2011). Testing study and constitutive modeling of relaxation behaviors of three clayey soils, Journal of Geotechnical and Geoenvironmental Engineering. under review.

Conference Papers

[1] **TONG Fei** and YIN Jianhua (2011). Influence of sand content on the stress-strain behavior of silica sand mixed bentonite in CRS condition, Proc. of the Geo-Frontiers 2011 Conf., ASCE, 10.1061/41165 (397) 275.

[2] **TONG Fei** and YIN Jianhua (2011). Influence of sand content on the non-linear creep and swelling behaviors of bentonite in oedometric condition, Proc. of the 14th Asian Regional Conf. on Soil Mechanics, Hong Kong, Vol. 1, pp. 138 (Extended abstract).

[3] **TONG Fei** and YIN Jianhua (2011). Experimental study on settling-consolidation behavior of Hong Kong marine deposits, Proc. of Int. Postgraduate Conf. 2011, Hong Kong, Vol. 1, pp. 415-420.

ACKNOWLEDGEMENTS

I would like to express my deepest gratitude to my supervisor, Professor Jian-Hua Yin, for his encouragement and close supervision of the present study. It was his supports and experienced guidance that made this work possible. The experience of working with Professor Yin has appreciably influenced my professional development and perspectives.

Financial supports from research grants (G-U663 and G-YG60) and studentship of The Hong Kong Polytechnic University are gratefully acknowledged.

I would also like to express my appreciation to Professor Zhu Guofu for his consistent help in reviewing papers and the thesis.

I would like to express my thanks to Dr. Zhu Honghu, Dr. Hong Chengyu, Mr. Pei Huafu, Mr. Xu Dongsheng, Mr. Borana Lalit, Mr. Feng Weiqiang and Mr. Leung Y.P. in the Soil Mechanics Laboratory of Department of Civil and Structural Engineering in The Hong Kong Polytechnic University for their suggestions and assistance to me for conducting laboratory tests.

Finally, I would like to express my sincere thanks to my dear parents, my wife, teachers, and friends whose love, encouragement and friendship over the last three years let me reach a new level in my life.

TABLE OF CONTENTS

LIST OF TABLES

LIST OF FIGURES

Chapter 1

Introduction

1.1 Background

Soil is an important material containing natural resources. Soil ground either directly or indirectly supports various types of structures like a dam, a skyscraper, a bridge or even a sewage system. Properties and behaviors of soils are important for design and construction of geotechnical structures. Natural soil can be formed by gradual weathering of rock with a relatively long period of time and composed of particles of broken rock that have been altered by chemical and environmental processes including weathering and erosion. Soil with particle size less than 0.002 mm is known as clay material. Most soils, particularly clayey soils, are viscous, which makes soils exhibit time dependent stress-strain-strength characteristics. Since 1953, soil rheology mechanics has been recognized as an independent branch of soil mechanics. Consolidation analysis of soils with and without vertical drains taking into consideration time dependent effect is of practical and theoretical importance in geotechnical engineering.

Rheology is a science devoted to studying changes in stress-strain states of real material over time. Rheological theories, such as elasticity, plasticity and viscosity theories, are developed to describe the behavior of real materials. The time-dependent deformation of a real material depends on its elastic, plastic, and viscous properties. Description of the deformation of real bodies often becomes an

insurmountable task. Hence deformation of real bodies is generally described by models considering simplified characteristics or the characteristics of ideal bodies. This kind of models is known as rheological models.

Five typical process related to the viscosity of soils are encountered, namely creep, swelling, stress relaxation, strain rate (or loading-rate) dependency and long-term strength. The viscous deformation with time under a constant load is called creep; while the opposite of the process of creep is swelling. As for stress relaxation, the strain is maintained constant, while stress decreases with time. Strain rate effects mean that the stress-strain behavior of soil changes with strain rate or loading-rate. Under a sustained stress for a long time, the strength (for example undrained shear strength) of a soil may decrease, and this decreased strength is the so-called long-term strength.

The time dependency of the stress–strain behavior of soft soils, especially soft clay, is generally too important to be ignored (Graham *et al.*, 1983). When a soil is loaded under a constant total vertical stress in one-dimensional conditions, it continues to settle after dissipation of the excess pore pressures, which is known as creep. Estimating creep settlement has been an interesting area of research for a long time (Bjerrum, 1967; Berre and Iversen, 1972; Leroueil et al., 1985; Yin and Graham, 1994 and 1999).

Due to the large-scale increasing need of land for buildings and infrastructure, a number of reclamation works have been constructed in Hong Kong over the last two decades. This trend will continue for the near future. Bentonite in civil

engineering applications is used traditionally as a thixotropic and support in diaphragm walls and foundations. For the design of the reclamation and superstructures, an accurate prediction on both the short-term and long-term settlements in the design analyses is indispensable. If the long-term settlement is too large to be tolerated for the superstructures, it may be necessary to improve the bentonite. Therefore, a better understanding of behaviors of bentonite is required before application.

The term Bentonite has been commonly used for any plastic, colloidal, and swelling clay. It is highly a colloidal and plastic clay with unique swelling characteristic that can expands several times of its original volume when comes in contact with water. Bentonite could be found in almost all countries and in rocks of a wide variety of ages. The properties of bentonite are similar to those of clay, which means soft, water absorbability under saturation. Due to its highly absorbent nature and swelling property, it could be used in soil modification and seepage reduction. Many bentonites are of great commercial value. They are used in decolorizing oils, in bonding molding sands, in the manufacture of catalysts, in the preparation of oil well drilling mud, and also in numerous other relatively minor ways. Sodium bentonite can be used in oil well drilling as a component and in the sealing of subsurface disposal systems, etc. Calcium bentonite is an excellent absorbent of ions in water or even oil; therefore it can be used in decolorizing oils.

Recently much attention has been paid on disposal of high-level radioactive wastes, either as spent fuel or as the by-products of nuclear fuel reprocessing

(Daniel and Wu, 1993; Alawaji, 1999). For this purpose, large areas of deep ocean sediments are available, providing vast space free from seismic and tectonic disruption. Due to its low hydraulic conductivity, micro-porous structure, good sorption properties and plasticity, bentonite is included in buffer and backfill materials in most high-level waste (HLW) repository concepts (Jedinakova-Krizova, 1998). As an effective barrier, bentonite protects the canister and restricts the movement of radionuclides released from the waste packages after canister failure.

Marine clays in the seabed have typically high water content and high compressibility. Appropriate prediction of the soil behavior regarding consolidation and deformation has critical impacts on design, construction and maintenance. These behaviors are particularly time-dependent, requiring reliable soil description and understandings. With the reclamation works in many coastal areas in Hong Kong, comprehensive site investigations on marine deposits (Yim, 1983; Koutsoftas *et al.*, 1987) have been performed. The investigations revealed a characteristic seabed soil profile of upper marine clay, alluvial crust, lower marine clay and lower alluvium above residual soil and granite bedrock in most coastal areas of Hong Kong. The marine clay, hereinafter, is referred to as Hong Kong Marine Deposits (HKMD). Reclamation on this foundation of HKMD generally induces a number of geotechnical problems. A typical example is the reclamation at the site of Chek Lap Kok international airport of Hong Kong.

Besides reclamation, many other earth works may suffer problems related to the time-dependent behavior of soils. Creep displacements and gradual failure of

large masses of seabed sediments are a common occurrence on continental slopes and rises (Silva *et al.*, 1991). Many slopes, retaining walls, earth dams and buildings on soft soils, failed due to creep of soil.

Due to the significance, the viscous effects have been studied extensively in last decades. The study of time-dependent stress-strain behavior mainly uses two approaches: one is experimental study, and the other is numerical modeling including constitutive modeling and its application. From experimental investigation, the time-dependent stress-strain behavior can be measured and understood. Meanwhile some useful empirical equations may be obtained and used directly in practice. To predict more accurately the behavior of geotechnical structures with complex boundary conditions, it is necessary to perform numerical modeling using a proper constitutive model for the soil. Detailed reviews of the previous studies on viscous effects of soils are presented in Chapter 2.

1.2 Objectives

The time-dependent behavior of clayey soils has gained concern worldwide. Although the behavior has been studied extensively in the past, the problem is far from being solved. Most test data in various conditions are needed to clarify the properties of clayey soils. As for the constitutive modeling, most of the models proposed are only valid for a certain stress stage. Each model more or less has limitations. For the real design of soil structures, an accurate prediction on both the

short-term and long-term settlements in the design analyses is indispensable. Further work is in need to make constitutive model predict well the time-dependent behavior of clayey soils.

The main objective of this research is to investigate the stress-strain behavior of clayey soils with both creep and swelling and to develop a general constitutive model for clayey soils in saturated condition. To this end, the work is carried out in two aspects: (a) experimental investigation on the time-dependent stress-strain behavior (creep and swelling) of the Silica Sand Mixed Bentonite (SMB) soils and Hong Kong Marine Deposits (HKMD) soils and (b) elastic viscoplastic modeling considering swelling effect and application of the model.

To examine the viscosity of SMB soils with different sand proportion (50%, 60%, 70%, 80% and 90%, respectively), a series of oedometer tests, constant-strain rate oedometer tests, consolidated undrained triaxial tests and isotropic consolidation are conducted. For HKMD soils, oedometer tests, constant-strain rate oedometer tests with relaxation and settling column tests are carried out. The elastic viscoplastic (EVP) approach is commonly accepted to build constitutive models. However the development of the EVP model is not perfect so far. In this thesis, the 1D and 3D EVP models in Yin and Graham (1989, 1994 and 1999) are extended to consider the swelling effect (called EVPS model). The EVPS model is applied on specific soils for different loading conditions such as constant rate of strain (CRSN) loading, relaxation, unloading/reloading, etc.

Appreciation of the time-dependent behaviors of these soils is essential for

developing theories of consolidation and for interpreting field settlement in any reclamation project.

1.3 Organization

This thesis includes ten chapters and an appendix as follows:

In **Chapter 1**, significance of studies on the viscous effects of soils is discussed. Research background and objective of the current study are presented.

In **Chapter 2**, previous studies and research outcomes on the time-dependent stress-strain behaviors are reviewed, including experimental investigation, numerical modeling and constitutive modeling. Five important viscous phenomena of soils are discussed. They are creep, swelling, stress relaxation, strain rate (or loading-rate) dependency and long-term strength.

In **Chapter 3**, testing apparatus and techniques in this study are introduced. Two typical clayey soils Sand Mixed Bentonite (SMB) and Hong Kong Marine Deposits (HKMD) are described. Basic physical properties of soil samples are obtained in this chapter.

In **Chapter 4**, experimental results of one-dimensional oedometric compression tests with multi-stage loading and unloading/reloading on specimens of bentonite mixed with different sand contents are presented. Based on the test results, the influence of sand contents on time-dependent stress-strain behavior of the bentonite-sand mixture under 1D straining is examined with special attention to the

nonlinear creep behavior and swelling behavior.

In **Chapter 5**, the effects of strain rate and sand content on the one-dimensional compressibility of SMB soils are investigated by a series of CRSN tests with step-changed strain rates. The stress-strain relationships of three samples with different sand content (50%, 60%, and 80%, respectively) are presented. The compression index and the rebounding index are discussed.

In **Chapter 6**, test study of the time-dependent relaxation behaviors of SMB and HKMD are focused. Relaxation tests are conducted to measure the changes of the effective stress with time in 1D straining condition. Relaxations are performed both in loading stage and unloading stage.

In **Chapter 7**, the stress-strain behaviors of SMB under isotropic consolidation condition and triaxial undrained CRSN condition are investigated. The influences of sand content (60% and 70%) and strain rates are examined. Variations of deviator stress and excess porewater pressure with vertical strain are presented and discussed.

In **Chapter 8**, test results of a series of one-dimensional settling column consolidation tests and conventional oedometer tests on HKMD are presented. The complete consolidation behavior of Hong Kong marine deposits both in self-weight condition and in oedometer condition is examined. Influences of soil concentration and settling velocity are also investigated in this chapter.

In **Chapter 9**, creep, swelling and strain rate effects observed in above chapters are analyzed. Based on the test data and the 1D Elastic Visco-Plastic (1D EVP)

model developed by Yin and Graham (1989 and 1994), a new 1D Elastic Visco-Plastic model considering both creep and swelling (namely 1D EVPS) is proposed. The data from the multi-stage oedometer tests are used to calibrate the new model. Then, the calibrated new model is used to simulate the step-changed constant rate of strain compression tests for comparison. In this way, the new model is verified. The new 1D EVPS is further used to simulate CRSN tests with a single strain rate, relaxation in creep or swelling region and constant rate of stress tests.

In **Chapter 10**, based on the classic Cam-clay model and EVPS model proposed by Yin and Tong (2011), Elastic Visco-Plastic model considering swelling (EVPS) in triaxial stress state is proposed as an extension to the 1D EVPS model. The function and application of this model are presented in this chapter. The SMB samples are adopted to perform isotropic consolidation test and triaxial constant rate of strain (CRSN) test. Calibration of all the parameters in this model can be done from isotropic consolidation test. Simulation on triaxial CRSN test validates this model.

In addition, an analytical solution of Elastic Visco-Plastic model considering Swelling (EVPS model) in 1D relaxation condition has been derived and presented in the Appendix. The derived analytical solution from the EVPS model can predict relaxation behaviors both in creep region and in swelling region. Simulations of relaxation tests on HKMD and SMB verified the solution by comparison with results of laboratory tests.

In this thesis, following the convention in soil mechanics, all compressive stress and compressive strain are positive ("+"). Tables and Figures are placed at the end of each chapter.

Chapter 2

Literature Review

The effects of time on the response of soil are a salient feature of soils, in particular, for clayed soils. In general, there are two types of time-dependent behaviors. One is due to the interaction of free pore water and soil skeleton called consolidation phenomena of soils with small permeability and the other is generated by the inherent viscous characteristics of soil skeleton. Studies in the literature are mainly focused on (a) the experimental investigations of two viscous phenomena, *i.e*. creep and strain rate dependency and (b) the developments of constitutive model for the time-dependent stress-strain behavior. The following sections are intended to give a review of the literatures on these two aspects. Because the properties of bentonite are similar to clay, the reviews of literature are mainly on clays.

2.1 General Consolidation Theories

The theory of consolidation occupies a unique place in the history of geotechnical engineering. The one-dimensional theory was first proposed by Terzaghi (1943) based the underlying assumptions:

a. The soil is fully saturated;

b. Water and soil particles are incompressible;

c. Darcy's law is valid;

d. Compression and flow are one-dimensional (vertical);

e. The relation between effective stress and strain is linear;

f. External loading is applied suddenly and remains constant;

g. Clay layer is homogeneous; and

h. Strains are small.

These simplified assumptions lead the formulation of the well-known equation

$$\frac{\partial u}{\partial t} = c_v \frac{\partial^2 u}{\partial z^2} \tag{2-1}$$

where c_v is the vertical coefficient of consolidation; u is excess pore pressure; z is vertical co-ordinate; and t is elapsed time. Terzaghi's work forms the basis for all studies of consolidation as well as other subjects related to the deformation and flow of fluids through porous media (Gibson *et al.,* 1981).

For many clays, the assumptions made in this basic Terzaghi theory are not grossly in error and, in view of the difficulties in predicting in-situ soil parameters, the correlation between predicted and observed behavior is good. Therefore, application of this theory is still popular with possible refinements by means of the methods proposed by Skempton and Bjerrum (1957) and Schiffman and Gibson (1964); and in special problems by paying attention to the stress path (Lambe, 1964). However, the basic Terzaghi theory is oversimplified for a lot of situations. A number of consistently observed experimental facts clearly do not conform to the Terzaghi theory (Buisman, 1936; Gray, 1936; Leopards and Girault, 1961). After careful examinations of various factors influencing the consolidation behavior, Barden and Berry (1965) indicated that a main source of error was in the assumed

elastic behavior of the soil skeleton, which did not take into consideration of the structural viscosity of the soil.

2.2 Viscosity of Soils

Tolerance of settlement of earth structures after construction is always very limited. However the viscous behaviors of soils influence the settlement dramatically. Particularly the recent reclamation works in Hong Kong on soft marine deposits induce many geotechnical problems in terms of excessive creep deformation, ground heaving, and uneven settlement, etc.

The classic case due to viscosity is differential settlement of the famous Tower of Pisa. Under 514 kPa mean pressure on a 280 m^2 annular foundation, the tower had tilted more than two meters to one side since the completion of construction.

Most soils have viscosity, which makes the soils exhibit time-dependent stress-strain characteristics (Graham *et al.*, 1983b; Mitchell, 1993). The time dependency of the stress–strain behavior of soft soils, especially soft clay, is generally too significant to be ignored (Graham *et al.*, 1983; Tatsuoka *et al.,* 2001 and 2002). Generally speaking, soils all exhibit more or less viscosity. Sand also shows time-dependent behavior (Suklje, 1969; Murayama *et al.*, 1984). Clayey soils containing clay mineral montmorillonite show strong creep and swelling characteristics. Both creep and swelling characteristics have a significant influence on the deformation and failure of geotechnical structures (Yin and Tong, 2011).

The total area of Hong Kong is approximately 100 km^2, accommodating a population of 7 million. Hong Kong is one of the world's largest and most vibrant trading economies. 64% of the Hong Kong land area is natural hillside. To accommodate the population and economic development, many slopes are formed for land development to cope with the rapid development of Hong Kong. Many buildings and highways are constructed adjacent to slopes, and many cut and fill slopes are formed to suit for the construction. Hong Kong is famous for slope failures, with an average of about 300 slope failures each year (GEO, 2008). In slope inspections, slow movement of natural slopes is an evident of the time-dependent viscosity of soils. According to Skempton (1964), landslide occurring to railway embankment in England is attributed to loss of strength of clayey soils as a result of creep effect. After investigation on dam failures, Vyalov (1986) further indicated that the progressive displacement is induced by the time-dependent behavior of soils.

There have been numerous researchers (Singh and Mitchell, 1968; Silva *et al*., 1991; Tian *et al.*, 1994; Nicholson *et al.*, 1996; Yin, 1999b) who concentrated their efforts on the experimental study of the viscous behavior of clayey soils. A few tests were performed on direct simple shear apparatus (Tian *et al.*, 1994). Some creep tests were carried out on the isotropic stress conditions with special procedures (Holtzer *et al.*, 1973; Yoshikuni *et al.*, 1994). Other conventional tests used for investigating the creep behavior are triaxial compression tests. It is clear that the time-dependent behaviors of soils, especially clayey soils, play a significant part in

geotechnical design and practice.

2.3 Creep Behavior

2.3.1 Compression of Soils

In geotechnical engineering, the consolidation of soils comprises three distinct phases corresponding to three different phenomena (Figure 2.1).

a. Instantaneous settlement, before the expulsion of water, corresponding to the undrained deformation of soil.

b. Primary settlement (or hydrodynamic consolidation), corresponding to the dissipation of the interstitial pressure, u. The duration of this phase (for u=0) can be estimated, provided the configuration of the layer, compressibility and permeability are known.

c. Secondary settlement, which is the consequence of creep, obeys a linear law in the logarithm of time. This additional settlement, which is practically negligible in the case of consolidated or over-consolidated soils, is, contrarily, of considerable importance for mud and soft clays.

In the time-dependent deformation (secondary consolidation), the coefficient of secondary consolidation C_α, is helpful in determining the creep settlement at the end of primary consolidation and is often considered to be the slope of the linear portion of the void ratio (or compression) versus the logarithm of time curve in the secondary compression region. It is noted that the secondary consolidation is the

creep settlement after the end of the primary consolidation. In fact, creep occurs during the whole consolidation process (Yin and Graham, 1999).

2.3.2 Two Hypotheses on Creep Compression

Estimation of the creep settlement has been an interesting area of research for a long time. In engineering practice, two hypotheses, Hypothesis A and Hypothesis B have been adopted for the estimation of the creep (or 'secondary) compression (Yin and Graham, 1996). Hypothesis A assumes that creep occurs only after the end of primary consolidation (after completion of dissipation of porewater pressure). Based on this hypothesis, the total settlement is equal to the settlement before the time at the end of primary consolidation (t_{EOP}) plus the settlement after t_{EOP}. Hypothesis A predicts that soil layer thickness, and hence the time required for porewater pressure dissipation (t_{EOP}), has no effect on the end of primary (EOP) compression curve (Zhu, 1999). In this approach, Terzaghi 's consolidation theory is used to calculate the settlement before EOP and a separated coefficient of secondary consolidation $C_{\alpha z}=-\Delta e / \Delta \log t$ is used to calculate secondary compression. The total settlement is calculated as below:

$$S_{total} = S_{primary} + S_{second} \qquad (2\text{-}2)$$

$$= U_v S_f + 0 \qquad \text{for } t<t_{EOP,\,field}$$

$$= U_v S_f + C_{\alpha\varepsilon} H \log(t / t_{EOP,field}) \qquad \text{for } t>t_{EOP,\,field}$$

where U_v is the vertical average degree of consolidation; S_f is the final primary compression; and H is the height of soil layer.

Hypothesis B assumes the creep occurs during the whole consolidation process. Based on this hypothesis, the EOP compression curve will depend on the thickness of the soil layer as shown in Figure 2.2(a) (Zhu, 1999). The total settlement for a soil is simplified by Yin (2011) as below:

$$S_{total} = S_{"primary"} + S_{creep} \tag{2-3}$$

$$= U_v S_f + \frac{C_{\alpha e}}{1+e_o} H \log \frac{t_o + t_e}{t_o} \quad \text{for a normally-consolidated soil at } t_e>0$$

$$= U_v S_f + \frac{C_{\alpha e}}{1+e_o} H \log \frac{t + t_{e2}}{t_o + t_{e2}} \quad \text{for a over-consolidated soil at } t_e>0$$

where t_o is a material parameter; e_o is initial void ratio; t_e and t_{e2} are equivalent times.

The logarithmic function has a limitation that may cause a serious error in the estimation of long-term settlement. The limitation is that, when the time is infinite, the settlement is infinite. This is certainly incorrect. Results of long term creep tests have shown that the relationship of creep strain to log (time) is not a straight line (Leroueil *et al.*, 1985). The slope of the graph of creep strain against log (time), commonly denoted by coefficient of "secondary" consolidation decreases with time. Thus, the use of logarithmic function may overestimate the creep settlement.

2.3.3 Creep Description

Creep is a continuous deformation of soil under constant loading. When time goes by, the soil creeps (volumetric creep) more but the creep rate decreases with time. Maschyan (1995) has shown many examples emphasizing the creep behavior

of clayey soils. There have been numerous researchers (Bjerrum, 1967; Singh and Mitchell, 1968; Duncan and Buchignani, 1973; Vaid and Campanella, 1977; Tavenas *et al.*, 1978; Silva *et al.*, 1991; Tian *et al.*, 1994; Nicholson *et al.*, 1996; Yin, 1999b) having concentrated their efforts on experimental studies of the creep behavior of clayey soils.

The conventional drained creep test (or oedometer test) can be adopted to study the nonlinear creep behavior of soils in 1D straining. It can reflect the time-dependent stress-strain behaviors of soils in most soil foundations, embankments and other earth works. The 1D straining has a special physical meaning in geotechnical practice including soil foundations, embankments or other earth works. As presented in Silva *et al.* (1991), Tian *et al.* (1994), Nicholson *et al.* (1996), Zhu (2000) and Cheng and Yin (2003), creep behavior both in oedometric condition and triaxial condition are extensively examined.

In triaxial creep tests, the creep behaviors are typically divided into primary, secondary and tertiary periods of creep. At low stress level, there is normally no tertiary creep (Zhu, 2000). Singh and Mitchell (1968) proposed a simple semi-empirical equation for the interrelationship among creep rate, stress level and time. The equation was implemented into time-dependent constitutive models in Kavazanjian and Mitchell (1980) and Borja and Kavazanjian (1985) to estimate the creep strain. The equation was further modified and improved in Mitchell (1993).

In addition to undrained experimental investigations on creep, a number of drained triaxial creep tests were also conducted. Bishop and Lovenbury (1969),

Tavenas *et al.* (1978), Tian *et al.* (1994), Nicholson *et al.* (1996) and Silva and Brandes (1996) gave different suggestions on interpretation of creep behavior. However no practical use is available from small stress level to high stress value at failure.

The secondary consolidation phase (creep) is usually characterized by the secondary compression index $C_\alpha = -\Delta e/\Delta \log t$, where e is void ratio and t is elapsed time. The creep coefficient C_α is considered to be the slope of the linear portion of the void ratio versus logarithm of time curve in the secondary compression region. It is noted that this coefficient is not a constant, but varies with time (Yin, 1999). Mesri and Godlewski (1977) showed that C_α is related to the compression index C_c of the soil and more precisely, that the ratio C_α/C_c is constant for a given soil. This has been confirmed for a large variety of geotechnical materials by Mesri (1973) and many other researchers.

For creep behavior, actually there are volumetric creep which causes no failure and deviatoric creep which ultimately leads to rupture. It is critical to develop a proper constitutive model to consider both creep behaiors, which can be further implemented into numerical simulation for reasonable interpretation and prediction of the creep behavior of soils in varied stress states from different initial stress condition. Experimental and constitutive studies on the creep behavior in different scales and conditions are of significant importance for understanding the time-dependent stress-strain behaviors.

2.4 Swelling Behavior

Clayey soils have been encountered in many parts of the earth for construction of civil projects. In general speaking, clayey soils exhibit more or less both creep and swelling behavior. Creep happens during the whole consolidation process with very little (almost none) excess porewater pressure after primary consolidation. The swelling behavior has been discussed in academic conference and forum (Nelson and Miller, 1992; Al-Rawas and Goosen, 2006). Swelling is the reverse stage of the consolidation process - increasing in volume of a soil due to absorption of water within the voids when the applied stress is reduced. It is represented by the unloading curve (decompression curve) marked in Figure 2.5. The compression due to consolidation is never fully recoverable on unloading and a load-unload-reload cycle produces a hysteresis loop of the form denoted in Figure 2.3.

In this thesis, swelling is completely different from rebounding. Rebounding is associated with decrease in effective stress while swelling happens due to the viscous property of soils with constant effective stress. Swelling occurs when overconsolidated clays are allowed free access to water on unloading because of their great affinity for water. Overconsolidated clay when unloaded possesses very high suction tensions within the soil skeleton. These draw water into the voids causing the volume of voids to increase and the soil to swell, and eventually-often rapidly-to disintegrate. However, swelling can be prevented by constraining the clay to maintain its original volume. The pressure required to prevent swelling is known as the swelling pressure and can be quite large.

Swelling has been observed in clayey soils in oedometer condition (Tong and Yin, 2011). Dakshanamurthy (1978) summarized two main reasons for swelling: water adsorption to clay particles and double-layer repulsion. El-Sohby and Rabba (1981) divided the factors of swelling into three main aspects. The first is concerned about the physical properties of the soil. The second group refers to the environment and placement condition of the soil. The third group is related to the type of water used in wetting. Actually any value of water content exceeding the shrinkage limit will contribute to swelling behavior. Lambe and Whitman (1959) reported that swelling ability varies with the clay mineral and decreases in the order: montmorillonite, illite, attapulgite and kaolinite. Swelling also depends considerably on the exchangeable ion present. El-Sohby and Mazen (1983) confirmed the above results and indicated that the exchangeable ions in particular affect the values of the swelling pressure and the amount of swelling. Sivapullaiah *et al.* (1996) defined three distinct phases of swelling: intervoid swelling, primary swelling and secondary swelling. A slow and continuing swelling with time after primary swelling is called secondary swelling and yields a linear relationship between strain and logarithmic time (Figure 2.6).

Clayey soils containing clay mineral montmorillonite show strong creep and swelling characteristics. Both creep and swelling characteristics have a significant influence on the deformation and failure of geotechnical structures. Clayey soils normally contain one or more of clay minerals of kaolinite, illite, and montmorillonite (Mitchell, 1993; Liu *et al.*, 2011; Xiao *et al.*, 2011). An essential

characteristic of all smectite minerals is their swelling ability to absorb tremendous amounts of water into their sheet structures. The ability of smectite to absorb water is due in part to the inherently small grain size of individual smectite crystals (typically much less that 2 μ) and to the fact that individual sheets possess a negative surface charge which tends to attract polar molecules. The water nearest to the particle is strongly held and appears to have a high viscosity.

Kaolinite consists of the basic structure of a single silica sheet and a gibbsite sheet with relative strong hydrogen bonding between the two sheets. Illite has a basic structure consisting of a gibbsite sheet combined with two silica sheets with relatively weak bonding due to non-exchangeable potassium ions between the two basic structures. Smectite has the same structure as illite. The spacing between two basic structures is occupied by water molecules and exchangeable cations other than potassium, resulting in a very weak bond (Mitchell, 1993). The surfaces of clay mineral particles carry residual negative charges. The negative charges result in cations present in water in the voids being attracted to the clay surfaces. A double layer is formed as the negatively charged particle surface and the adsorbed and dispersed later of cations. A clay particle is surrounded by a layer of adsorbed water. The water nearest to the particle is strongly held and appears to have a high viscosity. The absorbed water can move relatively freely parallel to the particle surface. All these physicochemical properties contribute to the creep and swelling of clayey soils containing the clay minerals.

The research on the creep and swelling of clayey soils has been very active

with a long history. The clayey soils containing montmorillonite have high swelling potential and cause ground heave with addition of water, resulting in damages to foundations and other geotechnical structures. Such soils are also called expansive soils. Expansive soils occur in many parts of the world. Considerable research in this area has been reported over the past three decades. "The First International Research and Engineering Conference on Expansive Clay Soil" was held at Texas A & M University, USA, 30 Aug to 3 Sept 1965. After this a series of such conferences were held in different regions (Snethen, 1980; Al-Rawas and Goosen, 2006). Some books were published on this topic (Chen, 1988; Nelson and Miller, 1992; Katti and Katti, 1994; Al-Rawas and Goosen, 2006). The swelling properties of smectite (bentonite) can be utilized for certain applications, for example, as a buffer material for sealing of nuclear fuel waste. Gray *et al.* (1984), Dixon and Woodcock (1986) and Graham *et al.* (1989) reported a mixture of sodium-based bentonite and medium quartz as a buffer material for sealing nuclear fuel waste in Canadian Nuclear Fuel Waste Management Program. Marcial *et al.* (2002) studied the high stress compression of bentonites as buffer materials. Komine (2008) studied and proposed theoretical equations on hydraulic conductivities of bentonite-based buffer and backfill for underground disposal of radioactive wastes. Mitachi (2008) reported lab test results of mechanical behaviour of bentonite-sand mixtures as buffer materials. The research on the sand-bentonite mixtures as buffer materials is still very active. The swelling potential of the sand-bentonite mixture with addition of water can automatically close the fractures or small gaps in the soil and solidified

nuclear fuel waste cylinder. It shall be noted that swelling can occur from dry/unsaturated condition when inundated with water until saturated condition (Fredlund and Raharadjo, 1993). Figure 2.5 shows a typical plot of void ratio versus vertical stress where there is an initial swelling with addition of water and then compression/consolidation and rebound (Nelson and Miller, 1992). Figure 2.6 shows the time-dependent swelling behaviour of soil-bentonite mixtures, where there is an evidence of "secondary swelling" (Hashim and Muntohar, 2006). In the past, the heave/swelling pressure of the expansive soils was determined mainly with the addition of water. The expansive soils should exhibit time-dependent swelling in a saturated condition. But this has not well investigated before. To my knowledge, little work has been done on the development of a general constitutive model for the time-dependent stress-strain behavior of saturated expansive soils exhibiting both creep and swelling. The study on the soils in a saturated condition is less complicated than that in an unsaturated condition. But the outcomes from the research will provide a basis for future development of constitutive models for soils in a general unsaturated condition.

2.5 Stress Relaxation

Stress relaxation is frequently encountered in geotechnical engineering practice, for instance, short-term change in lateral earth pressure after the installation of support system, and changes in horizontal stress and porewater pressure around

penetrating devices immediately after penetration has stopped (Zhu, 2000). Previous studies on relaxation assumed that stress relaxation and creep are based on the same mechanisms. The viscoplastic strain increment changes the material structure and thus takes effect on both creep and relaxation. This assumption however has neither been proved in experimental studies nor in field applications. It is generally believed that creep may be used to establish a basic constitutive law for geo-materials while results from stress relaxation test can be used to verify the creep law.

Relatively few investigators have studied stress relaxation in soils. Relaxation tests have been used in the past less frequently than conventional creep tests. It was, however, considered that relaxation testing represented an important alternative for studying the rheological properties of a material (Lacerda and Houston, 1973; Ladanyi and Benyamina, 1995). From stress relaxation tests, the parameters of creep can be estimated (Lacerda and Houston, 1973; Ladanyi and Benyamina, 1995). Furthermore, in some cases, for instance in failure states it is more convenient to study time-dependent stress-strain behavior using a relaxation test than using a creep test, because in the latter the failure states only last a very short time.

Yoshikuni *et al.* (1994, 1995a, b) conducted special oedometer tests with different phases of consolidation and relaxation. When the drainage is closed, the tests may be considered as a kind of stress relaxation test with a constant volume strain. In the tests, they found that the increase of pore water pressure is considerable, and the magnitude of pore water pressure is related to the consolidation period of time after which the relaxation started. The higher the strain

rate at which secondary consolidation is stopped, the higher is the generated excess pore water pressure. Holtzer *et al.* (1973) reported similar results in isotropic consolidation tests.

Actually 1D relaxation tests on a saturated clayey soil can be performed both in "creep region" and in "swelling region" (Tong and Yin, 2011). "Swelling" here is not the swelling in unsaturated soils. "Swelling" here occurs in a saturated soil and is caused by the time-dependent expansion of the skeleton of the saturated clay plates with negative charge due to the movement of the absorbed water with dipole attraction to the clay surface (Mitchell, 1993). Swelling is the reverse behavior to creep in a saturated soil.

In undrained triaxial relaxation tests, no existence of a limiting equilibrium stress or principal stress difference was obtained in 24 hours (Vialov and Skibitsky, 1961; Wu *et al.*, 1962). Similar findings were reported by Akai *et al.* (1975) that no limiting value was available for about 10000 minutes of relaxation tests on two remoulded saturated clays. Oda and Mitachi (1988) conducted a series of undrained triaxial stress relaxation tests on four saturated remoulded clays. The results displayed a limiting equilibrium stress. The slope of the principal stress difference versus logarithm of time curve depends on the axial strain level prior to the stress relaxation test. Moreover, Wu *et al.* (1962) and Arai (1985) performed stress relaxation tests after constant rate of strain loading. Lacerda and Houston (1973) carried out a set of stress relaxation tests and indicated that the ratio of principle stress difference over the deviator stress at the beginning of relaxation was linear

with logarithm time. The curve slope was independent of confining pressure. An empirical equation was developed by Lacerda and Houston (1973) for the decayed deviator stress by inverting the Singh and Mitchell's (1968) equation. Consequently, the decay of deviator can be expressed as

$$\frac{q}{q_0} = 1 - s\log\left(\frac{t}{t_0}\right) \quad , \text{ for } t > t_o \tag{2-4}$$

where q_0 is the deviator stress just at the beginning of stress relaxation, q is the deviator stress at any time t, and s is a parameter. A number of stress relaxation tests on undisturbed San Francisco Bay Mud, a remoulded kaolinite, clean quartz sand and compacted clay by Lacerda and Houston (1973) confirmed the validation.

In these tests, the pore water pressure does not vary significantly. Lacerda and Houston (1973) found that "the variation of pore pressure during the relaxation is very small." Similar conclusions were obtained by Sheahan *et al.* (1994) from the results of K_o-consolidated undrained triaxial compression relaxation tests on resedimented Boston Blue Clay. They also found that a single specimen could be used reliably for multiple relaxation tests. Hicher (1988) found that the undrained triaxial stress relaxation test on a remoulded bentonite does not generate pore pressure variation at the strains of 2% and 4%; however, the pore pressure slightly increased in the test with a constant strain of 6%, *i.e.*, at large strain, relaxation will result in the increase of pore pressure.

2.6 Strain Rate Effects

The stress-strain behavior of saturated clays can be significantly affected by the rate of loading, and has been studied with a long history. In the last four decades, numerous papers have been published on the subject of strain rate effects on soil behavior, especially for soft soils (Bjerrum, 1967; Graham *et al.*, 1983a, b; Leroueil *et al.*, 1985; Olson, 1998). The experimental studies of strain rate effects mainly adopted two approaches: one is investigation using oedometer tests, and the other using triaxial tests.

As early as in Buisman (1936), it has been recognized that time could be an important factor during the deformation of soil. In the early 1960's, Crawford (1964) emphasized the importance of strain rate effects on clay behavior and the fact that oedometer test results depend on the testing technique used. Following the pioneering work of Buisman (1936), Taylor (1943) and Casagrande and Wilson (1951), the effects of strain rate on the behavior of clays have been studied by numerous researchers (Crawford, 1959; Richardson and Whitman, 1963; Bjerrum, 1967, 1973; Alberro and Santoyo, 1973; Vaid and Campanella, 1977; Graham *et al.*, 1983a; Lefebvre and Leboeuf, 1987; Lo Presti *et al.*, 1996; Sheahan *et al.*, 1996 and Zhu *et al.*, 1999). Bjerrum (1967), Berre and Iversen (1972), Mesri and Godlewski (1977) and Leroueil *et al.* (1985) among others carried out comprehensive lab studies in oedometer (1D straining) condition. The research on the strain rate-dependency of soil behavior received added attention in recent years due to a large number of constructions on soft ground on-shore, near-shore or offshore.

Most of the oedometer tests investigating the strain rate effects of clayey soils were constant rate of strain (CRSN) tests, such as the tests done by Crawford (1964), Tavenas and Leroueil (1977), Vaid *et al.* (1979), Leroueil *et al.* (1983), Silvestri *et al.* (1985), and Graham *et al.* (1983a). All the test results revealed that the strain rates affect the compression curves of clays and the pre-consolidation pressures. Higher vertical strain rate results in higher vertical effective stress in oedometer CRSN tests. The longer the application of the load, the smaller the pre-consolidation pressure reached in oedometer creep tests. Other kinds of oedometer tests, such as constant rate of loading tests (Jarrett, 1967; Burghignoli, 1979), stage loading tests (Larsson, 1981; Leroueil *et al.*, 1985; Leroueil *et al.*, 1996), controlled gradient tests (Shields, 1974; Leroueil *et al.*, 1983), confirmed the results.

Leroueil (1988) and Leroueil and Marques (1996) examined the importance and practical implication of strain rate effects. The pre-consolidation pressure and effective stress at any strain or void ratio measured in CRSN tests were larger than those measured in conventional 24-hour tests. The typical ratio of effective stress in CRSN test over that in conventional oedometer test equaled to 1.25.

Vaid *et al.* (1979) presented test results of both oedometer tests and isotropically-consolidated triaxial compression/creep tests on a natural clay. Sheahan *et al.* (1994, 1996) carried out studies on time-dependent triaxial relaxation behavior of a resedimented clay and rate-dependent undrained shear behavior of a saturated clay. Koutsoftas *et al.* (1987) and Lee and Ng (1999) among a few others carried out site investigations and lab studies on the properties and behavior of

marine deposits in seabed of Hong Kong. They found that the marine deposits were dark grey clayey silts or silty clay which contained illite. There are many other researchers who have done a lot of lab tests on the time-dependent behavior, mainly on creep of saturated soils. But few researchers have done tests to investigate the time-dependent creep and swelling of saturated soils together.

2.7 Constitutive Models

From experimental investigations, empirical equations or strain-time relationships are usually proposed to explain and fit the test results. Many researchers (Singh and Mitchell, 1968; Garlanger, 1972; Murakami, 1979; Murayama, 1984 and Feda, 1992) adopted empirical equations to predict the time-dependent stress-strain behaviors under simple conditions. Accuracy and assumptions were also discussed in related publications. However the basic limitation of these approaches is that the equations are only valid for the very stress conditions on which the equations are derived. Only under a certain condition these equations simulate behaviors of soils at certain aspects (Zhu, 2000). This is the reason why researchers later followed viscous elastic approach or elastic viscoplastic approach to describe viscous behaviors of soils.

In order to relate the structural viscosity of soils to such coefficients as compression indices familiar to us, C_c, C_α and so on, efforts have also accumulated in formulating a constitutive equation by use of such indices. Bjerrum (1967) was

the first to successfully interpret a variety of consolidation phenomena by a simple conceptual model. His concept and model have caused influences on the research done thereafter. Nearly all the consolidation models that constructed using the common compression indices have been based more or less on his model.

Bjerrum's conceptual model (1967) shown in Figure 2.4(a) is characterized by a single instantaneous compression curve (sedimentation curve or perfect consolidation test curve) and by a family of approximately parallel compression curves each of which is drawn for an equal time after the compression of a clay layer. The model was developed for a normally consolidated young clay or aged clay layer. Contrary to the separation of the compression of a clay layer into a primary and a secondary contribution, Bjerrum (1967) divided the compression into two components as shown in Figure 2.4(b): (a) an 'instant compression' which occurred simultaneously with the increase in effective pressure and caused a reduction in void ratio until an equilibrium value was reached at which the structure effectively supported the overburden pressure; and (b) a "delayed" compression' representing the reduction in volume at unchanged effective stress. At any given value of the overburden pressure and void ratio there corresponded an "equivalent time" of sustained loading, and a certain rate of delayed consolidation (or creep strain), independent of the way in which the clay has reached these values.

Under the action of an overburden load, the clay layer in situ starts to consolidate from the initial state point, *A*. If there was no hydrodynamic lag, the soil would deform first along *AB'C'* and then along *C'D*. The process from *A* to *C'* is the

primary (instant) stage and the *C'D* is the secondary (delayed) stage under a constant intergranular stress. However, no exact definition of instant time, equivalent time or constitutive model were given by Bjerrum (1967).

The viscous, non-recoverable deformation and rearrangement of clay particles make the time-dependent effects happen all the time. A realistic constitutive model for viscous stress-strain behaviors is the key element to predict and evaluate long-term performance of geotechnical structures. In this area some works have been done since Casagrand and Wilson (1951), followed by Bjerrum (1973), Vaid and Campanella (1977) and Graham *et al.* (1983b), etc.

A large number of constitutive models have been proposed for the time-dependent stress-strain behavior of saturated soils so far. Most of the 3D models are based on the viscoplasticity framework of Perzyna (1963, 1966), including, for example, models suggested by Zienkiewicz and Cormeau (1974), Adachi and Oka (1982), Borja and Kavazanjian (1985), Desai and Zhang (1987), Kaliakin and Dafalias (1990), Kutter and Sathialingam (1992), and Adachi *et al.* (1998) and Vermeer and Neher (1999). Detailed approaches used in these models are different. The most difficult part in these models is how to derive the scaling function that controls the magnitude of viscoplastic strain rates and how to determine the model parameters. In modeling 1D time-dependent stress-strain behavior, Leroueil *et al.* (1985) and Kim and Leroueil (2001) among others proposed 1D constitutive models for the strain rate dependent stress-strain behavior of clays. More recently, many experimental findings and constitutive models are

published including Kelln *et al.* (2008a and 2009), Yin and Tong (2011). Kelln *et al.* (2008b) developed analytical EVP model to describe time-dependent behavior of soft estuarine soil and presented triaxial test results in different conditions. Also numerical simulation was carried out to solve and verify the EVP model (Kelln *et al.*, 2008a and 2009). However, none of the above 1D and 3D models can consider both the time-dependent creep and swelling characteristics of saturated soils.

Some early laboratory tests (multi-staged loading, constant rate of strain oedometer tests and triaxial compression/creep/relaxation tests) were carried on a sand-bentonite mixture (proposed as a buffer material for storage of Canadian nuclear wastes) and re-constituted illite (Yin and Graham, 1989; Yin, 1990; Yin and Graham, 1994). A large number of oedometer and triaxial tests were further performed on a re-consolidated Hong Kong marine deposits (HKMD) (Zhu *et al.*, 1999; Zhu and Yin, 2000 and 2001) and undisturbed HKMD (Cheng and Yin, 2006; Yin and Cheng, 2006). Yin (1999a, b) studied and proposed a new nonlinear creep function for the nonlinear creep behaviour of the HKMD. It is seen from the previous test data that there is a loop in an unloading/reloading cycle. This loop is likely related to the swelling property of the soil.

Based on the work of Bjerrum (1967), Yin and Graham (1989, 1994) and Yin (1990) developed the "equivalent time" concept and proposed other concepts such as "reference time" line, etc. Based on these concepts and understanding, Yin and Graham (1989 and 1994) proposed a general one-dimensional elastic viscoplastic equation as

$$\dot{\varepsilon}_z = \frac{\kappa}{V}\frac{\dot{\sigma}_z^{'}}{\sigma_z^{'}} + \frac{\psi^c}{V}\frac{1}{t_o^c}\exp[-(\varepsilon_z - \varepsilon_{zo}^{rc})\frac{V}{\psi^c}]\left(\frac{\sigma_z^{'}}{\sigma_{zo}^{'rc}}\right)^{\frac{\lambda}{\psi^c}} \quad (2\text{-}5)$$

where κ/V is a constant for elastic behavior (V is specific volume), λ/V is a constant for the slope of a "reference time" line (similar to the normally consolidated compression line), ψ^c/V is a creep parameter (similar to the "secondary" consolidation coefficient, but defined differently), t_o^c is a creep parameter in units of time, $\sigma_{zo}^{'rc}$ is a constant parameter in units of stress locating the "reference time" line with $\varepsilon=0$. The same names of the parameters κ/V and are λ/V used in the Cam-Clay model (Roscoe and Burland, 1968) for modeling the unloading/reloading behavior and the normally consolidated behavior of clays under isotropic loading.

This elastic viscoplastic (EVP) model for the time-dependent stress-strain behaviour of soils is based on the “equivalent time” concept under 1D straining condition and has been verified using test data of five different remolded and natural clays. The 1D EVP models have been adopted and used in modeling and analyzing soft soils by others (Sun, 1999; Nash and Ryde, 2000; O'Loughlin, 2000). This 1D EVP model is used here as the basis for developing a new 1D EVP model for clayey soils exhibiting both creep and swelling characteristics. Recently, many experimental findings and constitutive models are published including Kelln *et al.* (2008a and 2009), Yin and Tong (2011).

Garlanger (1972) proposed a constitutive model also based on Bjerrum (1967)’s work. The relation of e-$\sigma^{'}$-t is expressed in (2-6). The soil layer will trace the path $AB^{'}C^{'}D$ in Figure 2.4 (a).

$$-\dot{\varepsilon} = \frac{\alpha e}{\sigma'}\frac{\partial \sigma'}{\partial t} + \frac{\beta e}{t_t}\left(\frac{e}{e_v}\right)^{t\beta}\left(\frac{\sigma'}{\sigma_v}\right)^{\gamma} \tag{2-6}$$

where t_t is the time governing instant line; e_v and σ_v are the e and σ at the yield point, respectively; α, β and γ are constants related to the compression indexes C_c, C_r and C_α.

Den Haan (1996) used an intrinsic time to describe the creep rate. The equation is similar to the work of Garlanger (1972) in form:

$$\dot{\varepsilon} = \frac{\alpha}{\sigma'}\frac{\partial \sigma'}{\partial t} + \beta \exp\left(\frac{-\varepsilon}{c}\right)(\sigma')^{bc} \tag{2-7}$$

where α, β, b and c are constants related to the compression indexes C_c, C_r and C_α.

Considering the whole viscous behavior in $AB'C'D$, Mesri and Rokhsar (1974) adopted the following relations to compute consolidation.

$$-\dot{\varepsilon} = \frac{\alpha}{\sigma'}\frac{\partial \sigma'}{\partial t} + \frac{0.434 C_\alpha}{t}\min\left(\frac{e_o - e}{e_o - e_p}, 1\right) \tag{2-8}$$

where "min" means minimum; e_o and e_p are the void ratio at A and C', respectively.

Yoshikuni *et al.* (1974, 1995) further assumed that equal creep rate lines are a family of straight lines on the *e*-logσ' plane and a new constitutive equation was proposed.

$$\begin{cases} -\dot{\varepsilon} = \dfrac{0.434 C_r}{\sigma'}\dfrac{\partial \sigma'}{\partial t} + \dfrac{\sigma'}{10^{\lambda}} \\ \lambda = \dfrac{e_o - e}{C_r} + \dfrac{C_\beta - C_\alpha}{C_\alpha}\log\dfrac{\sigma'}{\sigma_o'} + \log\eta_o \end{cases} \tag{2-9}$$

where σ_o' and η_o denote initial state; C_β is actually equal to C_c.

For the time-dependent stress-strain behaviors in three dimensions, Yin *et al.* (2002) proposed a new elastic viscoplastic (3D EVP) constitutive model of normally

consolidated and overconsolidated clays. A limit for the creep volume and a new smooth loading surface on the π plane are incorporated in this model. Using calibration in 1D stressing condition, the 3D EVP model is expressed as:

$$\dot{\varepsilon}_{ij} = \frac{1}{2G}\dot{S}_{ij} + \frac{\kappa}{3V}\frac{\dot{p}'}{p'}\delta_{ij} + \frac{\psi_o}{Vt_o}\left(1+\frac{\varepsilon_{vm}^{r}-\varepsilon_{vm}}{\varepsilon_{vml}^{vp}}\right)^{2} \times \exp\left[\frac{V}{\psi^{c}}\left(-(\varepsilon_{vm}-\varepsilon_{vmo}^{rc})+\frac{\lambda}{V}\ln\frac{p_m'}{p_{mo}^{'rc}}\right)\right]\frac{\partial F}{\partial \sigma_{ij}'} \tag{2-10}$$

where *G* is the shear modulus; The loading surface and features of this model are illustrated in Figure 2.7.

In these constitutive models, the total strain rate is divided into several components including elastic strain rate, plastic strain rate, viscoelastic strain rate and viscoplastic strain rate. Some earlier models (termed as over-stress models) are based on the framework proposed by Perzyna (1966), in which elastic viscoplastic modeling is adopted. The models proposed by Adachi and Oka (1982), Katona (1984), Kaliakin and Dafalias (1990) among others belong to this type. As recommended in Bjerrum (1967), total strain rate generally consists of elastoplastic part plus creep part/viscous part (termed as non-stationary flow surface model). The 'instant compression' and 'delayed compression' concepts have been adopted by Borja and Kavazanjian (1985), Kutter and Sathialingam (1992) and Yin and Graham (1989, 1994, and 1999).

2.8 Self-weight Consolidation

Construction on marginal land is becoming increasingly necessary for economic reasons. Foundation soils for these projects, such as soft clays and peats, typically have high water content, high compressibility, and low shear strength. The successful design, construction, operation, and in some cases reclamation of such projects involve prediction of geotechnical behavior in terms of hydraulic conduction, settlement and shear strength, often as a function of time. This in turn requires reliable soil characterization and modeling that account for differences in behavior as compared to conventional soils.

Sedimentary soils are formed initially through a process of sedimentation either in sea or in fresh water. Three main sedimentation stages are defined in Figure 2.8 with respect to the concentration degree as Clarification regime, Zone-settling regime, and Compression regime (Fitch, 1983). Kynch (1952) was groundbreaking in that it allowed the characterization of the settling characteristics of a pulp based on a single batch sedimentation test. This provided the basis for so-called "zone-settling," wherein a settling suspension is divided into three zones, a consolidating zone at the bottom, a clear zone at the top, and a suspension zone between them. In consolidation settling, no discrete flocs are formed and the interface settles at a constant rate. The settling types of the dredged clay in seawater are mainly of zone settling and consolidation settling (Imai, 1980). The settling rate of dredged clay is viewed as a key factor in land reclamation projects.

Study on self-weight settling of incompressible solids was initiated by Kynch

(1952), and subsequently developed by Mc-Roberts and Nixon (1976). The sedimentation process described by Kynch was intensively studied and modified by Scott (1966) and Tiller (1981). The term "self-weight consolidation" was initially proposed by Been and Sills (1981). The settling rate in this consolidation is slow and soil layers gradually form on the bottom of the water. In this sense, the bottom sediment consolidates due to its self-weight lying above. Finally this consolidation results in very soft sediments at the top with density increasing till bottom.

The fundamental mechanism of self-weight consolidation was successfully interpreted by Mikasa (1965), who defined the specific volume f as $f= 1+e$, where e is the void ratio. The relationship between the volume ratio f and effective stress p is used for the estimation of the final settlement, and the relationship between the coefficient of permeability k and void ratio e is in need for the estimation of the settling rate. Generally, the void ratio of the sediment is crucial in sedimentation and consolidation analysis (Abu-Hejleh *et al.*, 1996; Liu and Znidarcic, 1991). Nishimura *et al.* (1992) reported that the permeability had a significant impact on the simulation results in consolidation analysis. The f-p and the k-e relationships, for numerical analysis of the self-weight consolidation, can be determined by the hydraulic consolidation test (Imai, 1981) or by the centrifugal model test (Mikasa and Takada, 1984). These relationships can also be determined in a CRSN consolidation (Umehara and Zen, 1982).

Self-weight consolidation recently becomes one of the major challenges in many engineering problems on the seashore (Mcvay *et al.*, 1986). The settling type

of marine clays in seawater shifts from zone settling to self-weight consolidation when the initial water content decreases to less than about 1000% (Imai, 1980). The zone settling rate of a clay suspension with high water content is so rapid that it is difficult to estimate. It has also been commonly accepted that the traditional consolidation theories are inadequate to explain the self-weight consolidation (Sills, 1995). In this consolidation field, two hypothesizes exist. One claimed such consolidation started at the base, which was supported by majority of researchers including Imai (1981) and the other considered contradictively that the consolidation commenced at the drainage surface-the top, which was approved by Li and Williams (1995).

In reality, there is no sharp transition time from sedimentation to consolidation (Li and Williams, 1995). When the interface of sediment rises for consolidation, sedimentation occurs in the suspension slurry. Major arguments on the interface/boundary were discussed in Been and Sills (1981). Based on Been and Sills' results, the typical void ratio of the sediment surface at the end of settling lies between 6~7, and the value reaches 9~10 when the effective stress is first measured. Tan (1995) proposed an expression for effective stress estimation considering electrochemical effect:

$$\sigma' = \sigma - u - \sigma_{\gamma}(t) \tag{2-11}$$

where σ_{γ} is the contribution from the time-dependent electrochemical force. The void ratio at the transition point is found to be about 6 (Been and Sills, 1981; Tan *et al.*, 1990a).

Secondary compression or creep effect, on the other hand, can be important for high water content soils, especially those that contain organic matter. Settlement behavior referred to "tertiary compression" is also observed. This creep-like behavior has been attributed to biodegradation and gas generation. However recent studies have illustrated that treatment of the specimens for bacterial activity does not entirely remove the effect. Consolidation testing of marine clays using traditional geotechnical testing methods is not practically possible. Among the conventional consolidation apparatuses, the settling column test is suitable for sedimentation and self-weight consolidation analysis.

2.9 Large Strain Consolidation

The large strain consolidation is generally associated with thick layer of compressible soils with considerable high water content (more than 200%). The deformation behaviors of self-weight consolidation and large strain consolidation under additional load are still not yet well understood. Even under significant load, the large strain consolidation alone will take effect.

Early consolidation analysis was generally based on conventional constitutive models. Initiated by Terzaghi's linear elastic model, Taylor and Merchant (1940), Gibson and Lo (1961) proposed linear elastoviscous model; Barden and Berry (1965) developed nonlinear elastoviscous model; Garlanger (1972) introduced an elastoviscous plastic model. A summary of typical constitutive models is illustrated

in Figure 2.9.

It has been proved that the classic Terzaghi's theory is unsatisfactory when the strains involved are substantial (order of 20% or more) or when the self-weight consolidation takes place (Schiffman, 1958). Solution for this large stain consolidation was first proposed by Gibson *et al.* (1981). Lee and Sills (1981), Been and Sills (1981) among others who have made effort in verifying the theory in self-weight consolidation stage on soft soils. Kim *et al.* (1995) described another method to describe the consolidation of soft clays.

The magnitude and settling rate in large strain consolidation of soft soils/slurries are the main topics in various researches. It was generally recognized that the large consolidation deformations when starting with initial void ratios as high as 15 became problematic when working with small-strain formulations. Formulations allowed for the non-linear behavior of void ratio and permeability are also necessary for the analysis of large-strain problems. Olson and Mesri (1970), Tan *et al.* (1990) and Tan (1995) carried out large strain consolidation tests and indicate that the e-σ' curve in low stress range are dependent of initial water content. Following Gibson's theory, Carrier III and Beckman (1984) used the finite element approach to study the stress-large strain behavior and suggested the e-σ' relationship and hydraulic conductivity:

$$\begin{cases} e = \alpha\left(\dfrac{\sigma'}{P_{atm}}\right)^{\beta} + \varepsilon \\ k = \mu\dfrac{(e-\lambda)^{\nu}}{1+e} \end{cases} \tag{2-12}$$

where α, β, ε, v and μ are all empirical parameters.

After determining these parameters, relationship between sedimentation height and elapsed time is proposed:

$$h = a\left(\frac{w}{A}\right)^{b} t^{c-b} \tag{2-13}$$

where h is the height of sediment; w is the weight of material mass; A is the size of disposal area; t is the elapsed time; and a, b, c are all analytical coefficients from computer runs.

Gibson *et al.* (1981), Lee and Sills (1981), Cargill (1982) also proposed different equations to predict the time factor curve and settling rate for large strain consolidations.

Generally, mud flocs are subjected to sedimentation before self-weight consolidation. As a result, the averaged distance between aggregates becomes of the same order as their averaged size at a certain stage, and these aggregates join together to form a volume-filling network. This is usually referred to as the "gel point", and it marks the transition from sedimentation to consolidation (Sills, 1995). Once the volume-filling network is formed, the layer is subjected to self-weight consolidation. From the gel point, excess pore water pressure is transferred to effective stress. Soft soils/slurries during sedimentation to consolidation undergo both viscous and plastic deformations. The deformation can be divided into two phases: (a) in the first one, viscous deformation happens and gradually switches to plastic deformation. The viscous part is time-dependent and irreversible. The

transition point is likely to be smooth. Behavior in this phase can be described by a dashpot (viscous part) and a spring (plastic part); (b) in the second phase, the deformation is viscoplastic and also after transition point, plastic deformation dominates.

Based on the theory for saturated soils by Terzaghi (1943), Bo *et al.* (1997) modified the spring model and add a gap between two springs. The model is feasible in that in large strain consolidation, initial load is taken by water. Until the soil particles contact with each other, the "springs" contact and the real effective stress can be measured. In this sense, the early phase of large strain consolidation is governed by hydraulic conductivity while the later one is stress-dependent.

Following the basic law of mass conservation, balance of movement and energy conservation, Gibson *et al.* (1967) proposed the governing equation (2-14) with the assumption that soil grains are homogeneous and pore fluid and solid are incompressible.

$$\pm\left(\frac{\rho_s}{\rho_f}-1\right)\frac{d}{de}\left(\frac{k(e)}{1+e}\right)\frac{\delta e}{\delta z}+\frac{\delta}{\delta z}\left(\frac{k(e)}{\rho_f(1+e)}\frac{d\sigma'}{\delta e}\frac{\delta e}{\delta z}\right)+\frac{\delta e}{\delta t}=0 \qquad (2\text{-}14)$$

In the above equation, two coordinate systems are used. As shown in Figure 2.10, the soil element *ABCD* at *t=0* is denoted with independent variable "*a*" and the same element at subsequent time "*t*" is to be located at unknown distance by dependent variables. It is noted that the boundary condition is always that $a=a_o$.

The non-linear finite strain consolidation theory (Gibson *et al.*, 1981) is generally accepted as the basic law for consolidation description in engineering field. The prediction of the behavior is however greatly influenced by various forms of the constitutive equations employed. Quite a few relationships that can be applied to highly porous media have been reported regarding mine sludge materials and very high water content soft organic clays (Abu-Hejleh and Znidarcic, 1992; Abu-Hejleh *et al.*, 1996). Somogyi (1979) defined permeability changes for one dimensional consolidation as $k = Ce^D$; C and D are empirical parameters. Znidarcic and Liu (1989) illustrated that the compressibility of high water content soils during consolidation could be characterized by $e = A(\sigma' + Z)^B$; A, B and Z are also material parameters. Regarding the relation of permeability and void ratio, Den Haan (1996) defined a *natural compression line* (NCL) by the equation $\ln\frac{1+e}{1+e_o} = -\lambda^* \cdot \ln\frac{\sigma'}{\sigma_o'}$, considering λ^* as a true material constant. Bartholomeeusen *et al.* (2002) and Hawlader *et al.* (2008) have reviewed some of the formulations.

2.10 Summary and Conclusions

In this chapter, previous studies on the time-dependent stress-strain behaviors are reviewed. Five important viscous phenomena of soils are presented and discussed. It is no doubt that the time-dependent characteristics of soils have indispensible impact on geotechnical structures, from building foundations, to slopes, embankments, retaining walls and dams. The engineering problems of

excessive settlement/deformation, ground heaving, differential settlement and the time-dependent stress-strain-strength behavior have attracted much attention in engineering design, construction and maintenance. More and more public attentions have been paid to this issue. Reliable interpretation, modeling and prediction of these behaviors are essential in settlement control and safety evaluation of structures.

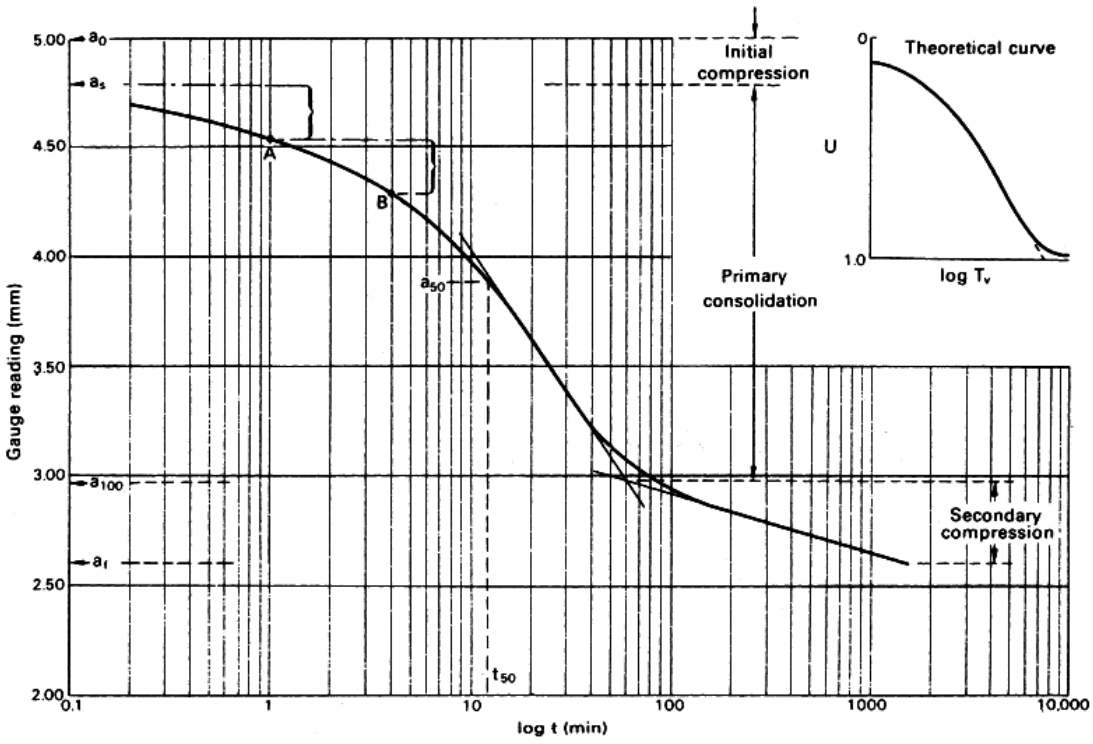

Figure 2.1 Typical consolidation curve and estimation in log scale (Craig, 2004)

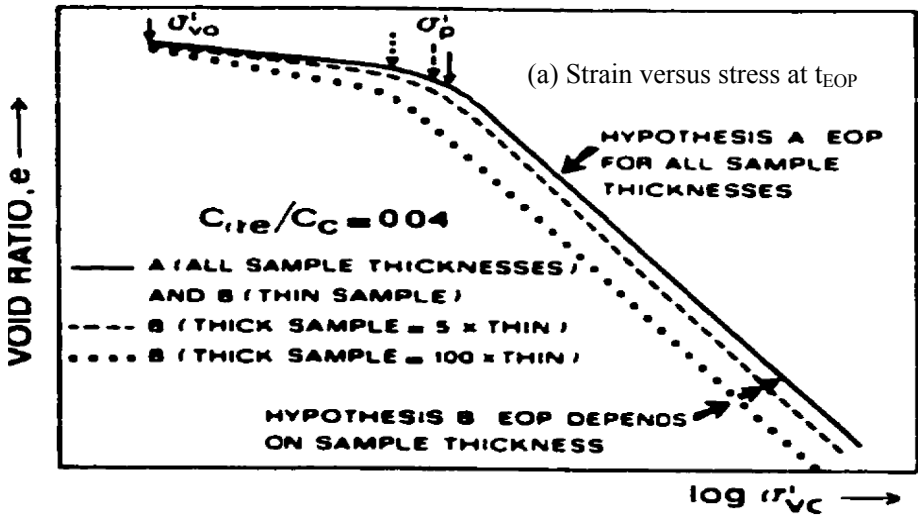
σ'vo
σ'p
(a) Strain versus stress at tEOP
HYPOTHESIS A EOP FOR ALL SAMPLE THICKNESSES
Cr/Cc = 0.04
A (ALL SAMPLE THICKNESSES) AND B (THIN SAMPLE)
B (THICK SAMPLE = 5 x THIN)
B (THICK SAMPLE = 100 x THIN)
HYPOTHESIS B EOP DEPENDS ON SAMPLE THICKNESS
VOID RATIO, e
log (σ'vc)

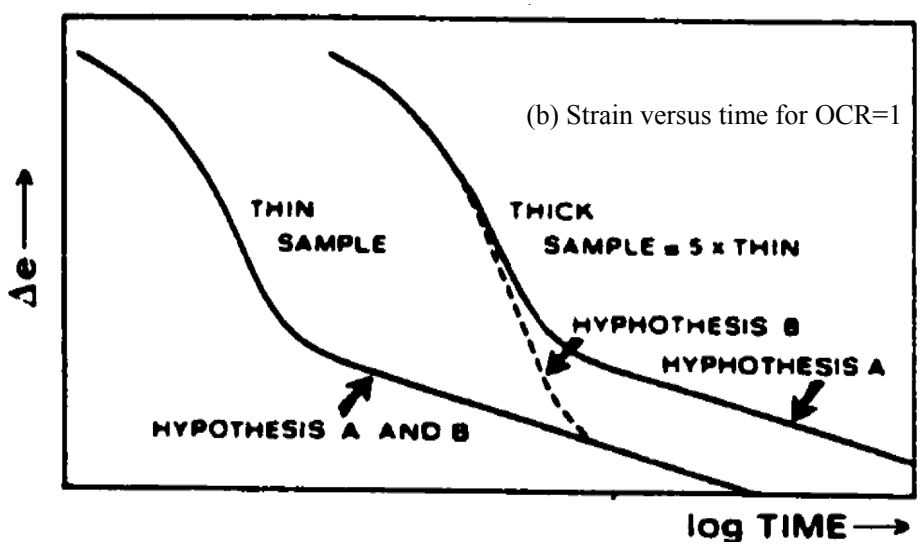

Figure 2.2 Illustration of Hypotheses A and B - (a) relationship of strain versus stress and (b) relationship of strain versus time (Leroueil *et al.*, 1988)

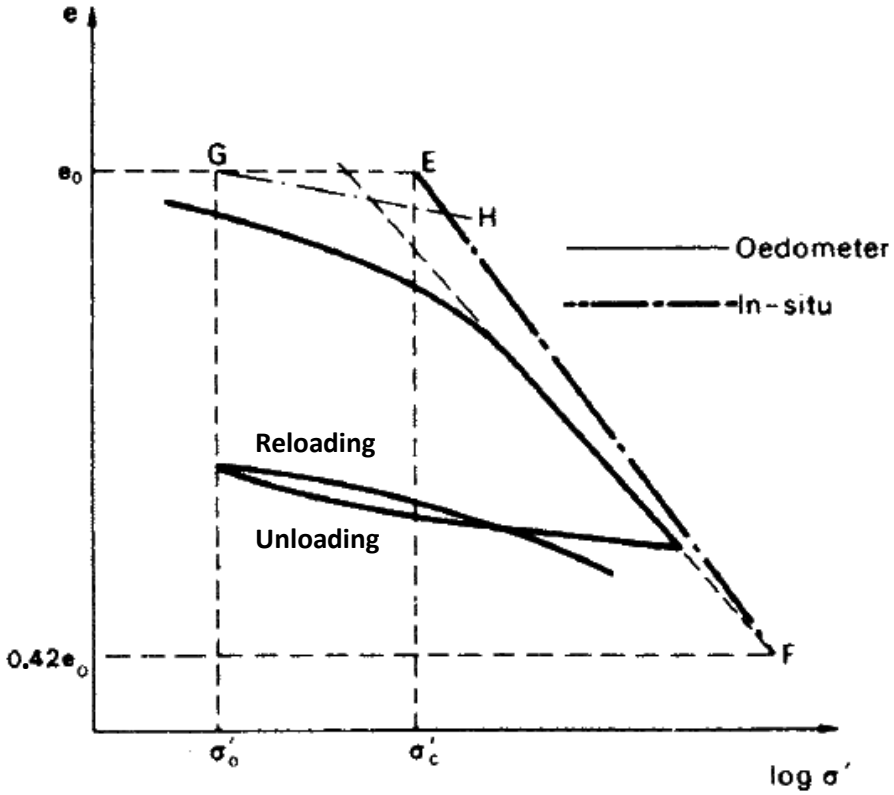

Figure 2.3 Unloading and reloading in compression (Craig, 2004)

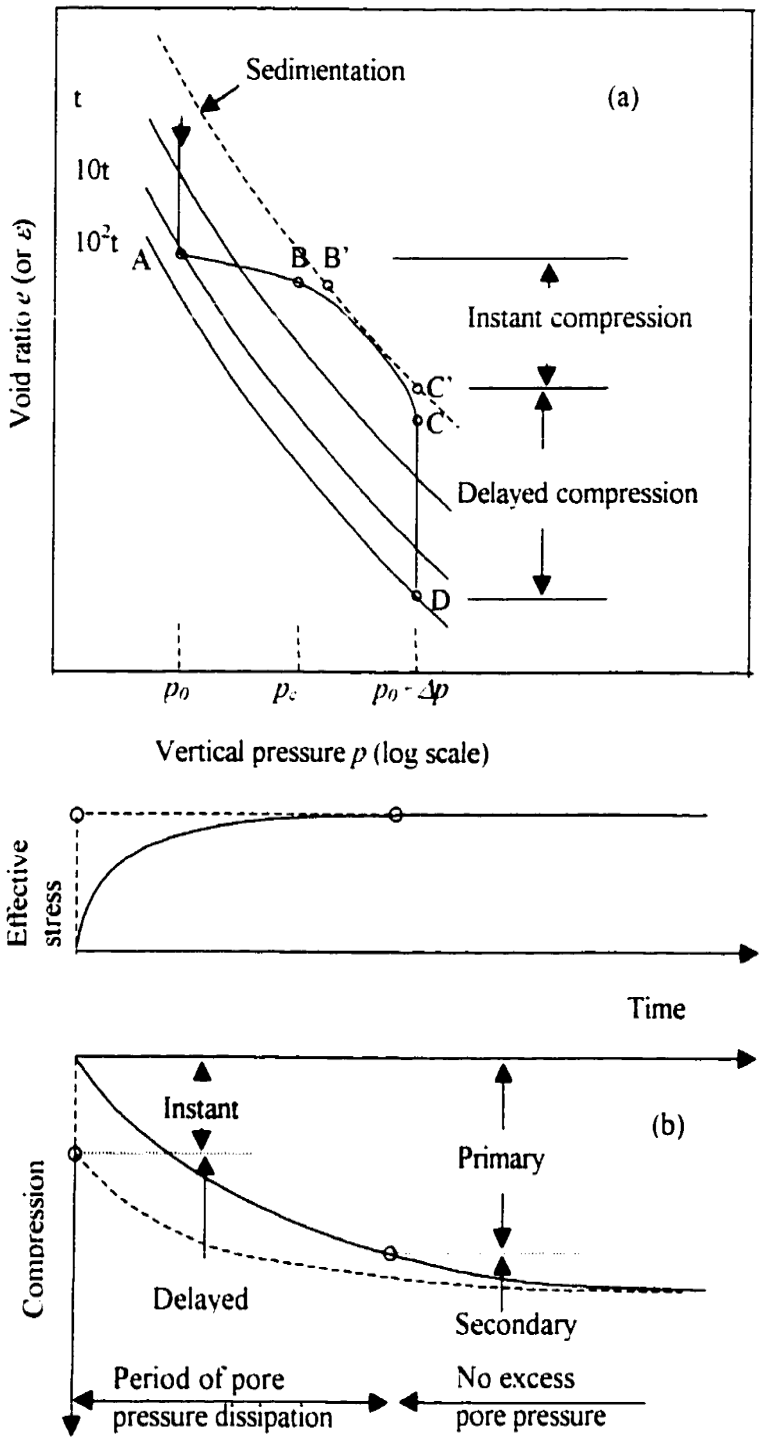

Figure 2.4 Compression model proposed by Bjerrum (1973) - (a) consolidation process of a soil layer and (b) definition of different consolidation stage

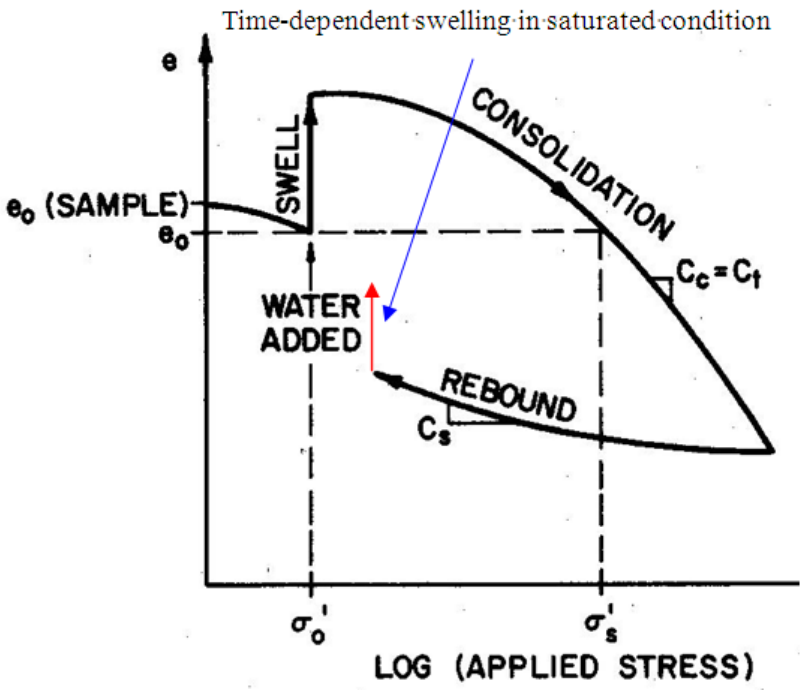

Figure 2.5 Typical plot of consolidation-swell test results (Nelson and Miller, 1992)

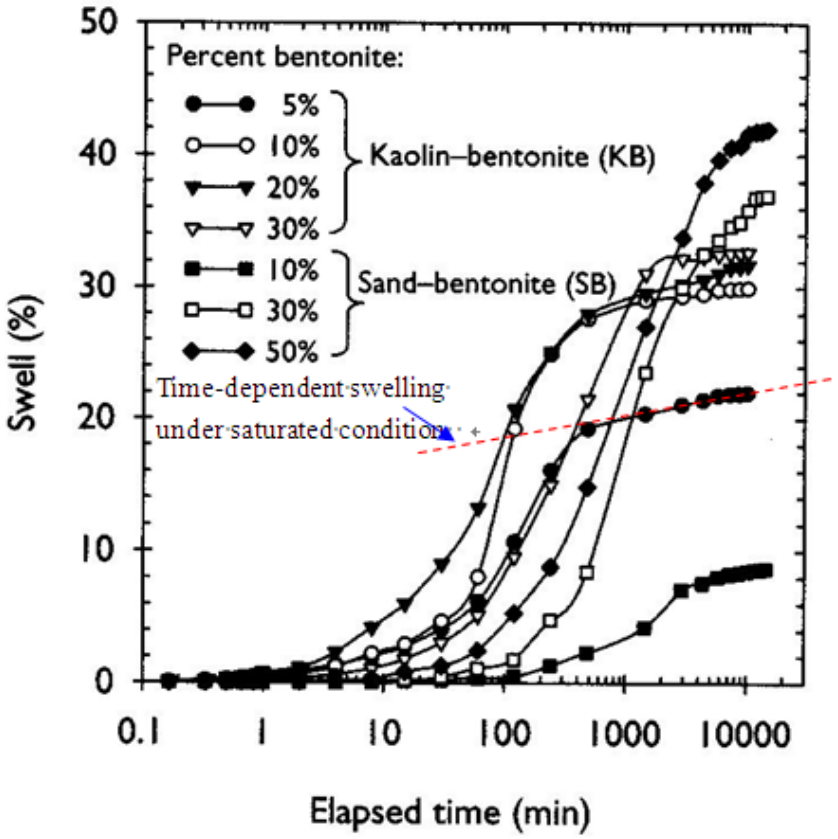

Figure 2.6 Swelling behavior of soil-bentonite mixtures (Hashim and Muntohar, 2006)

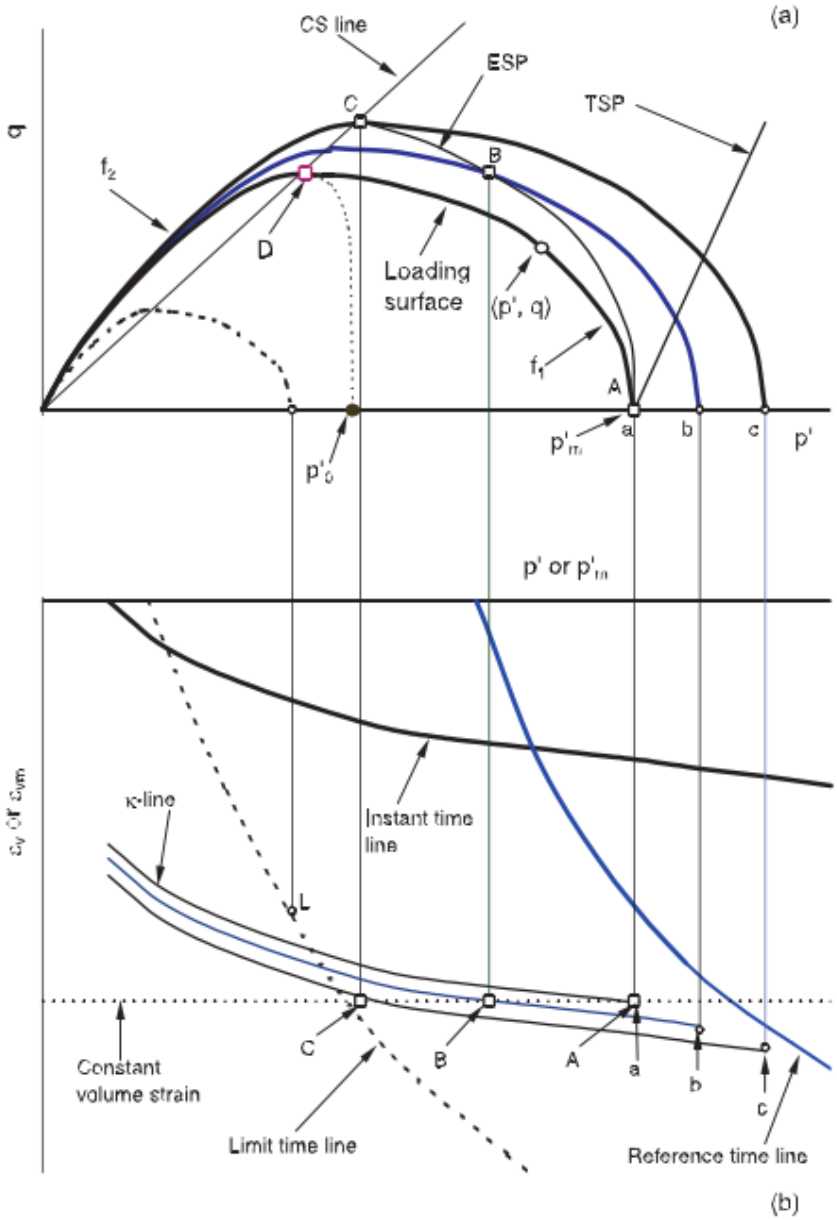

Figure 2.7 Illustration of (a) loading surfaces, total stress path (TSP) and effective stress path (ESP) in $q - p^{'}$ space and (b) corresponding ε_v (or ε_{vm}) versus $p^{'}$, instant timeline, reference time line and limit timeline for isotropically consolidated, undrained triaxial test at constant axial strain rate (Yin *et al.*, 2002)

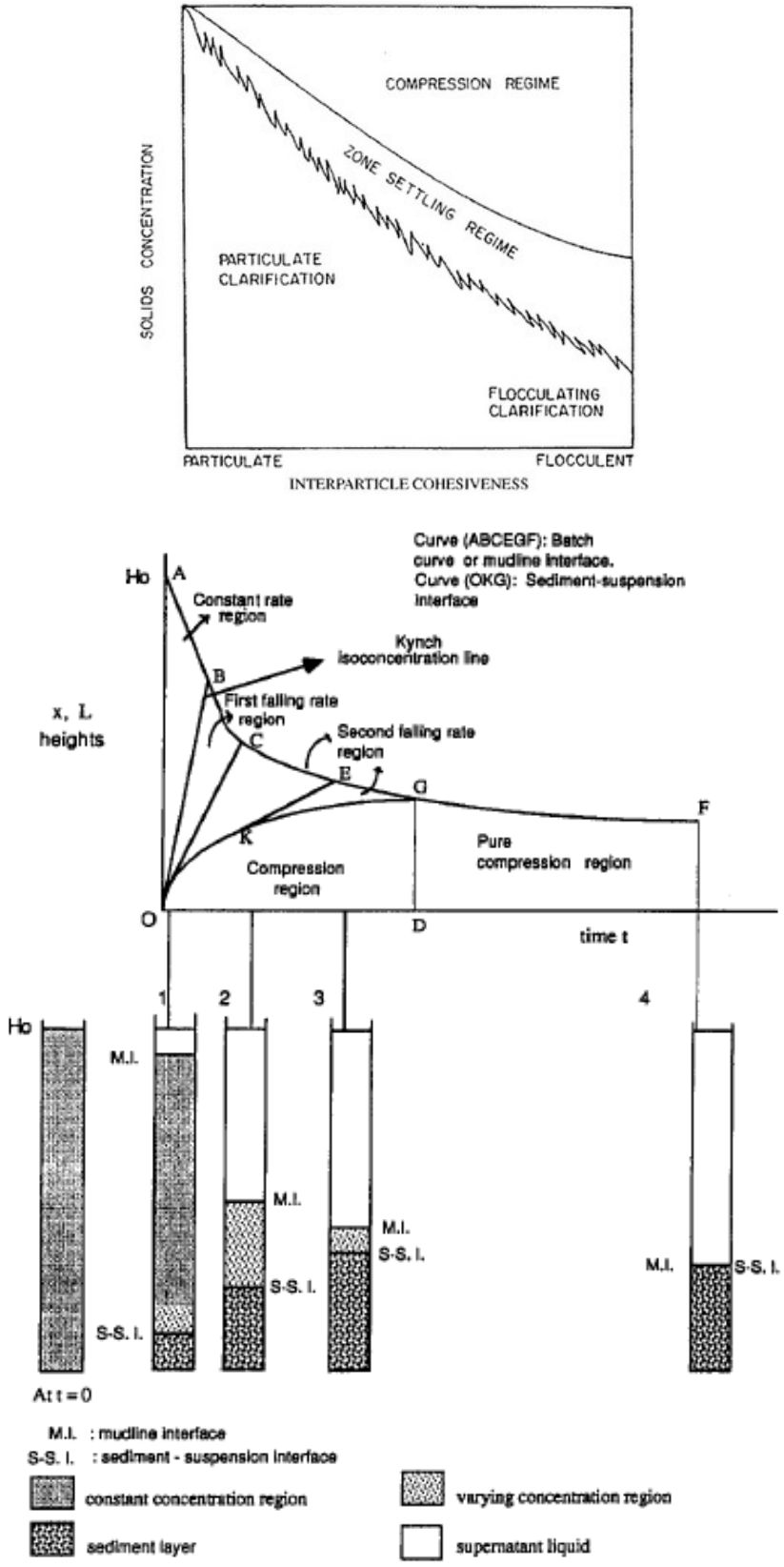

Figure 2.8 Typical settling regimes in settling column test (Fitch, 1983; Panayiotis, 1997)

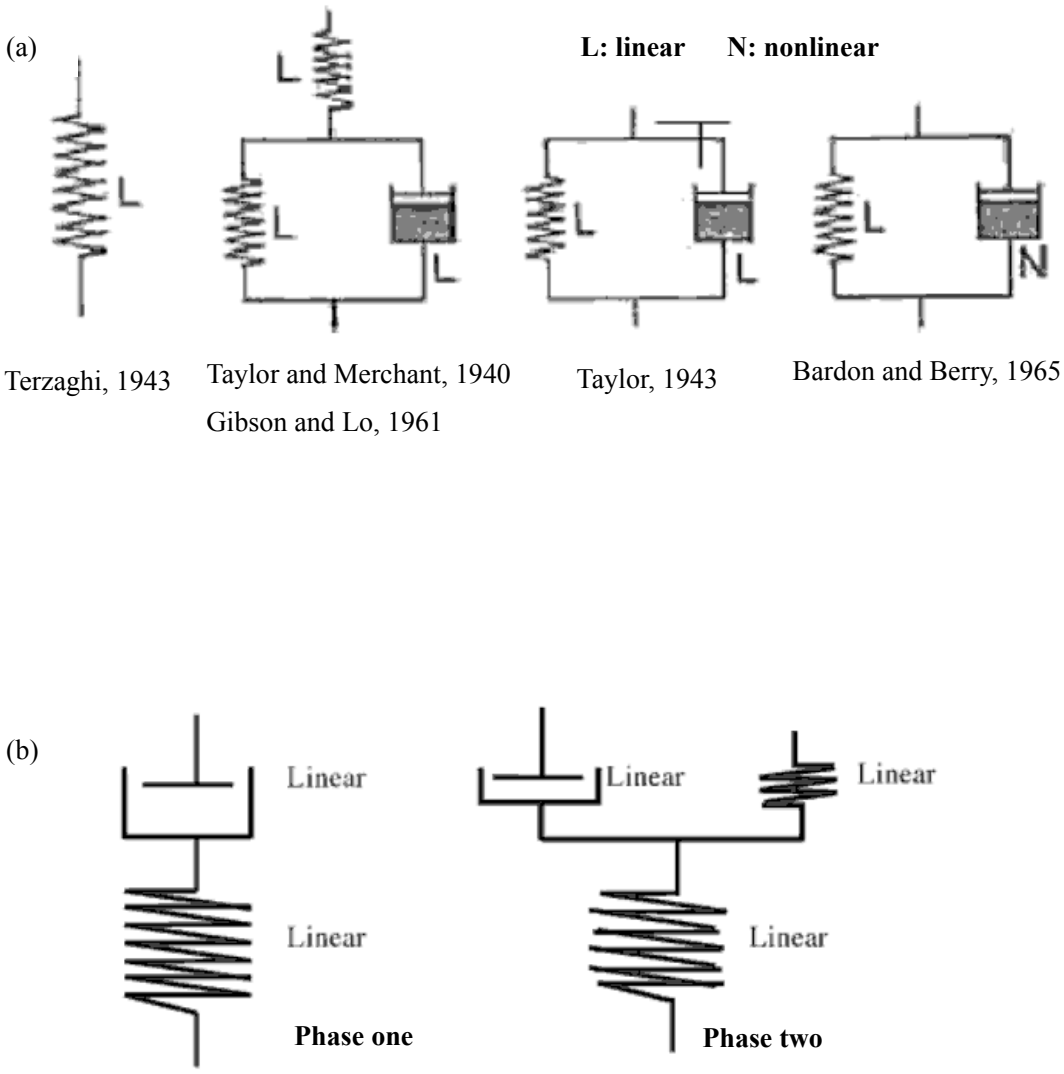

Figure 2.9 Illustration of (a) typical constitutive models in soil mechanics (Extended from Zhu, 2000) and (b) viscoplastic model in large strain consolidation

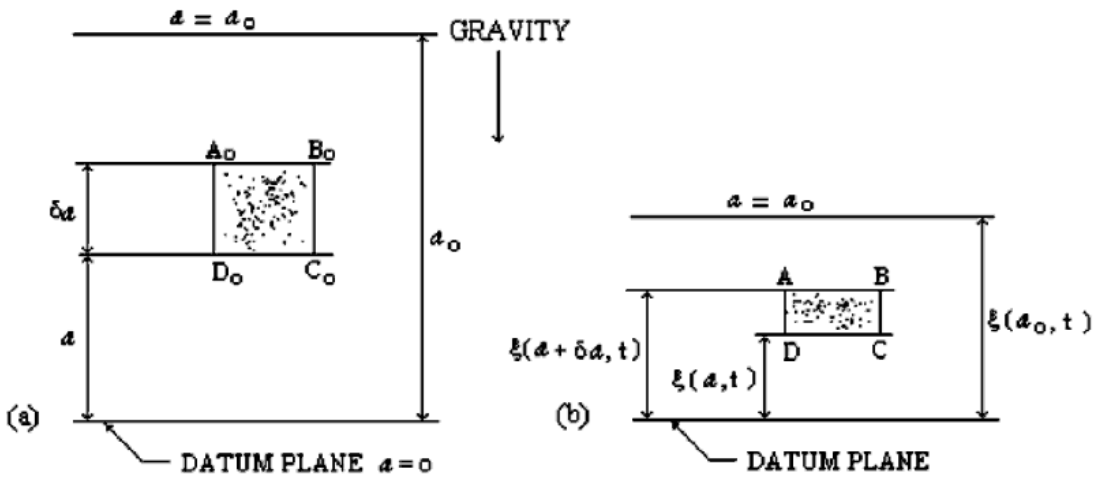

Figure 2.10 Lagrangian and convective coordinates - (a) initial configuration at time *t=0* and (b) configuration at time *t>0*. (Gibson *et al.*, 1967)

Chapter 3

Testing Apparatus and Soil Properties

3.1 Introduction

This chapter introduces the apparatuses and soil materials used in the present study. Results from oedometer tests and isotropic consolidation tests will be used to calibrate the proposed EVPS model in Chapter 9 and Chapter 10 while CRSN tests will be used to verify the model. The SMB soils and HKMD soils with fair viscosity are tested in different stress conditions. The basic properties of the two soils are determined. The apparatuses and testing techniques for various tests are described in details and preparations of soil specimens for each testing are also presented.

3.2 Multi-stage Oedometer Tests

Ahead of the oedometer test, the soil slurry should be pre-consolidated in the large-diameter steel tank. The purpose of pre-consolidation is to allow the specimen to consolidate similar to nature condition underground and to reduce the time for consolidation of specimens. Due to low permeability of the bentonite, it would take about 1.5 months to finish the pre-consolidation.

An electric dial-gauge was installed to measure the pre-consolidation settlement. The loading was added one after another once the settlement was steady. The final pre-consolidation was 24 kPa.

After the pre-consolidation stage, samples were extracted from the

pre-consolidation tank. Specimens with a height of 19 mm and 70 mm in diameter were placed in the oedometric cell. Side friction was minimized using silicone grease. Porous stones attached with filter papers were placed on the top and bottom of the specimens. In all cases, drainages were allowed at the top of the specimens. Oedometer tests were carried out using the Wykeham Farrance conventional oedometers with the maximum capacity of vertical stress 20 MPa. The loadings were applied suddenly in multiple stages. At certain stress level, the loading was reduced in stages and then increased again in two cycles.

The duration of some loading stages was up to 7 days in order to measure the coefficient of secondary consolidation more accurately. Results from the odometer tests are presented and discussed in the following section. All the tests were carried out under the constant laboratory temperature of 20±1°C.

All oedometer specimens were prepared from piston tube samples following the procedures in BS 1377 Part 1 (1990). Saturated filter papers were placed between the specimen and the porous stones to prevent any clogging of the porous stone by clay particles. All the specimens had been allowed to be saturated under the atmosphere for 36 hours.

Every set of the oedometer rings, moveable porous stones and the top cap had to be cleaned and checked so that they fitted to one another. An excessive gap due to the differences in their diameters greater than about 2 mm will result in the clay specimen being squeezed out of the retaining ring. This large gap can also cause an apparent large settlement and compressibility coefficient for the tested soils,

especially during the first stress increment and any successive large stress increment. Therefore, unfitting parts were forbidden for all the tests. The required consolidation stress was applied by placing known weights on the lever arm. In order to ensure that the calculated stresses were applied to the specimen, the lever arm was balanced first with the oedometer cell filled with water and the weights of the ring and the soil specimen.

When an increment of stress is applied to the oedometer test specimen there is an instantaneous increase in pore pressure equal to the stress increment. As drainage occurs the pore pressures decrease and the effective stresses increase, until drainage is complete and the change in effective stress is equal to the applied total stress increment everywhere.

3.3 Constant Rate of Strain (CRSN) Tests

The constant rate of strain (CRSN) testing system, based on the recommendation of Head (1985), is designed for this study. The CRSN oedometer test used consists of 100 mm diameter and 20 mm deep base plate, which is mounted onto the existing base of a triaxial cell. Since the interpretation of CRSN test results require excess pore water pressure at the base to be measured, a small hole together with pressure transducer is installed to measure the pore water pressure. A 63.5 mm diameter ring with a height of 17 mm confines the soil sample to ensure one-dimensional compression. In order to achieve single drainage condition, contact between the sample ring and the bottom plate is sealed by an

O-ring, resulting in single drainage at the top through a coarse porous stone attached to the top cap.

Before the test, the base plate has to be de-aired and saturated. The sand mixed bentonite sample, after extrusion from the Shelby tube, is trimmed to the required size in the sample retaining ring. A filter paper is placed at the bottom of the specimen, preventing the entry of soil particles during testing.

After assembling the specimen, the sample retaining ring, side ring, top cap, top coarse porous stone and base plate in the CRSN apparatus, the cell is placed on the motorized loading frame. A load cell is fixed in position to the frame and the loading piston is brought in contact with the loading plate (top cap) in order to maintain specimen height. The axial force is measured by means of a load gauge of 3 kN capacity attached to the loading frame. De-aired water is used to fill the cell. The strain rates for all CRSN tests were applied in a sequence as follows: $+1\times10^{-5}$ 1/sec, $+1\times10^{-4}$ 1/sec, $+1\times10^{-6}$ 1/sec, $+1\times10^{-7}$ 1/sec, $+1\times10^{-5}$ 1/sec, -1×10^{-5} 1/sec (unloading), $+1\times10^{-5}$ 1/sec (reloading), $+1\times10^{-4}$ 1/sec, $+1\times10^{-6}$ 1/sec, $+1\times10^{-7}$ 1/sec, $+1\times10^{-5}$ 1/sec, -1×10^{-5} 1/sec (unloading), $+1\times10^{-5}$ 1/sec (reloading). All tests were done under the laboratory temperature of 20 ± 1°C in order to minimize the temperature effect.

3.4 Settling Column Consolidation Tests

A total of five settling column samples were taken from five locations for consolidation tests. All these five locations are situated in Yuen Long, the North

West New Territories. The settling column consolidation tests were carried out according to the procedure proposed by Merckelbath (2000). A total of 15 tests were conducted using three different starting concentrations of 20, 50 and 100 g/1 for each soil sample. The settling column is setup according to Berlamont *et al.* (1993) suggestion. A total of 10 perspex columns with an internal diameter of 130mm and a height of 1 m (volume=3.14x0.065x1= 0.01327 m^3) are used. In the setup, ruler length is about 100 cm; distance between two ruler ticks is 1 cm with readable resolution 0.1 cm.

When designed amount of sample and water are well mixed, they are poured into the column for self-consolidation. The settling level together with settling time is recorded manually. After the whole consolidation terminates, a special transparent plastic tube with an internal diameter of 3 mm and very thin thickness (0.05 mm) is used to suck soil at certain depth into the tube. The weight of the tube is measured so that the density is determined. The soil is pushed out and put into a glass container. The container with the wet soil is weighed to get the wet mass. The container with the wet soil is then out in an oven to dry for 24 hours at the standard temperature 105°C to get the dry mass. The water content is then determined.

3.5 Sample Basic Properties and Preparation

Bentonite is a subgroup of the smectite family of clays, for example, sodium montmorillonite with sodium ions is also called sodium bentonite. Considerable

swelling of smectite (bentonite) can occur due to additional water being adsorbed between the combined structural sheets. Bentonite and silica sand mixture has been ever selected as potential buffer and backfill materials for marine radioactive waste repository design (JNC, 2000). Silica present in aqueous media can interact with clayey materials in different ways: precipitation, adsorption, or mineralogical evolution of clays to form more silica rich clays (Bruun-Hansen *et al.*, 1994). Once the two materials get mixed, Bentonite is associated with a high cation exchange capacity, a high swelling potential and a low hydraulic conductivity, while silica sand is associated with high thermal conductivity and strong mechanical properties.

Before the CRSN and MSL tests, the sand mixed with bentonite (SMB) slurries were pre-consolidated in the large-diameter steel tank with 24 kPa vertical pressure to reduce the time for consolidation of specimens. Due to low permeability of the bentonite, it would take about 1.5 months to finish the pre-consolidation. During the process, an electric dial-gauge was installed to measure the settlement. Loading was imposed successively until settlement stabilized.

Five different proportions of silica sand mixed bentonite are employed to conduct various tests in this thesis. The ratios of silica to mixture by dry mass are respectively 50%, 60%, 70%, 80% and 90%. The silica used is BS4550 Pt 5-fraction D300 μm-150 μm. The basic properties (plastic limit, liquid limit, plastic index and specific gravity) are determined and summarized in Table 3-1. The samples are prepared in slurry with 1.5 times liquid limit of these mixtures inside containers.

Marine deposits (MD) in the seabed are clayey silt or silty clay containing clay

mineral illite with moderate creep and swelling potential. Most marine deposits encountered in Hong Kong are silt and sand with different clay contents and have low undrained shear strength (Yin, 1999a). The thickness of Hong Kong marine deposits (HKMD) is between a few meters to more than 20 m. Currently more and more reclamation work have been done in Hong Kong, most of which are on HKMDs. With the reclamation works of coastal areas in Hong Kong, comprehensive investigations on HKMD have been conducted. Yim (1983) and Koutsoftas *et al.* (1987) reported a characteristic seabed soil profile of upper marine clay, alluvial crust, lower marine clay and lower alluvium above residual soil and granite bedrock in most coastal areas of Hong Kong. Reclamation on this foundation of HKMD generally induces a number of geotechnical problems in that an additional load of greater than 250 kPa in reclamations may be applied on the soft HKMD.

Behaviors of HKMD are time-dependent, requiring reliable soil description and understandings. Reasonable prediction of the behavior from both field tests and laboratory tests can improve design, construction, and maintenance of the structures.

Five Hong Kong marine clays with fair viscosity are used from around Nam Sang Wai and Mai Po, Hong Kong (Figure 3.1) for self-weight settling, CRSN, relaxation and oedometer tests. They are MD08, MD19, MD3a, MD17 and MD12, respectively. Before self-weight consolidation, basic properties including water content and specific gravity are determined and presented in Table 3-2 and Table 3-3.

Table 3-1 Basic properties of bentonite specimens with different sand contents

Sand proportion	**50%**	**60%**	**70%**	**80%**	**90%**
Water Content (%)	211.5	159.0	124.5	88.5	57.9
Liquid Limit w_L (%)	146	106	83	59	39
Plastic Limit w_P (%)	30	29	27	26	23
Plastic Index I_P (%)	116	77	56	33	16

Table 3-2 Basic properties of five HKMD samples

Sample ID	**3a**	**08**	**12**	**17**	**19**
Water Content (%)	177.0	76.7	94.6	68.8	71.0
Bulk Density (g/cm^3)	1.71	1.89	2.03	2.01	1.75
Specific Gravity	2.56	2.58	2.54	2.62	2.52

Table 3-3 Basic properties of HKMD samples used in settling column tests

Sample ID	Plastic limit w_P (%)	Liquid limit w_L (%)	Plasticity index I_p (%)	Particle size distribution (%)			
				Clay	Silt	Sand	Gravel
3a	30	64	34	27	52	21	0
19	31	59	28	30	43	25	2
17	29	58	29	33	35	29	3
12	32	58	26	27	42	30	1
08	29	52	23	25	41	33	3

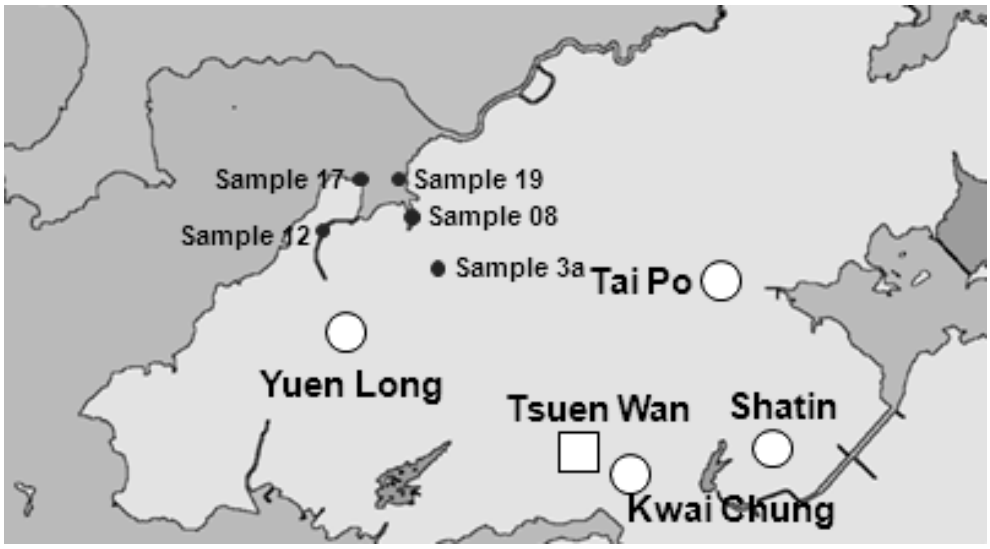

Figure 3.1 Locations of five HKMD samples (Yin and Tong, 2010)

Chapter 4

Creep and Swelling Behaviors on SMB from Oedometer Tests

4.1 Introduction

The time-dependent behavior of clayey soils has attracted much concern. Due to the viscous nature, especially the swelling property, bentonite is selected as buffer and backfill material for marine radioactive wastes disposal. This chapter is intended to investigate the creep and swelling behavior of bentonite mixed different sand contents under oedometeric condition. Appreciation of the sand influence on compressibility, creep, and swelling of bentonite-sand mixtures is essential for developing theories for modeling this type of soils and field applications.

This chapter presents experimental results from one-dimensional oedometric compression tests with multi-stage loading and unloading/reloading on specimens of bentonite mixed with different sand contents. The sand contents are 50%, 60%, and 70%, respectively in terms of the dry mass of sand over the dry mass of the mixture. Using the test results, this chapter examines the influences of sand contents on time-dependent stress-strain behavior of the bentonite-sand mixture in 1D straining with special attention to the nonlinear creep and swelling behaviors. Test results are analyzed and parameters are obtained. Moreover, a nonlinear creep function proposed by Yin (1999a) for Hong Kong Marine Deposits has been adopted to describe the nonlinear creep behavior of the bentonite-sand mixture. Influence of sand proportion on parameter selection is also discussed.

4.2 Testing Materials and Program

Three different proportions of silica sand mixed bentonite are adopted for the creep and swelling study. The silica used in this thesis is BS4550 Pt 5-fraction D150 μm - 300 μm. The basic properties (plastic limit, liquid limit, plastic index and specific gravity) are presented in Table 3-1. The samples are prepared in slurry with 1.5 times liquid limit of these mixtures inside containers.

After the pre-consolidation stage, samples were extracted from the pre-consolidation tank. Specimens with 70 mm in diameter and a height of 19 mm were placed in the oedometric ring. Side friction was minimized using silicone grease. Porous stones attached with filter papers were placed on the top and bottom of the specimens. In all cases, drainages were allowed at the top of the specimens. Oedometer tests were carried out using the Wykeham Farrance conventional oedometers with the maximum capacity of vertical stress 20 MPa. Typical oedometer test results are shown in Figure 4.1. The loadings were applied suddenly in multiple stages. At certain stress level, the loading was reduced in stages and then increased again for two cycles.

The duration of some loading stages was up to 7 days in order to measure the coefficient of secondary consolidation more accurately. Results of the odometer tests are presented and discussed in the following section. All the tests were carried out under the constant laboratory temperature of 20±1°C.

All oedometer specimens were prepared from piston tube samples following the procedures in BS 1377 Part 1 (1990). Saturated filter papers were placed between the specimen and the porous stones to prevent any clogging of the porous stone by clay particles. All the specimens had been allowed to be saturated under the atmosphere for 36 hours.

Every set of the oedometer rings, moveable porous stones and the top cap had to be cleaned and checked so that they fitted to one another. An excessive gap due to the differences in their diameters greater than about 2 mm will result in the clay specimen being squeezed out of the retaining ring. This large gap can also cause an apparent large compression and compressibility coefficient for the tested soils, especially during the first stress increment and any successive large stress increment. Therefore, unfitting parts were forbidden for all the tests. The required consolidation stress was applied by placing known weights on the lever arm. In order to ensure that the calculated stresses were applied to the specimen, the lever arm was balanced first with the oedometer cell filled with water and the weights of the ring and the soil specimen.

When an increment of stress is applied to the oedometer test specimen there is an instantaneous increase in pore pressure equal to the stress increment. As drainage occurs the pore pressures decrease and the effective stresses increase, until drainage is complete and the change in effective stress is equal to the applied total stress increment everywhere. The loading procedural is displayed in Table 4-1.

4.3 Test Results and Discussions

As illustrated in Figures 4.2~4.4, long duration oedometer tests on the bentonite-silica sand mixture clearly show the large contribution of creep to the total compression. Similar results are obtained for swelling to the total rebounding effect. The "primary" consolidation normally finishes within one day. Beyond t=1440 mins, it could be seen that the compression of SMB specimen continues at a very slow rate. The distinct characteristics of non-linear creep strains with the natural logarithm of time are found for the undisturbed bentonite-silica sand mixture. For the stress increments with a long period of loading time, the creep strain eventually has a tendency to lie on a horizontal asymptote, *i.e.* a creep strain limit.

The multi-staged oedometer test curves of vertical strain versus time (log scale) are presented in Figure 4.2 for 70% sand content; Figure 4.3 for 60% sand content; and Figure 4.4 for 50% sand content. Generally, the strain increment enlarges with higher normal stress. For 70% sand sample, the strain increment for a loading increased from 400 kPa to 800 kPa is approximately 6%, while the biggest increment of 13.8% occurs from 50 kPa to 100 kPa. Compared with the behavior of 70% sand sample, low sand proportion implies more dramatic compression. For 50% sand sample, the strain increment for a loading increased from 400 kPa to 800 kPa is approximately 11%, while the biggest increment also occurs from 50 kPa to 100 kPa, which reaches 17.2%. The above behavior is due to the different sand content. Less sand content results in low resistance against loading.

The relationships between the axial strain (ε_a) and vertical effective stress (σ'_v)

in log scale at the end of the "primary" consolidation are plotted in Figure 4.5(a) for 70% bentonite-silica sand mixture, Figure 4.5(b) for 60% bentonite-silica sand mixture and Figure 4.5(c) for 50% bentonite-silica sand mixture. To normalize the effect of initial void ratio, it is better to present stress-strain relationship in the form of ε_a- $log\sigma'_v$ rather than e-$log\sigma'_v$. Based on the test results, the generally accepted C_c-which is compression index is used to describe the relationship between strain at the end of the "primary" consolidation and log effective stress for the whole range of normal consolidation)-could be determined. In fact, according to the test results, C_c is not a constant at each stress level but primarily increases to a maximum value near the pre-consolidation pressure, then decreases with increasing effective stress. This change becomes more pronounced in the case of cementation between the soil particles. Meanwhile, the rebounding index C_r could also be obtained. Values of C_c, C_r and how they are affected by sand proportion would be discussed later.

4.4 Discussions on C_c, C_r, C_α and C_s

Walker (1969) suggested that highly sensitive clays with a high compressibility would exhibit relatively high rates of the "secondary" compression. Mesri *et al.* (1975) showed a linear relationship between C_α and C_c for Chicago blue clay and Mexico City clay, respectively. The concept of constant C_α/C_c ratio was used to characterize the compression behavior of a wide range of natural soils (Mesri and Godlewski, 1977). The C_α/C_c concept is based on the assumption that, for any natural soil, the ratio of C_α/C_c is constant for any time, effective stress and void ratio

during the "secondary" compression (Mesri and Godlewski, 1977).

Oedometer test results of vertical strain against effective vertical stress in log scale are presented in Figure 4.5. The compression index C_c, unloading/reloading (or swelling) index C_r, the coefficient of secondary consolidation C_α can be determined using the test data in Figure 4.2~4.4 and summarized in Table 4-2.

As shown in Table 4-2, the compression index C_c is obviously bigger than the rebounding index C_r for all oedometer tests. With the sand proportion increase, all the relevant coefficients decrease gradually.

The decrement from C_{c1} to C_{c2} (from 0.43 to 0.089) for 70% silica sand mixed bentonite is higher than that for 60% silica sand mixed bentonite (from 0.457 to 0.135). The same trend could be found for samples with sand contents from 60% to 50%. It shows that the soil with more sand has low compressibility.

The rebounding index decreases with higher sand proportion: 0.13 on average for 50% sand sample; 0.08 on average for 70% sand sample. It means that the sample with higher mixing proportion of bentonite is easier to rebound. This is due to the high swelling behavior of bentonite.

However, compared with C_r and C_c mentioned above, the creep behavior coefficient C_α is apparently much smaller (about 20% of the rebounding index), which decreases once the normal pressure increases. This occurs because after first creep, the specimens behave less creep during second loading. During creep, the specimens re-arrange its skeleton to a denser structure which is more difficult to be compressed. The denser structures of the specimens also make them rebound less

easily during the second swelling. Values of C_α/C_c for various sand contents are also summarized in Table 4-2. It is assumed that, for any natural soil, the ratio of C_α/C_c is constant for any time, effective stress and void ratio during the "secondary" compression (Mesri and Godlewski, 1977). Some factors such as normal pressure and the sand content will affect the ratio. SMB soils with low sand content always have high C_α/C_c ratio. Ratios of C_α/C_c could be verified by Mesri and Godlewski's work, that is the C_α/C_c ratio for natural soils lies in a narrow range of 0.025-0.l.

Based on the results, the swelling behavior is less obvious than the creep behavior, but the strain versus time curves all approach horizontal lines. The data also show that the creep and swelling behavior are becoming more obvious with the sand content decreases. For the total vertical strain, the specimen with the highest sand proportion reaches 47.9%, whereas the specimen with the lowest one reaches 66.0%.

4.5 Determination of Time at EOP

To assess the behavior during creep, it is necessary to distinguish the behavior between the "primary" consolidation and "secondary" consolidation. The end of the "primary" consolidation (EOP) can be defined in terms of excess porewater pressure measurements or by means of graphical methods. Although the former is the most accurate, the graphical methods will be adopted since porewater pressures are not measured in conventional oedometer tests.

Considering that the creep happens in both secondary consolidation and in primary consolidation, it is believed that good fitting cannot be achieved for the creep strain versus creep time curves by the Casagrade's method as well as the Taylor's method (Robinson and Allam, 1996).

In order to overcome such deficiencies caused by non-linear creep effect, the $t^{0.5-\inf}$ method was employed for t_{EOP} estimation, which has the advantages of both the Taylor's $t^{0.5}$ method and the inflection point method (Cour, 1971; Robinson, 1997; Mesri *et al.*, 1999).

Based on the method, the time of EOP as well as the strain at t_{EOP} are calculated and listed in Table 4-3 for specimens with different sand proportions. It is seen that when the sand content decreases, the time to finish the primary consolidation increases. Meanwhile, high normal stress effectively shortens the time of primary consolidation.

It should be mentioned that the inflection point would disappear as a result of a small load increment ratio like 0.2 (Mesri *et al.*, 1999). It is recommended that a load increment ratio within the range of 0.5-1 (Mesri *et al.*, 1999) be used for the laboratory tests so that the inflection point would appear on the *logt* consolidation curve at the degree of consolidation of 70.25%. While the inflection point at about U=70.25% forms the basis of determining the EOP, the creep effects which become pronounced for U>60% (Sridharan *et al.*, 1995) are less compared to the standard methods of Taylor (U=90%) and Casagrade (U=100%).

4.6 1D Non-linear Function and Parameters Identification

Creep also occurs during the "primary" consolidation (Yin and Graham, 1989, 1994 and 1996). The following creep equation has been proposed by Yin and Graham (1989 and 1994) and also used by Niemunis and Krieg (1996).

$$s = \frac{C_\alpha}{1+e_o} H_0 \log \frac{t+t_o}{t_o} \tag{4-1}$$

where C_α is the "secondary" consolidation coefficient defined before; and t_o is a curve-fitting parameter related to the initial creep rate (or the choice of a reference time line). Normally, t_o is chosen as the time equal to the end of the "primary" consolidation (t_{EOP}) from oedometer tests. The t_o is not equal to t_{EOP} calculated from the field consolidation conditions and is considered to be a material parameter. It is noted that the "instant" compression is simply calculated using the stress-strain curve from the end of the "primary" consolidation data of the laboratory oedometer tests.

Although there is a good progress in the expression of creep strain using equation (4-1), an obvious obstacle is still unsolved, that is, when the time is infinite, the compression becomes infinite. This is not realistic to our common sense.

To develop an empirical relation for predicting the creep settlement, Yin (1999) proposed a non-linear creep function with a creep strain limit and found that this function can fit well one-dimensional creep test data of remoulded HKMD. In this study, the non-linear creep function proposed by Yin (1999) is adopted for the evaluation of the time-dependent creep axial strain of the undisturbed SMB under

one-dimensional condition. The non-linear creep function is expressed as

$$\Delta\varepsilon_{\alpha}^{vp} = \frac{(\psi_o^{'}/V)\ln[(t+t_o)/t_o]}{1+((\psi_o^{'}/V)/\Delta\varepsilon_{l\alpha}^{vp})\ln[(t+t_o)/t_o]} \tag{4-2}$$

where $\Delta\varepsilon_{\alpha}^{vp}$ is the creep strain not including an instantaneous strain; the superscript "*vp*" and subscript "*a*" denote viscoplastic deformation and axial strain variation respectively; *t* is the creep time for the creep strain $\Delta\varepsilon_{\alpha}^{vp}$; $\psi_o^{'}/V$, t_o, and $\varepsilon_{l\alpha}^{vp}$ are three constant parameters, for which the definitions and determination methods are discussed in details later. The subscript "*o*" for the parameters, $\psi_o^{'}/V$ and t_o represents that they are parameters defined when *t*=0. As *t* is a variable, the term $ln[(t+t_o)/t_o]$ can be also considered together as a variable. Thus, equation (4-2) is in fact a hyperbolic function which was first used to fit the stress-strain relationships of soils by Kondner (1963).

Equation (4-2) can be given in an alternative way

$$\frac{\ln[(t+t_o)/t_o]}{\Delta\varepsilon_{\alpha}^{vp}} = \frac{1}{\Delta\varepsilon_{l\alpha}^{vp}}\ln(\frac{t+t_o}{t_o}) + \frac{V}{\psi_o^{'}} \tag{4-3}$$

where $\psi_o^{'}/V$ (Yin and Graham, 1989 and 1994) is a material parameter larger than zero and *V* is the specific volume. It is noted that $\psi_o^{'}/V$ is a constant value in Yin and Graham (1989, 1994). However $\psi_o^{'}/V$ may vary with the vertical effective stress (Mesri and Godlewski, 1977; Yin, 1999).

Equation (4-3) is a form of *y*=*kx*+*b*, in which $1/\Delta\varepsilon_{l\alpha}^{vp}$ is the slope and $V/\psi_o^{'}$ is the *y*-intercept. If the test data produces a straight line on the $\ln(\frac{t+t_o}{t_o})$ against $\frac{\ln[(t+t_o)/t_o]}{\Delta\varepsilon_{\alpha}^{vp}}$ plot, the key parameters can be determined.

It should be emphasized that t_o cannot be chosen arbitrarily by comparing the fitting effect when using different t_o; inappropriate t_o would result in incorrect $\psi^{'}/V$ and $\varepsilon_{l\alpha}^{vp}$ (Yin, 1999). Other than being a curve fitting parameter, t_o serves as starting point to account the creep strain and is the time referring to the real elapsed time determining the position of the referring time line (Yin and Graham, 1989 and 1994). It is suggested that t_o be equal to the time at the end of primary consolidation, t_{EOP}.

By appropriately selecting t_o, the test data can be fitted well by a straight line in the $\ln(\frac{t+t_o}{t_o})$ against $\frac{\ln[(t+t_o)/t_o]}{\Delta\varepsilon_{\alpha}^{vp}}$ plot. Figure 4.7 and Figure 4.8 show the curve-fitting results under different normal effective pressure. The influence of different sand proportions on fitting parameters is illustrated in Table 4-4. Actually, the quality of simulation is highly dependent of the accuracy of $\psi^{'}/V$ and $\varepsilon_{l\alpha}^{vp}$, and hence of R^2 for the straight line fitting. By examining Table 4-4, one can find that both V/ψ_o and $\varepsilon_{l\alpha}^{vp}$ decrease with the vertical effective stress increases. For given normal effective pressure, $V/\psi_o^{'}$ and $\varepsilon_{l\alpha}^{vp}$ increases with the increase of sand content. Under a normal effective pressure of 100 kPa, $V/\psi_o^{'}$ is 16.19 for the 70% specimen. By contrast, the value is only 10.04 for 50% sample.

If the effective stress $\sigma_v^{'}$ is considered, formulations of the two parameters with both loading time and sand content could be summarized. Yin (1999) has already developed a linear relationship between these two parameters with $\log\sigma_v^{'}$.

4.7 Summary and Conclusions

In this chapter, three types of silica sand mixed bentonite samples in term of different sand content are tested to examine the creep and swelling behavior under oedometer condition. Conclusions could be drawn as follows:

a. Non-linear creep and swelling behaviors have been observed from the 1D multi-stage oedometer tests on sand mixed bentonite specimens. Both behaviors occur less obviously under higher stress condition. After first creep and swelling, both the creep coefficient and the swelling coefficient decreases.

b. The $t^{0.5-\inf}$ method was employed for t_{EOP} estimation, which provides the theoretical framework for further parameters determination for non-linear function. Then Yin (1999)'s function has been adopted to simulate the creep settlement for the SMB samples. A good agreement is obtained between the test data and modeling results. Appropriately selecting t_o and strain at t_{EOP} ensures a good quality in curve fitting. More accurate prediction is dependent of long duration of oedometer test.

c. The sand content exerts an indispensible impact on soil behaviors. Soil with higher sand content has lower compressibility. With the increase of sand contents, the oedometric characteristics of SMB specimens have: (1) small compression, (2) high resistance against loading, (3) low value of C_c, C_r, C_α and C_s, (4) low ratio of C_α/C_c and C_s/C_r, (5) less time at t_{EOP}, and finally (6) high value of V/ψ_o and $\varepsilon_{l\alpha}^{vp}$. Sand content has become a key parameter determining the behaviors of SMBs.

d. Ratios of C_α/C_c, C_s/C_r and C_s/C_c show non-linear relationship for SMB. All the three ratios over sand content follow hyperbolic curves, hence keep relatively constant finally. For SMB samples with varied sand content, ratio of swelling coefficient against rebounding index C_s/C_r lies in 0.11 consequently.

Table 4-1 Loading procedure in oedometer tests (44 days in total)

	Load (kPa)	Duration (day)		Load (kPa)	Duration (day)		Load (kPa)	Duration (day)
1	0-10	1	8	10-25	1	15	100-50	7
2	10-25	1	9	25-50	1	16	50-100	1
3	25-50	1	10	50-100	1	17	100-200	1
4	50-100	7	11	100-200	1	18	200-400	1
5	100-50	1	12	200-400	7	19	400-800	2
6	50-25	1	13	400-200	1			
7	25-10	7	14	200-100	1			

Table 4-2 Creep and swelling indexes for different bentonite samples

Sand proportion	**50%**	**60%**	**70%**	**80%**	**90%**
Compression index C_c	0.315	0.296	0.260	0.243	0.104
Rebounding index C_r	0.130	0.113	0.092	0.054	0.021
Creep coefficient $C_{\alpha 1}$ (σ_v=100 kPa)	0.0304	0.0263	0.0227	0.0062	0.0025
Creep coefficient $C_{\alpha 2}$ (σ_v =400 kPa)	0.0191	0.0141	0.0120	0.0051	0.0023
C_α/ C_c (σ_v =100 kPa)	0.0965	0.0889	0.0873	0.0255	0.0240
C_α/ C_c (σ_v =400 kPa)	0.0606	0.0476	0.0462	0.0210	0.0221
Swelling coefficient C_{s1} (σ_v =10 kPa)	0.0284	0.0251	0.0160	0.0085	0.0033
Swelling coefficient C_{s2} (σ_v =50 kPa)	0.0173	0.0131	0.0124	0.0062	0.0024
C_{s1}/ C_r (σ_v =100 kPa)	0.2185	0.2221	0.1739	0.1574	0.1571
C_{s2}/ C_r (σ_v =400 kPa)	0.1331	0.1159	0.1048	0.1148	0.1143
C_{s1}/ C_c (σ_v =100 kPa)	0.0902	0.0848	0.0615	0.0350	0.0317
C_{s2}/ C_c (σ_v =400 kPa)	0.0549	0.0443	0.0477	0.0255	0.0230

Table 4-3 Determination of time at EOP

Sand proportion		**70%**	**60%**	**50%**
100 kPa	EOP (min)	1300	1600	2020
	Strain at EOP (%)	11.2	10.8	13.0
400 kPa	EOP (min)	1200	1460	1900
	Strain at EOP (%)	7.4	7.6	12.0

Table 4-4 Summary of the curve-fitting parameters for SMB with different sand contents

Normal stress		**70% sand**	**60% sand**	**50% sand**
	t_o	1300	1600	2020
100 kPa	V/ψ_o	16.19	15.02	10.04
	ε_{la}^{vp}	0.0300	0.0293	0.0290
	t_o	1200	1460	1900
400 kPa	V/ψ_o	60.88	40.05	10.19
	ε_{la}^{vp}	0.0236	0.0234	0.0222

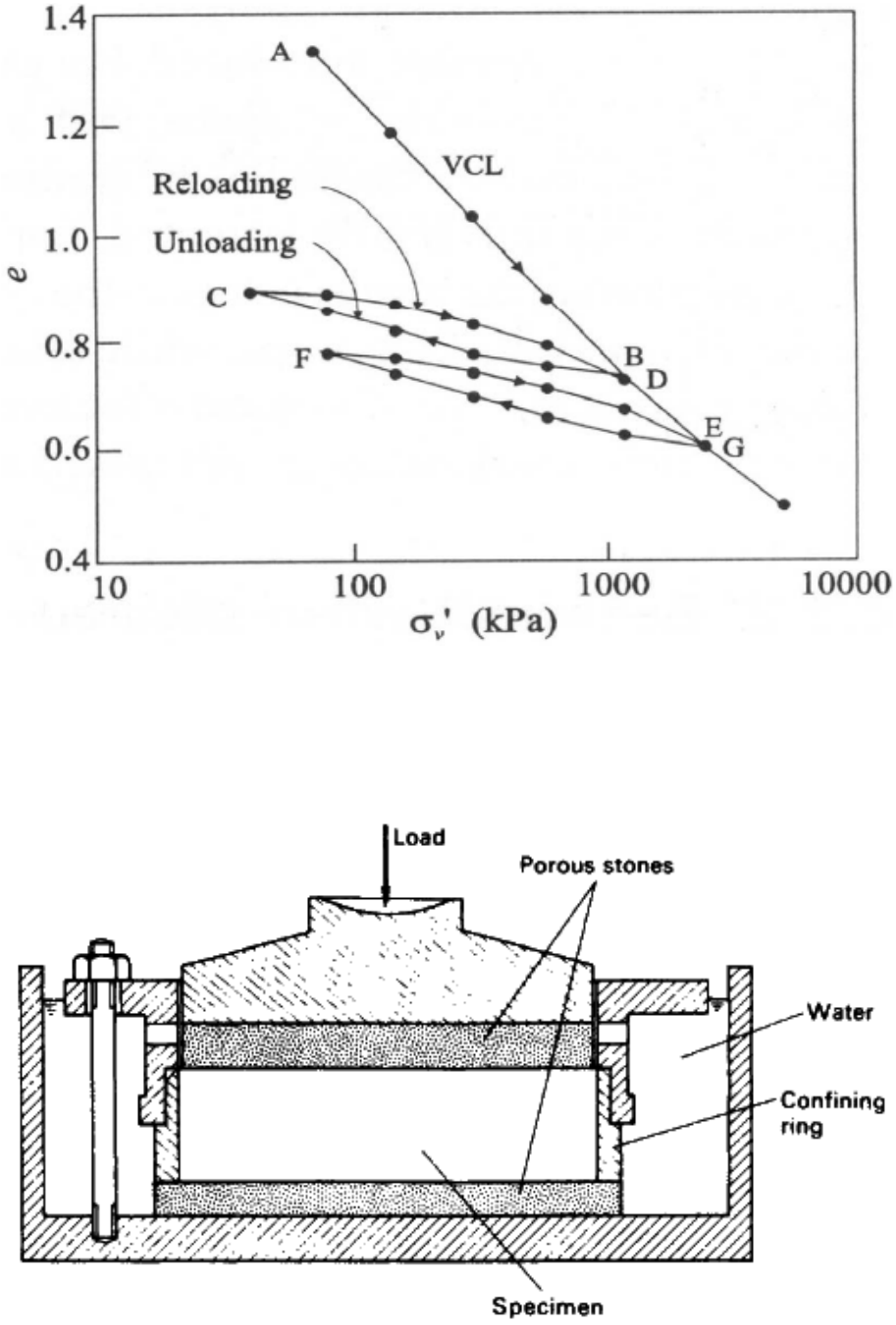

Figure 4.1 Typical creep curves and the oedometer (Craig, 2004)

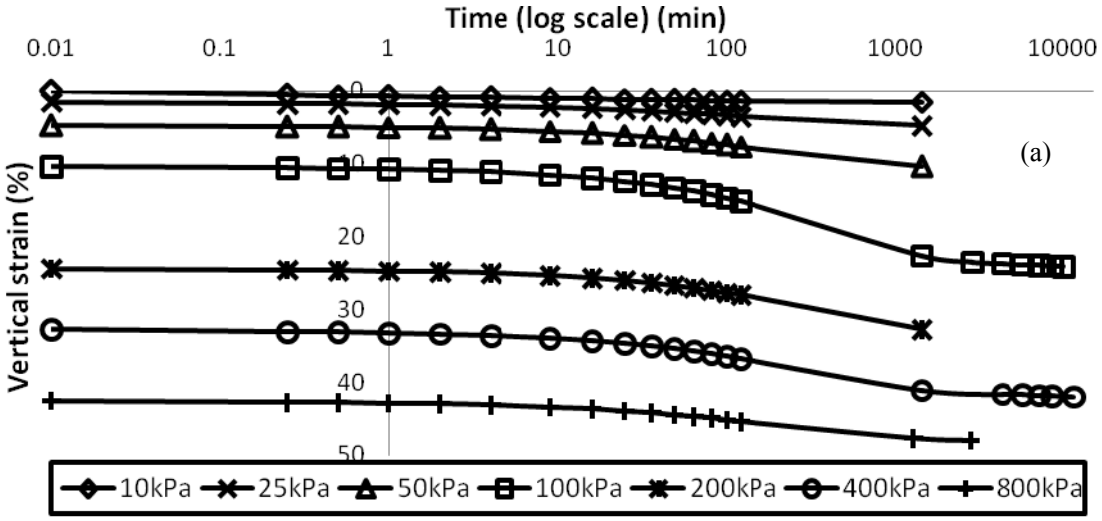

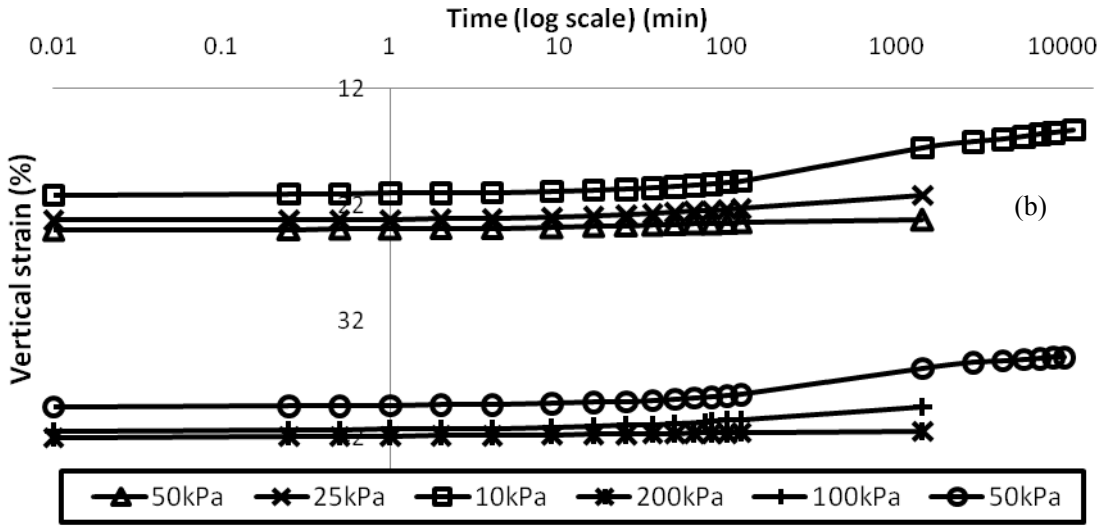

Figure 4.2 Vertical strain against time in log scale for 70% sand mixed with 30% bentonite - (a) loading and (b) unloading

(a)

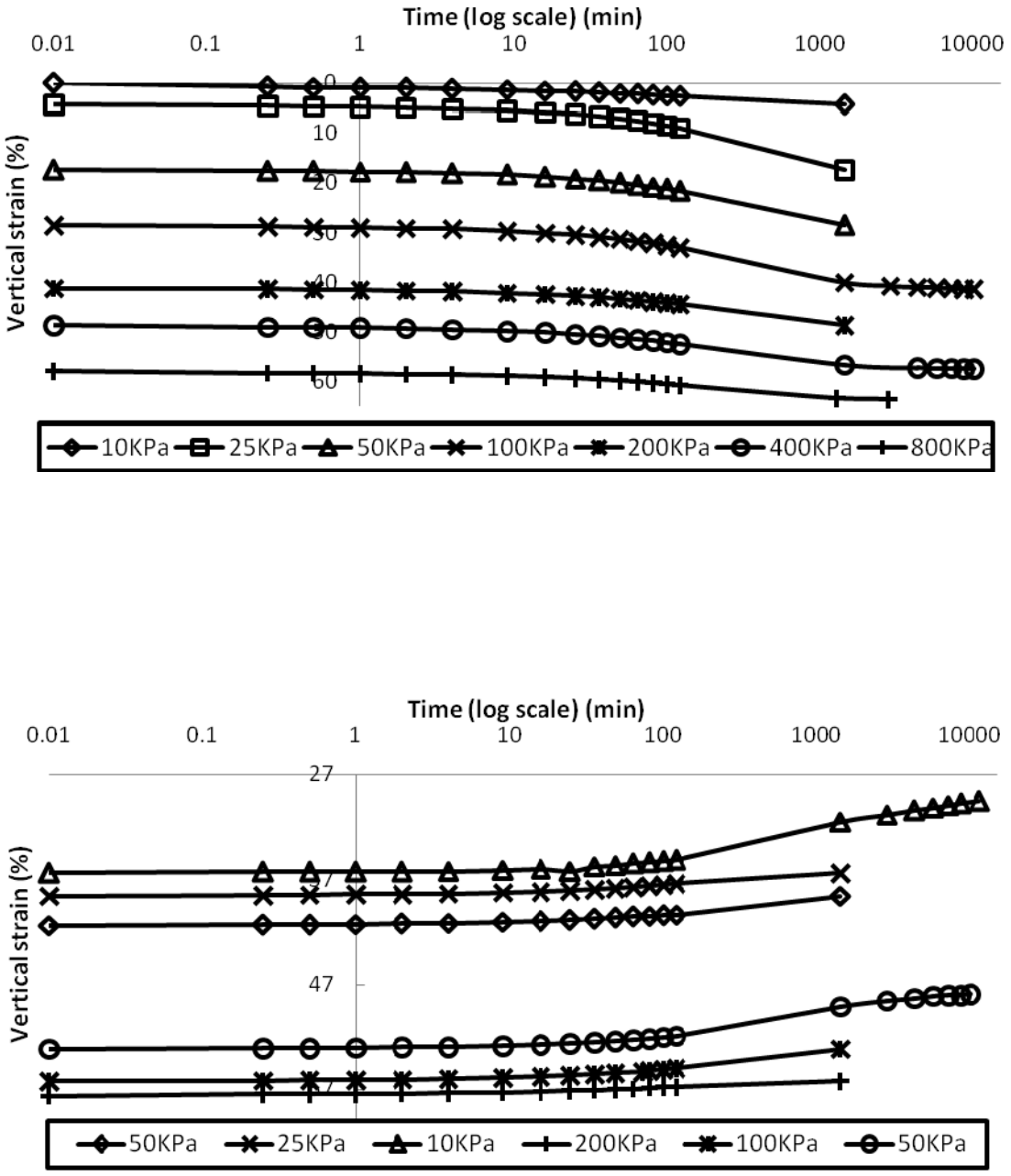

Figure 4.3 Vertical strain against time in log scale for 60% sand mixed with 40% bentonite - (a) loading and (b) unloading

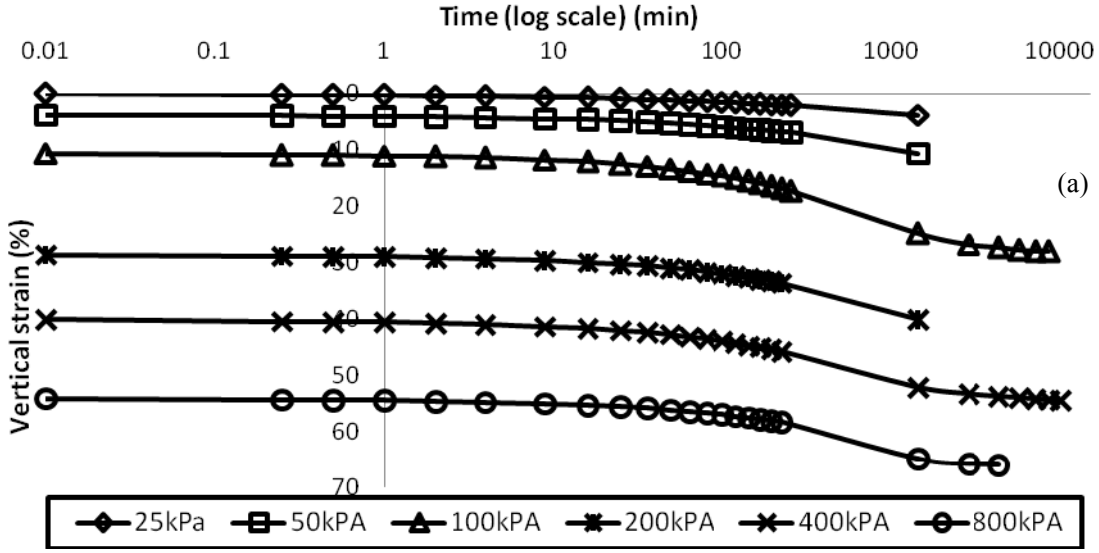

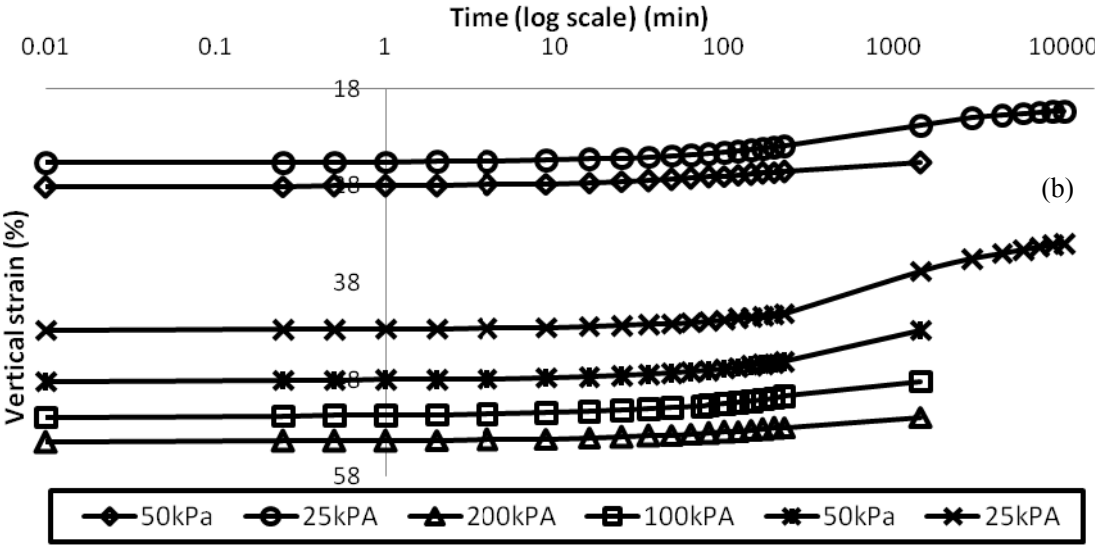

Figure 4.4 Vertical strain against time in log scale for 50% sand mixed with 50% bentonite - (a) loading and (b) unloading

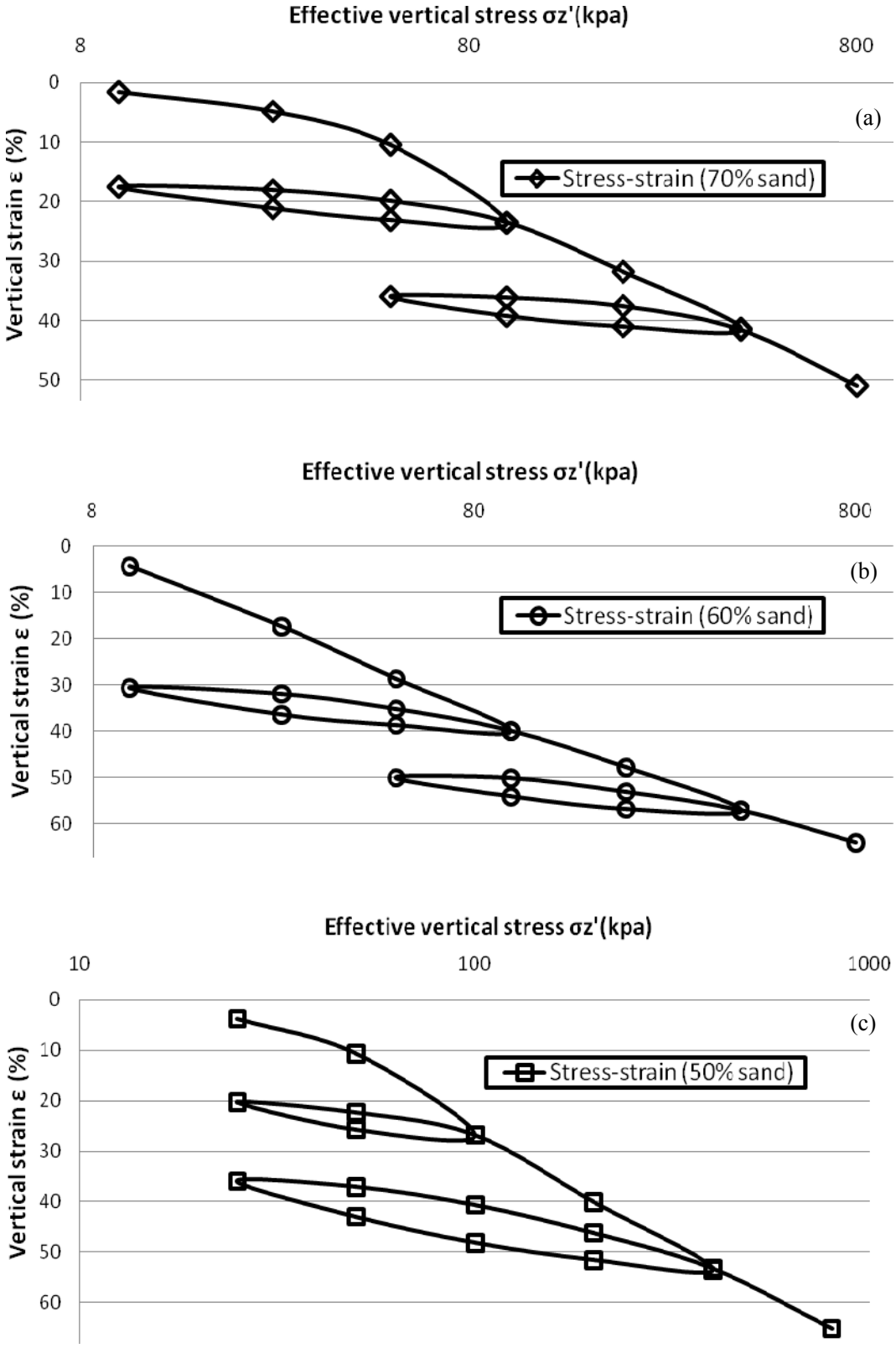

Figure 4.5 Vertical strain against effective vertical stress in log scale - (a) 70% sand content, (b) 60% sand content, and (c) 50% sand content

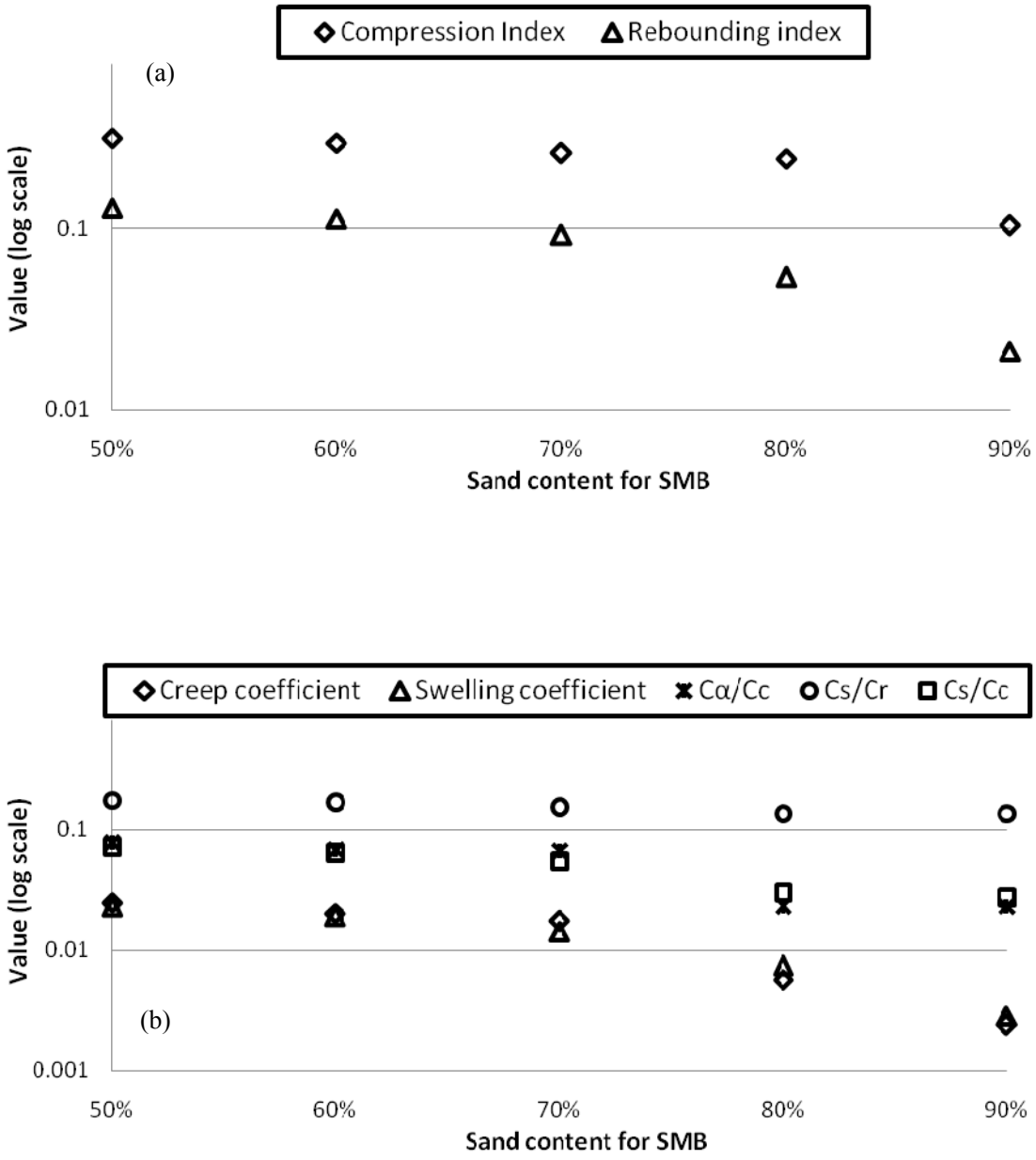

Figure 4.6 Relationships of sand content against relevant indexes/coefficients in log scale - (a) compression index C_c and rebounding index C_r and (b) creep coefficient C_α, swelling coefficient C_s, ratios of C_α/ C_c, C_s/ C_r, and C_s/C_c

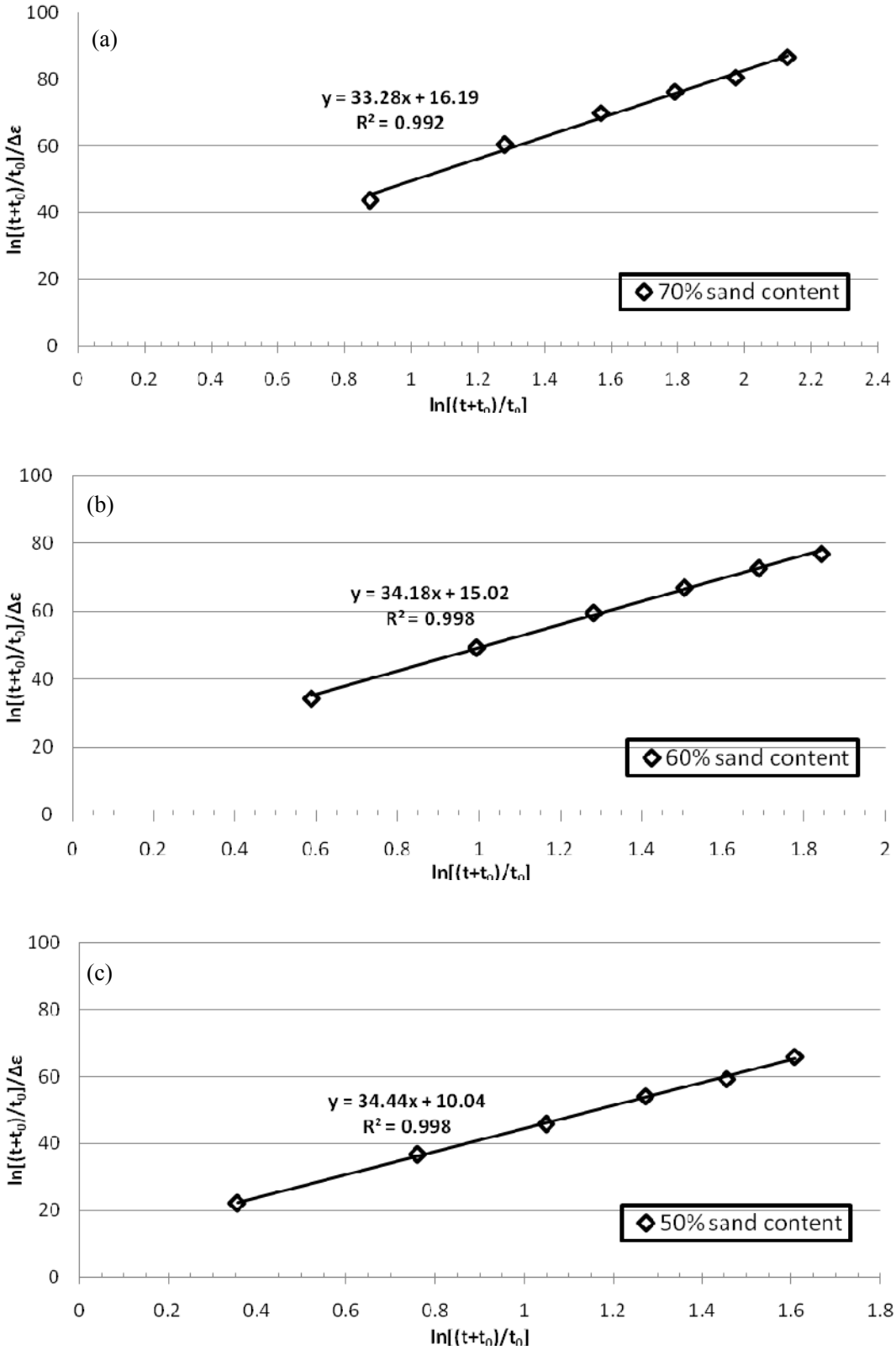

Figure 4.7 Curve fitting by a straight line under 100 kPa normal stress - (a) 70% sand content, (b) 60% sand content, and (c) 50% sand content

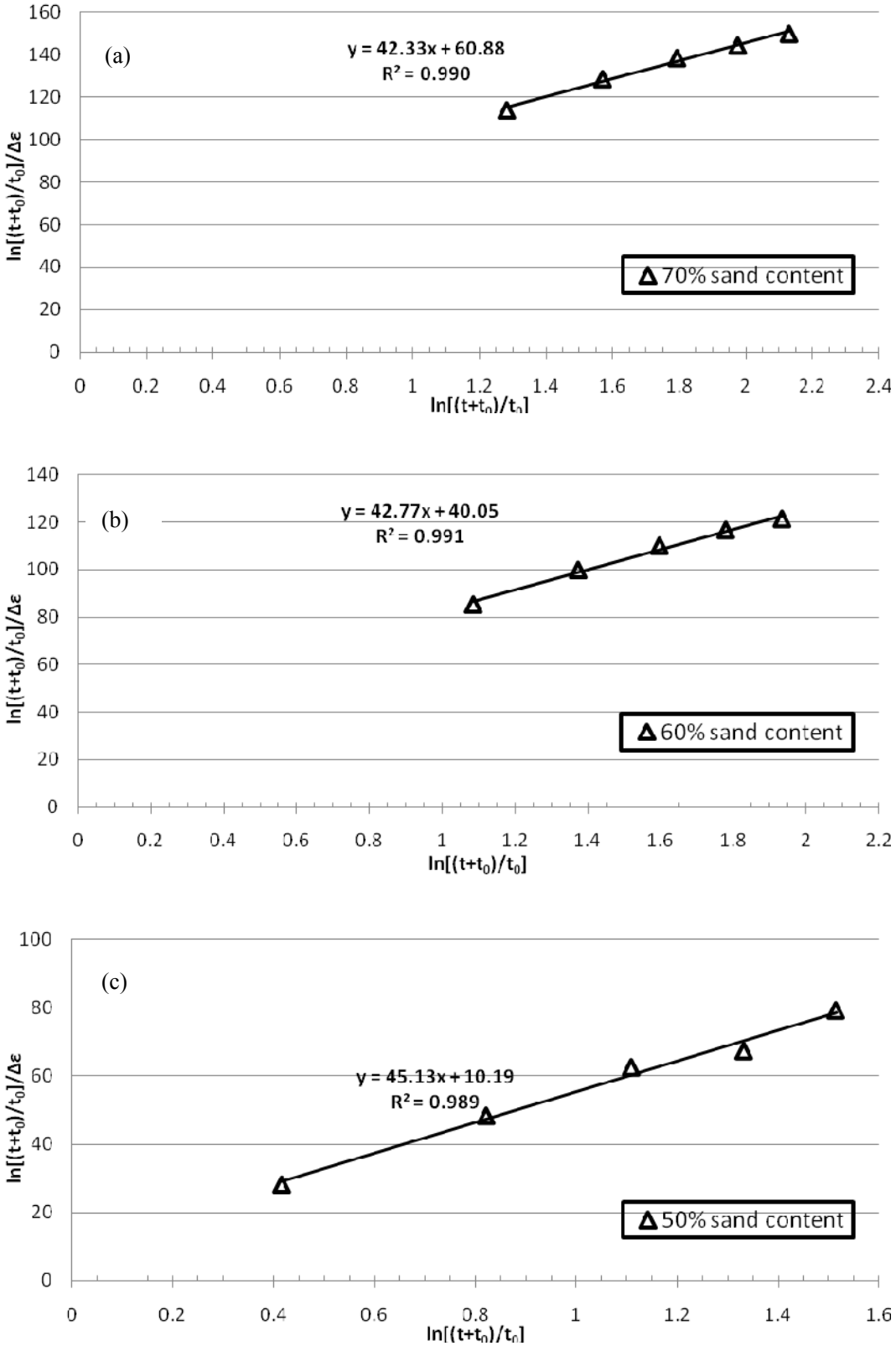

Figure 4.8 Curve fitting by a straight line under 400 kPa normal stress - (a) 70% sand content, (b) 60% sand content, and (c) 50% sand content

Chapter 5

Strain Rate Effects from CRSN Tests on SMB in 1D Straining

5.1 Introduction

In this chapter, the constant rate of strain (CRSN) test is used to examine the strain rate effects of clayey soils. To better understand the time-dependent behavior of the fully saturated Silica Sand Mixed Bentonite (SMB), the influence of sand content on strain rates effects is evaluated under 1D CRSN condition.

To study the strain rate effect and sand content impact on the one-dimensional compressibility, a series of CRSN tests are conducted with step-changed strain rates. All the stress-strain test results of three samples with different sand contents (50%, 60%, and 80%) are presented in this chapter.

The stress-strain behavior of saturated SMB exhibits considerable viscous characteristics. At a given rate in a CRSN test, the higher the strain rate, the higher the effective stress. Test results also show that the stress-strain behavior of saturated SMB can be significantly affected by the sand content. Specimen with higher sand content has less creep ability. The ratios of creep coefficient over compression index, C_α/C_c in CRSN tests are compared with those in MSL oedometer tests. The ratios in CRSN tests vary from 0.14 to 0.21, while these values are in the range of 0.20 to 0.41 in MSL oedometer tests. The influence of sand content on the creep parameter and swelling parameter is also discussed.

5.2 Testing Materials and Program

The constant rate of strain (CRSN) testing system, based on the recommendation of Head (1985), is used in this study (Figure 5.1). The CRSN oedometer test apparatus consists of 100 mm-diameter and 20 mm-thick base plate, which is mounted onto the existing base of a triaxial cell. Since the interpretation of CRSN test results require the excess pore water pressure at the base to be measured, a small hole is made and a porewater pressure transducer is installed. A 63.5 mm-diameter ring with a height of 17 mm confines the soil sample to ensure one-dimensional compression. In order to achieve single drainage condition, contact between the sample ring and the bottom plate is sealed by an o-ring, resulting in single drainage at the top through a coarse porous stone attached to the top cap.

Before the test, the base plate is de-aired and saturated. The sand mixed bentonite sample, after extrusion from the Shelby tube, is trimmed to the required size in the specimen retaining ring. A filter paper is placed at the bottom of the specimen, preventing the entry of soil particles during testing.

After assembling the specimen, the sample retaining ring, side ring, top cap, top coarse porous stone and base plate in the CRSN, the cell is placed on the motorized loading frame. A load cell is fixed in position to the frame and the loading piston is brought in contact with the loading plate (top cap) in order to maintain specimen height. The axial force is measured by means of a load gauge of 3 kN capacity attached to the loading frame. De-aired water is used to fill the cell.

Based on the criterion by Lee *et al.* (1993) for the strain rate selection for the

CRSN tests, the strain rate adopted for the CRSN tests should have an upper bound β value of 0.1, which $\beta = h_o^2 / c_v$ with $\dot{\varepsilon}$, h_o, c_v standing for the strain rate, initial specimen height and coefficient of consolidation, respectively. Premchitt *et al.* (1995) pointed out that high strain rates applied for the CRSN tests would induce too high porewater pressures. Since the strain rate adopted in all CRSN tests varied from 10^{-7}/s to 10^{-4}/s, and the coefficient c_v is found to be less than 20 m^2/yr, the corresponding value of β could be obtained to be 0.003<0.1. For the estimation of the c_v value, a solution $c_v = (\Delta p' / \Delta t) \cdot (H^2 / 2\Delta u)$ is employed in which $\Delta p'$ is the effective vertical stress increment during a time interval, H is the height of the specimen during Δt, and Δu is the excess porewater pressure.

The strain rates for all CRSN tests were applied in a sequence as follows (Table 5-1): $+1\times10^{-5}$ 1/sec, $+1\times10^{-4}$ 1/sec, $+1\times10^{-6}$ 1/sec, $+1\times10^{-7}$ 1/sec, $+1\times10^{-5}$ 1/sec, -1×10^{-5} 1/sec (unloading), $+1\times10^{-5}$ 1/sec (reloading), $+1\times10^{-4}$ 1/sec, $+1\times10^{-6}$ 1/sec, $+1\times10^{-7}$ 1/sec, $+1\times10^{-5}$ 1/sec, -1×10^{-4} 1/sec (unloading), $+1\times10^{-4}$ 1/sec (reloading). The basic properties of all samples have been determined in Chapter 3. All tests were done under the laboratory temperature of 20±1°C in order to minimize the temperature effect.

5.3 Test Results and Interpretation

Results of the vertical strain versus effective vertical stress (*i.e.* ε_z–$log\sigma'_z$) under CRSN condition are shown in Figures 5.2-5.4. In the curves an abrupt reduction of

stresses denotes the stress relaxation process. A hyperbolic distribution is utilized here for porewater pressure estimation (Cheng and Yin, 2005). That is, the effective vertical stress for a CRSN test is calculated by the total vertical stress minus two thirds of the porewater pressure measured at the base of the specimen in the test.

From Figures 5.2-5.4, it is clear that, while changing the applied strain rate the compression curve jumps from one constant rate of strain curve to another, which is consistent with the finding of Leroueil *et al.* (1985). For a specimen with given percentage of silica sand, the stress always increases with the increase of strain. The stress-rate dependent curves corresponding to each strain rate can be notified by interpolating and joining the measured portions of the respective strain rate curves, as shown by dotted lines. These curves are very similar in shape. They prove that the ε_z versus $log\sigma'_z$ relationship for the silica sand mixed bentonite is a function of the strain rate. At a given strain rate, there is a unique relationship between the strain and effective vertical stresses measured, which also agrees with the findings of Leroueil *et al.* (1985).

The test results illustrate that at a given strain, the higher the strain rate, the higher the effective stress, which is consistent with the findings of Crawford (1965), Jarret (1967), Smith and Wahls (1969), Vaid *et al.* (1979) and Leroueil *et al.* (1983, 1985). For a given strain, samples with higher sand content will have higher effective stress. For example, at a strain of 16%, the vertical effective stress is 61.6 kPa for the specimen with 50% sand content and 75.2 kPa for the specimen with 80% sand content.

5.4 CRSN Test Results on C_c, C_r and C_α

The compression index C_c and rebounding (unloading/reloading) index C_r for different strain rates can be determined using the test data in Figures 5.2~5.4. It is found that the compression curves for each strain rate are nearly parallel, which indicates that C_c for each strain rate is almost the same. The compression index C_c and rebounding index C_r with respect to different sand content are summarized in Table 5-2. Generally, C_c and C_r decrease with increase of sand contents. The data also indicate that C_c is obviously larger than C_r for all CRSN tests.

It is observed that the compression index C_c decreases with the increase of sand contents: C_c=0.186 on average for specimen with 80% sand content; C_c=0.198 on average for specimen with 60% sand content and C_c=0.218 on average for specimen with 50% sand content. With sand content increased from 50% to 80%, C_c slightly decreases by 0.032. There is no sudden decrease in the value C_c.

The rebounding index C_r increases with the increase of sand contents: C_r=0.0219 on average for specimen with 50% sand content; C_r=0.0233 on average for specimen with 60% sand content; and C_r=0.0275 on average for specimen with 80% sand content. There is no sudden increase in the value of C_r. With the sand content increased from 50% to 80%, C_r slightly increases by 0.0056.

For the comparison of coefficients in CRSN and in MSL, similar creep coefficient and the ratio of C_α/C_c are determined. Mesri and Choi (1979) suggested that the relationship between $\sigma_p^{'}$ and strain rate in strain-controlled consolidation

tests is analogous to the creep incremental load tests. Mesri and Castro (1987) proposed that the strain rate effect on the pre-consolidation pressure can be examined by the following equation using C_α/C_c:

$$(\sigma_v')_i/(\sigma_v')_j = [(\dot{\varepsilon}_a)_i/(\dot{\varepsilon}_a)_j]^{C_\alpha/C_c} \tag{5-1}$$

To determine C_α/C_c, equation (5-1) can be rewritten as

$$\frac{C_\alpha}{C_c} = \frac{\ln(\sigma_v')_i - \ln(\sigma_v')_j}{\ln(\dot{\varepsilon}_a)_i - \ln(\dot{\varepsilon}_a)_j} \tag{5-2}$$

The average values of C_α/C_c for different sand content at a strain rate of 10^{-7} /s are calculated using equation (5-2). These values are compared with the ratios in MSL_{24} tests. Relevant coefficients and indexes are all summarized in Table 5-2. For all SMB specimens, the calculated and measured data show a good agreement. However results from CRSN tests are smaller than those obtained from the MSL tests. It is assumed that, for any natural soil, the ratio of C_α/C_c is constant for any time, under given effective stress and void ratio during creep as in Mesri and Godlewski (1977). Some factors such as normal pressure and the sand content will affect the ratio. SMB soils with lower sand content always have higher C_α/C_c ratios. Ratios of C_α/C_c can be verified by Mesri and Godlewski's work, that is, C_α/C_c is equal to 0.04±0.01 for inorganic clays and 0.05±0.01 for organic clays.

5.5 CRSN Test Results on Pre-consolidation Pressure

The strain rate dependency can be examined by the pre-consolidation pressure σ_p' (or "apparent" pre-consolidation pressure) as well. Different strain rates induce

different "apparent" pre-consolidation pressures. At each strain rate, it is noted that there is an abrupt change in the compressibility near the pre-consolidation pressure. This behavior well defines the relationship between ε_z and $\log\sigma_z^{'}$. The stress-strain curves after the "apparent" pre-consolidation pressure are approximately parallel.

The "apparent" pre-consolidation pressures $\sigma_p^{'}$ corresponding to each strain rate from the CRSN tests on SMB specimen with different sand contents are shown in Table 5-3, The relationship between the "apparent" $\sigma_p^{'}$ and strain rate applied is plotted and represented by a fitting line in Figure 5.5. It shows that when a higher strain rate is applied, the "apparent" $\sigma_p^{'}$ is higher. With a higher sand content in SMB, the increase rate of the "apparent" $\sigma_p^{'}$ due to strain rate increase is higher. Even for specimens with the same sand content, the difference between the pre-consolidation pressures induced by two different strain rates appears to apply to the entire stress-strain curve up to 20% strain level. The change in the pre-consolidation pressure due to the change of strain rate is a good indicator of the strain rate effect.

It has been reported that the stress-strain curves from the constant rate of strain tests are generally different from those generated in the MSL_{EOP}. Leroueli (1996) stated that the pre-consolidation pressure produced by the CRSN tests ($\sigma_{pCRS}^{'}$) would be 25% higher than that obtained from the conventional 24-hr oedometer tests MSL_{24} ($\sigma_{pOED}^{'}$). Previous researches on the CRSN tests and MSL_{24} tests for other natural clay gave the ratio $\sigma_{pCRS}^{'}/\sigma_{pOED}^{'}$ generally in the range of 1.3 to 1.5.

In this chapter, the ratio $\sigma'_{pCRS} / \sigma'_{pOED}$ is calculated for the strain rate ranged from 1.9×10^{-3} 1/s to 1.9×10^{-6} 1/s in the CRSN tests using oedometer results at t_{EOP}. The average $\sigma'_{pCRS} / \sigma'_{pOED}$ associated with the strain rate is listed in Table 5-4. This ratio is obviously dependent on the sand content of SMB. For a given sand content, the ratio is larger at higher strain rate. It should be mentioned that the pre-consolidation pressure for the step-changed consolidation tests are estimated by interpolation or extrapolation of the consolidation curves.

5.6 Discussion on C_s/C_r Ratio

In both CRSN and MSL tests on soils, a loop in an unloading/reloading cycle is observed, which has been convinced relevant to the swelling property. Opposite to the definition of consolidation, swelling stands for the reverse behavior (to move upward). From oedometer results in Chapter 4, the swell-time relationship demonstrates that swelling continues to occur for a long time after the primary swelling (rebounding) stage, coming to a "second swelling". The "second swelling" is true swelling under given effective stress, reverse to creep. The swelling rate is only dependent of time but independent of stress condition.

For saturated expansive soils, swelling (secondary swelling) can be observed in unloading stage. With the effective stress decrease, the strain decreases continuously but more and more slowly (Figure 5.2). In CRSN tests, SMB specimens with lower sand content exhibit greater swelling potential and this behavior becomes less

obvious when sand content exceeds 60 percents (Figure 5.4). To examine the swelling property both in CRSN and in MSL, the coefficient of swelling, C_s should be obtained first. In Figure 5.2 during unloading, an analogical stress point σ'_{sCRS} to "pre-consolidation" can be found. A similar equation is used to determine the C_s and C_s/C_r.

$$(\sigma'_s)_i/(\sigma'_s)_j = [(\dot{\varepsilon}_s)_i/(\dot{\varepsilon}_s)_j]^{C_s/C_r} \tag{5-3}$$

where $(\dot{\varepsilon}_s)_i$ is strain rate.

The C_s/C_r ratio is then computed for each specimen and listed in Table 5-2. The results are verified with the values from oedometer tests. The C_s/C_r ratio from CRSN varies from 0.11 to 0.154, which is quite close to that from MSL. However in Table 5-2 all the values from CRSN are lower than those from MSL. From the table, obvious creep and swelling are obtained for SMBs. Specimens with lower sand content have higher creep and swelling properties. The C_α/C_c ratio decreases from 0.0596 for a specimen with 50% sand content to 0.0121 for a specimen with 80% sand content. The C_s/C_r ratio changes from 0.154 for a specimen with 50% sand content to 0.110 for a specimen with 80% sand content. The results show that swelling occurs even in saturated SMBs, although sand content plays an important role.

5.7 Summary and Conclusions

The stress-strain behavior of silica sand mixed bentonite under CRSN

condition was studied in the chapter. The influences of sand content as well as strain rates were examined. The following conclusions could be drawn:

a. In the CRSN tests with step-changed strain rate on fully saturated SMB (Sand Mixed Bentonite) samples, a unique stress-strain-strain rate relationship is obtained under one-dimensional compression. For a given strain rate, there is a unique relationship between the measured strain and effective vertical stresses.

b. Strain rate effects can be clearly observed. The "pre-consolidation pressure", is higher under higher strain rate applied. On average, for the SMB specimen with constant sand content, σ'_p under strain rate 1×10^{-7} s^{-1} is only 42% of the σ'_p under strain rate 1×10^{-4} s^{-1}.

c. The SMB specimens exhibit viscous behaviors, among which the sand content has an essential impact. For specimens with sand content in the range of 50% to 80% and loaded at a given strain rate, the higher the sand content, the higher the effective vertical stress at a given strain. For example, at a strain of 16% (strain rate=10^{-4} s^{-1}), the vertical effective stresses are 61.6 kPa and 75.2 kPa for SMB with 50% sand content and for SMB with 80% sand content, respectively.

d. C_c and C_α/C_c decrease with the increase of sand contents. For sand content changed from 50% to 80%, C_c slightly decreases by 0.032. For the rebounding index C_r, the opposite trend exists with a small increment of 0.0056. Values of C_s/C_r from CRSN tests change from 0.11 to 0.154 with the reduction of sand content, which is quite close to those from MSL.

e. For a SMB sample with higher sand content, the increase rate of the "apparent"

σ'_p versus strain rate increase is also higher. Compared with σ'_{pOED} in 24 h standard MSL tests, higher sand content and higher strain rate will result in higher $\sigma'_{pCRS} / \sigma'_{pOED}$. The $\sigma'_{pCRS} / \sigma'_{pOED}$ ratio lies in a narrow range between 0.87 and 1.67.

Table 5-1 CRSN loading schedule

No.	Strain Rate (1/sec)	Strain (%)	Settlement (mm)	No.	Strain Rate (1/sec)	Strain (%)	Settlement (mm)
1	1×10^{-5}	5	0.95	8	1×10^{-4}	11	1.90
2	1×10^{-4}	7	1.33	9	1×10^{-6}	12	2.09
3	1×10^{-6}	8	1.52	10	1×10^{-7}	12.5	2.28
4	1×10^{-7}	8.4	1.596	11	1×10^{-5}	13	2.47
5	1×10^{-5}	9	1.71	12	-1×10^{-4}	11.5	Unloading
6	-1×10^{-5}	7.5	Unloading	13	1×10^{-4}	16	3.04
7	1×10^{-5}	10	1.9	Total strain = 16%			

Table 5-2 Summary of compression index C_c and rebounding index C_r for CRSN tests

Sand Content	**50%**	**60%**	**80%**
Average Compression Index C_c	0.218	0.198	0.186
Average Rebounding Index C_r	0.0519	0.0533	0.0575
C_α (Creep Coefficient) / C_c (CRSN)	0.0596	0.0472	0.0121
C_α (Creep Coefficient) / C_c (MSL)	0.0606	0.0476	0.0130
C_s (Swelling Coefficient) / C_r (CRSN)	0.154	0.149	0.110
C_s (Swelling Coefficient) / C_r (MSL)	0.176	0.169	0.136

Table 5-3 "Apparent" pre-consolidation pressures under different strain rates in the CRSN tests

Strain Rate	**50% sand content**	**60% sand content**	**80% sand content**
1×10^{-4} 1/sec	24 kPa	30 kPa	45 kPa
1×10^{-5} 1/sec	21 kPa	26 kPa	33 kPa
1×10^{-6} 1/sec	18 kPa	24 kPa	23 kPa
1×10^{-7} 1/sec	16 kPa	21 kPa	14 kPa

Table 5-4 Comparison of pre-consolidation pressures by CRSN and MSL tests ($\sigma'_{pCRS}/\sigma'_{pOED}$)

Strain Rate	**50% Sand content**	**60% Sand content**	**80% Sand content**
1×10^{-4} 1/sec	1.54	1.67	1.62
1×10^{-5} 1/sec	1.32	1.42	1.48
1×10^{-6} 1/sec	1.18	1.21	1.25
1×10^{-7} 1/sec	0.87	0.95	0.92

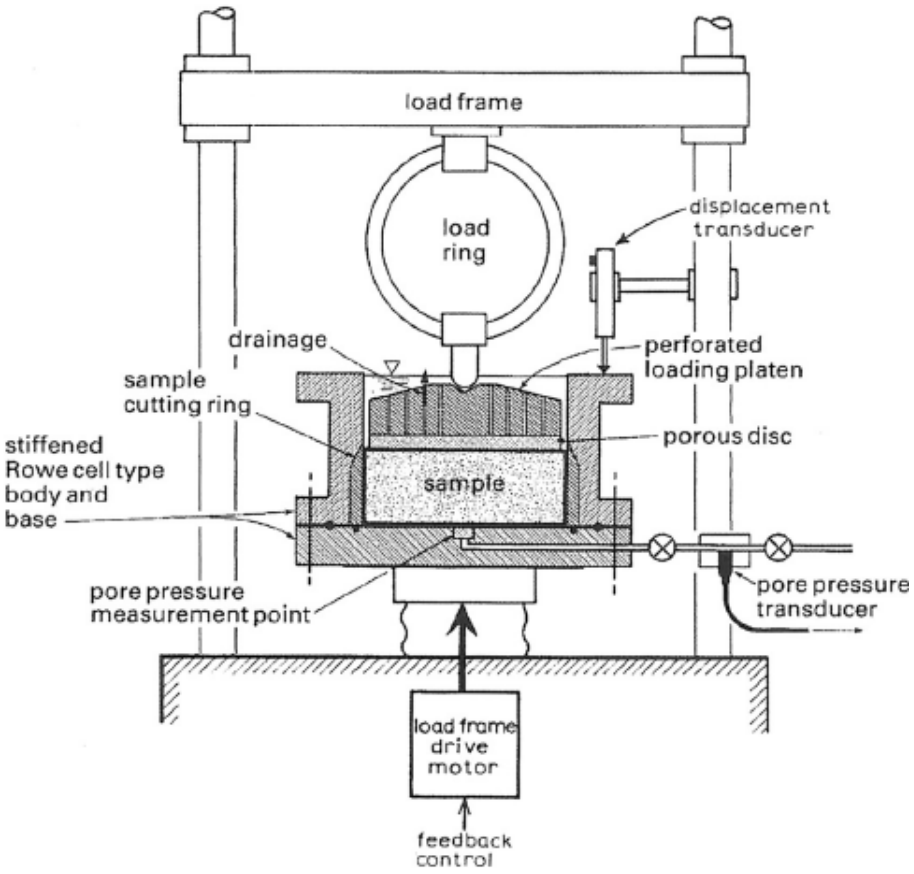

Figure 5.1 Schematic view of the CRSN testing system (Head, 1985)

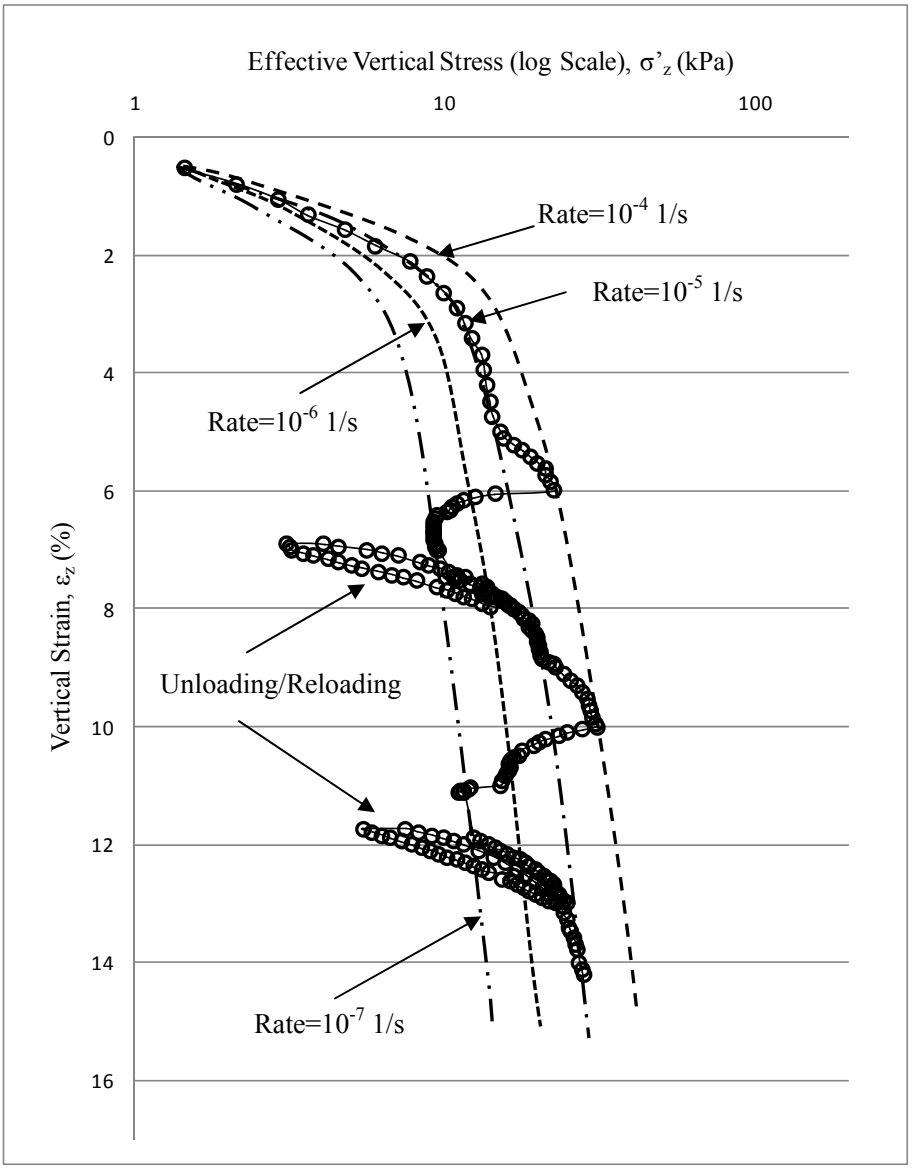

Figure 5.2 Relationship between vertical strain and vertical effective stress for SMB with 50% sand content

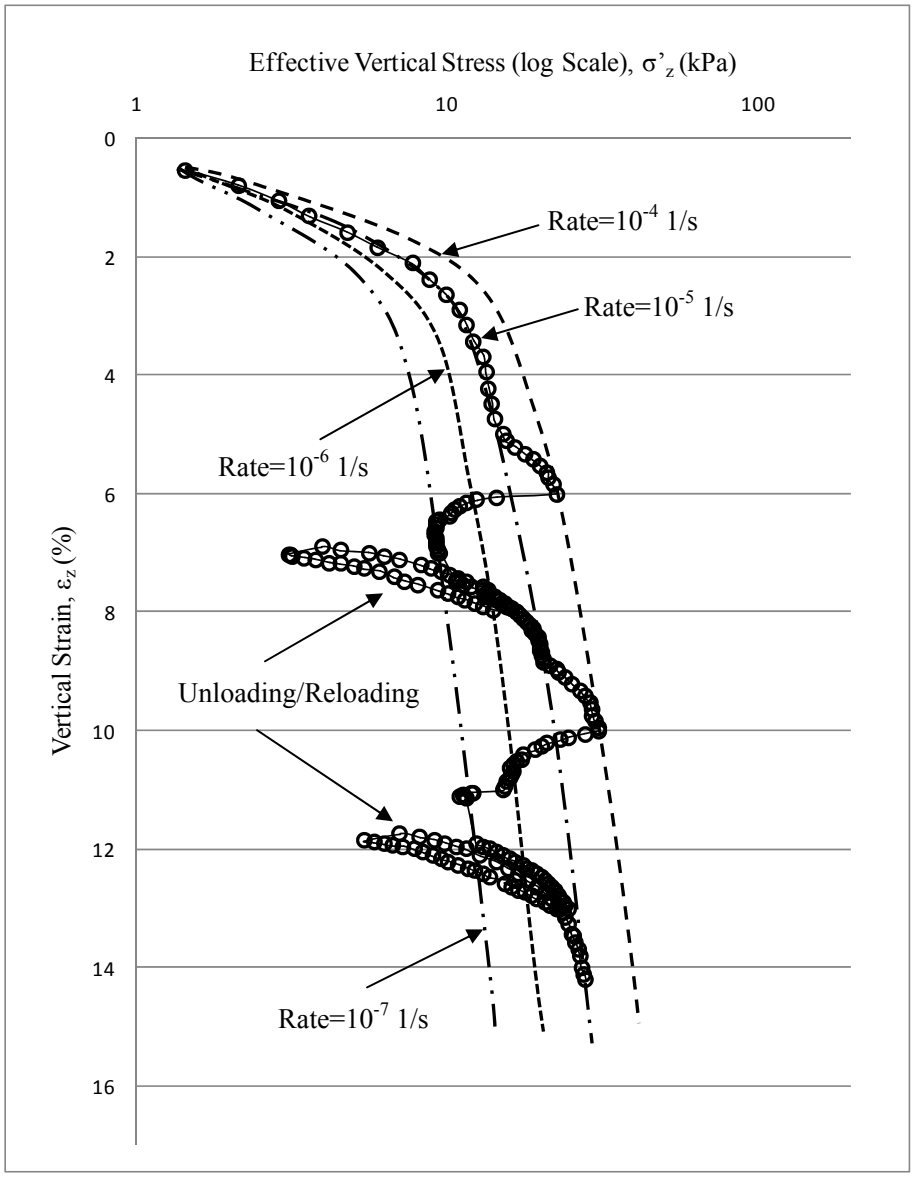

Figure 5.3 Relationship between vertical strain and vertical effective stress for SMB with 60% sand content

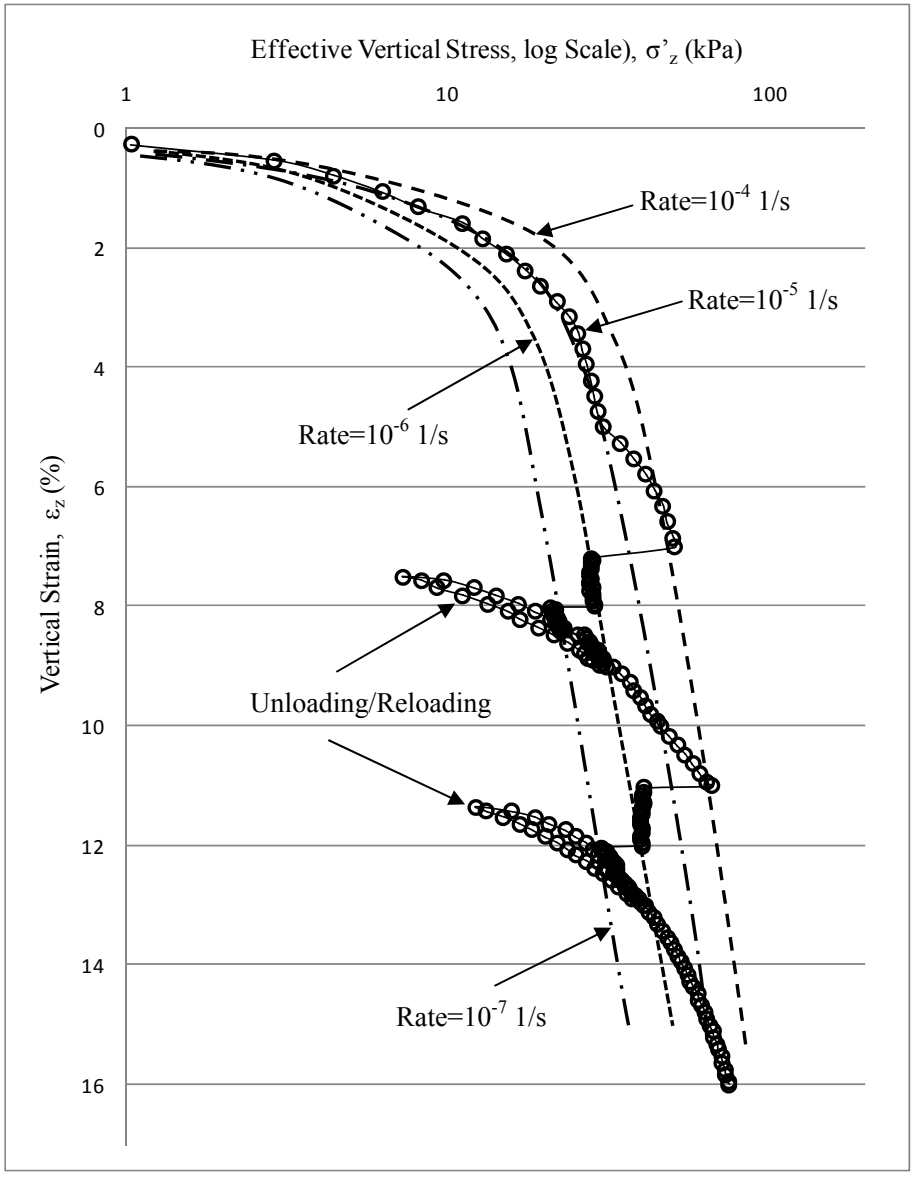

Figure 5.4 Relationship between vertical strain and vertical effective stress for SMB with 70% sand content

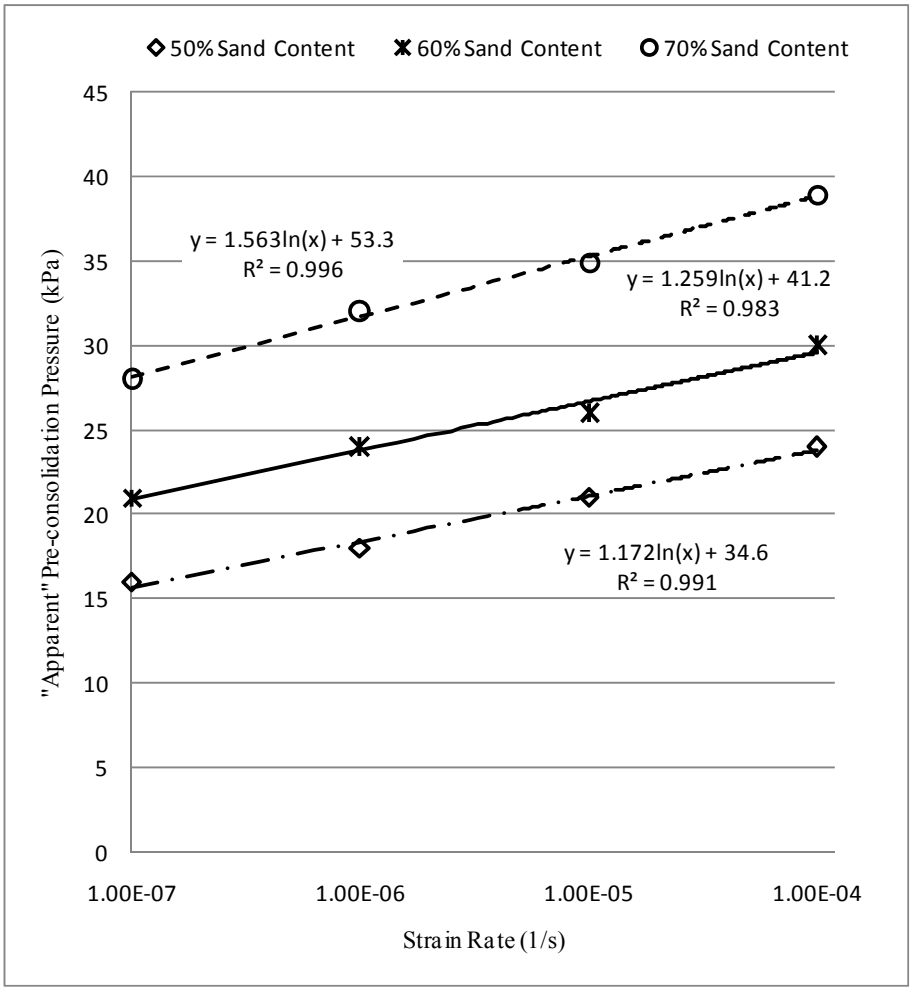

Figure 5.5 Relationship between "apparent" pre-consolidation pressure and strain rate

Chapter 6

Stress Relaxation Behaviors from Relaxation Tests on Two Types of Clayey Soils in 1D Straining

6.1 Introduction

Stress relaxation, one of the significant time-dependent phenomena in clayey soils, has been observed in excavations and other constructions, such as the short term change in lateral earth pressure after installation of supporting system in excavations. In this chapter, Hong Kong marine deposits (HKMD) and a sand mixed bentonite (SMB) soil are investigated using relaxation tests. Relaxations are performed in both loading stage and unloading stage. The time-dependent relaxation behavior of clayey soils is examined. The relaxation tests were carried out in 1D straining condition.

6.2 Testing Materials and Program

The constant rate of strain (CRSN) testing system proposed by Head (1985) is used to perform CRSN tests with different strain rate. A relaxation test is actually a special CRSN test with zero strain rate ($\dot{\varepsilon}_z = 0$). A 63.5 mm diameter ring with a height of 17 mm confines the soil specimen to ensure one-dimensional compression.

The effect of relaxation on the specimens in creep region is demonstrated by switching off the CRS testing system after compression with a strain rate of $+10^{-5}$ 1/s. As in the MSL tests, the specimens were under a confined strain condition. The

change in stress is the main concern instead of compression in creep region. The effect of relaxation on the specimens in swelling region is observed by switching off the CRS testing system after unloading with a strain rate of -10^{-5} 1/s. Similarly at a given height, the effective stress is observed to increase with time.

6.3 Test Results and Discussions

Test results on HKMD and SMB soils under relaxation in both creep region and swelling region are presented in Figures 6.1~6.3. In a relaxation test in the creep region, as shown in Figures 6.1(a)~6.3(a), the height of the specimen is kept constant, and the effective stress is observed to decrease with time. All the three specimens are first loaded at the strain rate 10^{-5} 1/s up to 63.92 kPa for MD 3a, 98.39 kPa for MD 19 and 16.60 kPa for SMB, respectively, and then perform relaxation. The rate of reduction in effective stress is not constant throughout the process. A sharp decrease in effective stress is observed within about first 200 minutes for MD 3a and SMB; 500 minutes for MD 19 respectively after termination of the straining process. The change in effective stress is less significant since then, which indicates that the deformation of soil skeleton is finite.

In a relaxation test in the swelling region as shown in Figures 6.1(b)~6.3(b), all the three specimens are unloaded with constant strain rate -10^{-5} 1/s down to stress levels 21.29 kPa (for MD 3a), 48.27 kPa (for MD 19) and 14.90 kPa (for SMB), then relaxations start. In this way, the so-called “swelling pressure” can be obtained.

The recorded applied stress is the swelling pressure inside the specimen. Swelling pressure is defined as the pressure required to maintain the system at the required strain when it is allowable to absorb water. The increase is less noticeable compared to that under relaxation in creep region.

6.4 Summary and Conclusions

In this chapter, three types of soils (HKMDs and SMB) are tested to examine the time-dependent behavior in relaxation condition. Both the stress relaxation in creep regions and the stress increase in swelling regions are investigated. Conclusions could be drawn as follows:

a. Stress relaxations occur in both creep and swelling conditions. The "swelling pressure" observed in swelling relaxation test verifies that swelling occurs in saturated condition, especially for expansive soils.
b. Relaxation tests represent an important alternative for studying the theological properties of a soil. The HKMDs and SMB exhibit considerable viscosity. Relatively the SMB is more viscous than the HKMD in terms of creep and swelling abilities in relaxation tests.
c. Both in creep region and in swelling region, stress only changes dramatically within the first several hundred minutes after the termination of the straining process, which indicates that the deformation of soil skeleton is not infinite.

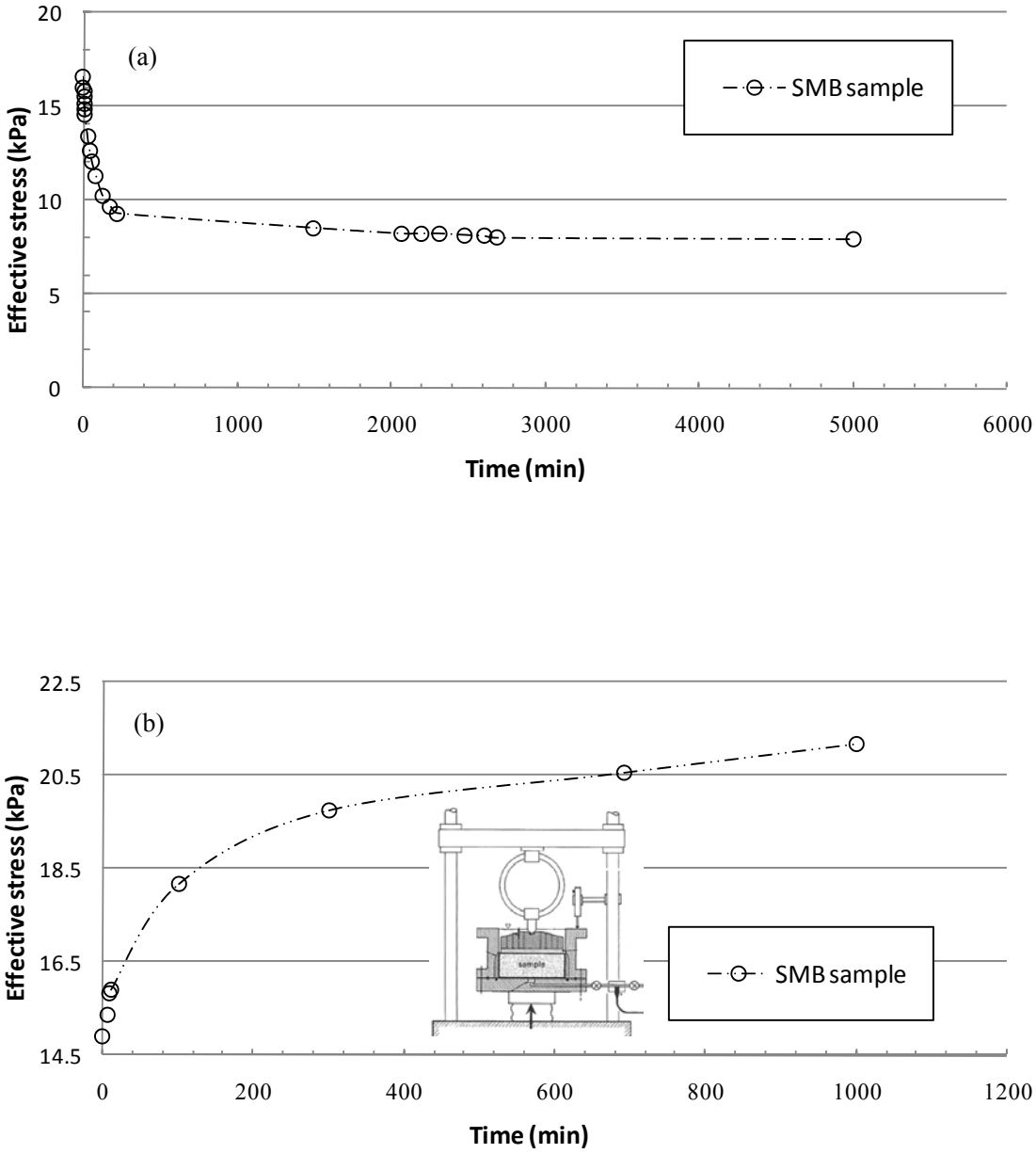

Figure 6.1 Relaxation results of SMB - (a) in creep region and (b) in swelling region

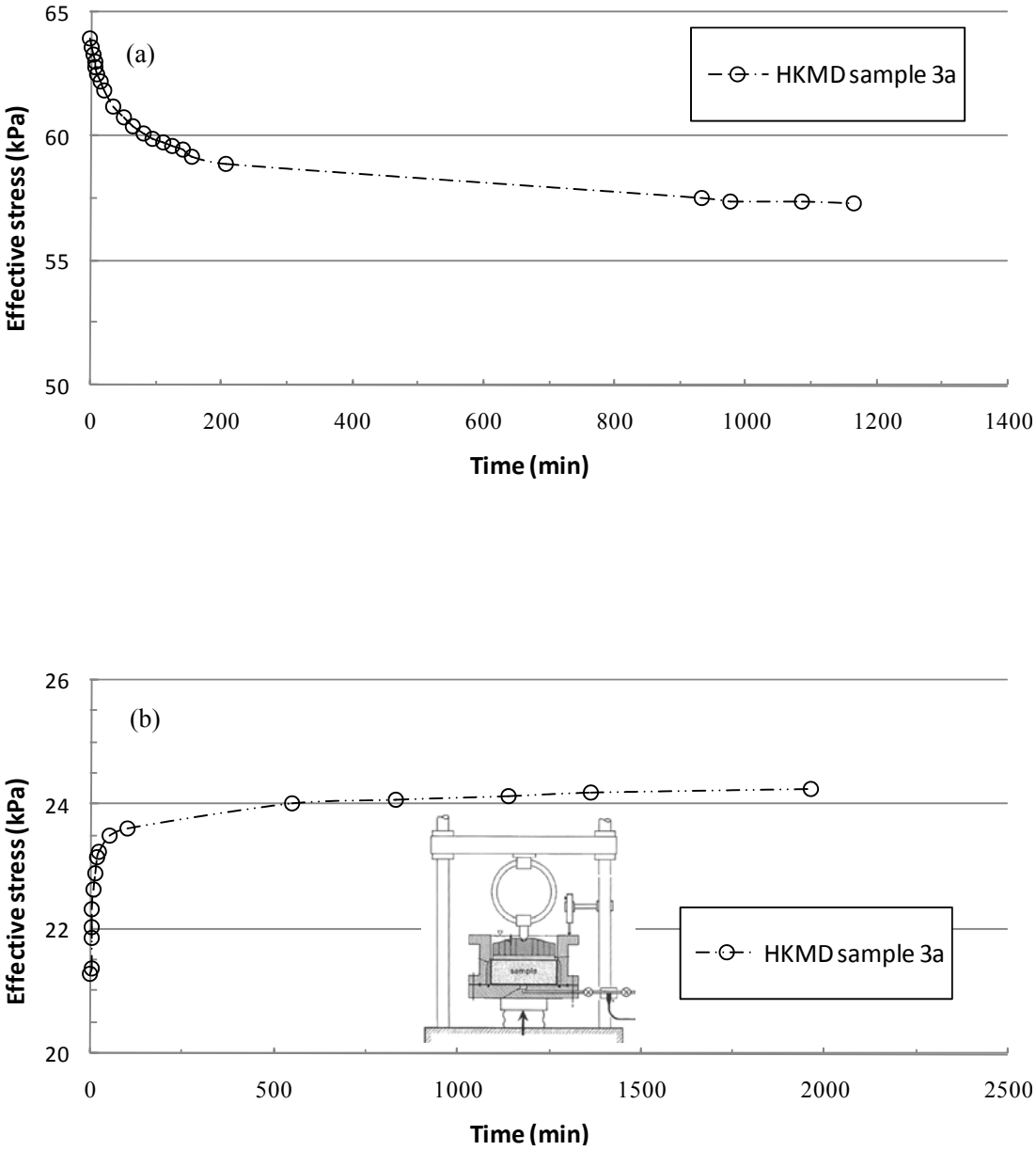

Figure 6.2 Relaxation results of MD3a - (a) in creep region and (b) in swelling region

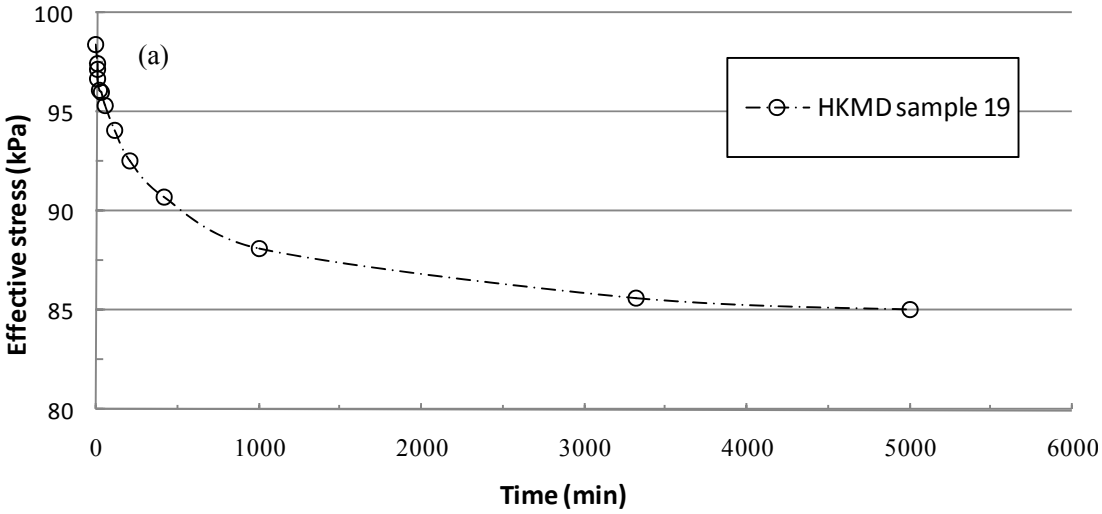

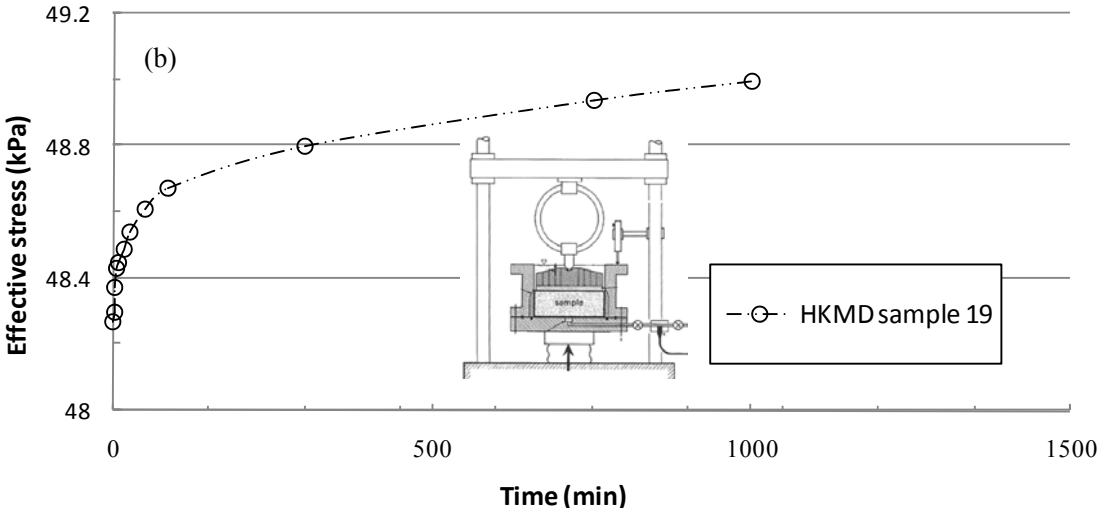

Figure 6.3 Relaxation results of MD19 - (a) in creep region and (b) in swelling region

Chapter 7

Strain Rate Effects from CRSN Tests on SMB in Triaxial Condition

7.1 Introduction

In Chapter 5, it is shown that the stress-strain behavior of the silica sand mixed bentonite can be significantly affected by the strain rates. To better understand the behavior of strain rate effect on SMB soils, isotropic consolidation and undrained triaxial CRSN tests on the SMB are carried out in this chapter. Samples with two sand proportions (60% and 70%) are tested under four different effective confining pressures. Curves of deviator stress versus axial strain, excess porewater pressure versus axial strain, and the total stress path (TSP) and effective stress path (ESP) are presented. Viscosities of soils both in isotropic condition and in CRSN condition are discussed.

7.2 Testing Materials and Program

Two silica sand mixed bentonite (SMB) samples are employed to conduct isotropic consolidation tests and triaxial CRSN tests. The mass fractions of silica sand in the mixture are 60% and 70%, respectively. The basic properties (plastic limit, liquid limit, plastic index and specific gravity) are presented in Section 3.5.

a) Isotropic Consolidation test

When the pre-consolidation is completed, specimens will be obtained by pushing vertically thin-wall PVC tubes of internal diameter of 38 mm into the tank.

Specimens of 38 mm in diameter and 76 mm in height are used. The isotropic consolidation tests are carried out in the Wykeham Farrance triaxial apparatus (Figure 7.1) under a sequence of all-round pressure. The test procedure does not have axial loading stage and only consists of saturation stage and consolidation stage. To ensure the saturation of the specimen, a back pressure of 100 kPa was imposed on each specimen and the B-value was greater than 0.98 to ensure fully saturation.

After saturation, the specimen was consolidated (creep for 3 days to 7 days), unloaded (swell for 3 days to 7 days) and reloaded (creep for 3 days to 7 days). The load was doubled for each incremental loading (loading and reloading). The load was halved for each decremental loading (unloading). The loading schedule is summarized in Table 7-1. The loading was applied by the difference between cell pressure and back pressure. All the back pressures were 100 kPa in each stage.

b) Undrained Triaxial CRSN test

According to conventional triaxial testing procedures, each sample was firstly saturated, secondly consolidated under isotropic confining pressure, and finally compressed in the Wykeham Farrance triaxial apparatus. Similar to isotropic consolidation test, specimens of 38 mm×76 mm are used and a back pressure of 100 kPa is applied. In the consolidation stage, net confining pressures (50 kPa, 100 kPa, 200 kPa, respectively) are applied to drain out the water. All the tests were carried out under the laboratory temperature of 20±1℃.

Once the consolidation degree exceeds 98%, undrained loading is applied. The axial load is gradually increased while the total confining pressure remains constant. The loading strain rates are in the following sequence: $+1\times10^{-5}$ 1/sec, $+1\times10^{-4}$ 1/sec, $+1\times10^{-6}$ 1/sec, $+1\times10^{-7}$ 1/sec, $+1\times10^{-5}$ 1/sec, -1×10^{-5} 1/sec (unloading), $+1\times10^{-5}$ 1/sec (reloading), $+1\times10^{-4}$ 1/sec, $+1\times10^{-6}$ 1/sec, $+1\times10^{-7}$ 1/sec, $+1\times10^{-5}$ 1/sec, -1×10^{-5} 1/sec (unloading), $+1\times10^{-5}$ 1/sec (reloading). During testing, the axial strain, axial load and porewater pressure are recorded manually.

Considering that the porewater pressure is measured at the base of the specimen in this study, there must be more or less a porewater pressure lag between the end and middle portions of the testing specimen. This is inevitable, especially for a rapid undrained shearing. To minimize this pore pressure lag, shorter specimens and side filter paper drains used in Zhu and Yin (2000) are adopted. The vertical side drain strips are placed beforehand and the effects of side drains had been corrected by using the method suggested by Head (1985).

7.3 Results and Discussions of Isotropic Consolidation Tests

Relationships of volume change against effective pressure (in log scale) are presented in: Figure 7.2 for SMB with 60% sand content (SMB60); Figure 7.3 for SMB with 70% sand content (SMB70). Similar to the results from oedometer tests, the volumetric strain increment enlarges with higher effective confining pressure. It is seen that the creep behavior is more obvious than the swelling behavior in

isotropic consolidation test, and both of them have a same trend to be horizontal line finally.

For the stress-strain behaviors in isotropic consolidation, a logarithmic function with the rebounding index C_r (κ/V) is commonly used in the unloading/reloading loop to fit stress-strain data. Parameter C_r (κ/V) is related to compression in the over-consolidated stage. When loading exceeds the pre-consolidation pressure (along the elastic line), deformation will be along the normal consolidation line with the slope C_c (the compression index). Similarly, by straight line fitting, other coefficients such as C_α (creep coefficient) and C_s (swelling coefficient) can be determined.

It should be noted that the volumetric strain rather than void ratio is used in present stress-strain relationships. The compression index and the rebounding index in isotropic consolidation are defined by $C_{c\varepsilon}$ and $C_{r\varepsilon}$. For the specimen with 70% sand content, $C_{c\varepsilon}$=0.29 and $C_{r\varepsilon}$=0.10.

7.4 Results and Discussions of Undrained Triaxial CRSN Tests

Results of six consolidated undrained triaxial CRSN tests with stepped changed strain rate are presented in Figures 7.4~7.9. For SMB60, Figures 7.4(a), 7.5(a) and 7.6(a) show curves of deviator stress versus axial strain under different confining pressures; while Figures 7.4(b), 7.5(b) and 7.6(b) illustrate the corresponding curves of excess pore water pressure versus axial strain. It is seen that both the deviator

stress and excess porewater pressure are affected by the axial strain rate. Similar to the curves in CRSN oedometer tests, when the strain rate is changed, the compression curve jumped from one constant rate of strain curve to another. The larger the strain rate, the higher the deviator stress. This effect is also found on the curve of excess pore water pressure versus axial strain. However, the strain rate influence on deviator stress is more significant than that on excess porewater pressure. The strain rate dependency is thus obvious and it has been anlyzed by many researchers (Vaid and Campanella, 1977; Graham *et al.*, 1983a; Lo Presti *et al.*, 1996).

The dotted stress-strain curves from triaxial CRSN tests corresponding to different strain rates are obtained by interpolating between the measured portions of the curves. These curves show clearly the characteristics of strain softening, that is, the deviator stress increases with the axial strain up to a peak and then decreases gradually. This phenomenon has been observed and examined by Graham *et al.* (1983a) in isotropic CU tests on undisturbed specimens; and Zhu (2000) on K_o-consolidated remoulded HKMD.

The total stress path (TSP) and effective stress path (ESP) for different confining pressure are illustrated in Figure 7.4(c), 7.5(c) and 7.6(c) for SMB60. In a compression tests, the specimen is loaded/unloaded by increasing/decreasing the axial stress while the radial stress is kept constant. The slope of total stress path is therefore equal to 3 all the time. The excess porewater pressure u recorded in triaxial CRSN tests is positive and generally less affected by the strain rate. The positive u

due to loading/unloading in compression is the difference between the total mean *p* and effective mean *p'* (horizontal distance between TSP and ESP).

Relationships of deviator stress against axial strain are demonstrated in Figures 7.7(a), 7.8(a) and 7.9(a) for SMB specimens with 70% sand content (SMB70) under different confining pressure. Relationships of corresponding excess pore water pressure against axial strain are also presented in Figures 7.7(b), 7.8(b) and 7.9(b). For SMB specimens with the same sand content, the deviator stress and excess porewater pressure are higher at a certain axial strain when the confining pressure increases. The deviator stress of SMB70 is also higher than that of SMB60 at a given axial strain and given confining pressure, which indicates the impact of sand content on the stress-strain behaviors.

Zhu (2000) suggested using the following equation (7-1) to consider the strain rate and OCR effects:

$$\rho_q = \Delta(q_f / \sigma_o^{'}) / \Delta \log \dot{\varepsilon}_a \qquad (7\text{-}1)$$

where q_f is the peak deviator stress; $\sigma_o^{'}$ is the effective confining pressure before shearing; $\dot{\varepsilon}_a$ is the strain rate corresponding to q_f; and ρ_q is the slope in $\log \dot{\varepsilon}_a$ versus $q_f / \sigma_o^{'}$ plot.

Plots of $\log \dot{\varepsilon}_a$ versus $q_f / \sigma_o^{'}$ for SMBs with different sand content are presented in Figure 7.10. The values of the slope are $\rho_q = 0.008$ for SMB60 and $\rho_q = 0.007$ for SMB70, which indicates strain rate has more influence on SMB60 due to its higher bentonite content. To compare the ρ_q parameters, Graham *et al.* (1983a) examined the strain rate influence by using the strain rate parameter $\rho_{0.1}$.

Sheahan *et al.* (1996) considered a general expression for the strain rate dependency. In this chapter, the parameter $\rho_{0.36}$ is adopted, which is written as:

$$\rho_{0.36} = \frac{\Delta S_u / S_{u,0.36}}{\log \dot{\varepsilon}_{z,peak} - \log 0.36} = \frac{\Delta(q_{f,peak} / q_{f,peak0.36})}{\log \dot{\varepsilon}_{z,peak} - \log 0.36} \tag{7-2}$$

where $\rho_{0.36}$ is the strain rate parameter defined at the reference axial strain rate 0.36% /h; $S_{u,0.36}$ is the reference undrained shear strength at the given strain rate; and ΔS_u is the strength increase corresponding to the increment in $\Delta \log \dot{\varepsilon}_z = \log \dot{\varepsilon}_{z,peak} - \log 0.36$. Actually, using $\rho_{0.1}$ or $\rho_{0.36}$ is based on the same principle as in Zhu (2000). The parameter $\rho_{0.36}$ is determined to be 3.6% on average for SMB60 and 2.7% on average for SMB70.

7.5 Summary and Conclusions

The stress-strain behavior of silica sand mixed bentonite under isotropic consolidation condition and triaxial undrained CRSN condition is investigated in this chapter. The influences of sand content and strain rates are also examined. The following conclusions can be made:

a. Non-linear creep and swelling behavior has been observed from the multi-stage isotropic tests on sand mixed bentonite specimens. Similar to those in oedometer condition, both behaviors occur less obviously under higher stress condition.

b. Both the deviator stress and excess porewater pressure are influenced by strain rate. Similar to the curves in CRSN oedometer tests, when the strain rate is changed, the compression curve jumps from one constant rate of strain curve to

another. The higher the strain rate, the higher the deviator stress and the excess porewater pressure. The influence on deviator stress is more significant than that on excess porewater pressure. Strain softening is observed on SMB specimens.

c. The sand content exerts an indispensible impact on soil behaviors. In isotropic condition, with the increase of sand content, SMB specimens exhibit lower compressibility and less viscosity. In undrained triaxial condition at a given axial strain and a given confining pressure, the CRSN curves of SMB specimens with higher sand content have higher deviator stress and porewater pressure.

Table 7-1 Loading schedule of isotropic consolidation test

Confining Pressure (kPa)	Duration (Day)	Confining Pressure (kPa)	Duration (Day)	Confining Pressure (kPa)	Duration (Day)
0 - 15	3	50 - 100	6	25 - 15	6
15 - 25	3	100 - 50	3	15 - 50	3
25 - 50	3	50 - 25	3	50 - 200	3

Table 7-2 Results from undrained triaxial CRSN tests

$\dot{\varepsilon}_a$ (%/h)	$\sigma_o^{'}$	q_f of SMB60 (kPa)	q_f of SMB70 (kPa)	$q_f / \sigma_o^{'}$ of SMB60	$q_f / \sigma_o^{'}$ of SMB70
0.036	50	31	35	0.62	0.70
0.36	50	36	42	0.72	0.84
3.6	50	42	53	0.84	1.06
36	50	49	58	0.98	1.16
0.036	100	33	44	0.33	0.44
0.36	100	38	56	0.38	0.56
3.6	100	50	66	0.50	0.66
36	100	67	78	0.67	0.78
0.036	200	102	107	0.51	0.54
0.36	200	123	131	0.62	0.66
3.6	200	149	167	0.75	0.84
36	200	182	186	0.91	0.93

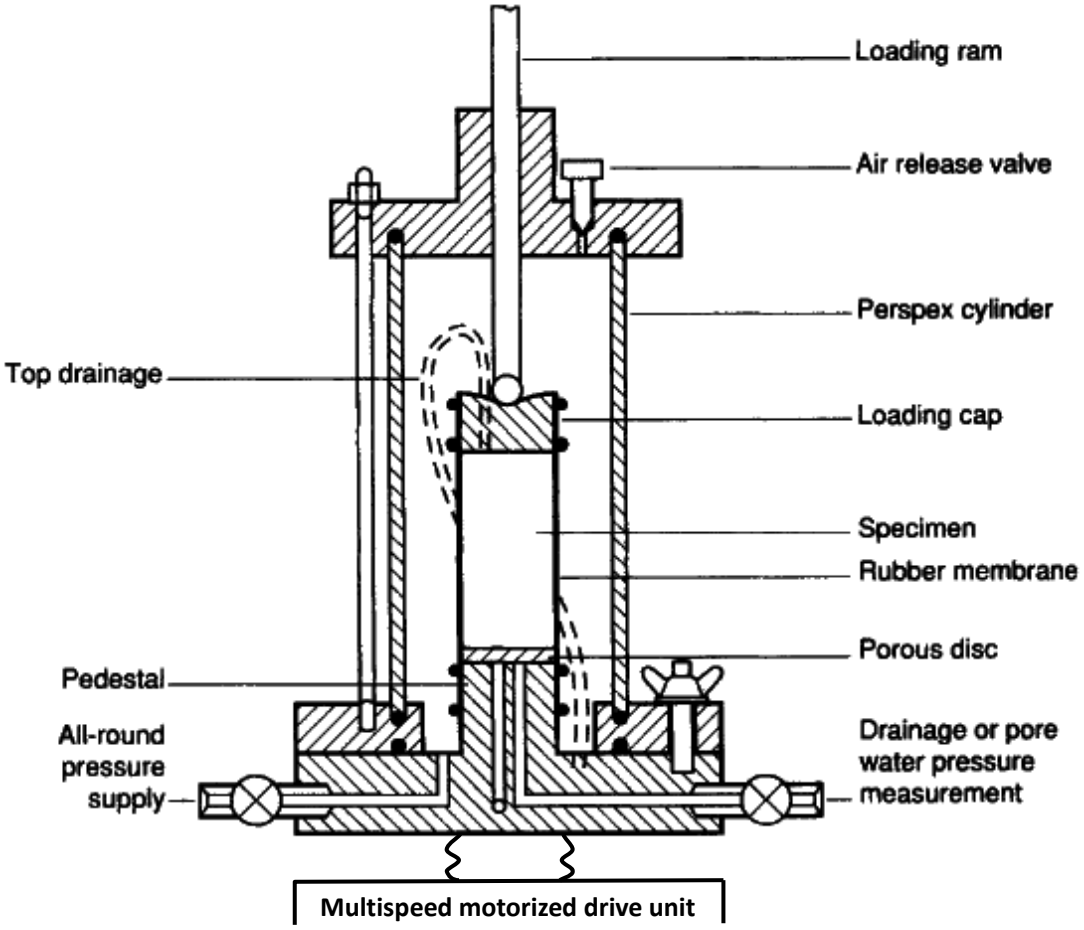

Figure 7.1 Schematic view of the triaxial CRSN testing system (Craig, 2004)

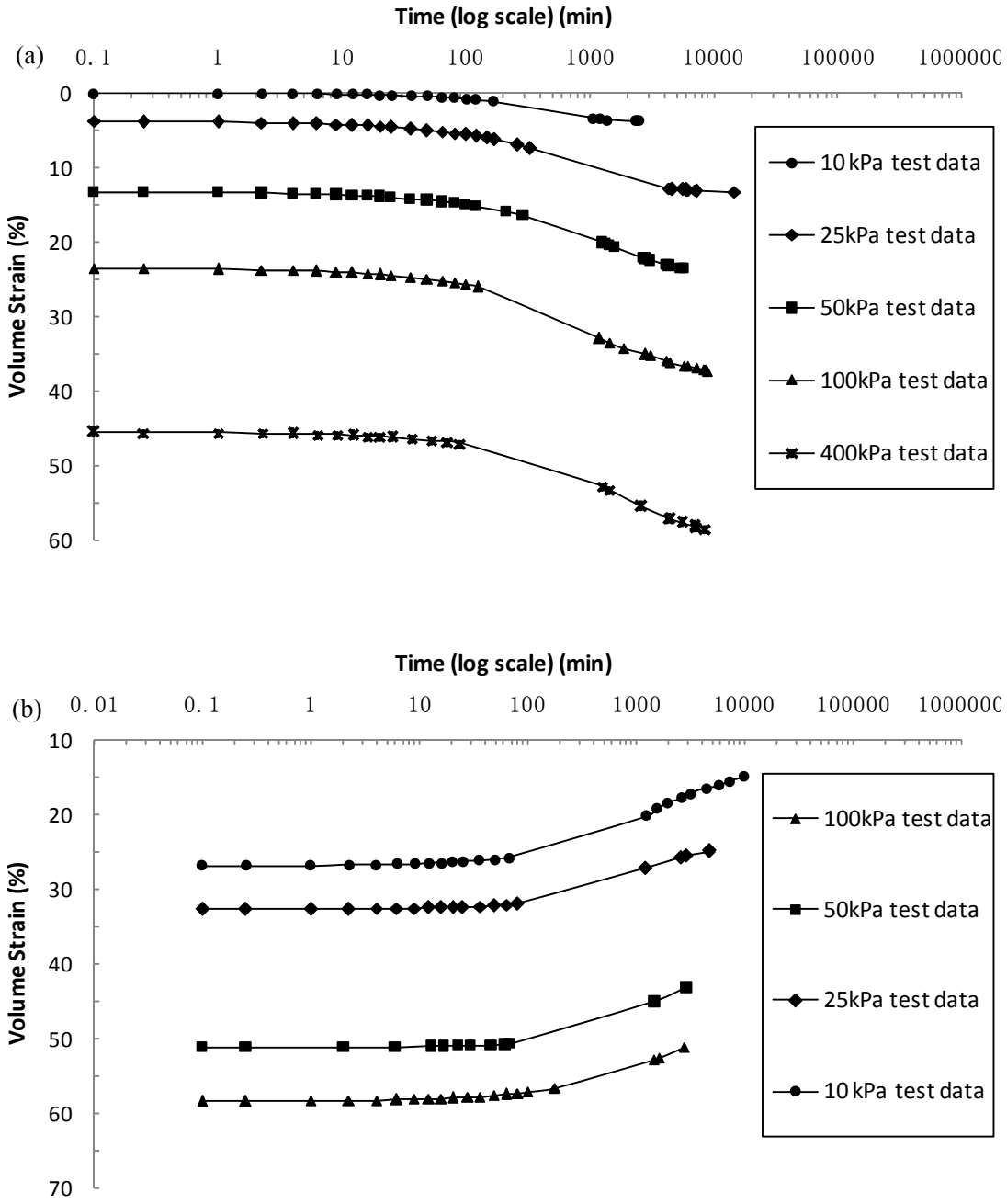

Figure 7.2 Isotropic consolidation data for SMB60 - (a) increase of volume strain with time and (b) decrease of volume strain with time

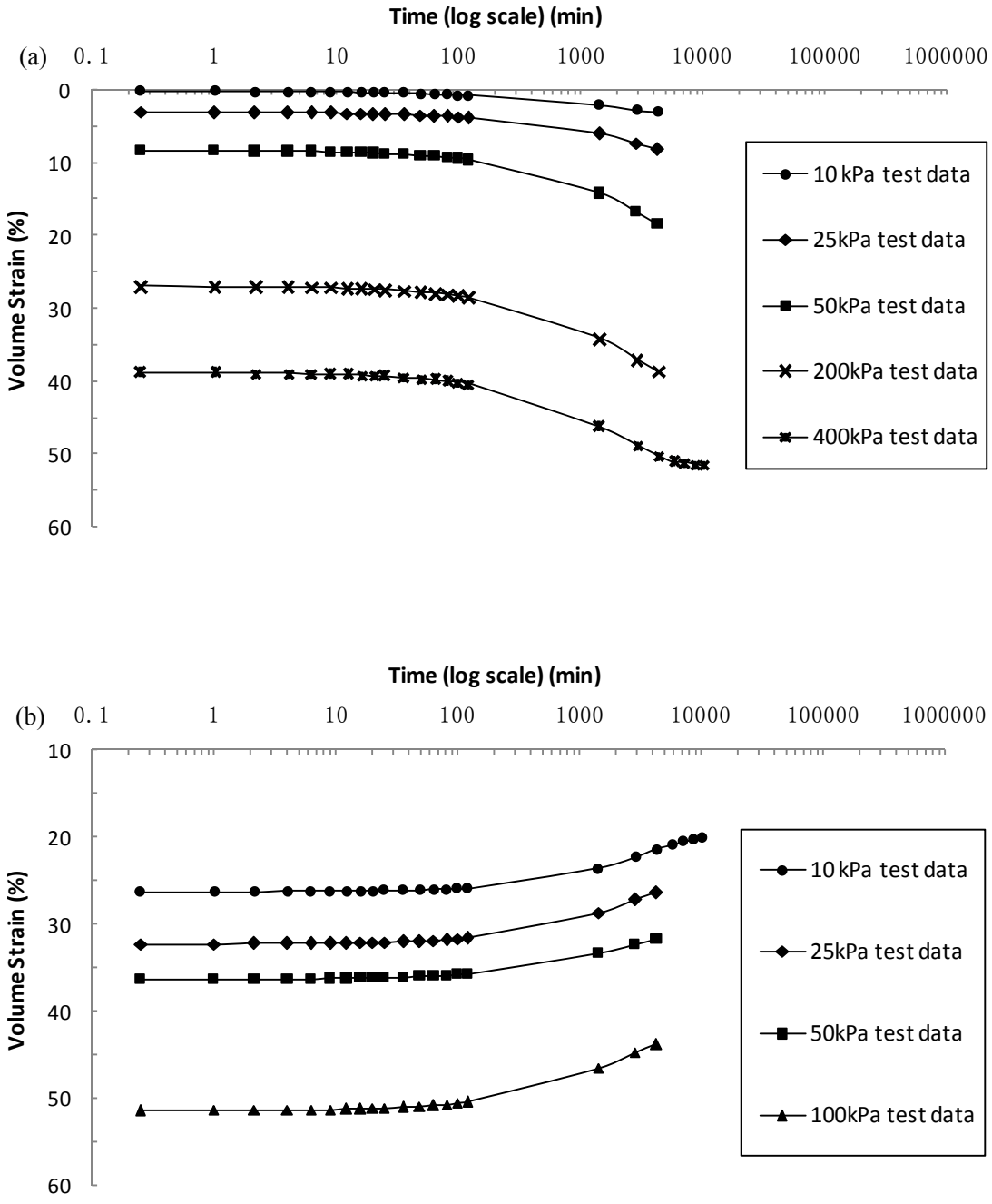

Figure 7.3 Isotropic consolidation data for SMB70 - (a) increase of volume strain with time and (b) decrease of volume strain with time

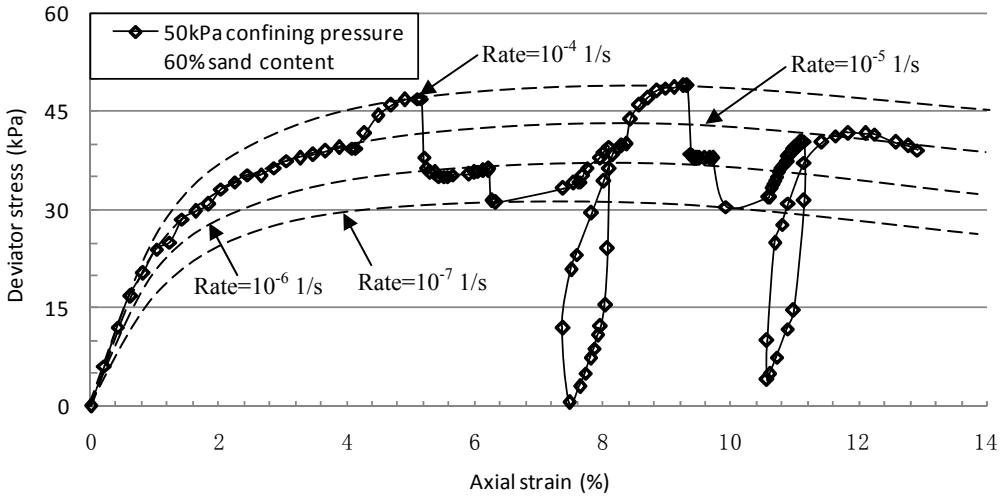

(a) Relationship between axial strain and deviator stress

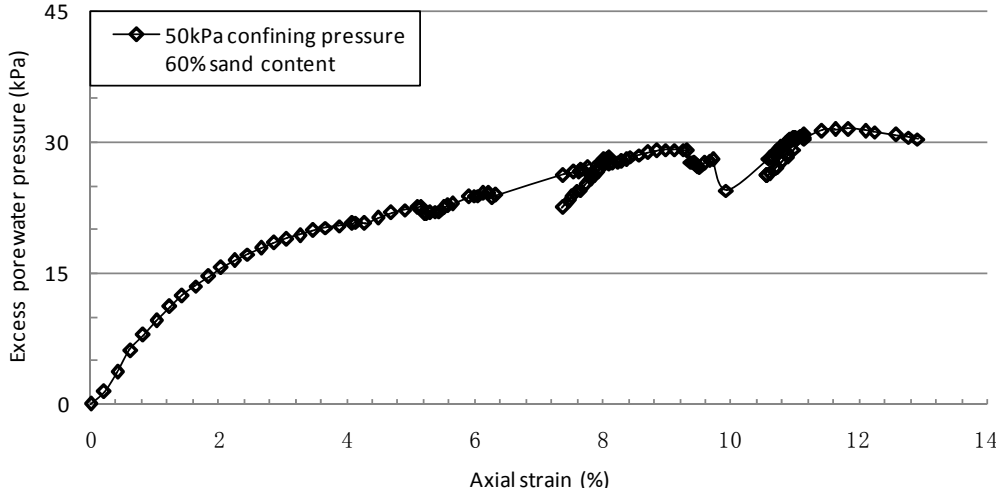

(b) Relationship between axial strain and excess porewater pressure

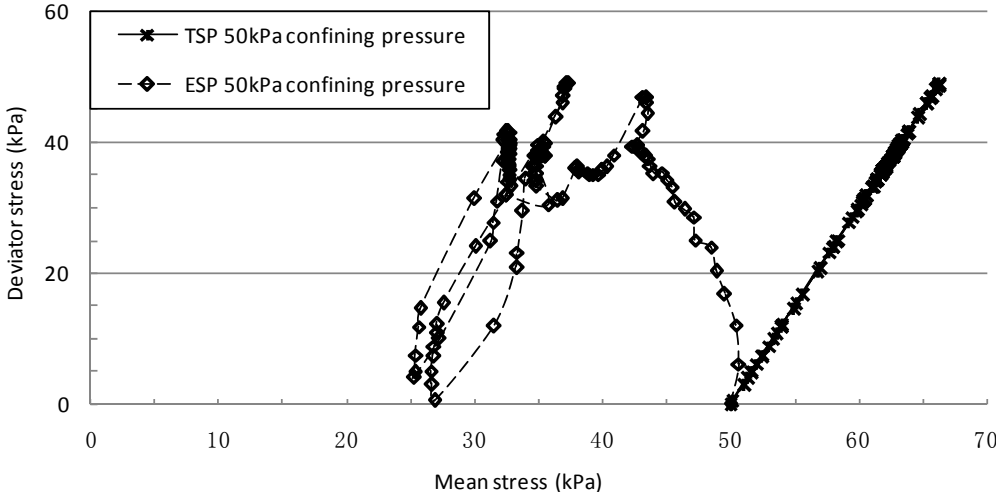

(c) The total stress path and effective stress path

Figure 7.4 Triaxial CRSN test results for SMB with 60% sand content under 50 kPa confining pressure

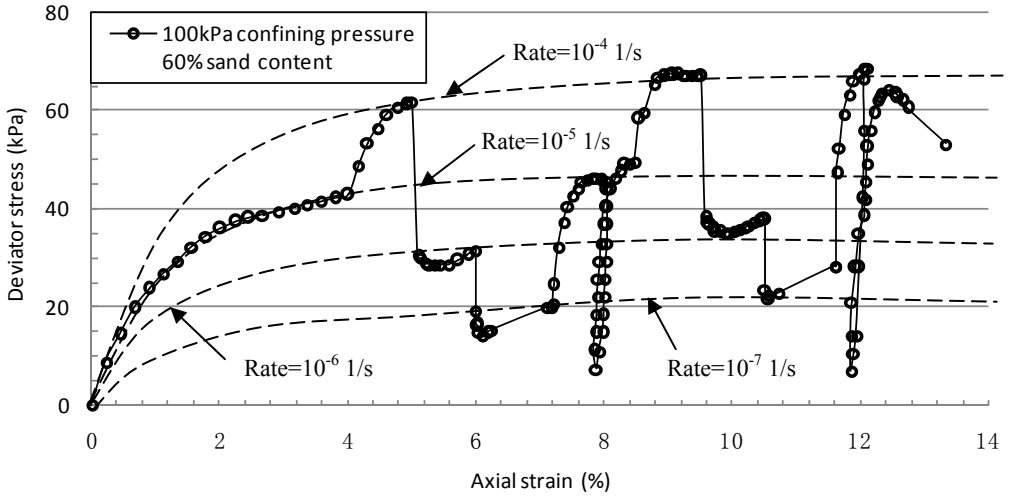

(a) Relationship between axial strain and deviator stress

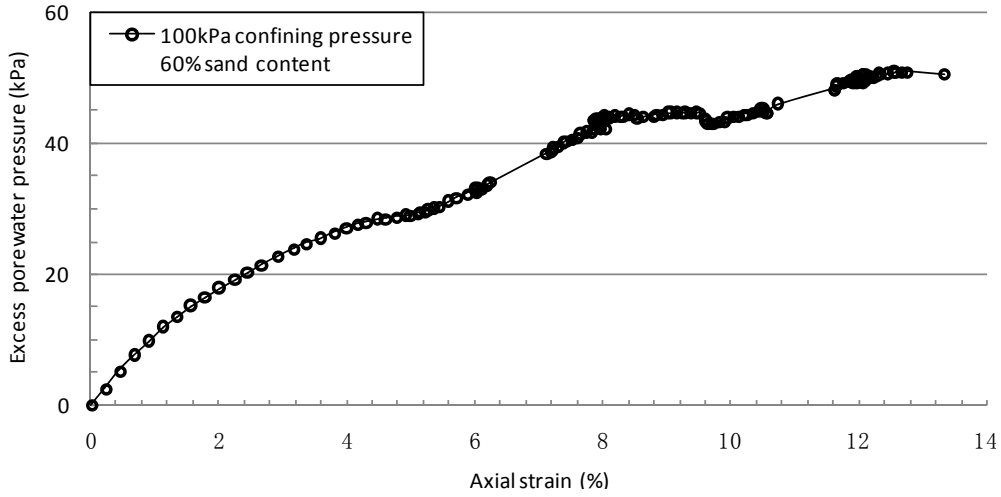

(b) Relationship between axial strain and excess porewater pressure

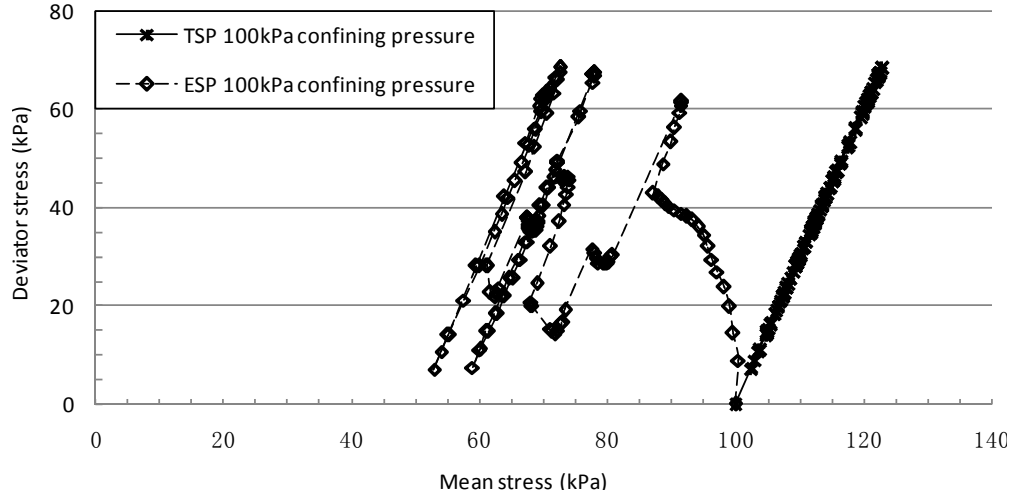

(c) The total stress path and effective stress path

Figure 7.5 Triaxial CRSN test results for SMB with 60% sand content under 100 kPa confining pressure

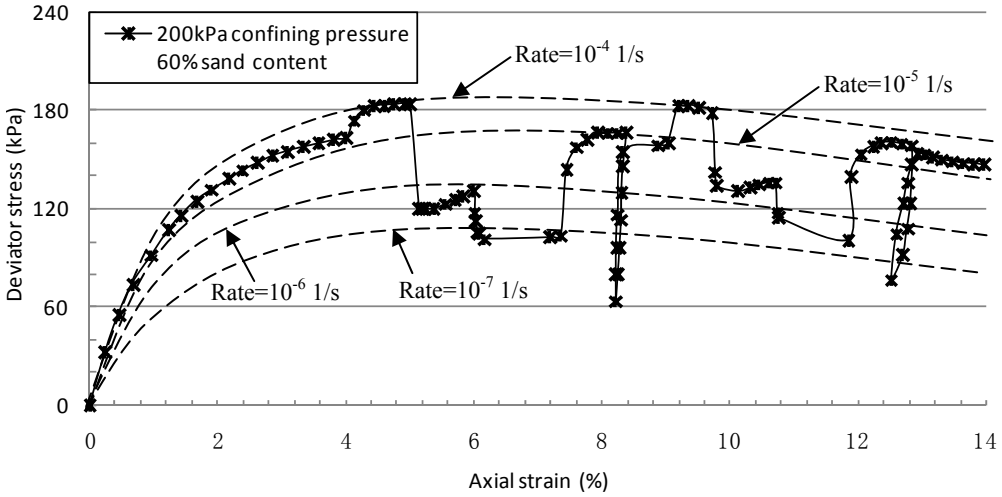

(a) Relationship between axial strain and deviator stress

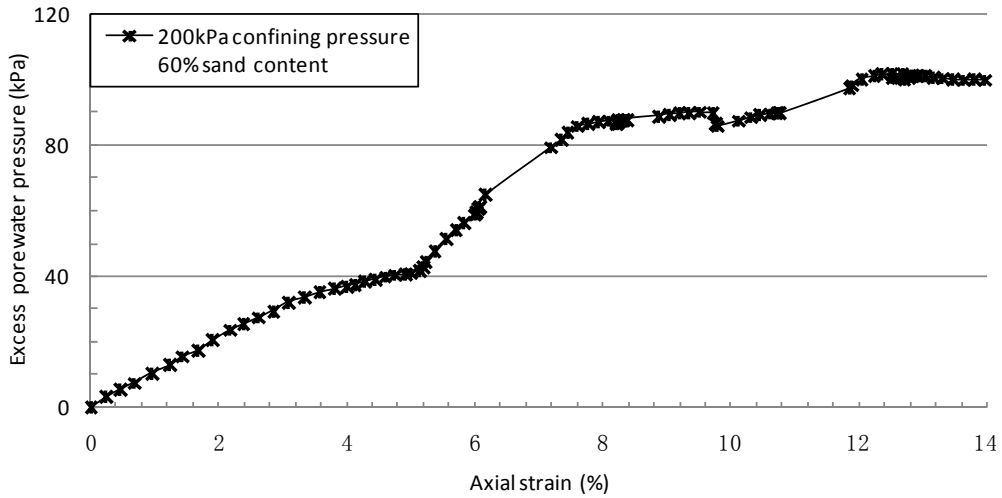

(b) Relationship between axial strain and excess porewater pressure

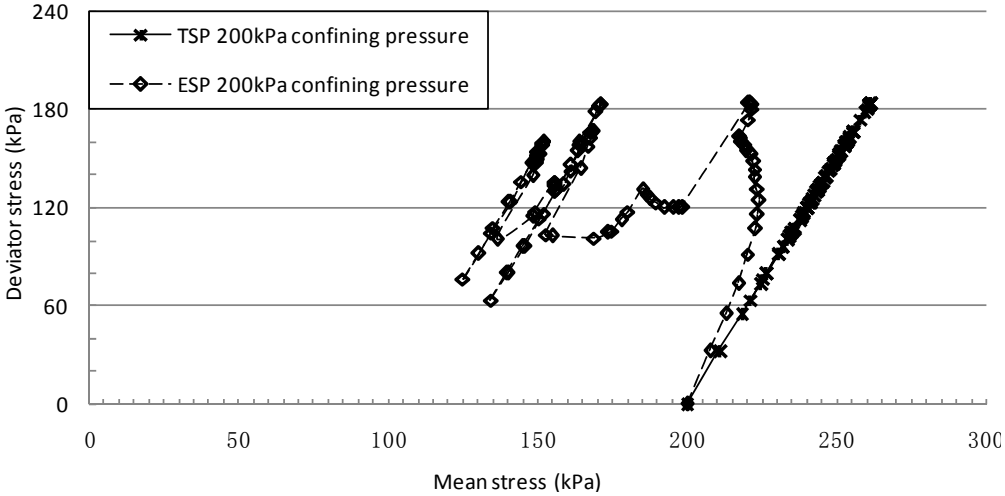

(c) The total stress path and effective stress path

Figure 7.6 Triaxial CRSN test results for SMB with 60% sand content under 200 kPa confining pressure

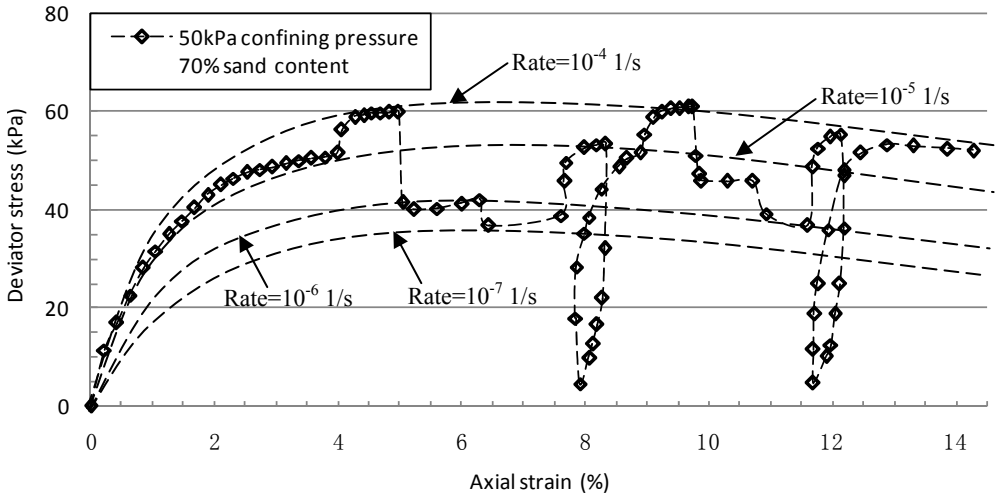

(a) Relationship between axial strain and deviator stress

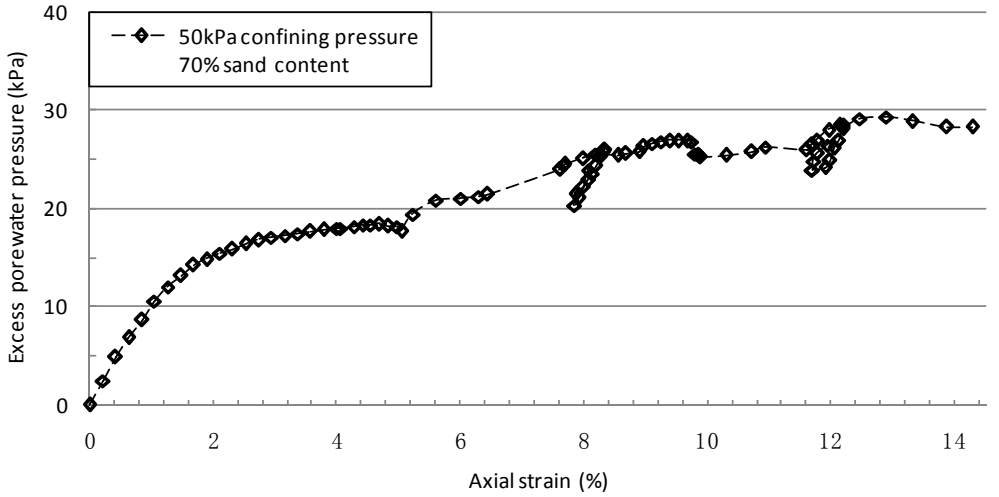

(b) Relationship between axial strain and excess porewater pressure

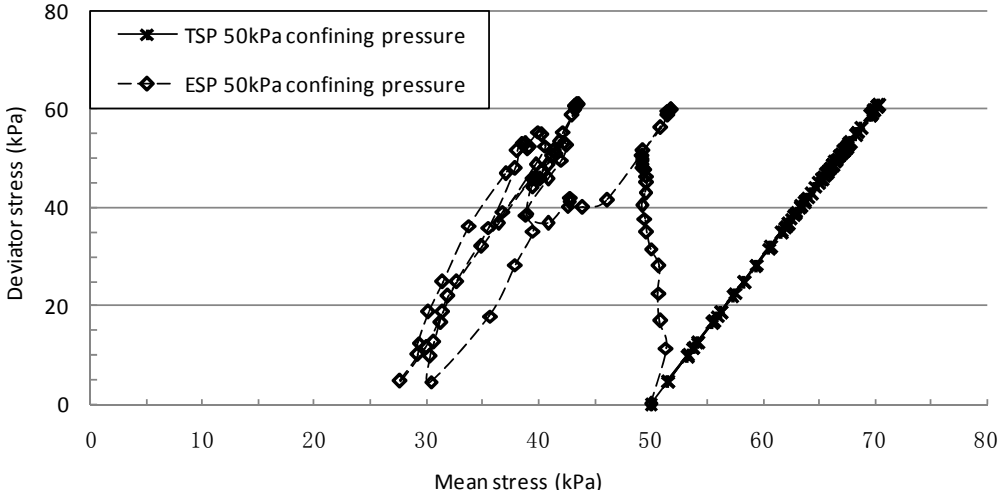

(c) The total stress path and effective stress path

Figure 7.7 Triaxial CRSN test results for SMB with 70% sand content under 50 kPa confining pressure

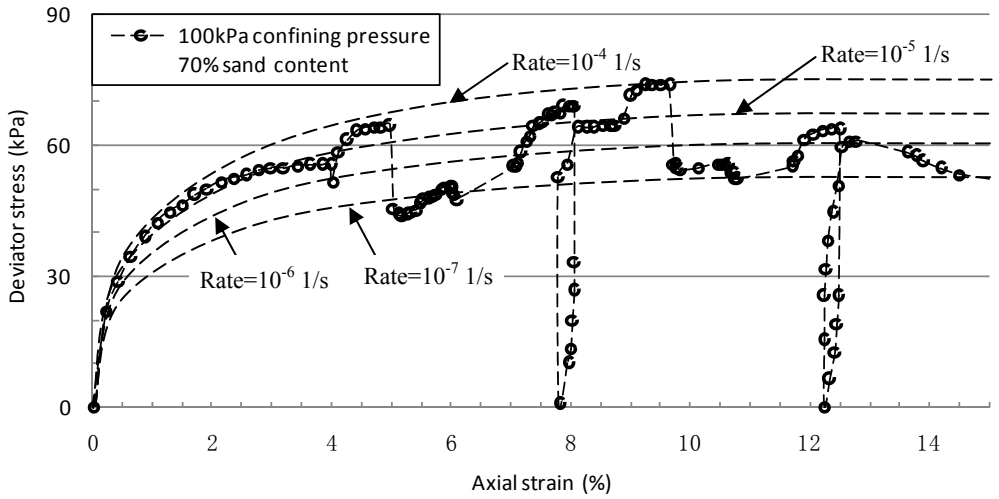

(a) Relationship between axial strain and deviator stress

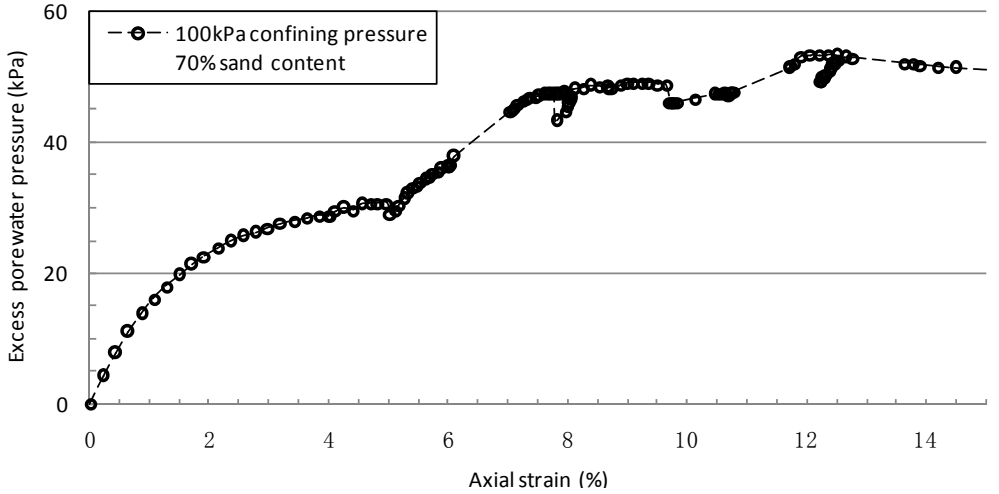

(b) Relationship between axial strain and excess porewater pressure

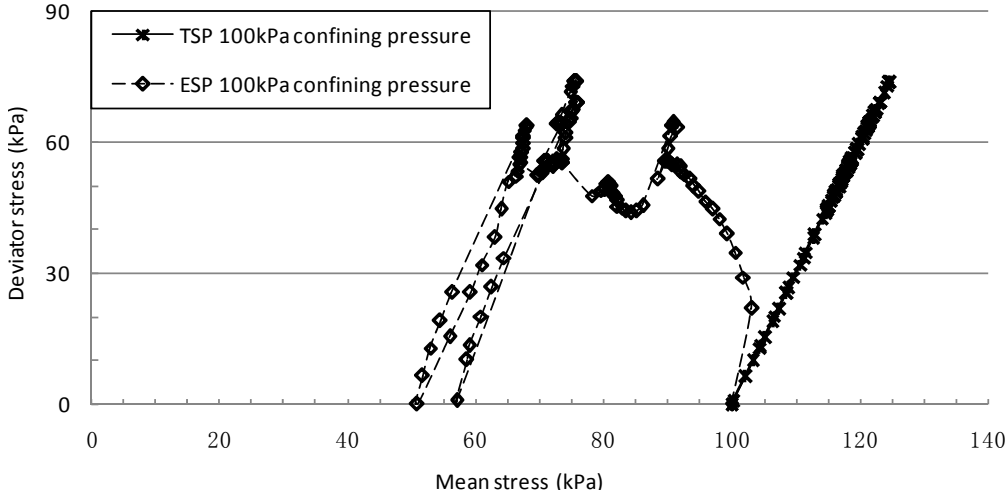

(c) The total stress path and effective stress path

Figure 7.8 Triaxial CRSN test results for SMB with 70% sand content under 100 kPa confining pressure

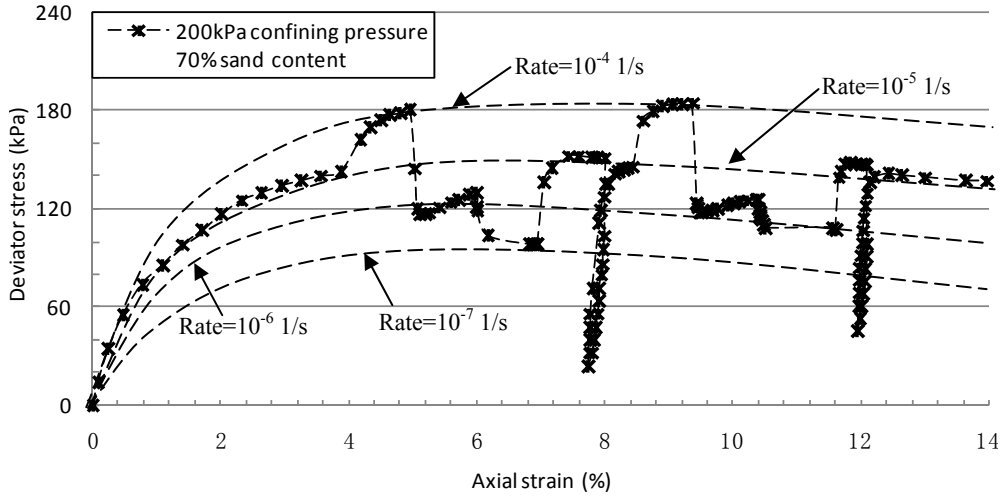

(a) Relationship between axial strain and deviator stress

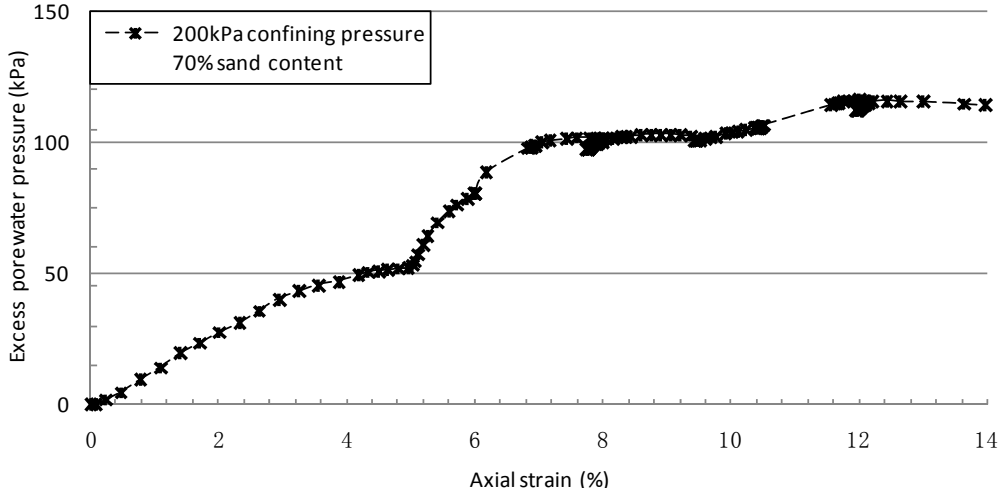

(b) Relationship between axial strain and excess porewater pressure

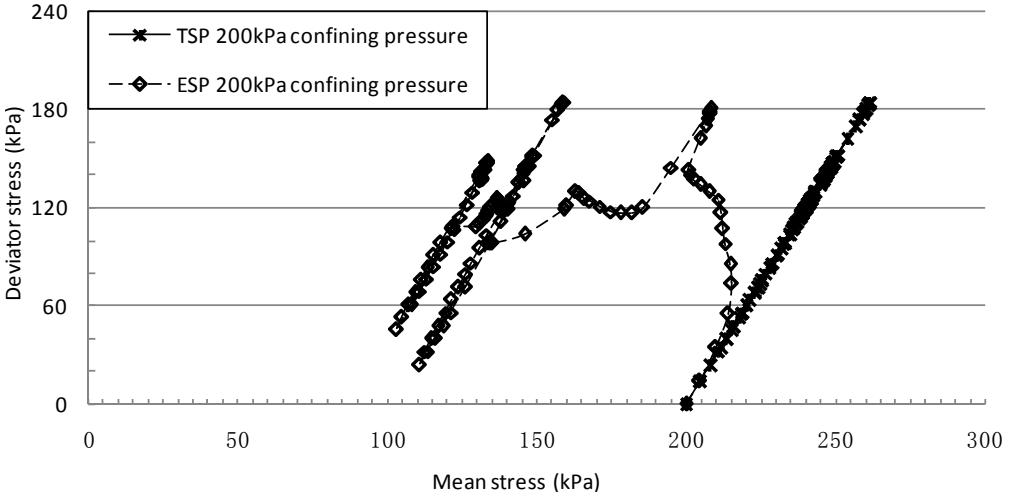

(c) The total stress path and effective stress path

Figure 7.9 Triaxial CRSN test results for SMB with 70% sand content under 200 kPa confining pressure

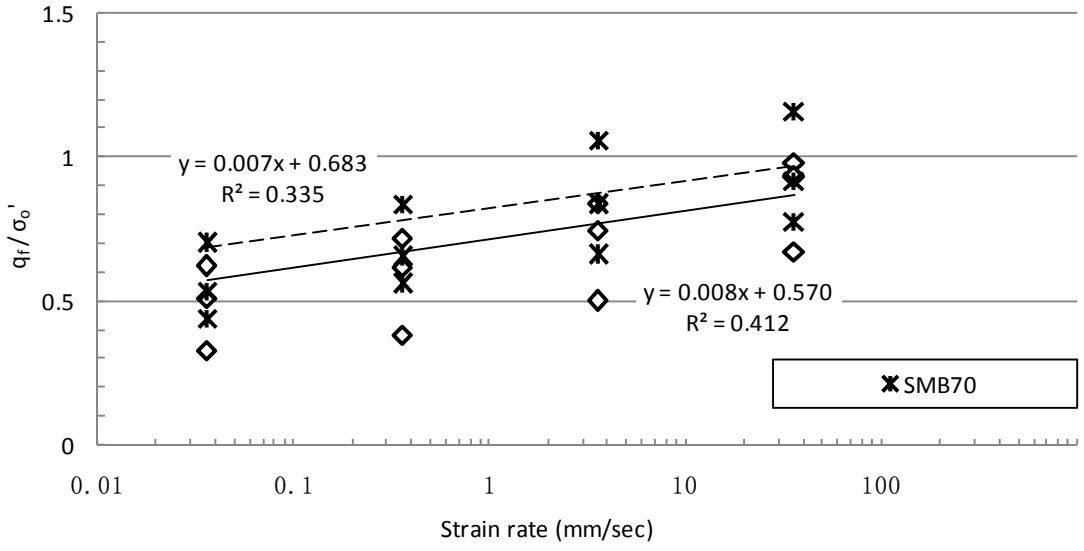

Figure 7.10 Relationship between $\log \dot{\varepsilon}_a$ and $q_f / \sigma_o^{'}$

Chapter 8

Self-weight Consolidation Behaviors from Settling Column Tests on HKMD

8.1 Introduction

The time-dependent feature of soft soils has gained intensive attraction in recent years. Due to the high water content and viscous property, the Hong Kong marine deposit (HKMD) frequently poses challenge to geotechnical practice, particularly to the reclamation in Hong Kong. A key issue related to reclamation design, foundation construction and maintenance is excess settlement/deformation of the ground. Formation of HKMD typically goes through sedimentation and self-weight consolidation. In this chapter, a series of one-dimensional settling column consolidation tests, together with conventional oedometer tests are conducted on the HKMD to examine the complete consolidation behavior of Hong Kong marine deposits both in self-weight condition and in oedometer condition. Applicable interpretation of consolidation of HKMD in wide stress range is critical to model this type of soils and field applications.

By normalizing parameter in settling stage, a unique complete relationship of effective stress, σ_z' against strain, ε_z could be established. Results reveal that the settling curve and settling rate are significantly affected by the sediment concentration in self-weight consolidation. After the primary self-weight consolidation, the settling rate is reduced in the "secondary self-weight

consolidation".

8.2 Testing Materials and Program

The soils were artificially sedimented at different initial water contents in order to obtain both segregated and homogeneous sediments. In settling column consolidation, initial water content of the soil-water suspension is one of the important factors controlling the settling behavior of soils (Imai, 1980; Sridharan and Prakash, 1999). The soil slurry is prepared with water content sufficiently high, yet maintaining the homogeneity (Sheeran and Krizek, 1971). At very high initial water contents, grain size sorting takes place, resulting in segregated sediments. In contrast, when the initial water content is below a limiting value, mutual mechanical interaction among the settling soil particles/flocs dominates, which results in homogeneous sediments.

The settling column setup by Berlamont *et al.* (1993) is adopted to establish total six perspex columns with internal diameter of 130 mm and height 1 m (volume=3.14×0.065×1= 0.01327 m^3). In this setup as shown in Figure 8.1, scale length is nearly 100 cm; distance between two ruler ticks is 1 cm with readable resolution 0.1 cm.

For a soil with given concentration (weight of dry mass of the soil over 0.001 m^3 of soil), and for a container of a given volume of 0.015 m^3, the soil dry mass M_s will be 1500 g. The mass of water is:

$$M_w = \rho_w V_w = \rho_w (V_{total} - V_{soild}) = \rho_w (V_{total} - M_s / G_s) \qquad (8\text{-}1)$$

where ρ_w is the density of water; G_s is the specific gravity of soil particles.

In order to avoid destruction of organic materials in soil during drying, the original wet soil is used to find the required dry mass. The original soil in a box is thoroughly mixed first to make the soil uniform. After this, two soil specimens are taken to find the initial water content w_i, of the soil. The dry density and the dry mass are calculated as follows:

$$\rho_d = \frac{\rho}{1+w} = \frac{M_s}{V} \quad M_s = V\frac{\rho}{1+w_i} = \frac{M}{1+w_i} \qquad (8\text{-}2)$$
$$M = M_s(1+w_i)$$

According to the procedure illustrated in Figure 8.2, once the weight of wet soil is determined, the raw soil of known water content and weight was mixed with the water to form slurry, and then the water content was increased to desired value. A high-speed rotary mixer is used to prepare the slurry. The soil-water mixture was thoroughly mixed and transferred to the test jar of 0.95 m in height for free settling. Then, the sedimentation and subsequent consolidation starts. The level of the interface between the clear water and sediment is recorded manually at a series of time intervals: 15 sec, 30 sec, 1 min, 2 min, 4 min, 8 min, 16 min…, until the completion of the whole consolidation.

The experiments were conducted using site water with a pH of about 7.2. Two soil samples in different colors with site water were tested. By varying the initial content, segregated and homogeneous sediments were obtained for the same soil. The sediments formed were left undisturbed for a sufficiently long time to allow the self-weight consolidation to complete for all practical purposes. Results from the

settling tests are presented and discussed in the following section. All the tests were carried out under the constant laboratory temperature of 20±1°C.

The time to reach full consolidation depends on the initial concentration of the sample used to fill the column. By doubling the concentration, the duration also (nearly) doubles, requiring a four times longer consolidation time. A very low initial concentration certainly results in a short experiment time, a thin final layer and a low effective stress. In these tests, the duration of time varied from about 7 days for soils with 20 g/l concentration to about two months for soils with 100 g/l concentration.

Berlamont *et al.* (1993) used a "conductivity probe" to measure the density of the soil along the soil thickness. Using this method calibration must be done properly. In this study, a direct method is used. After free-settling for sufficient time, the water above the sediment was siphoned out and a specially made spatula (bent horizontally at end) was inserted for sampling layer by layer from the top to the bottom of the sediment. The spatula is thin in diameter and will very slightly disturb the local soil samples. The soil is carefully transferred into glass containers. The container with the wet soil is put in an oven to dry for 24 hours at the standard temperature of 105°C and then weighed to get the dry mass. In this way, the water content distribution and hence, the void ratio profiles over the entire depth of the sediment were obtained based on equation (8-3).

$$\begin{aligned}
&\phi = \frac{V_s}{V} \\
&\rho_d = \frac{\rho}{1+w} = \frac{M_s}{V} \Rightarrow M_s = V\frac{\rho}{1+w} \\
&\rho_s = \frac{M_s}{V_s} \Rightarrow V_s = \frac{M_s}{\rho_s}; \rho_s = G_s\rho_w \\
&\phi = \frac{V_s}{V} = \frac{M_s}{V\rho_s} = \frac{V}{V\rho_s}\frac{\rho}{1+w} = \frac{1}{\rho_s}\frac{\rho}{1+w} = \frac{1}{G_s}\frac{\rho/\rho_w}{1+w}
\end{aligned} \tag{8-3}$$

where ϕ is the soil fraction (volume of solid mass over the total volume).

The effective stress at any depth was calculated using the effective weight of the soil mass above that depth. The segregated layers were carefully identified visually as the thin scrapped layers were taken out. Grain size analyses were carried out to confirm whether the sediments formed were homogeneous or segregated.

8.3 Settling Results and Discussions

Three typical marine clays (3a, 19 and 17, respectively) with fair viscosity are adopted from around Nam Sang Wai and Mai Po, Hong Kong for self-weight settling and oedometer analysis. Before self-weight consolidation, basic properties including water content and specific gravity have been illustrated in Chapter 3.

With settling column technique, one can get the compression curve over a very low stress range (Imai, 1981; Umehara and Zen, 1982; Scully, 1984). Combining the void ratio profile and the effective stress variation with depth, the void ratio-effective stress relationship can be established. Data are used to plot the compression curve (*i.e.*, *e-logσ'* or *w%-logσ'*) where *w%*, *e*, and *σ'* are the water content, void ratio, and the effective overburden pressure at any depth measured

from the top of the soil sediment, respectively. Typical settling results for each sample with different concentration degree (20 g/l, 50 g/l and 100 g/l, respectively) are illustrated in Figure 8.3~Figure 8.7.

For the HKMD slurries, water content is much higher than the liquid limit, therefore the soil grains flocculate in water. Although in settling some deformation occurs due to reduction of pore water, the pressure actually does not dissipate until the grains are in mutual contact. From this time real effective stress began to accumulate. Since the vertical burden is accumulated layer by layer, the effective stress can be obtained in a sequence illustrated in equation below.

$$\sigma_v^i = \sigma_v^{i-1} + \frac{\gamma_{i-1} d_{i-1} + \gamma_i d_i}{2}, \quad \gamma_i = \gamma_w \frac{G_s + e_i}{1 + e_i} \tag{8-4}$$

where γ_i is unit weight; G_s is specific gravity; γ_w is unit weight of water; d is layer thickness; e is void ratio; and i-1 stands for layer above.

Based on Figure 8.4(a) and 8.6(a), the *e-logσ'* curves are presented in term of great variation of void ratio over the depth of sediment. As the initial HKMD concentration is reduced (water content increased), the curve becomes steeper initially. The *e-logσ'* curves obtained due to self-weight consolidation are about to coincide even cross each other, which is consistent with finding by Sridharan and Prakash (2003).

When the stress is low, the *e-logσ'* curve indicates the extent of grain size sorting takes place during settling. After particle segregation, the self-weight consolidation takes place. Flatter curve means more homogeneity. In this sense, the

absolute case without self-weight consolidation will produce a horizontal line.

All the test results are proved to be reasonable. According to Merckelbach (2000) and Merckelbach and Kranenburg (2004a, b), the settlement of the interface *h (t)* may be expressed as:

$$h(t) = \left(\xi \frac{2-n}{1-n}\right)^{\frac{1-n}{2-n}} \left[K_K \frac{\rho_s - \rho_w}{\rho_w}(n-2)\right]^{\frac{1}{2-n}} t^{\frac{1}{2-n}} \tag{8-5}$$

where ρ_s is the density of the solid particles; ρ_w is the density of pore water and can be taken as 1.0 Mg/m^3; ζ is the material height, m; K_K is the permeability parameters; and n=2/(3-D), D is the fractal dimension.

The above equation can be rewritten in normal log scale as

$$\log h(t) = \log\left[\left(\xi \frac{2-n}{1-n}\right)^{\frac{1-n}{2-n}} \left(K_K \frac{\rho_s - \rho_w}{\rho_w}(n-2\right)^{\frac{1}{2-n}}\right] + \frac{1}{2-n}\log t \tag{8-6}$$

As demonstrated in equation (8-6), the parameters for settling interface are to be determined. In all the settling progress, the parameter K_K is a key factor governing permeability, which can further affect settling rate.

$$k = c_v m_v \gamma_w = K_k \cdot \phi^{\frac{-2}{3-D}} \tag{8-7}$$

where k is the permeability; φ is sediment volume fraction, namely the volume of the solid particles with respect to the total volume.

Note that equation (8-6) is a straight line, only valid for $t_1<t<t_2$. At $t=t_1$, the interface becomes clear and a single discontinuity remains. At $t=t_2$, the effective stress takes effect, and the assumption in equation (8-6) does not work anymore. The final density profile after self-consolidation exhibited in Figure 8.8 can be adopted to compute the effective stress parameter K_σ in equation (8-8). In Figure 8.8, the

slope of soil height over volume fraction becomes steeper once the soil concentration increases.

$$\log h(t-z) = \log\left(\frac{2K_\sigma}{(D-1)(\rho_s-\rho_w)g}\right) + \frac{D-1}{3-D}\log\phi \tag{8-8}$$

Then the effective stress can be determined.

$$\sigma_v^{'} = K_\sigma \cdot \phi^{\frac{2}{3-D}} \tag{8-9}$$

Additionally incorporating equation (8-8), the coefficients of consolidation c_v can be determined and summarized in Table 8-1. Value of c_v is obtained based on equation (8.10).

$$c_v = -\frac{k(1+e)}{\rho_w g}\frac{d\sigma^{'}}{de} = \frac{2}{3-D}\frac{K_\sigma K_K}{\rho_w g}\frac{1+e}{e} \tag{8-10}$$

It can be seen from Table 8-1 that the coefficient of consolidation increases gradually with reduction of HKMD concentration. The fractal dimension however increases once increasing the concentration degree. Another fact can be found that sample 19 consolidates “faster” than the sample 3a, which means sample 3a exhibits more viscous property. Surely the value of c_v will slightly vary depending on the void ratio and thickness of soil in column.

Extensive studies have been conducted on the relationship between strain and effective stress, particularly on the relevant C_c, C_r indexes. Early study by Skempton (1944) indicates the both the initial water content and the liquid limit W_L has a great impact on the consolidation behavior. Many researchers have already incorporated the W_L concept into compressibility estimation (Skempton, 1944; Terzaghi and Peck, 1967; Yoon *et al.*, 2004).

Butterfield (1979) assumes that the plot of log$V$ (V=1+e) and log$p$ shows a linear relationship, when the initial water content is fairly high. Then the Basic Compression Line is defined as

$$\log_e V = \log_e V_1 - \frac{\lambda}{V}\log_e p \tag{8-11}$$

where p is the consolidation pressure; V_1 is the specific volume at p=1 kPa and λ/V is slope of the compression line expressed by Yin and Graham (1989) as

$$\frac{\lambda}{V} = \frac{\Delta\varepsilon_z}{\Delta \ln \sigma_z^{'}} = \frac{-\Delta e}{V\Delta \ln \sigma_z^{'}} = \frac{-\Delta e \times 0.434}{V\Delta \log \sigma_z^{'}} = \frac{0.434}{V}\frac{-\Delta e}{\Delta \log \sigma_z^{'}} = \frac{0.434}{V}C_c \tag{8-12}$$

By differentiation of the above equation, a linear fundamental law between stress and strain can be obtained.

$$\frac{dV}{V} = \frac{\lambda}{V}\frac{dp}{p} \tag{8-13}$$

However in Figure 8.3(a), 8.5(a) and 8.7(a), the settling continues with time after the “linear region”, which indicates that the structure of HKMD forms during free settling process (deposition), thus making the void ratio smaller than that on the compression curve, which further causes creep (secondary compression) during the whole consolidation.

8.4 Concentration and Settling Rate

Typical settling curves of sample 19 and sample 17 in Figure 8.9 are selected for analysis of settling rate and accumulated settling velocity. Before the first 10min, soil particles initially convert into loose sediments, while their settling is quite slow.

After that, settling of soil particles accelerates, and a clear solid-liquid interface develops at the top of the column. This occurs because discrete flocs are formed from clay or colloid particles. As illustrated in Figure 8.3(a) and 8.5(a), the constant settling rate in this stage has been proved to be independent of soil type and concentration (Park *et al.*, 1992).

Relationships of settling rate against elapse time are demonstrated in Figure 8.10. It is found from the figure that the settling of sediment is closely related with soil concentration and distribution. The settling rate in this stage is dependent of soil type as well. Comparatively the soil concentration has more influence than soil type on settling rate profile. Soil particles continuously deposit on the bottom of the column to form a bed of loose structure. Particles in sediment with high concentration may easily contact with each other thus to reduce the settling rate.

Following the above "zone settling" (Imai, 1980), the void ratio is beyond 30 and gradually sedimentation transforms into self-weight consolidation. In fact, the transition point becomes less clear once the soil concentration increases. Compared with the zone settling, the settling rate of the solid-liquid interface becomes slow again. Moreover, self-weight consolidation starts at the bottom while the sedimentation process starts at the top.

8.5 Secondary Self-weight Consolidation

Drained creep in conventional oedometer condition has been a research interesting area with a long history (Berre and Iversen, 1972; Leroueil *et al.*, 1985; Yin and Graham, 1999). Mesri and Godlewski (1977) showed that C_α is related to the compression index C_c of the soil and more precisely, that the ratio C_α/C_c is constant for a given soil. The C_α/C_c concept has been confirmed for a variety of geotechnical materials by Mesri and Godlewski (1977) and many other researchers.

For settling column condition in Figure 8.3(a), 8.5(a) and 8.7(a), the soil continues to settle with time after the "linear region", which indicates that the structure of HKMD forms during free settling process (deposition), thus making the void ratio smaller than that on the compression curve, which further causes creep (secondary compression) during the whole consolidation.

As illustrated in Figure 8.9(b), for sample 17 with 100 g/l concentration in self-weight consolidation stage, the slope of the settling curve is determined to be 13.81 by curve fitting. Similarly to the creep behavior in oedometer condition, soils continue to settle after the self-weight consolidation. The settling rate is further reduced to 2.842 and this stage may be called the "secondary self-weight consolidation". The two corresponding slopes for sample 19 are determined to be 6.978 and 2.709, respectively.

It has been proved the C_α/C_c for natural soils ratio lies in a narrow range of 0.025~0. l. Once the C_α/C_c concept is adopted in self-weight consolidation, two ratios can be obtained: 0.21 for sample 17; and 0.39 for sample 19. More viscous

soil has higher C_α/C_c value. The secondary compression has more significant influence on the whole self-weight consolidation.

8.6 Complete One Dimensional Consolidation

After settling column tests, a series of multi-stage oedometer tests were also carried out on HKMDs. Ahead of the oedometer test, the HKMDs were pre-consolidated in the large-diameter steel tank to reduce consolidation time. The multi-staged oedometer results in vertical strain versus time (log scale) are presented in: Figure 8.11(a) for sample 19; Figure 8.12(a) for sample 3a. It can be seen that due to the creep effect, specimens continue to settle after the primary consolidation. Once the normal stress and strain in standard 24 h are plotted (Figure 8.11(b) and Figure 8.12(b)), the virtual compression line can be determined.

Combined with settling column results in last section, a complete consolidation curve is obtained for each sample. The curves presented in Figure 8.13 have been normalized in e/e_L, in which e_L is the void ratio at the liquid limit. It deserves mention that the gap between the settling column results and oedometer results is sealed by low stress CRSN test data. Furthermore, a linear equation is adopted to fit the test data so that a *Basic Compression Line* (BCL) is obtained for each HKMD specimen.

As illustrated in Figure 8.13(a) for sample 19, when effective stress is larger than 0.8 kPa, most of the data are plotted around the BCL. In the region σ'<0.8 kPa

(transition pressure), the void ratio is much bigger in that the sediment process enables soil particles to reform the structure. The void ratio of the sediment surface at the end of settling is found to be 10.5~15.6, slight bigger than those obtained by Been and Sills (1981). At around 1 kPa of effective stress, all the settling data approach to the BCL. As for sample 3a in Figure 8.13(b), the transition pressure is determined to be 1.1 kPa, and the surface void ratio at the end of settling is around 12.2~18.3. The BCL is much flatter compared with the line for sample 19.

Based on Figure 6-7, following equation (8-14) the C_{bc} index (*Basic Compression Index*) is obtained for each sample: 0.15 for sample 19; 0.09 for sample 3a. Relatively sample 19 shows more compressibility. Similarly from oedometer results, the *Basic Rebounding Index* C_{be} is determined to be 0.0175 for sample 19; and 0.0162 for sample 3a. Small rebounding indexes indicate low potential in swelling.

$$C_c = \frac{-\Delta e}{\Delta \log \sigma_z^{'}}$$
$$C_{bc} = \frac{-\Delta (e/e_L)}{\Delta \ln \sigma_z^{'}} = \frac{-\Delta e \times 0.434}{e_L \Delta \log \sigma_z^{'}} = \frac{0.434}{e_L} C_c \qquad (8\text{-}14)$$

where e_L is the void ratio at the liquid limit.

8.7 Summary and Conclusions

The complete consolidation behaviors of Hong Kong Marine Deposits both in settling column condition and in oedometer condition are studied in the chapter. The following conclusions can be made:

a. Typical settling curves of HKMD are obtained. The *e-logσ'* curves obtained due to self-weight consolidation are about to coincide even cross each other. The void ratios of the sediment surface at the end of settling are found to be 10.5~15.6 for sample 19; 12.2~18.3 for sample 3a; and 8.5~13.3 for sample 17. When the void ratio is about 4, the *e*-log *p* curves coincide to form a compression line.

b. The settling curves indicate a constant settling rate at zone settling, and then attain transition points, thereafter decreasing. Soils even exhibit viscosity in self-weight consolidation. After the primary self-weight consolidation, the settling rate is further reduced in the "secondary self-weight consolidation".

c. Soil concentration has critical influence on the settling property. In final density profile, the slope of soil height over volume fraction becomes steeper once the soil concentration increases. The coefficient of consolidation c_v is found to decrease when the soil concentration increases. With 100g/l concentration, the c_v value is 2.80×10^{-5} m^2/yr for sample 19; 1.89×10^{-5} m^2/yr for sample 3a; and 3.21×10^{-5} m^2/yr for sample 17.

d. Combined with settling column results, MSL results and CRSN results, a complete consolidation curve is obtained for each sample. The C_{bc} index is obtained for each sample: 0.15 for sample 19; 0.09 for sample 3a.

e. Soils even exhibit viscosity in self-weight consolidation. After the primary self-weight consolidation, the settling rate is further reduced in the "secondary self-weight consolidation". Soil with more viscosity has higher C_α/C_c value.

Table 8-1 Summary of parameters from the settling column tests

ID	Concentration	h (cm)	ξ (cm)	D	K_k (10^{-10} m/s)	K_σ (kPa)	C_v (m^2/yr)
3a	20g/l	95.80	1.18	2.57	0.40	54.35	3.99E-02
	50g/l	95.78	2.94	2.62	0.27	64.69	3.56E-02
	100g/l	96.06	5.89	2.69	0.05	144.40	1.89E-02
19	20g/l	98.18	1.20	2.60	0.79	45.08	7.53E-02
	50g/l	96.29	2.99	2.66	0.27	82.72	5.54E-02
	100g/l	99.30	5.98	2.71	0.07	133.79	2.80E-02
17	20g/l	98.18	1.20	2.60	0.79	45.08	9.80E-02
	50g/l	96.40	2.88	2.62	4.09	64.72	6.86E-02
	100g/l	96.57	5.75	2.63	1.14	106.46	3.21E-02

Table 8-2 Summary of parameters from the MSL oedometer tests

ID	Final height (mm)	Final water content (%)	C_v (m^2/yr)
3a	10.66	35.25	8.81E-02
19	12.10	29.60	9.06E-02
17	12.58	27.88	9.57E-02

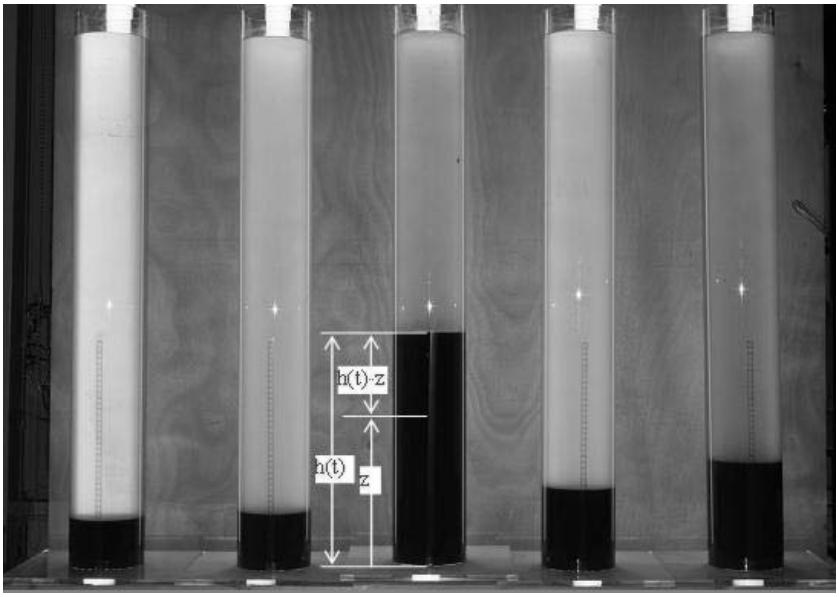

Figure 8.1 Column setup to for settling column tests (Berlamont *et al.*, 1993)

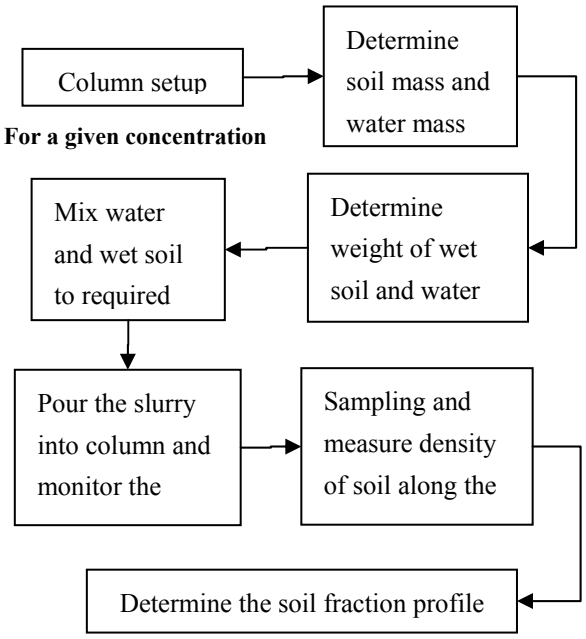

Figure 8.2 Flow chart of the experiment procedure

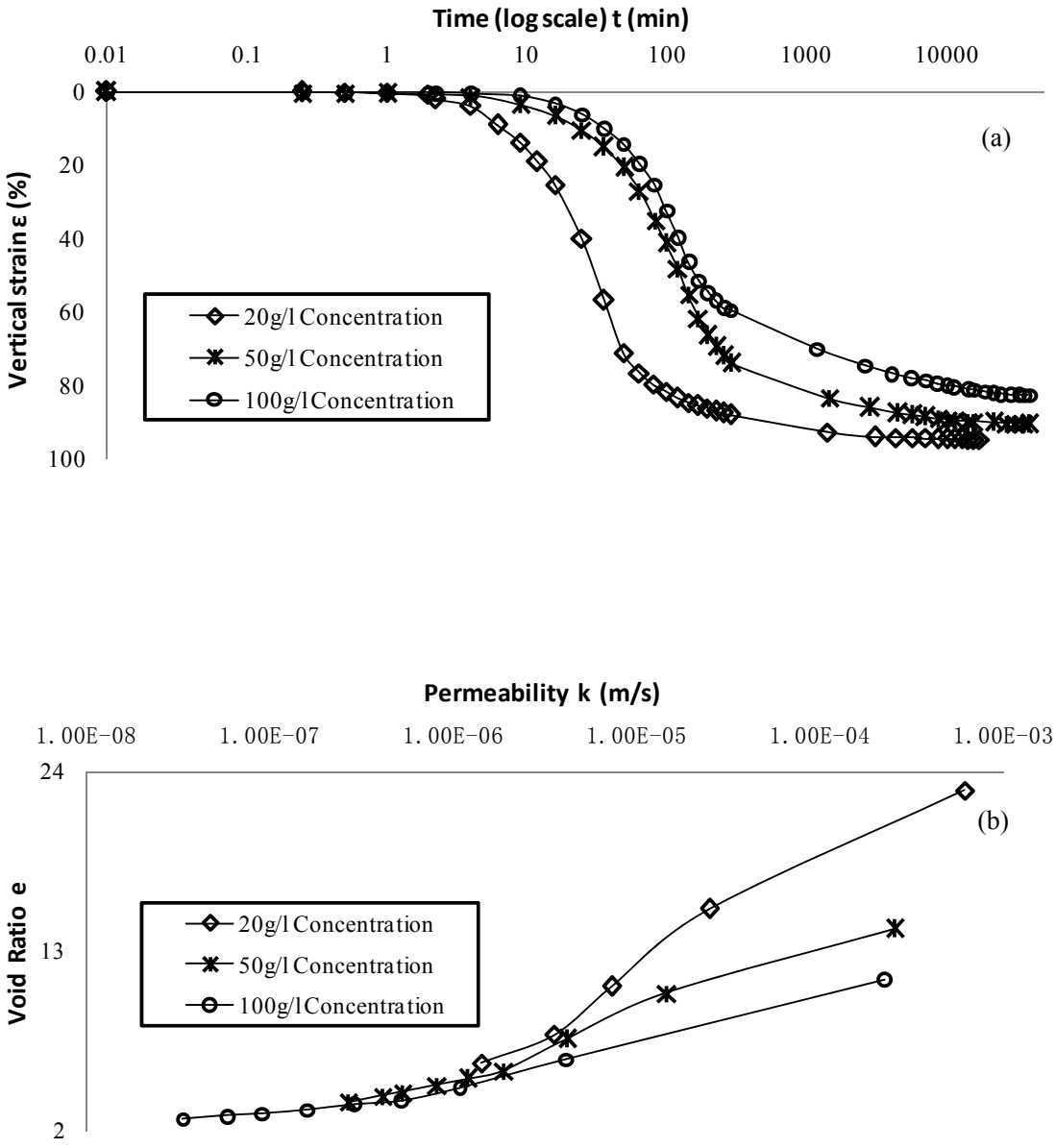

Figure 8.3 Consolidation of sample 19 - (a) relationships of vertical strain against elapse time and (b) relationships of permeability against void ratio

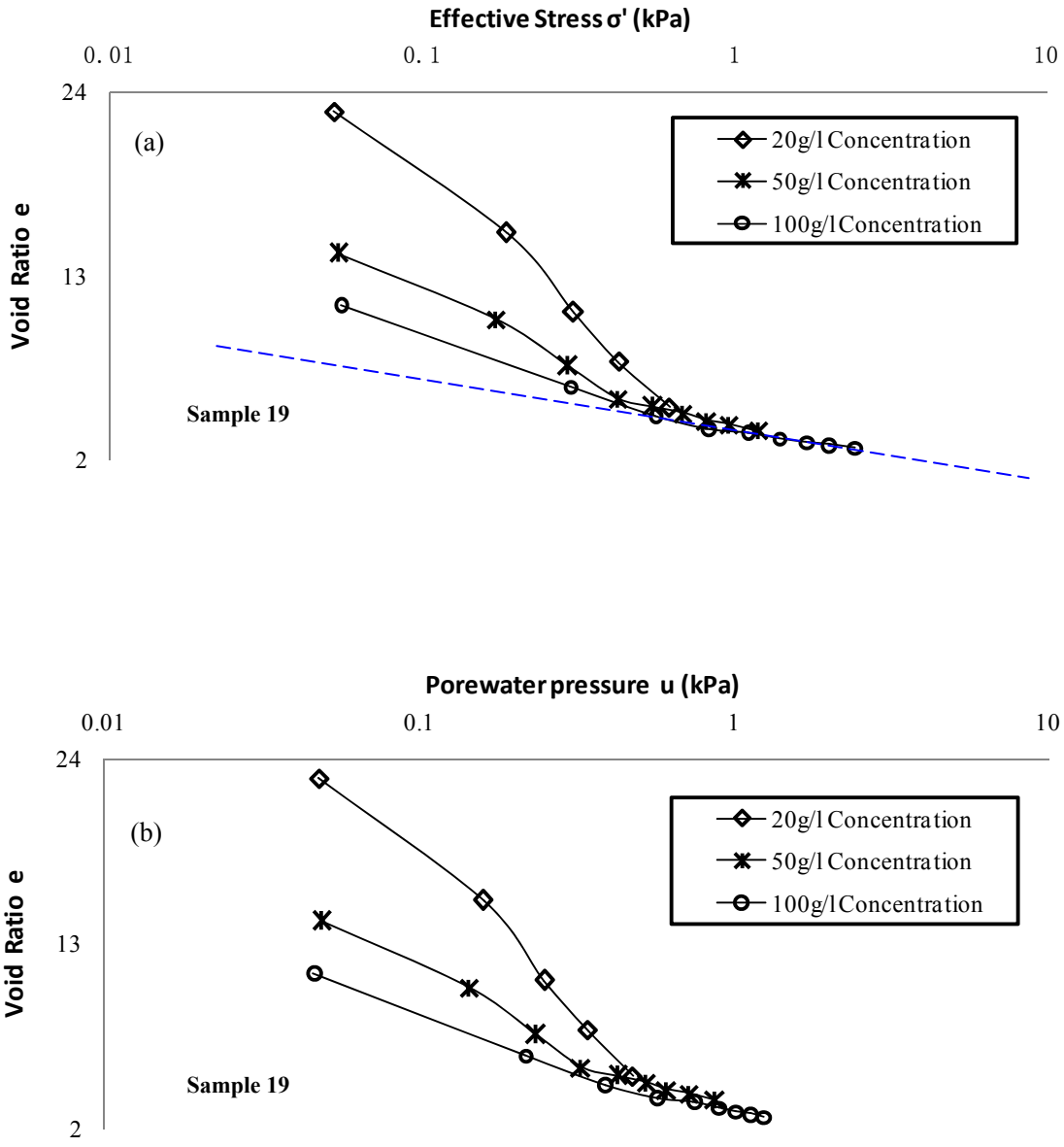

Figure 8.4 Consolidation of sample 19 - (a) relationships of effective stress against void ratio and (b) relationships of porewater pressure against void ratio

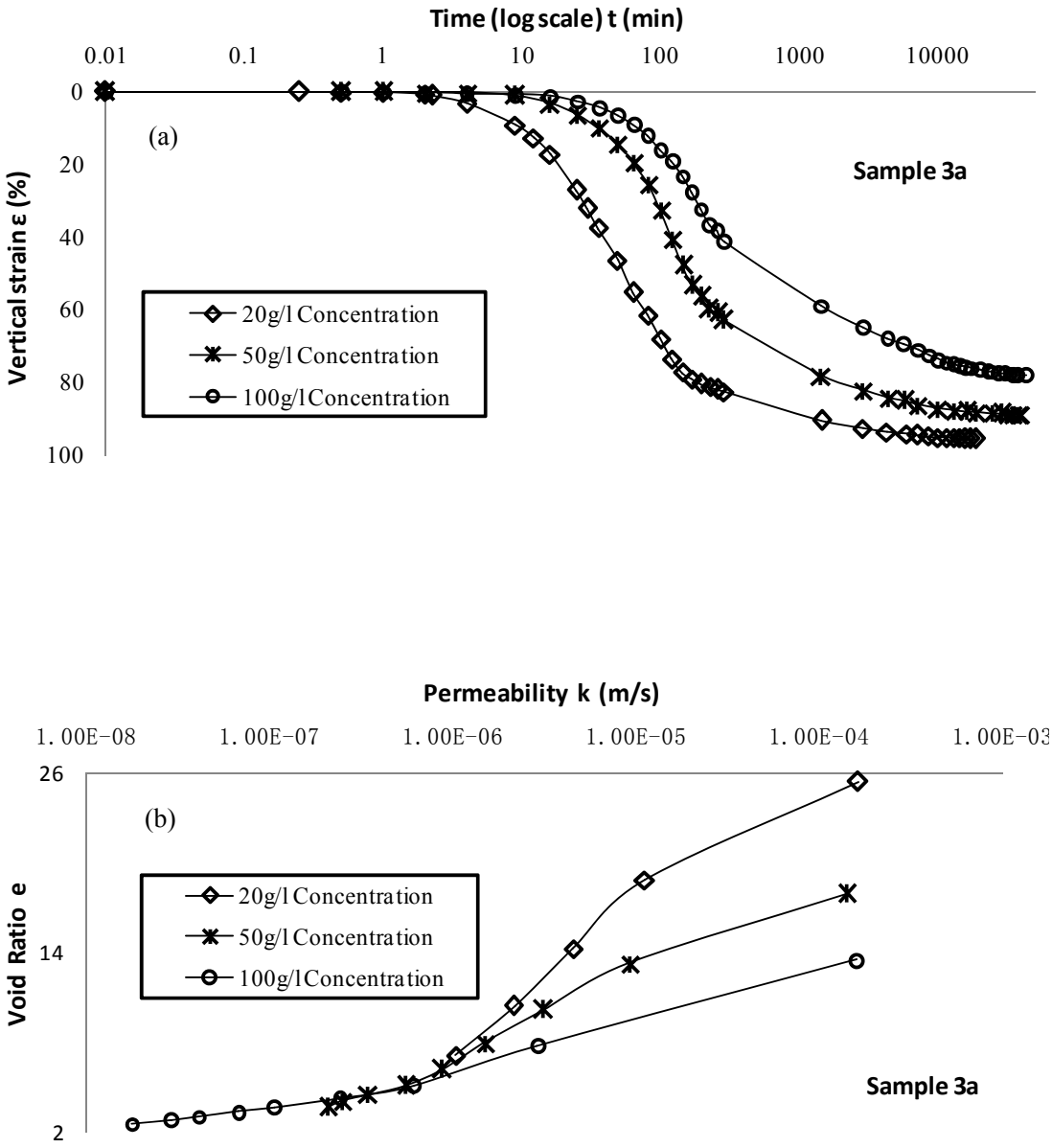

Figure 8.5 Consolidation of sample 3a - (a) relationships of vertical strain against elapse time and (b) relationships of permeability against void ratio

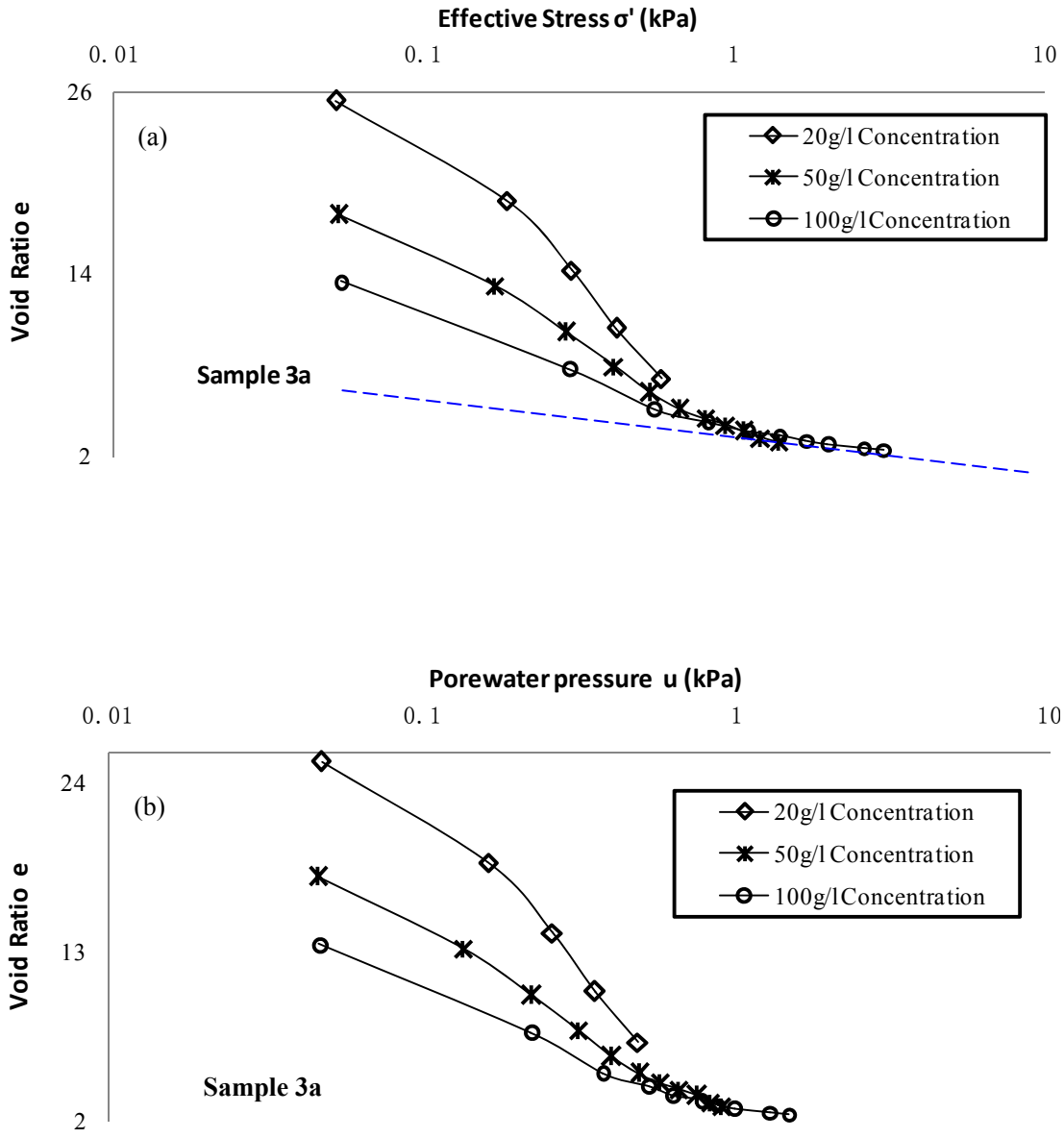

Figure 8.6 Consolidation of sample 3a - (a) relationships of effective stress against void ratio and (b) relationships of porewater pressure against void ratio

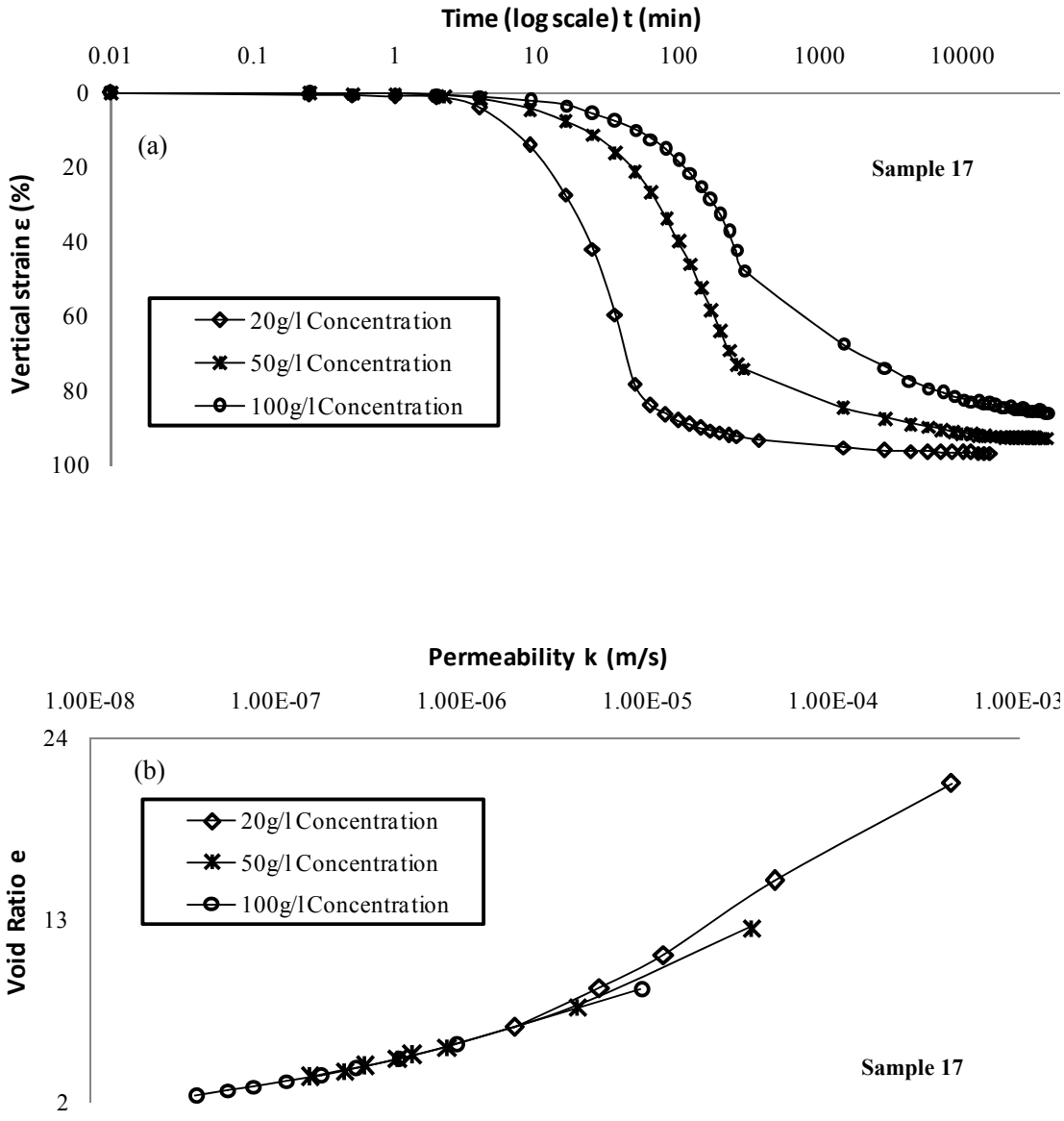

Figure 8.7 Consolidation of sample 17 - (a) relationships of vertical strain against elapse time and (b) relationships of permeability against void ratio

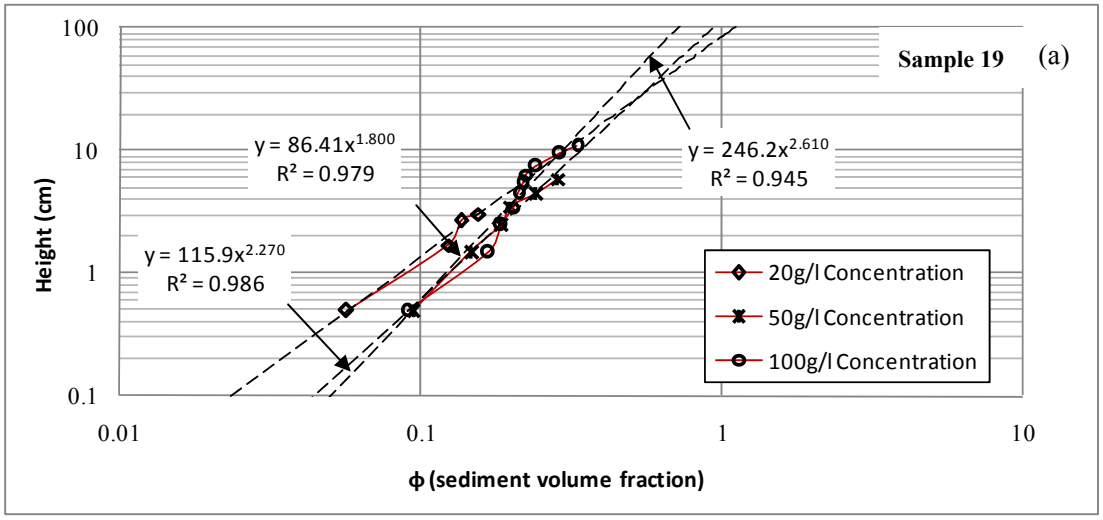

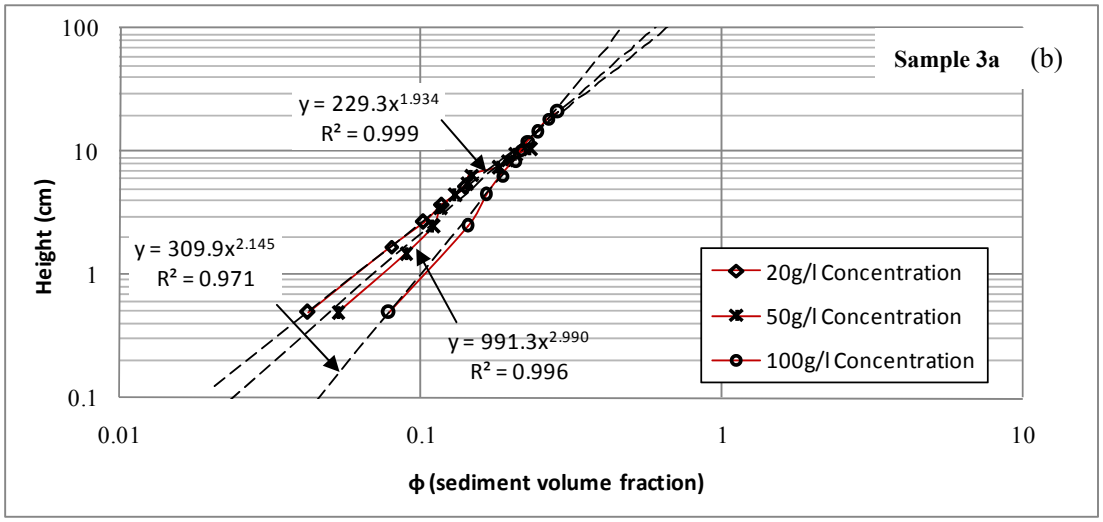

Figure 8.8 Relationships of sediment height against volume fraction after consolidation

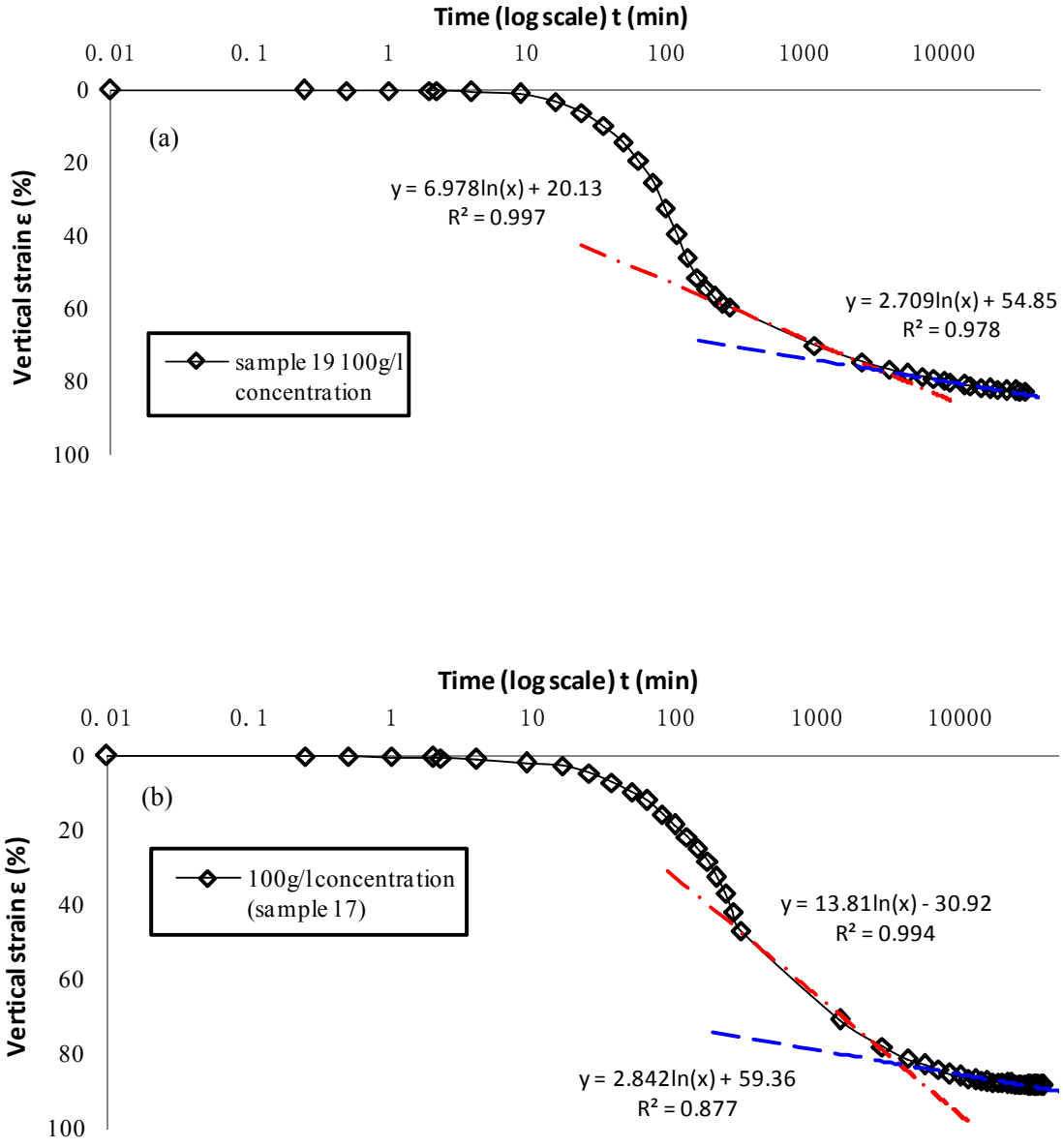

Figure 8.9 Curve fitting for relationships of vertical strain against elapse time in self-weight consolidation - (a) sample 19 with 100 g/l concentration and (b) sample 17 with 100 g/l concentration

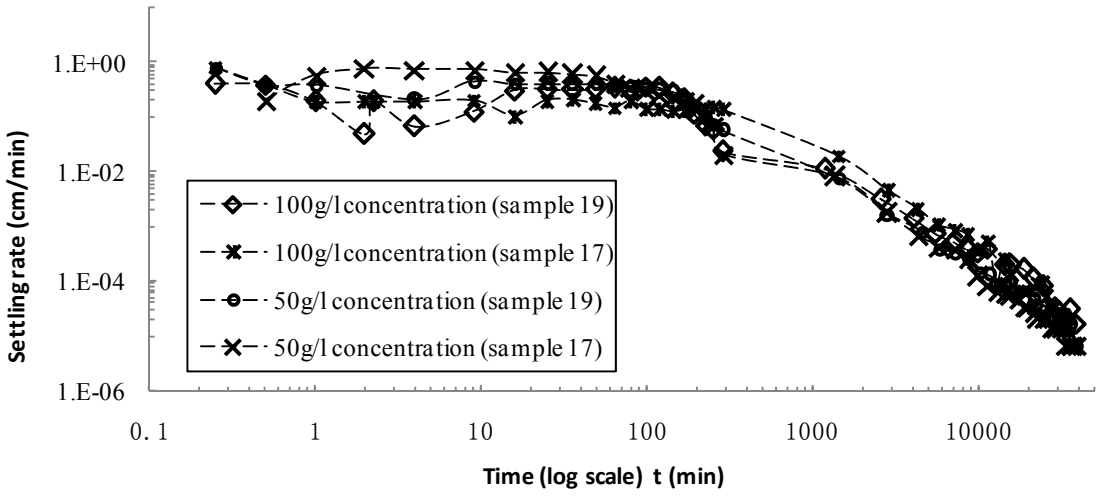

Figure 8.10 Relationships of settling rate against elapse time

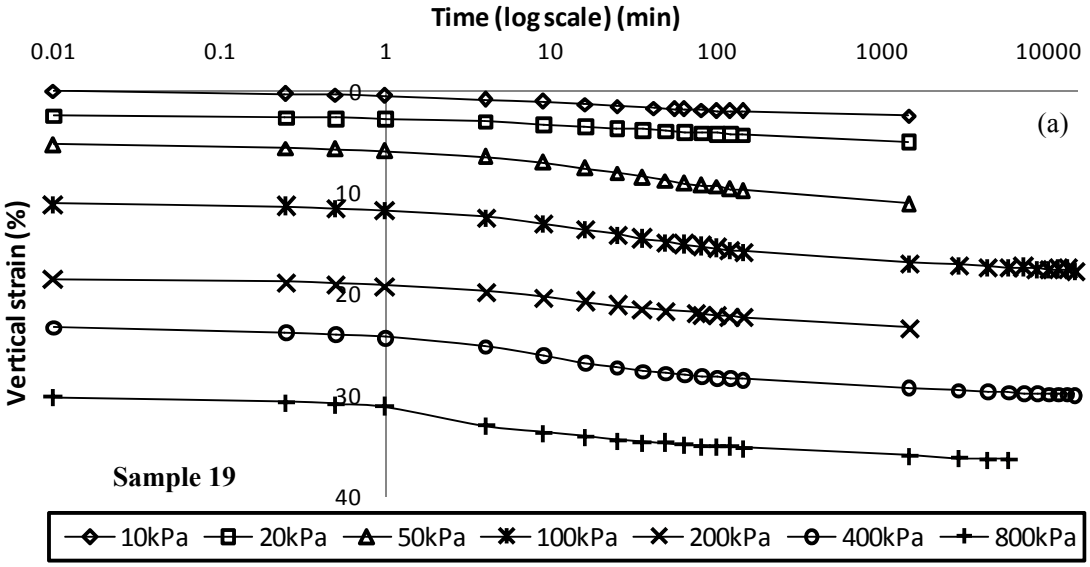

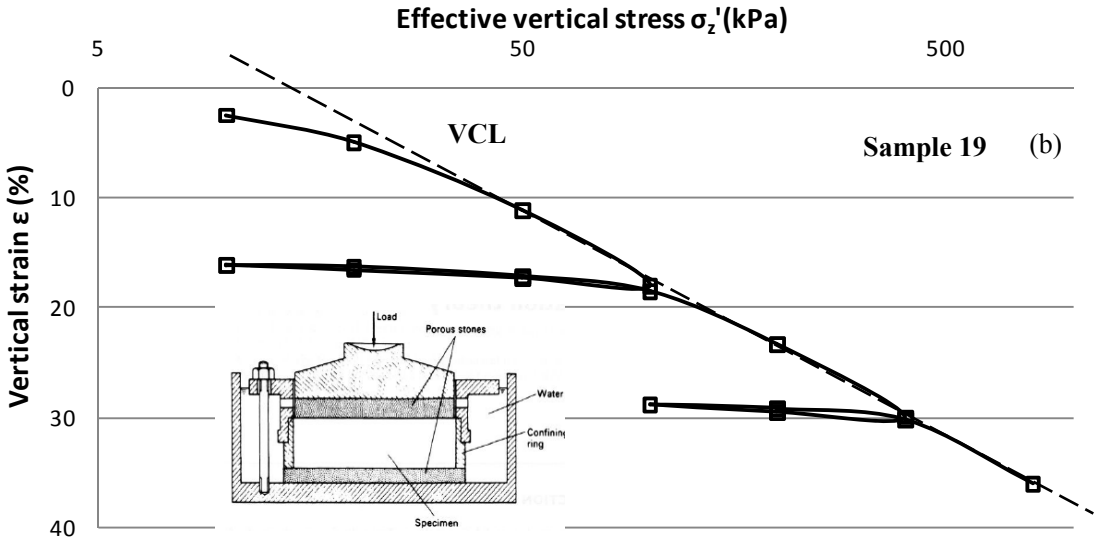

Figure 8.11 Oedometer consolidation of sample 19 - (a) relationships of vertical strain against elapse time under different normal pressure and (b) relationships of vertical strain against effective stress

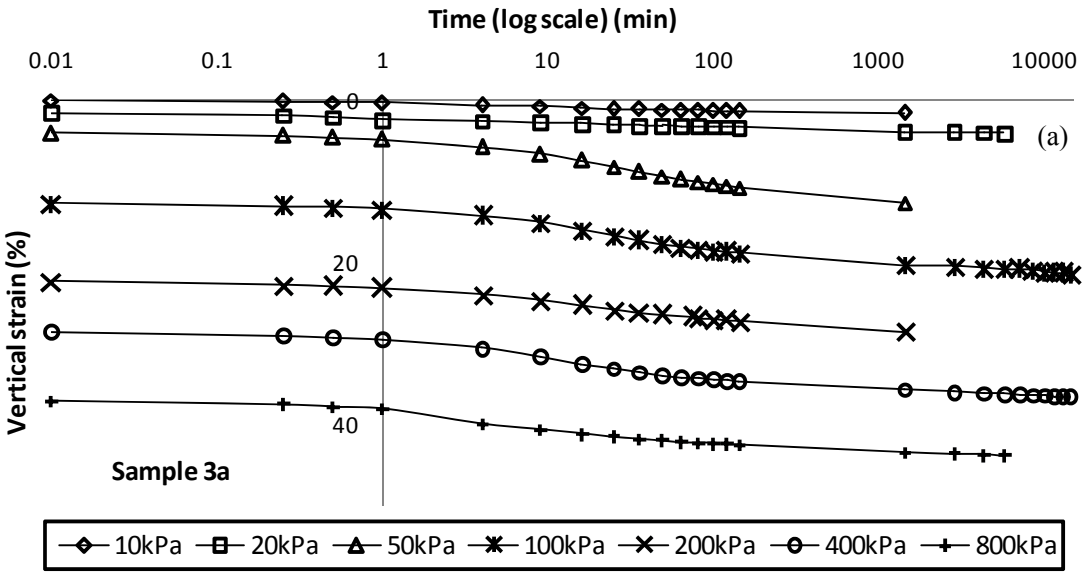

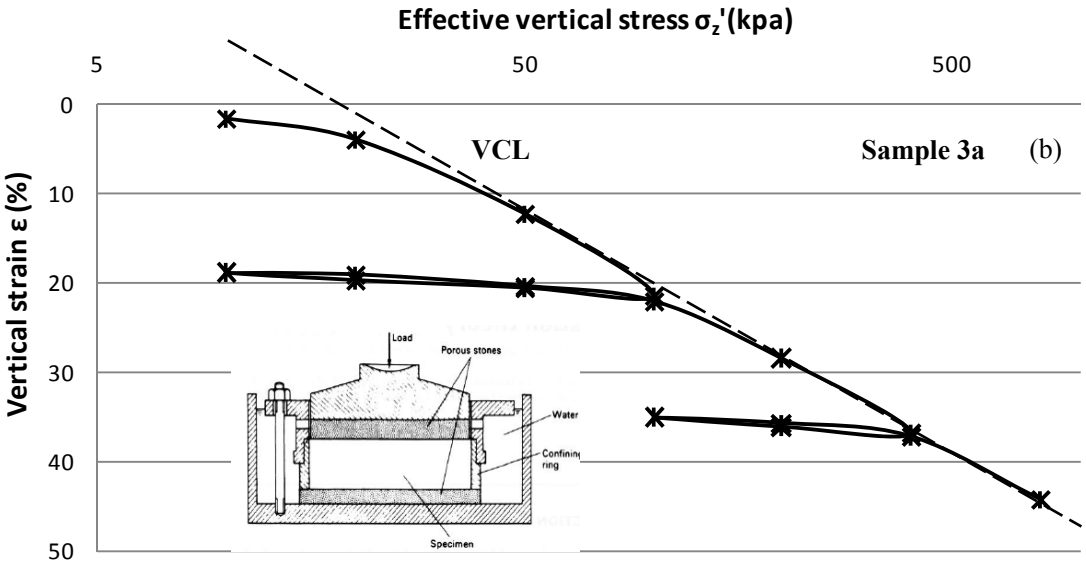

Figure 8.12 Oedometer consolidation of sample 3a - (a) relationships of vertical strain against elapse time under different normal pressure and (b) relationships of vertical strain against effective stress

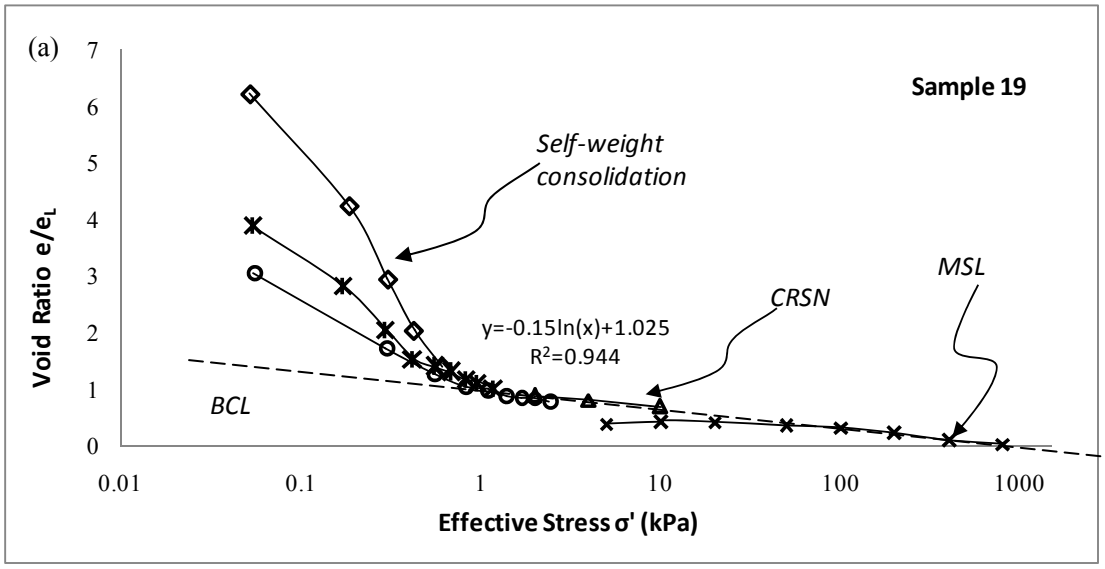

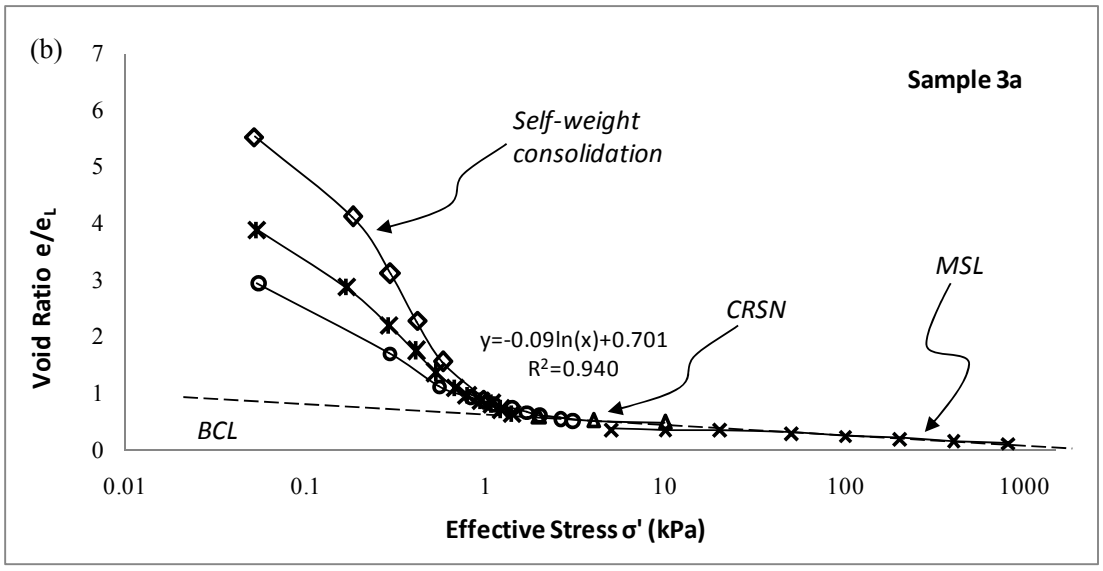

Figure 8.13 Complete relationships of effective stress against e_L/e - (a) sample 19 and (b) sample 3a

Chapter 9

1D EVPS Modeling and Verification

9.1 Introduction

In generally speaking, clayey soils exhibit more or less both creep and swelling. Clayey soils containing clay mineral montmorillonite show strong creep and swelling characteristics. Both creep and swelling characteristics have a significant influence on the deformation and failure of geotechnical structures. In this chapter, creep, swelling and strain rate effects in above chapters are observed and discussed. Based on the test data and a 1D Elastic Visco-Plastic (1D EVP) model developed by Yin and Graham (1989, 1994), a new 1D Elastic Visco-Plastic model considering both creep and swelling (called 1D EVPS) is proposed. The data from the multi-stage oedometer tests are used to calibrate the new model. Afterwards, the new model is used to simulate the step-changed constant rate of strain compression tests and make a comparison. In this way, the new model is verified. The new 1D EVPS is further used to simulate CRSN tests with a single strain rates, relaxation in creep or swelling region and constant rate of stressing tests. It is found that the new model can simulate well the strain (or stress) rate effects, loops in unloading/reloading, stress relaxation in the creep region or stress increase in the swelling region, which are all caused by both creep and swelling of the soil.

9.2 The Time-dependent Stress-Strain Behaviour of SMB

Basic properties of Bentonite and silica sand mixture has been discussed in Chapter 3. In this chapter, the sample of 30% Bentonite and 70% silica sand (by dry weight) was prepared in slurry with 1.5 times of liquid limit of these mixtures inside containers. The silica used was BS4550 Pt 5-fraction with diameter 150 μm to 300 μm while the bentonite had diameter 0.1 μm to 0.5 μm.

The bentonite and silica sand mixture was pre-consolidated in cylindrical tank. The basic properties of the sample are specific gravity G_s=2.57, liquid limit w_L =83%, plastic limit w_P =28%, plasticity index I_P =55%, initial water content w=124.5% and initial void ratio e_o=5.5 (after re-consolidation but before odometer testing).

(a) Multi-stage oedometer test

Odometer tests were carried out using Casagrande type of odometers. The loading was applied suddenly and in multi-stages. Subjected to the loading from 10 kPa to 800 kPa, the specimen had been under compression up to 44 days. At certain stress level the loading was reduced (reloading) and increased again (reloading). The multi-staged oedometer results in vertical strain versus time (log scale) are presented in: Figure 9.1(a). The relationships of the axial strain (ε_z) against vertical effective stress ($\sigma_z^{'}$) in log scale at standard 24 h are plotted in Figure 9.1(d).

(b) CRSN test

To study the strain rates effect on the one-dimensional compressibility, a

stress-strain CRSN result on 70% bentonite specimen is illustrated in Figure 9.2. The effective vertical stress in a CRSN test is calculated by the total vertical stress minus two thirds of the porewater pressure measured.

9.3 Development of a New 1D EVPS Model in 1D Straining Condition

The new model is based on the previous 1D EVP model proposed by Yin (1990) and Yin and Graham (1989 and 1994). Some important concepts such as "elastic" time line, "reference" time line, and "equivalent" time lines are shown in Figure 9.3 in the plot of the vertical effective stress $\sigma_z^{'}$ in ln-scale and vertical strain ε_z. It is noted in Figure 9.3 that the stress is plotted in natural log-scale. It is well known that the compression in over-consolidated range is approximated as a straight line and expressed as:

$$\varepsilon_z^e = \varepsilon_{zi} + \frac{\kappa}{V} \ln \frac{\sigma_z^{'}}{\sigma_{zi}^{'}} \tag{9-1}$$

where $V = 1 + e_o$, called specific volume and e_o is the initial void ratio; κ / V is the slope; $(\varepsilon_{zi}, \sigma_{zi}^{'})$ is a point on the κ / V line. The strain ε_z^e in equation (9-1) is considered elastic. The elastic strain rate is obtained by differentiating equation (9-1):

$$\dot{\varepsilon}_z^e = \frac{\kappa}{V} \frac{\dot{\sigma}_z^{'}}{\sigma_z^{'}} \tag{9-2}$$

As explained by Yin and Graham (1989, 1994), a reference time line with a slope λ / V is introduced as:

$$\varepsilon_z^{rc} = \varepsilon_{zo}^{rc} + \frac{\lambda}{V} \ln \frac{\sigma_z^{'}}{\sigma_{zo}^{'rc}} \tag{9-3}$$

where λ / V is the slope of the reference time line; $(\varepsilon_{zo}^{rc}, \sigma_{zo}^{'rc})$ is a point on the λ / V line.

The creep is described (Yin and Graham, 1989 and 1994) by:

$$\varepsilon_z^c = \frac{\psi^c}{V} \ln \frac{t_e^c + t_o^c}{t_o^c} \tag{9-4}$$

where ψ^v / V is the slope of the plot of ε_z^c and ln (t_e^c); t_e^c is the equivalent time defined by Yin and Graham (1989, 1994) and be equal (or related) to the normal duration time *t*; t_o^c is a parameter with unit of time to mark the beginning of creep.

The creep rate is obtained by differentiating equation (9-4):

$$\dot{\varepsilon}_z^c = \frac{d\varepsilon_z^c}{dt_e^c} = \frac{\psi^c}{V} \frac{1}{t_e^c + t_o^c} \tag{9-5}$$

According to the definition of the equivalent time and the reference time line (Yin and Graham, 1989 and 1994), the total strain at any point in the creep region in Figure 9.3 is considered to be the strain occurred for the soil to creep from the reference time line to this point, that is:

$$\varepsilon_z = \varepsilon_z^{rc} + \varepsilon_z^c = \varepsilon_{zo}^{rc} + \frac{\lambda}{V} \ln \frac{\sigma_z^{'}}{\sigma_{zo}^{'rc}} + \frac{\psi^c}{V} \ln \frac{t_e^c + t_o^c}{t_o^c} \tag{9-6}$$

From equation (9-6), the equivalent time can be expressed as:

$$\frac{\psi^c}{V}\ln\frac{t_e^c+t_o^c}{t_o^c}=\varepsilon_z-\varepsilon_{zo}^{rc}-\frac{\lambda}{V}\ln\frac{\sigma_z^{'}}{\sigma_{zo}^{'rc}}$$

$$\frac{t_e^c+t_o^c}{t_o^c}=\exp[\left(\varepsilon_z-\varepsilon_{zo}^{rc}\right)\frac{V}{\psi^c}]\left(\frac{\sigma_z^{'}}{\sigma_{zo}^{'rc}}\right)^{-\frac{\lambda}{\psi^c}} \tag{9-7}$$

$$\frac{1}{t_e^c+t_o^c}=\frac{1}{t_o^c}\exp[-\left(\varepsilon_z-\varepsilon_{zo}^{rc}\right)\frac{V}{\psi^c}]\left(\frac{\sigma_z^{'}}{\sigma_{zo}^{'rc}}\right)^{\frac{\lambda}{\psi^c}}$$

When the soil has the swelling potential, when the soil specimen is subjected a large unloading to a point as shown in Figure 3, the specimen will have swelling, that is, upward movement. This swelling is similar to the creep (down), but in the opposite direction (up) and is described as:

$$\varepsilon_z^s=-\frac{\psi^s}{V}\ln\frac{t_e^s+t_o^s}{t_o^s} \tag{9-8}$$

where ψ^s/V is the swelling parameter and may be called the swelling coefficient; t_o^s is a swelling parameter; t_e^s is the "equivalent" time for swelling strain (Yin and Graham, 1994). The swelling here refers to the swelling after the rebounding process. Since the logarithmic function is used to describe swelling, swelling will come to infinity. If a soil has the same creep and swelling potential, a time-independent line will be generalized in Figure 9-1. Differentiating equation (9-6) with the "equivalent" time:

$$\dot{\varepsilon}_z^s=\frac{d\varepsilon_z^s}{dt_e^s}=-\frac{\psi^s}{V}\frac{1}{t_e^s+t_o^s} \tag{9-9}$$

As shown in Figure 9.3, the slope of the reference time line for swelling is assumed to be the same as that of the reference time line for creep. According to the definition of the equivalent time and the reference time line (Yin and Graham, 1989

and 1994), the total strain at any point in the swelling region is considered to be the strain occurred for the soil to swell from the reference time line to this point, that is:

$$\varepsilon_z = \varepsilon_z^{rs} + \varepsilon_z^{s} = \varepsilon_{zo}^{rs} + \frac{\lambda}{V}\ln\frac{\sigma_z^{'}}{\sigma_{zc}^{'rs}} - \frac{\psi^s}{V}\ln\frac{t_e^s + t_o^s}{t_o^s} \tag{9-10}$$

From equation (9-8), the equivalent time can be expressed as:

$$\frac{\psi_s}{V}\ln\frac{t_e^s + t_o^s}{t_o^s} = -(\varepsilon_z - \varepsilon_{zo}^{rs}) + \frac{\lambda}{V}\ln\frac{\sigma_z^{'}}{\sigma_{zo}^{'rs}} \tag{9-11}$$

From the above, we have:

$$\frac{1}{t_e^s + t_o^s} = \frac{1}{t_o^s}\exp[\left(\varepsilon_z - \varepsilon_{zo}^{rs}\right)\frac{V}{\psi^s}]\left(\frac{\sigma_z^{'}}{\sigma_{zo}^{'rs}}\right)^{-\frac{\lambda}{\psi^s}} \tag{9-12}$$

One new feature in the new 1D model is addition of the strain rate due to swelling and related mathematical equations. The total strain rate $\dot{\varepsilon}_z$ is the sum of elastic strain rate $\dot{\varepsilon}_z^e$, visco-plastic creep strain rate, $\dot{\varepsilon}_z^c$ and swelling strain rate, $\dot{\varepsilon}_z^s$ (all compression as positive "+"):

$$\dot{\varepsilon}_z = \dot{\varepsilon}_z^e + \dot{\varepsilon}_z^c + \dot{\varepsilon}_z^s \tag{9-13}$$

Using equations (9-2), (9-5) and (9-9), equation (9-13) can be written as:

$$\dot{\varepsilon}_z = \frac{\kappa}{V}\frac{\dot{\sigma}_z^{'}}{\sigma_z^{'}} + \frac{\psi^c}{V}\frac{1}{t_e^c + t_o^c} - \frac{\psi^s}{V}\frac{1}{t_e^s + t_o^s} \tag{9-14}$$

Using equation (9-7) for $\frac{1}{t_e^c + t_o^c}$ and equation (9-12) for $\frac{1}{t_e^s + t_o^s}$, equation. (9-14) can be expressed as:

$$\begin{aligned}\dot{\varepsilon}_z = {} & \frac{\kappa}{V}\frac{\dot{\sigma}_z^{'}}{\sigma_z^{'}} + \frac{\psi^c}{V}\frac{1}{t_o^c}\exp[-\left(\varepsilon_z - \varepsilon_{zo}^{rc}\right)\frac{V}{\psi^c}]\left(\frac{\sigma_z^{'}}{\sigma_{zo}^{'rc}}\right)^{\frac{\lambda}{\psi^c}} \\ & - \frac{\psi^s}{V}\frac{1}{t_o^s}\exp[\left(\varepsilon_z - \varepsilon_{zo}^{rs}\right)\frac{V}{\psi^s}]\left(\frac{\sigma_z^{'}}{\sigma_{zo}^{'rs}}\right)^{-\frac{\lambda}{\psi^s}}\end{aligned} \tag{9-15}$$

Equation (9-15) is a general constitutive model for the time-dependent stress-strain behaviour of full saturated soils exhibiting both creep and swelling in 1D straining. This model is valid for all loading conditions such as constant rate of strain (CRSN) loading, relaxation, unloading/reloading, etc. This new model may be called one-dimensional Elastic Visco-Plastic model considering Swelling, namely 1D EVPS model.

9.4 Calibration of the 1D EVPS Model

In the development of the earlier one-dimensional Elastic Visco-Plastic (1D EVP) model, Yin and Graham (1989, 1994) proposed a rigorous method with complicated relationships for determining all model parameters. Later, Yin and Graham (1996, 1999) proposed a simple method for determination of all these parameters. For easy determination of the model parameters and easy applications of the new model, the same simple method is used for determining all parameters as in Yin and Graham (1996, 1999). The method and steps for determining all parameters are presented as follows.

Firstly, data from the multi-staged loading creep, unloading swelling and reloading test data in 1D straining will be used to determine all parameters in the new 1D EVPS model. The method used is similar to that in Yin (1990), Yin and Graham (1989, 1994). After this calibration, the new 1D EVPS will be used to simulate the stress-strain behavior of step-changed constant rate of strain tests in

oedometer (1D straining) condition. The simulated values are compared with data from the tests. In this way, the validation of this new model is examined.

It is noted that each vertical strain in Figure 9.1(d) is the strain at the end of 24 hour duration (1 day) under each vertical loading (vertical effective stress) in Figure 9.1(a) as one of the standard test procedures. The following method is based on this type of tests. This means that the stress-strain relationship in Figure 9.1(d) has 24 hour duration (1 day) already under each vertical loading (vertical effective stress).

(a) κ / V

The stress-strain in the over-consolidated range is very much elastic. In case, there is no over-consolidated range, the stress-strain in the unloading/reloading range is largely elastic. Fitting equation (9-1) to the ln (stress)-strain in the over-consolidated range or the unloading/reloading range, the parameter κ / V can be determined. If the stress is in log-scale, equation (9-1) is written as: $\varepsilon_z^e = \varepsilon_{zi} + \frac{\kappa}{V \log e} \log \frac{\sigma_z^{'}}{\sigma_{zi}^{'}}$. Clarified in Figure 9.4 using oedometer data, the slope is $\kappa / V / \log e = C_e / V$. It is well known that the compression index in the over-consolidated stage or unloading/reloading stage is C_e. The relationships are:

$$
\begin{aligned}
&\because C_e = \frac{-\Delta e}{\Delta \log \sigma_z^{'}};\ \frac{C_e}{V} = \frac{\Delta \varepsilon_z}{\Delta \log \sigma_z^{'}} \\
&\frac{\kappa}{V} = \frac{\Delta \varepsilon_z^e}{\Delta \ln \sigma_z^{'}} = \frac{-\Delta e}{V \Delta \ln \sigma_z^{'}} = \frac{-\Delta e \times 0.434}{V \Delta \log \sigma_z^{'}} = \frac{0.434}{V} \frac{-\Delta e}{\Delta \log \sigma_z^{'}} = \frac{0.434}{V} C_e \\
&\therefore \kappa = 0.434 C_e \\
&\frac{\kappa}{V} = 0.434 \frac{C_e}{V}
\end{aligned}
\tag{9-16}
$$

Based on Figure 9.4, $\kappa / V = 0.434 C_e / V = 0.014$. It is noted that C_e / V has been subjected a 24 hour loading duration.

(b) λ / V **and** $(\varepsilon_{zo}^{rc}, \sigma_{zo}^{'rc})$, $(\varepsilon_{zo}^{rs}, \sigma_{zo}^{'rs})$

As shown in Figure 9.4, a straight line is plotted along points in the normally consolidated ranges. The slope is $\lambda / V / \log e = C_c / V$. It is well known that the compression index in the normally consolidated stage is C_c. The relationships are:

$$\because C_c = \frac{-\Delta e}{\Delta \log \sigma_z^{'}};\ \frac{C_c}{V} = \frac{\Delta \varepsilon_z}{\Delta \log \sigma_z^{'}}$$

$$\frac{\lambda}{V} = \frac{\Delta \varepsilon_z}{\Delta \ln \sigma_z^{'}} = \frac{-\Delta e}{V \Delta \ln \sigma_z^{'}} = \frac{-\Delta e \times 0.434}{V \Delta \log \sigma_z^{'}} = \frac{0.434}{V} \frac{-\Delta e}{\Delta \log \sigma_z^{'}} = \frac{0.434}{V} C_c \quad (9\text{-}17)$$

$$\therefore \lambda = 0.434 C_c$$

$$\frac{\lambda}{V} = 0.434 \frac{C_c}{V}$$

From Figure 9.4, the slope is $C_c / V = 0.38$, so that $\lambda / V = 0.434 C_c / V = 0.16$. The interception point from the line fit in Figure 9.4 is $\sigma_{zo}^{'rc} = 16.5\ kPa$ and $\varepsilon_{zo}^{rc} = 0$. Similarly, reference line with the same slope is used to define swelling. It is found from Figure 9.4 that $\sigma_{zo}^{'rs}$ =3 kPa and $\varepsilon_{zo}^{rs} = 0$. It is noted that C_c / V has been subjected a 24 hour loading duration.

(c) ψ^c / V **and** t_o^c; ψ^s / V **and** t_o^s

To determine the two creep parameters (ψ^c / V and t_o^c) and the two swelling parameters (ψ^s / V and t_o^s), both the creep test duration and the swelling test duration shall last as longer as possible. As shown in Figure 9.1, these tests last for more than 10000 mins.

In equation (9-4), t_o^c is a creep parameter and is related to the creep rate at the starting point in the reference time line in the creep region (Yin and Graham, 1989 and 1994). Based on the previous study by (Yin and Graham, 1989, 1994, 1999a), if the stress-strain relationship in Figure 9.4 has 24 hour duration (1 day) already under each vertical loading (vertical effective stress), the creep parameter t_o^c can be taken as $t_o^c = 24$ hours .

Equation (9-4) with $t_o^c = 24$ hours is then used to fit the data in Figure 9.1(a) from the oedometer creep data to find ψ^c / V. In this fitting, the equivalent time t_e^c is equation (9-4) is taken as $t_e^c = t - t_o^c = t - 24 \text{ hours} = t - 1440 \text{ mins}$ in which t is the real duration under this vertical load. The curve fitting using equation (9-4) with $t_o^c = 24$ hours is shown in Figure 9.5(a) from which ψ^c / V is then determined as 0.00801.

Similarly, equation (9-8) with $t_o^s = 24 \text{ hours} = 1440 \text{ mins}$ is used to fit swelling data as shown in Figure 9.1(b). It is found that ψ^s / V to be 0.00704. It is noted that the equivalent time t_e^s for swelling in equation (9-8) is taken as $t_e^s = t - t_o^s = t - 24 \text{ hours} = t - 1440 \text{ mins}$, in which t is the real duration under this vertical load.

So far, all the parameters in equation (9-14) have been determined.

9.5 Simulation of 1D Constant Rate of Strain (CRSN) Test

Since equation (9-15) cannot be solved analytically, the Runge-Kutta method is chosen for its numerical solution. In the CRSN test, the strain rate $\dot{\varepsilon}_z$ is under

control and is kept constant ($\dot{\varepsilon}_z = C$). Staining starts from point ($\sigma'_{z,i}, \varepsilon_{z,i}$) and continues for a duration Δt. The total strain ε_z amounts to $C \times t$ at any time. Substituting all the parameters determined in the above section, equation (9-15) can be solved numerically for the stress-strain behaviour relation of the SMB. With varied strain rates in CRSN tests, the strain rate dependent behavior can be simulated. In this case, the final stress-strain state under the past CRSN loading with a strain rate is used for initializing a CRSN loading with a new strain rate. Figure 9.6 shows the simulation of a CRSN test with stepped changed strain rate and the corresponding laboratory results. The simulation agrees well with the test data. The simulation of CRSN tests with four different constant strain rates are better illustrated in Figure 9.7. The simulation using the 1D EVPS model can interpret well the strain rate effect on the stress-strain behavior in a CRSN condition, in which, at a given strain, the higher the strain rate, the higher the effective stress. Actually in stepwise CRSN tests, the strain rate effect is highly dependent on the ψ^c / V value, which indeed denotes the creep behavior of the soil. When the creep parameter ψ^c / V is small, strain rate effects are therefore reduced (Yin and Graham, 1994).

The swelling related parameter ψ^s / V, however, stands for the reverse behavior to creep. Swelling continues to occur for a long time under a given constant stress and after the elastic rebounding. The higher the value of ψ^s / V, the larger the swelling strain, and the more obvious the strain rate effect.

For examining more strain rate effects of saturated clays, under a given vertical

strain of 12%, the vertical effective stress is plotted against strain rate in Figure 9.8. In Figure 9.8, the creep parameter ψ^c / V is changed from 0.00801 to 0.004 and the swelling parameter ψ^s / V is charged from 0.00704 to 0.004. It is seen from Figure 9.8 that when the creep parameter is small (0.004), the strain rate effect is reduced. When ψ^c / V comes to zero, the behaviour degenerates to a simple elasto-plastic one (Yin and Graham, 1989 and 1994). As for the swelling parameter ψ^s / V, a small value of ψ^s / V (0.004) makes the stress higher under a low strain rate and reduces the strain rate effect. In other words, the swelling has a counter effect on the creep.

9.6 Analytical Solutions from the 1D EVPS model for Relaxation

When the soil is under relaxation condition, the total strain rate is zero. Equation (9-15) can be rewritten as:

$$-\frac{\kappa}{V}\frac{\dot{\sigma}_z^{'}}{\sigma_z^{'}} = \frac{\psi^c}{V}\frac{1}{t_o^c}\exp[-\left(\varepsilon_z-\varepsilon_{zo}^{rc}\right)\frac{V}{\psi^c}]\left(\frac{\sigma_z^{'}}{\sigma_{zo}^{'rc}}\right)^{\frac{\lambda}{\psi^c}} - \frac{\psi^s}{V}\frac{1}{t_o^s}\exp[\left(\varepsilon_z-\varepsilon_{zo}^{rs}\right)\frac{V}{\psi^s}]\left(\frac{\sigma_z^{'}}{\sigma_{zo}^{'rs}}\right)^{-\frac{\lambda}{\psi^s}} \tag{9-18}$$

In general form, the equation can be written as:

$$Ay^{'} = By^m - Cy^n \tag{9-19}$$

where m>n and the factor B and C are both tiny value.

Using change of variables, equation (9-17) can be further transformed to:

$$z^{'} = \frac{B(1-n)}{A} - \frac{C(1-n)}{A}z^{m-1} \tag{9-20}$$

Assume $\frac{B(1-n)}{A}=k$ and $\frac{C(1-n)}{A}=a$, when $\left|\frac{C(1-n)}{A}\right|<0.01$, the perturbation method is applied to solve the function. Using the Taylor series expansion and truncating at the third item (refer to Appendix for detail), we have

$$z=(kt)^{m-1}+\frac{ak^{m-1}t^{m}}{m}+\frac{2a^{2}(m-1)k^{m-1}t^{m+1}}{m(1+m)}+\frac{6a^{3}(m-1)(m-2)k^{m-1}t^{m+2}}{m(1+m)(2+m)} \quad (9\text{-}21)$$

Input the parameter in the EVPS model, finally equation (9-18) is expressed as:

$$\begin{aligned}
(\sigma_z')^{\psi^c/(\lambda-\psi^c)} &= \frac{\psi^c\psi^s(\lambda/\psi^c-1)(\sigma_{zo}'^{rc})^{-\lambda/\psi^c}t^{\lambda/\psi^s}}{t_o^c\kappa\lambda}\cdot\exp(-(\varepsilon_z-\varepsilon_{zo}^{rc})V/\psi^c)\cdot \\
&\left[\frac{\psi^s(1-\lambda/\psi^c)\exp(-(\varepsilon_z-\varepsilon_{zo}^{rs})V/\psi^s)(\sigma_{zo}'^{rs})^{-\lambda/\psi^s}}{t_o^s\kappa}\right]^{\lambda/\psi^s-1} \\
&+\frac{2(\psi^c)^2\psi^s(\lambda/\psi^s-1)(\lambda/\psi^c-1)^2(\sigma_{zo}'^{rc})^{-2\lambda/\psi^c}t^{1+\lambda/\psi^s}}{(t_o^c)^2\kappa^2\lambda(1+\lambda/\psi^s)} \\
&\cdot\exp(2(\varepsilon_z-\varepsilon_{zo}^{rc})V/\psi^c)\cdot\left[\frac{\psi^s(1-\lambda/\psi^c)\exp(-(\varepsilon_z-\varepsilon_{zo}^{rs})V/\psi^s)(\sigma_{zo}'^{rs})^{\lambda/\psi^s}}{t_o^s\kappa}\right]^{\lambda/\psi^s-1} \\
&+\frac{6(\psi^c)^3\psi^s(\lambda/\psi^s-2)(\lambda/\psi^c-1)^3(\sigma_{zo}'^{rc})^{-3\lambda/\psi^c}t^{2+\lambda/\psi^s}}{(t_o^c)^3\kappa^3\lambda(1+\lambda/\psi^s)(2+\lambda/\psi^s)}\cdot\exp(-3(\varepsilon_z-\varepsilon_{zo}^{rc})V/\psi^c) \\
&\cdot\left[\frac{\psi^s(1-\lambda/\psi^c)\exp(-(\varepsilon_z-\varepsilon_{zo}^{rs})V/\psi^s)(\sigma_{zo}'^{rs})^{\lambda/\psi^s}}{t_o^s\kappa}\right]^{\lambda/\psi^s-1} \\
&+\left[\frac{\psi^s(1-\lambda/\psi^c)\exp(-(\varepsilon_z-\varepsilon_{zo}^{rs})V/\psi^s)(\sigma_{zo}'^{rs})^{-\lambda/\psi^s}}{t_o^s\kappa}t\right]^{\lambda/\psi^s-1}
\end{aligned} \quad (9\text{-}22)$$

The main feature of EVPS model is that the total strain rate $\dot{\varepsilon}_z$ is sum of three parts including swelling strain rate. Two viscous parameters are used to define the creep strain and swelling strain. The proposed method in section 9.4 is to apply a mathematical function to fit t and ε_z^{tp} data after dissipation of excess porewater pressure under a given vertical stress. In this way critical parameters ψ^c/V and t_o^c, ψ^s/V and t_o^s in equation (9-12) have been determined. Next, the EVPS

model for 1D relaxation with known parameters is employed to simulate the behaviors of soils in relaxation tests.

9.7 Simulation of Stress Relaxation in Creep Region and Stress Increase in Swelling Region

In the past, investigators used relaxation tests to study time-dependent effects in addition to the conventional creep tests. Relaxation tests can represent an important alternative way for studying rheological behaviour of a material (Lacerda and Houston, 1973; Ladanyi and Benyamina, 1995; Yin and Graham, 1994). Meanwhile, the parameters of creep can be effectively estimated during relaxation process (Lacerda and Houston, 1973). To some extent, a relaxation test is more convenient to perform to study time-dependent stress-strain behaviours than using a conventional creep test, especially in failure states because in the latter a failure state only lasts for minutes (Ladanyi and Benyamina, 1995).

In modeling, relaxation is actually a special CRSN test with zero strain rate ($\dot{\varepsilon}_z = 0$). Yin and Graham (1994) adopted a 1D EVP model to simulate relaxation tests. Results showed that soil behavior is very sensitive to the creep parameters. In a relaxation test in the creep region, the height of the specimen is kept constant, and the effective stress is observed to decrease with time. However, in a relaxation test in the swelling region, similarly under a given height, the effective stress is observed to increase with time. In this way, the so-called “swelling pressure” can be obtained.

(a) Simulation of relaxation on SMB soils

The simulated results of two relaxation tests in the creep region and one relaxation test in the swelling region on SMB 70 are shown in Figure 9.9. It is noted that in a relaxation test in the creep region, the SMB specimen is compressed at a CRSN of $\dot{\varepsilon}_z = 10^{-5}\ 1/\text{sec}$ and then relaxation starts. It is seen in Figure 9.9 that the vertical effective stress decreases with time. In the second relaxation test in the creep region, the SMB specimen is compressed at a faster CRSN of $\dot{\varepsilon}_z = 10^{-4}\ 1/\text{sec}$ and then relaxation starts. It is seen in Figure 9.9 that the vertical effective stress decreases faster with time. In one relaxation test in the swelling region, the SMB70 specimen is unloaded at a CRSN of $\dot{\varepsilon}_z = -10^{-5}\ 1/\text{sec}$ and then relaxation starts. It is seen in Figure 9.9 that the vertical effective stress increases with time.

Simulations by EVPS model on SMB50 both in creep and swelling regions are shown in Figure 9.10. The input parameters are $\dot{\varepsilon}_z = 10^{-5}\ 1/\text{sec}$ with $\sigma_o^{'} = 16.60$ kPa for relaxation in creep region; $\dot{\varepsilon}_z = -10^{-5}\ 1/\text{sec}$ with $\sigma_o^{'} = 14.90$ kPa for relaxation in swelling region. It is seen that the simulation agrees well with the test data. The time-dependent behaviors can be seen clearly from the plots in Figure 9.10. The biggest feature in the modeling is that in swelling region the stress increase gradually with time resulting in "swelling pressure". The stress-time plot in the swelling region exhibits a reverse trend compared with the plots in creep region.

(b) Simulation of relaxation on HKMD soils

In section 9.4, all the parameters for HKMD soils in EVPS model have been fixed. In modeling as referred earlier, Yin and Graham (1994) adopted a 1D EVP model to simulate relaxation tests. Results showed that soil behavior is very sensitive to the creep parameters.

For MD 3a, curves in Figure 9.11 demonstrate the simulated results for relaxation tests by the EVPS model. It is found that the simulation agrees well with the test data in creep region. The simulated stress decreases rapidly within the first 100 min and the biggest error occurs at the end of the simulation. In contrast, simulations in swelling region indicate a quick stress rebound within the first 100 min. As reported by Yin and Tong (2011), the stress increases gradually with time in the swelling region, which results by the swelling pressure. Simulations by EVPS model on MD19 specimen is also presented in Figure 9.12. Using the parameters in Table 9-3, the EVPS model can easily predict the relaxation behaviors both in creep and swelling conditions.

If either the creep parameter ψ^c / V or the swelling parameter ψ^s / V is varied, the relaxation curves for MD 3a represented (the dot-dash lines) in Figure 9.13 change apparently. Higher value of ψ^c / V accelerates the stress reduction in creep relaxation while comparatively higher value of ψ^s / V accelerates the stress increase in swelling relaxation. In accordant with the findings by Yin and Graham (1994), the viscous parameters are very sensitive. Relatively speaking, the swelling parameter ψ^s / V is less sensitive compared with the creep parameter ψ^c / V. Once only the ψ^s / V changed from 0.00147 to 0.002 ($\psi^c / V = 0.00368$), the

stress increases at the time 2000 min only by 3.4%. Stress reduction however is 7.1% if only ψ^c / V is varied from 0.00368 to 0.007 ($\psi^s / V = 0.00147$). It deserves attention that in extreme condition, when both ψ^c / V and ψ^s / V equal to zero (no creep and no swelling), the EVPS model returns to the simplest case-constant stress, namely no relaxation.

9.8 Simulation of 1D Constant Rate of Stress (CRSS) Tests

The time dependent stress-strain behavior of saturated clays has been studied for years. This behavior can be significantly affected by the rate of loading, no matter in varied strain rate or varied stress rate. In constant rate of stress (CRSS) tests, $\dot{\sigma}_z$ is strictly controlled and kept constant. Simulations of CRSS tests with different stress rate are illustrated in Figure 9.14. The stress rates are 10 kPa/min, 1 kPa/min, and 0.1 kPa/min. Basic values of creep and swelling parameters are selected to be 0.00801 for ψ^c / V, and 0.00704 for ψ^s / V. Different from the previous EVP model, the new 1D EVPS model has both creep parameter ψ^c / V and swelling parameter ψ^s / V for simulation of the soil behavior with both creep and swelling. It is seen from Figure 9.14 that the stress-strain behavior is strongly dependent on the stress rates.

A parametric study is carried out using the new 1D EVPS model. The simulated stress-strain curves are shown in Figure 9.15. It is seen from Figure 9.15 that the creep parameter ψ^c / V has a profound influence on the stress-strain

relationship. A larger ψ^c / V value leads to more compression. The swelling parameter, however, has relatively longer effect on reversing the compression and finally makes the compression line a gentle slope.

Under the vertical effective stress of 120 kPa, the relationships between the stress rate and the vertical strain are simulated in Figure 9.16 for (a) ψ^c / V = 0.00801 and ψ^s / V = 0.00704; (b) ψ^c / V = 0.00801 and ψ^s / V = 0.004; and (c) ψ^c / V = 0.004 and ψ^s / V = 0.00704. As expected, the increment of strain becomes smaller once the creep parameter ψ^c / V is reduced to 0.004. However, the increment of strain becomes bigger once the swelling parameter ψ^s / V is reduced to 0.004. The latter is understandable since that the larger swelling parameter results in larger swelling strain and smaller total strain due to both creep and swelling.

So far, different soil behaviors in CRSN, relaxation, and CRSS tests are all simulated using the 1D EVPS model.

9.9 Summary and Conclusions

The concept of equivalent time is adopted to formulate a new one-dimensional Elastic Visco-Plastic model considering both creep and swelling behaviours (namely 1D EVPS model), for viscous soils under one-dimensional straining. From oedometer test results on silica sand mixed bentonite (SMB) specimens, all the parameters in the 1D EVPS model have been determined. This new model is then used to simulate the time-dependent (or rate dependent) stress-strain relations in

CRSN, relaxation and CRSS conditions. Conclusions are drawn as follows:

a. Swelling occurs even in saturated soils. The newly presented 1D EVPS model can consider both creep and swelling so that the unloading/reloading loop can be simulated.

b. A simple method is used to determine all parameters in the 1D EVPS model. Proper estimations of viscous parameters for both creep and swelling are essential to the 1D EVPS model. Totally eight parameters are needed to simulate the time-dependent behavior of a specific soil. Once all model parameters are determined, the model can predict all time-dependent (or strain-dependent) behaviors of a soil element under any loading condition in 1D straining.

c. Simulated results by using the 1D EVPS model agree well with data from a CRSN test. Using variable transfer and perturbation method, analytical solution is obtained for EVPS modeling in stress relaxation condition. The simulations by the solution from the EVPS model on relaxation tests also agree well with the test data.

d. The 1D EVPS model has been used to simulate relaxation tests and CRSS tests with different with different creep and swelling parameters. The simulated results are meaningful.

e. Based on the reference time line and the equivalent time line, both the creep parameter ψ^c / V and the swelling parameter ψ^s / V are needed in EVPS model to predict the viscous behavior of soils. Relatively the creep parameter is more sensitive than the swelling parameter.

f. The 1D EVPS model is powerful in describing viscous soil behaviors in a wide range of conditions, for example, stress relaxation, swelling pressure, pre-consolidation pressure, etc.

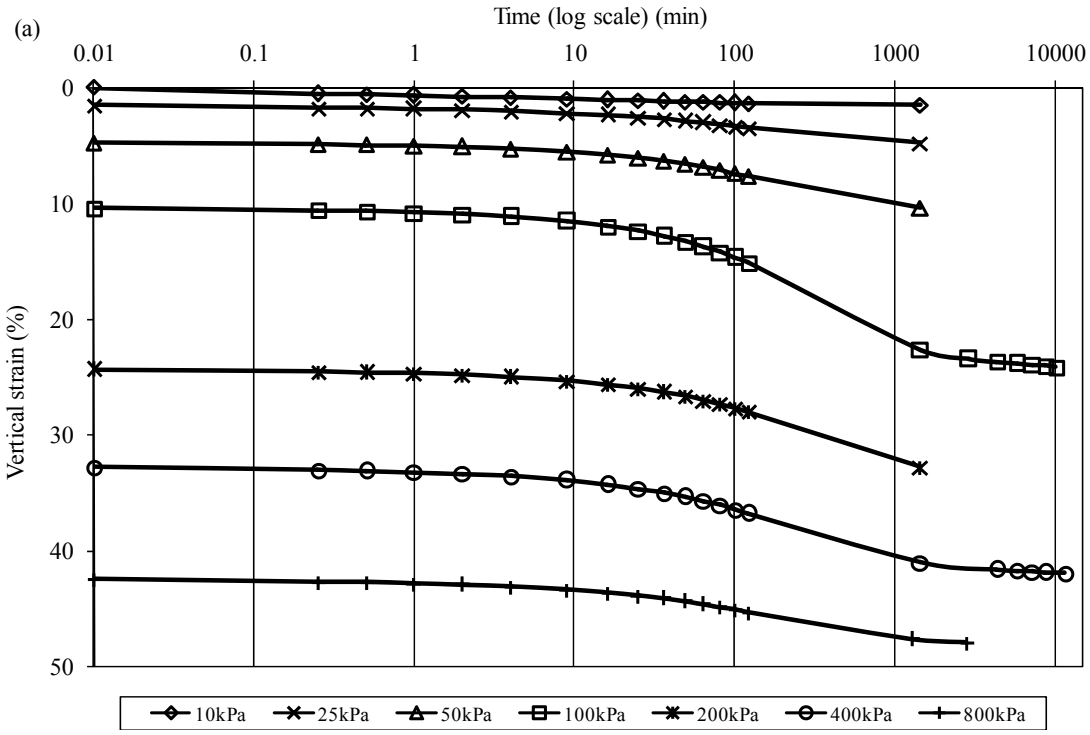

Figure 9.1(a) Initial loading stage of SMB70 from the multi-stage oedometer test

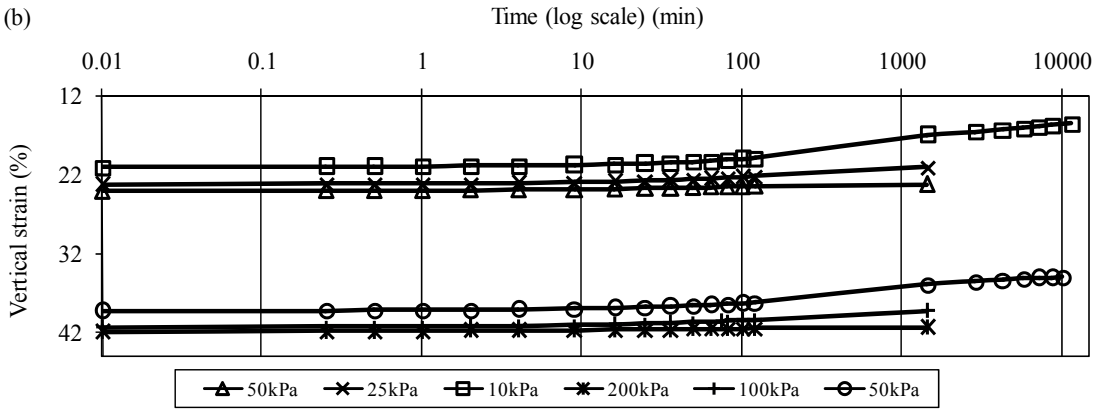

Figure 9.1(b) Unloading loading stage of SMB70 from the multi-stage oedometer test

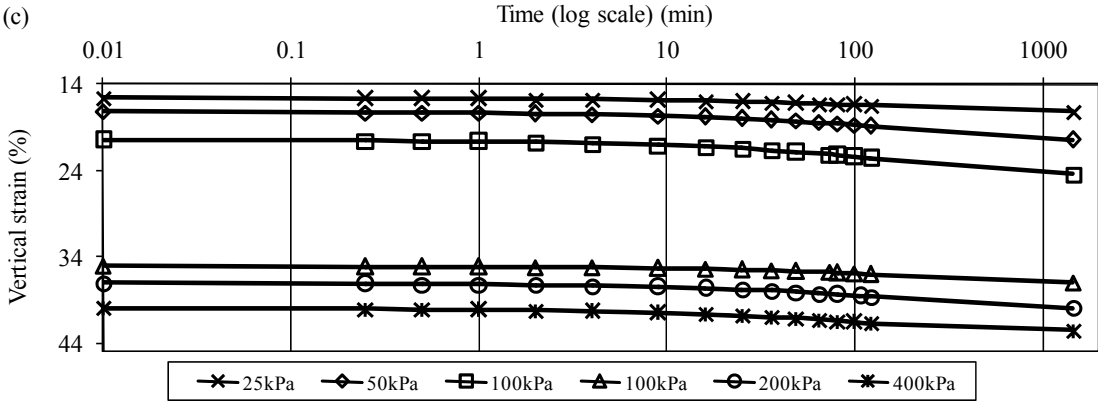

Figure 9.1(c) Reloading loading stage of SMB70 from the multi-stage oedometer test

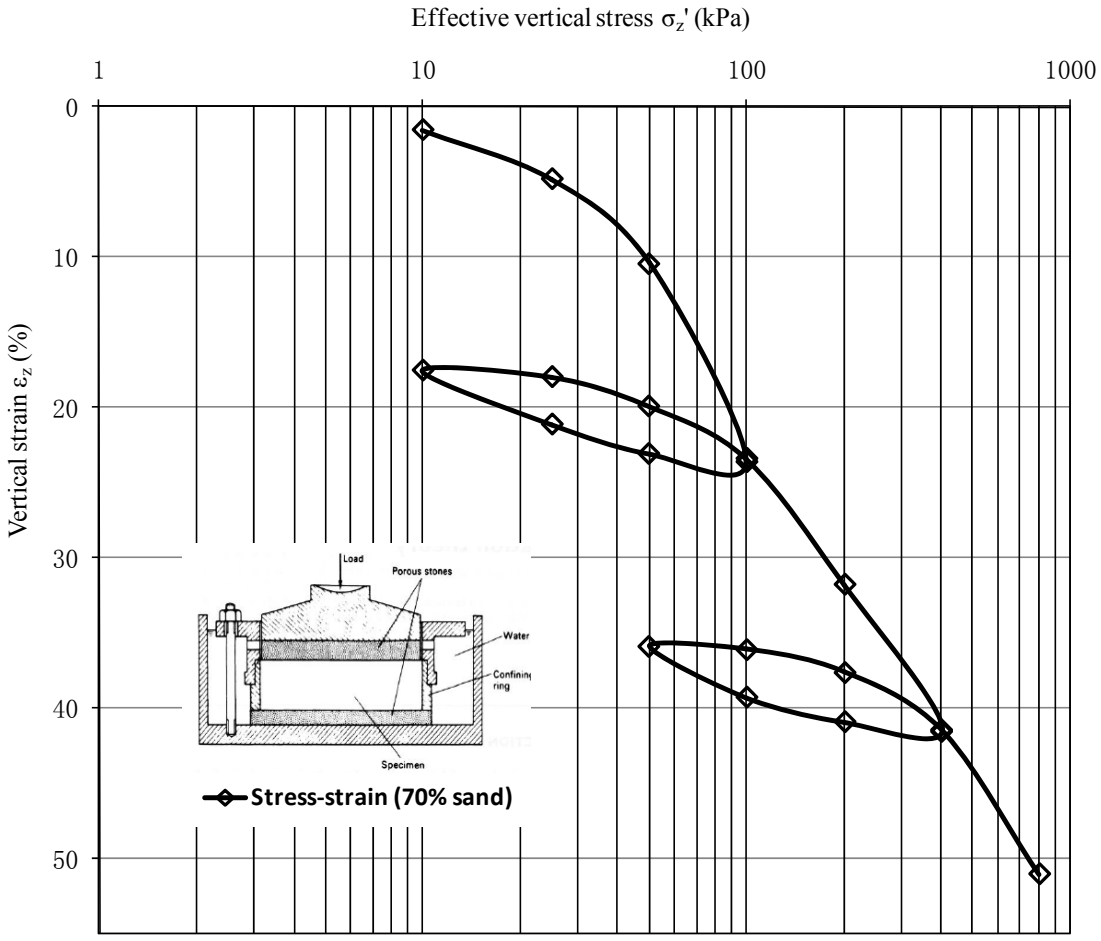

Figure 9.1(d) Relationship between the vertical strain and the vertical stress in log-scale at the end of primary consolidation

Figure 9.1 (a) initial loading stage of SMB70 from the multi-stage oedometer test, (b) unloading loading stage of SMB70 from the multi-stage oedometer test, (c) reloading loading stage of SMB70 from the multi-stage oedometer test, and (d) the relationship between the vertical strain and the vertical stress in log-scale at the end of primary consolidation

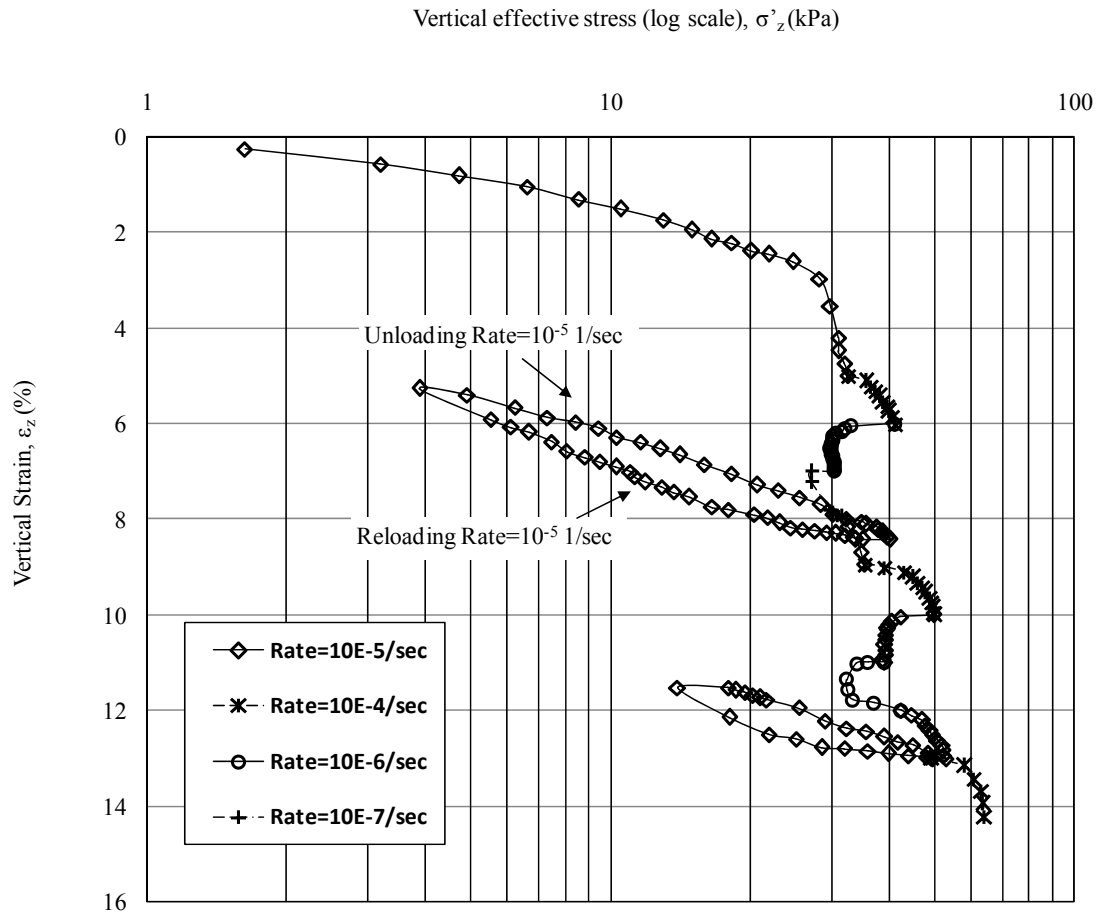

Figure 9.2 Results from the CRS test with step-changed strain rates and with unloading and reloading

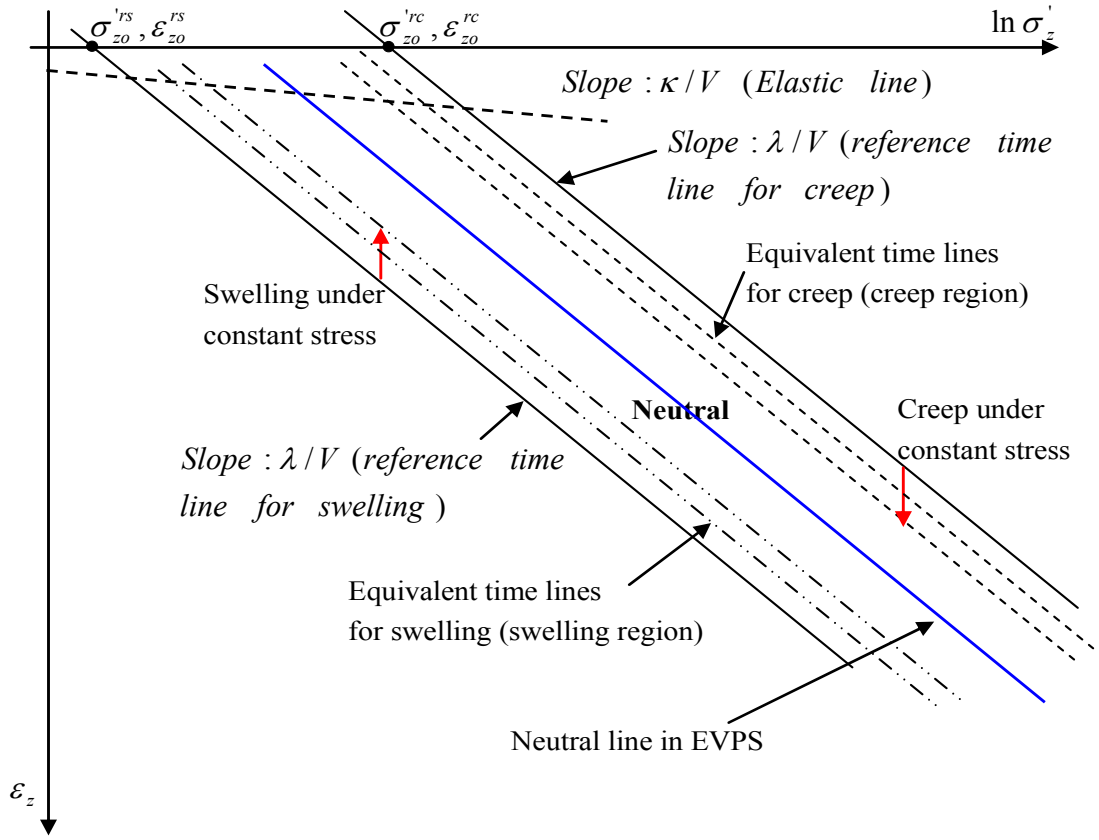

Figure 9.3 Conceptual illustration of creep, swelling, unloading/reloading loop, "elastic" line, "reference" time line, and "equivalent" time lines (extended from Yin, 1990; Yin and Graham, 1989, 1994 and 1999)

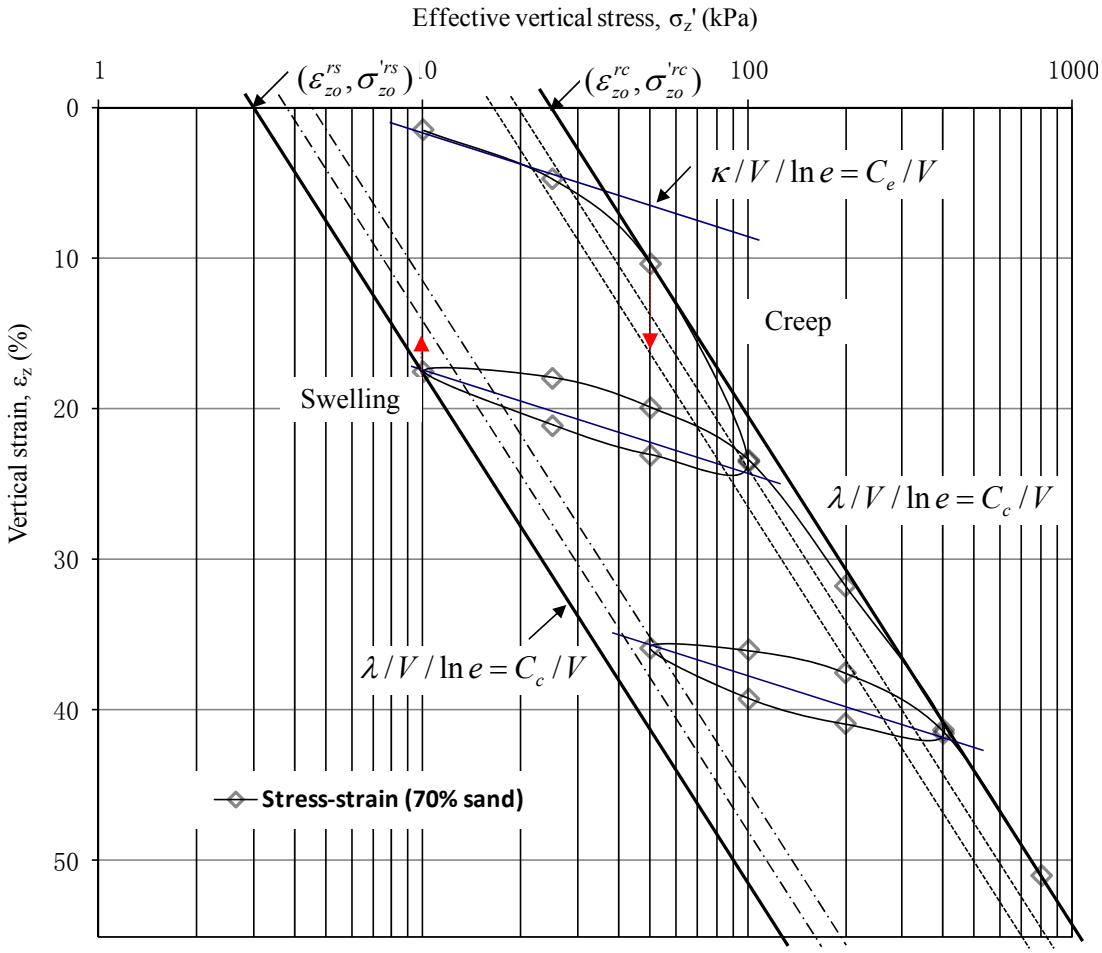

Figure 9.4 Determination of parameters in the EVPS model

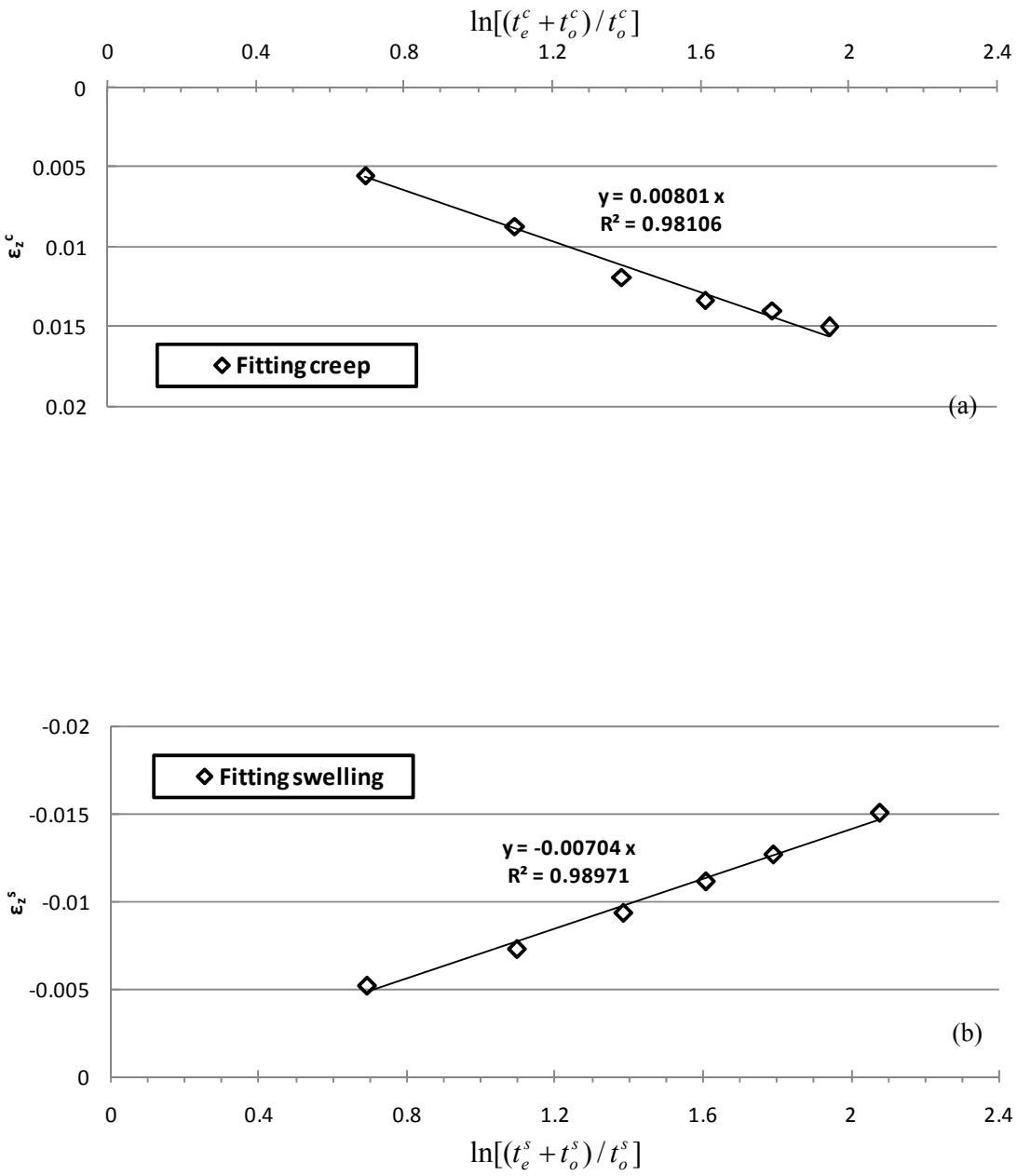

Figure 9.5 Determination of ψ^c / V and ψ^s / V in the EVPS model - (a) Fitting creep for SMB with 70% sand content and (b) Fitting swelling for SMB with 70% sand content

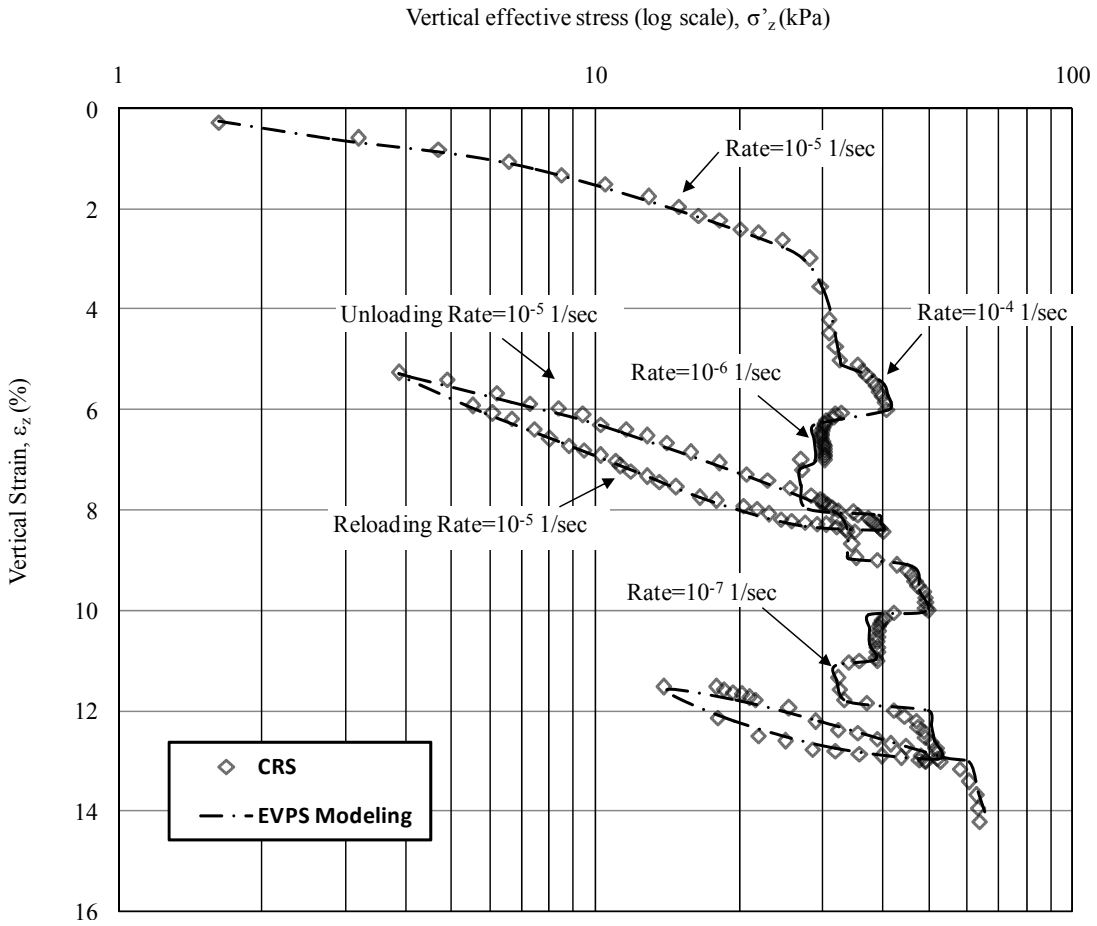

Figure 9.6 Comparison of modeling results with measured data from a CRS test with step- changed strain rates and with unloading and reloading

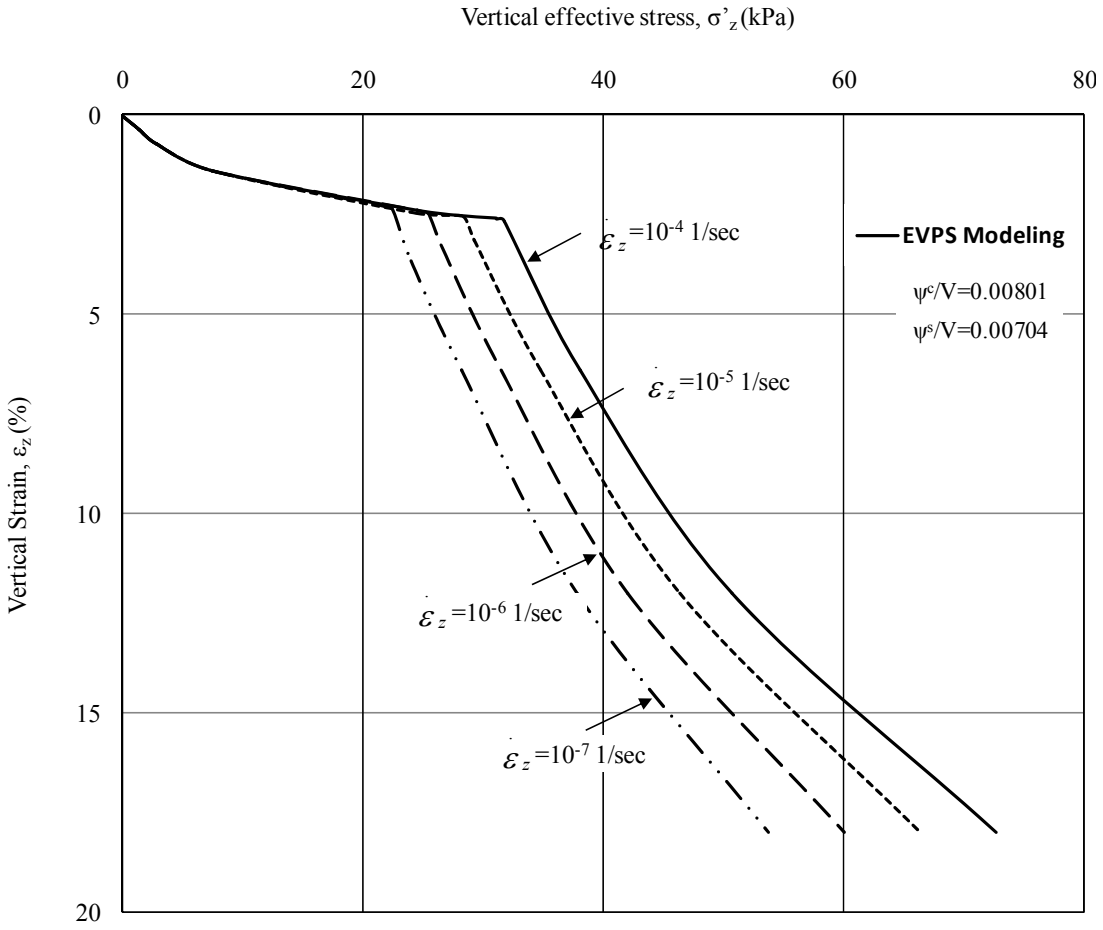

Figure 9.7 Simulation results for strain rate dependent stress-strain behavior in CSR tests using the EVPS model

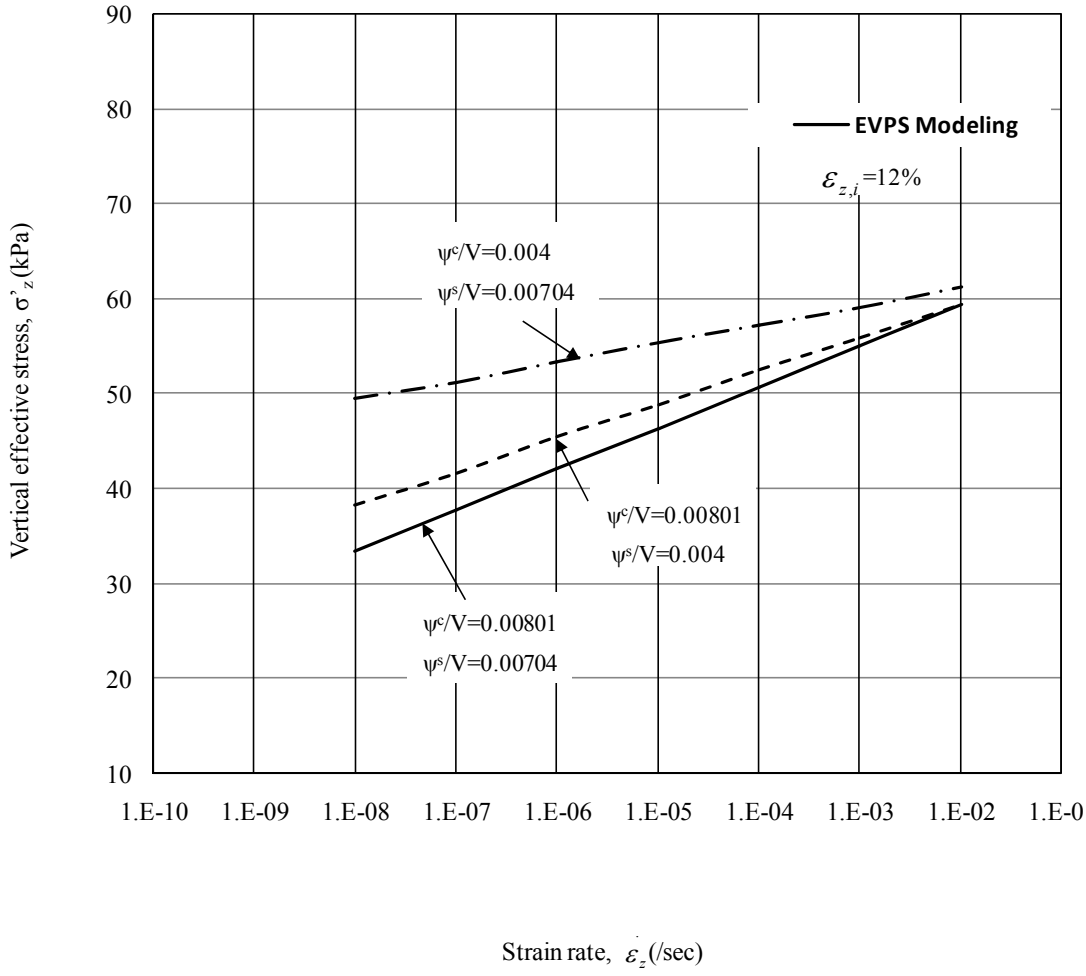

Figure 9.8 Strain rate effect with varied parameters

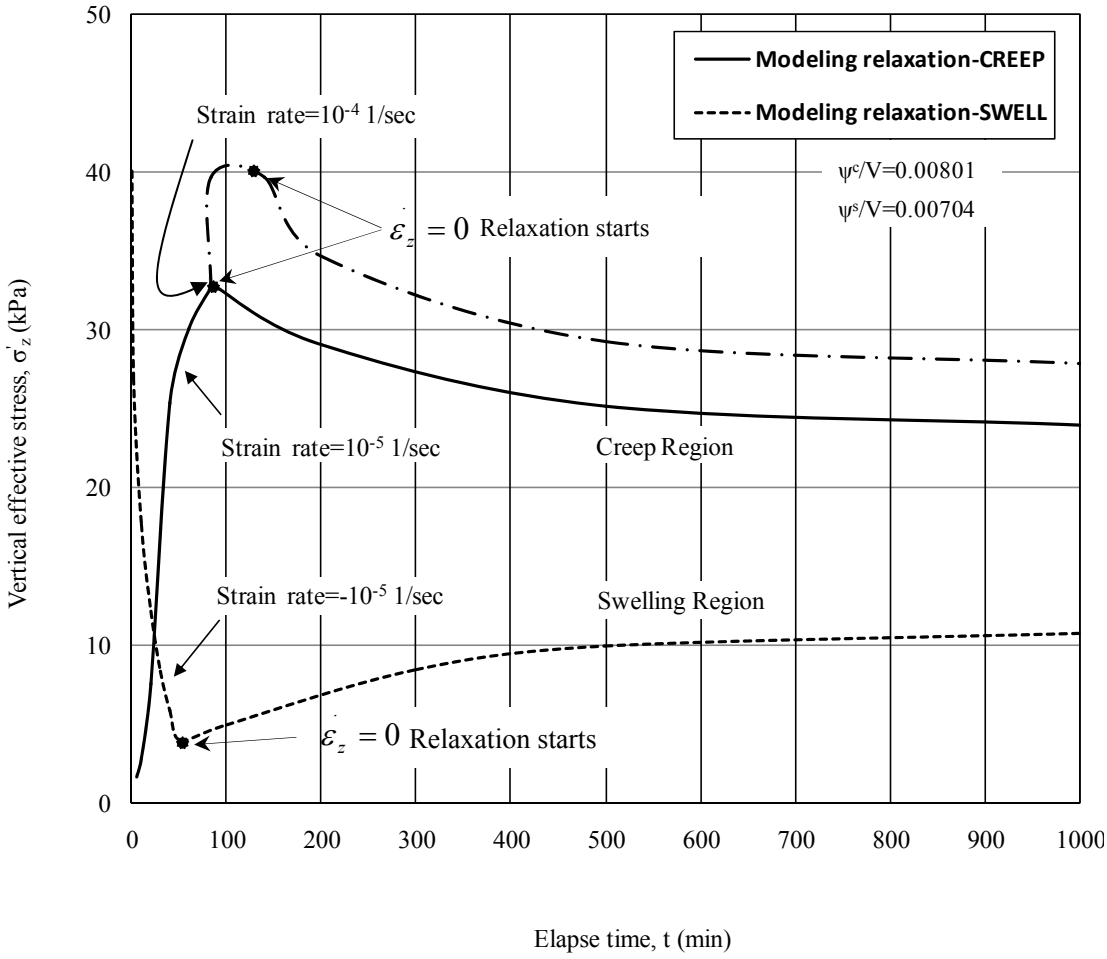

Figure 9.9 Simulation results for relaxations in both creep region and swelling region

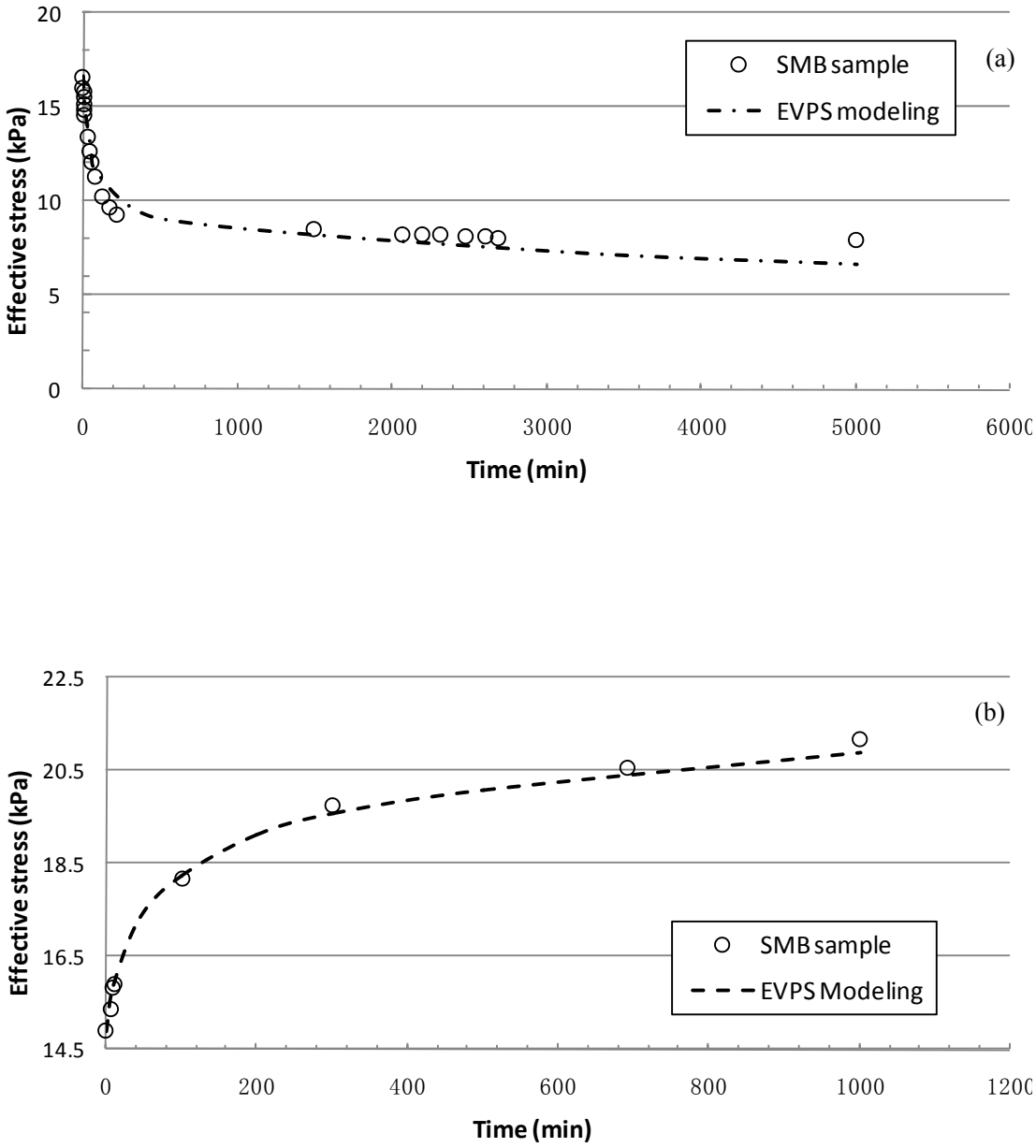

Figure 9.10 Simulation results for relaxation tests on SMB50 - (a) in creep region and (b) in swelling region

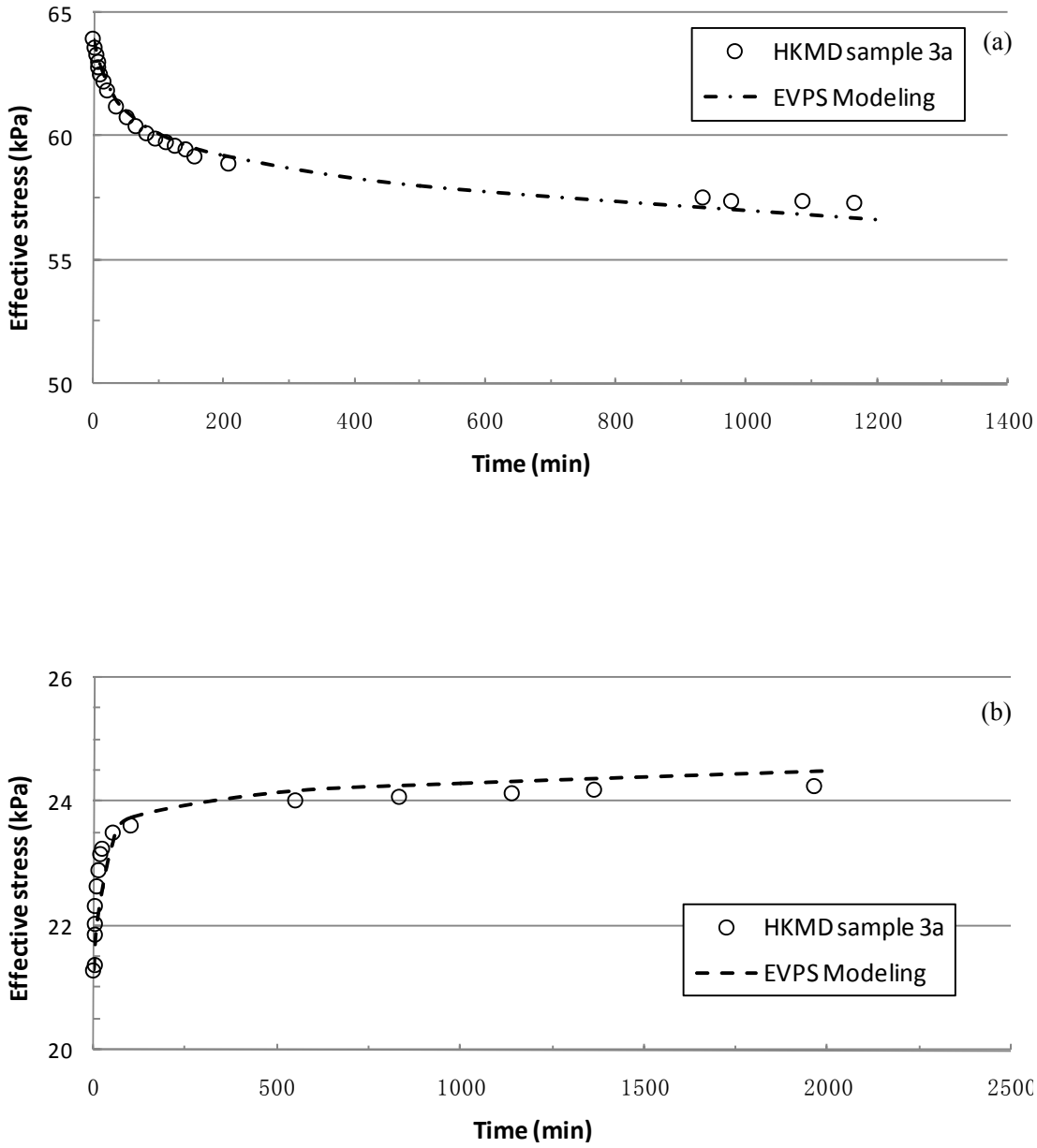

Figure 9.11 Simulation results for relaxation tests on MD 3a - (a) in creep region and (b) in swelling region

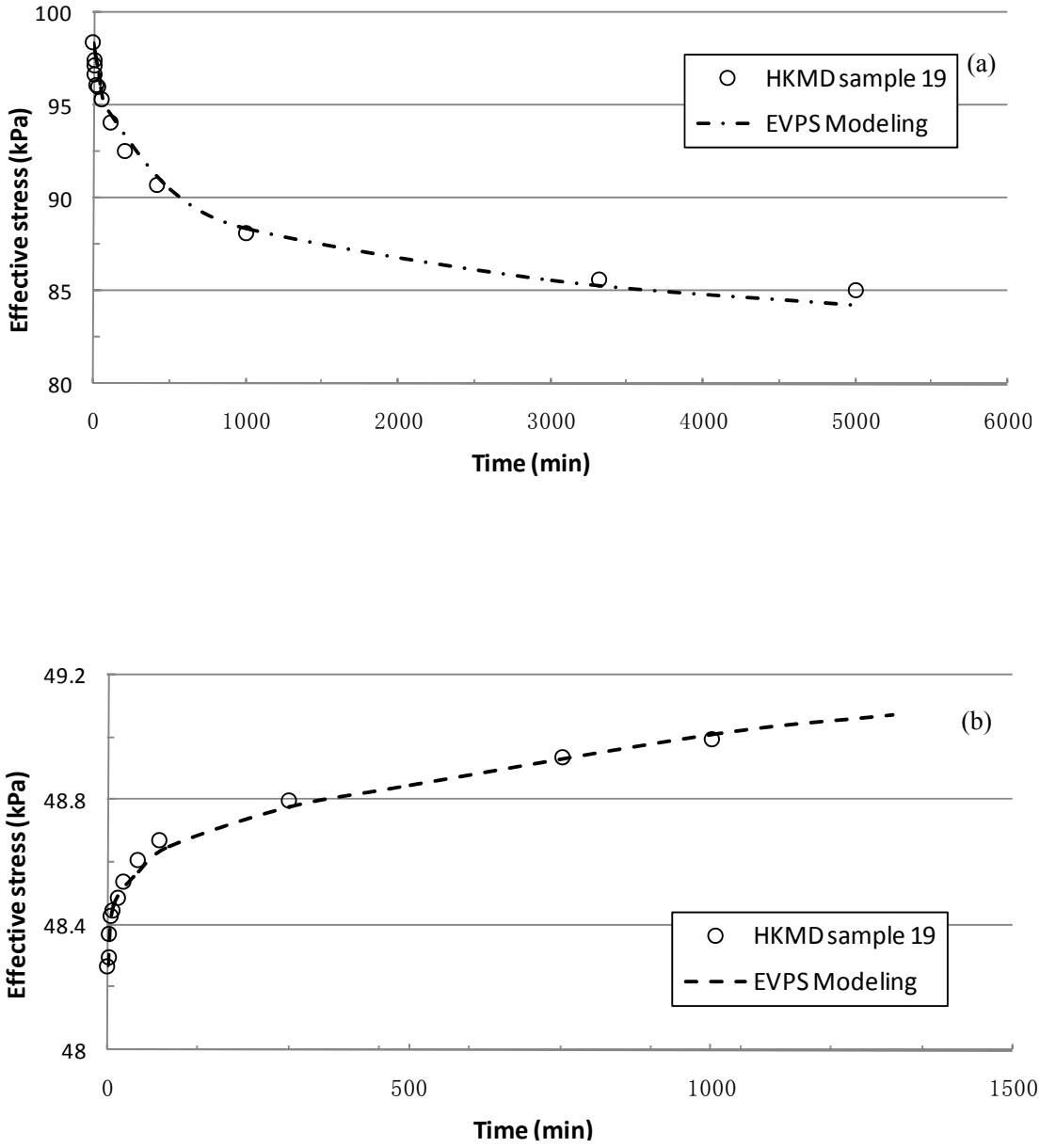

Figure 9.12 Simulation results for relaxation tests on MD 19 - (a) in creep region and (b) in swelling region

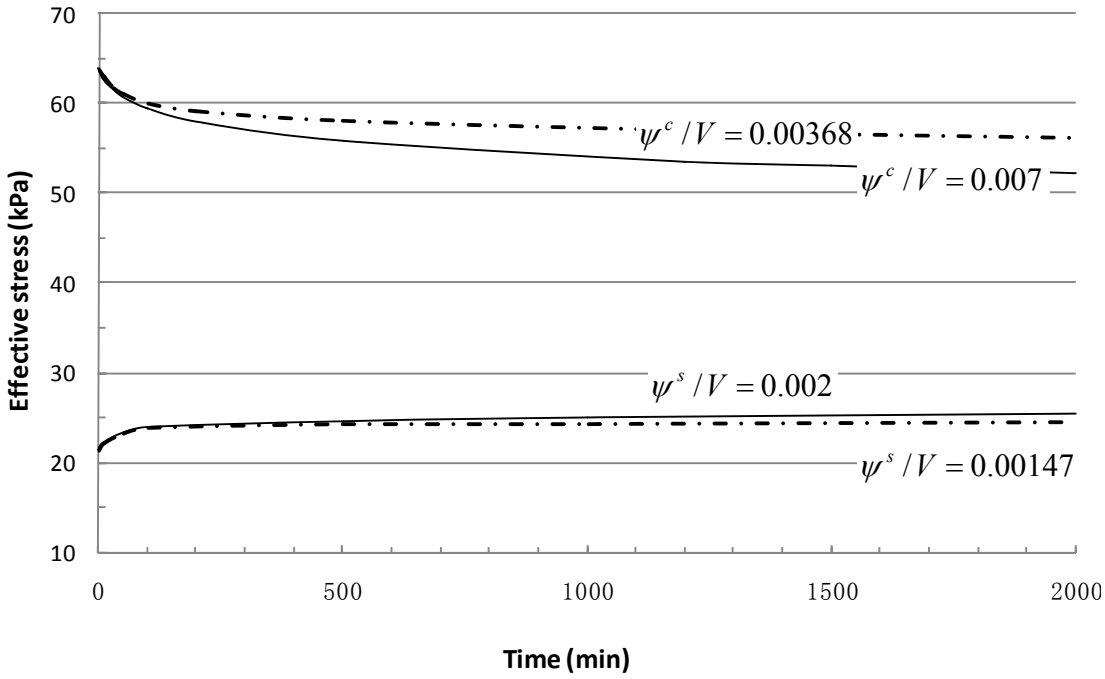

Figure 9.13 Relaxation simulation results by EVPS with varied parameters

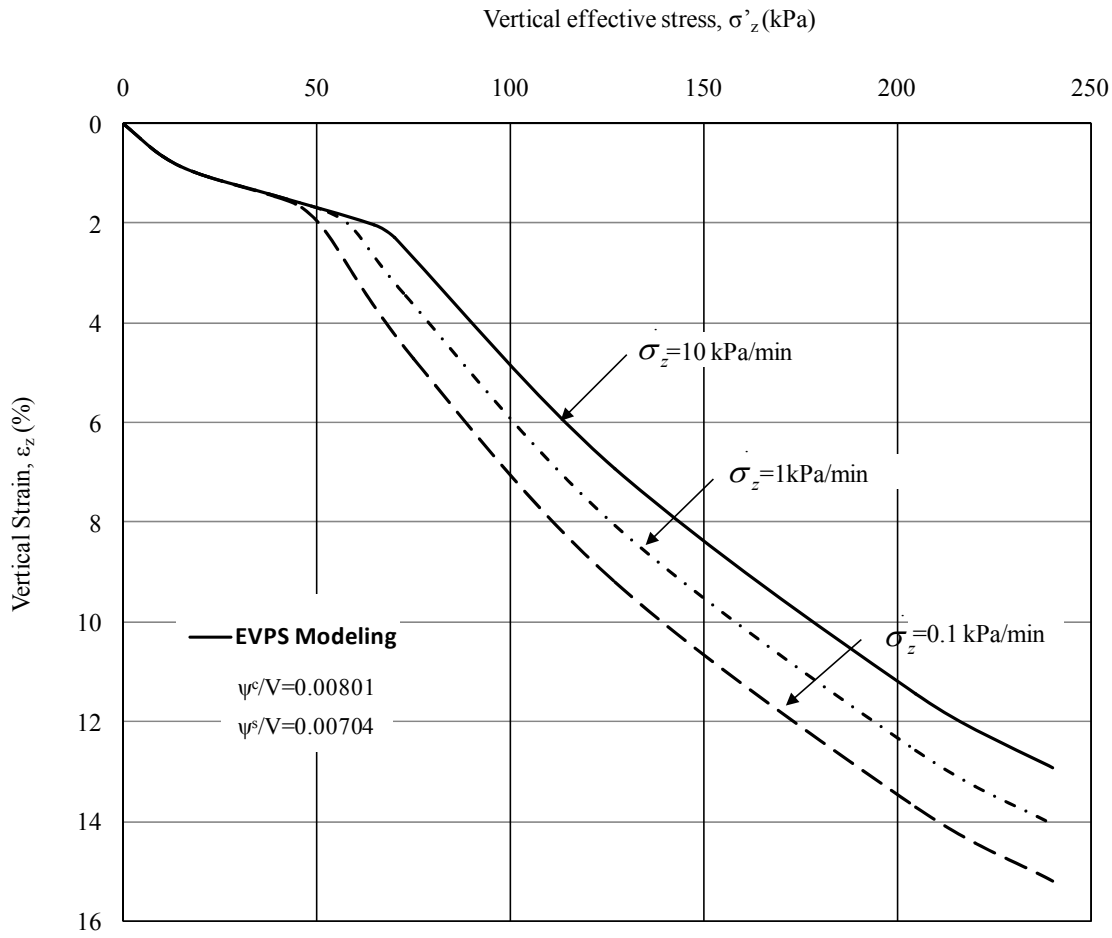

Figure 9.14 Simulation results of stress-strain behaviors for constant rate of stress tests

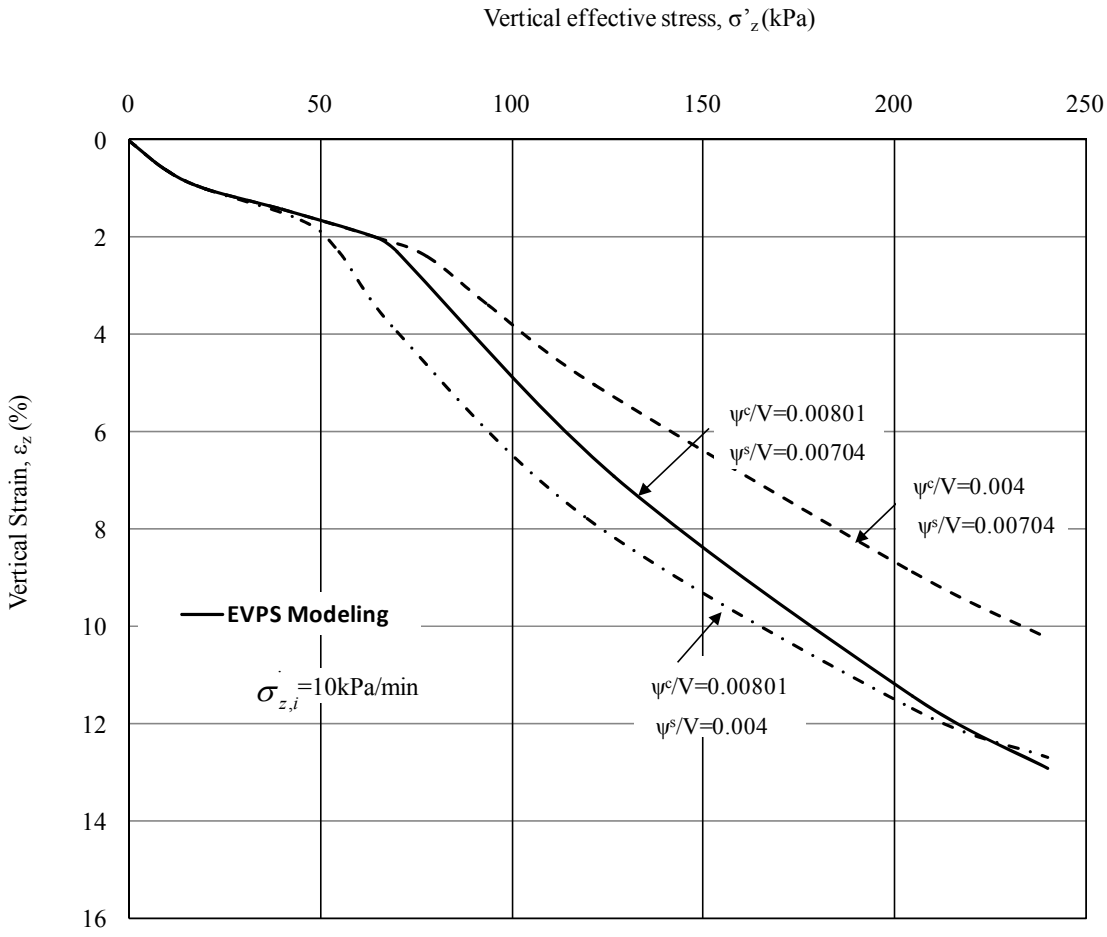

Figure 9.15 Simulation results for constant rate of stress tests with varied parameters

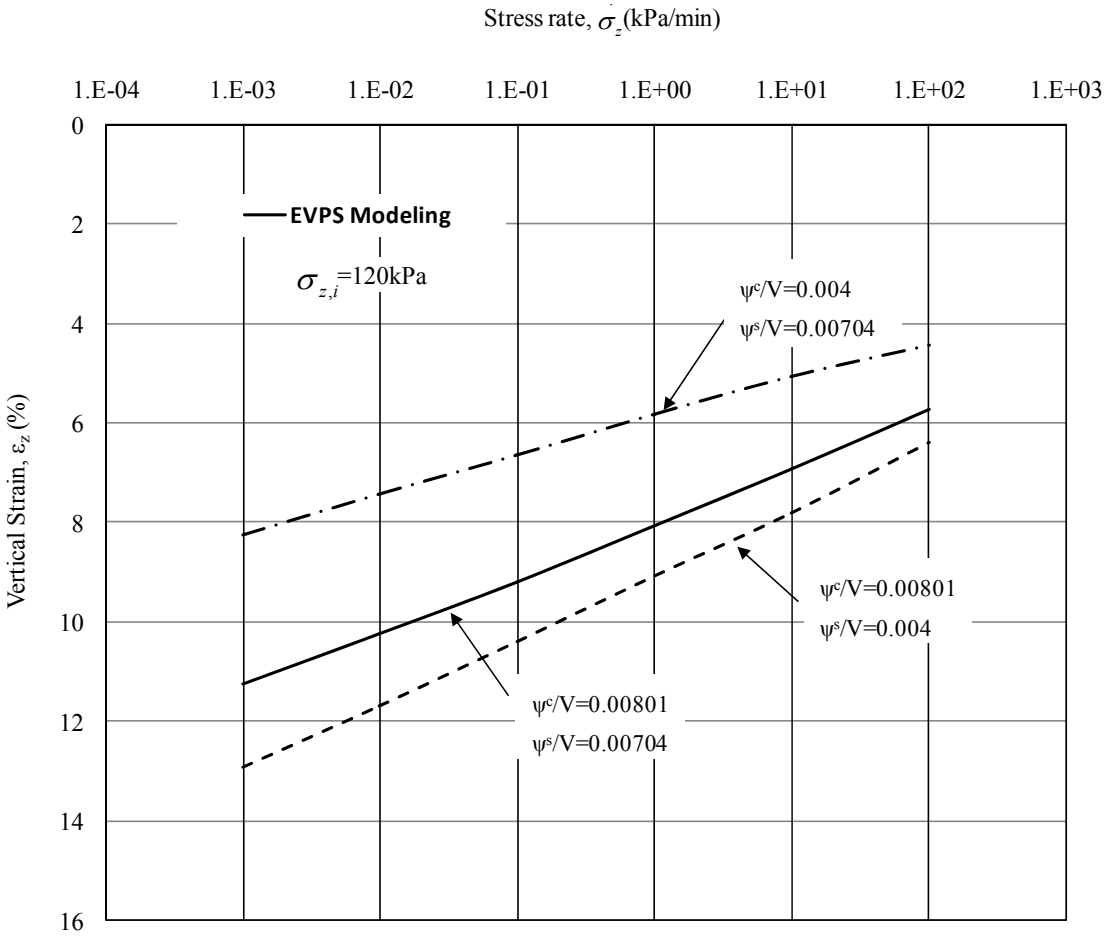

Figure 9.16 Stress rate effect with varied parameters

Chapter 10

3D EVPS Modeling and Verification

10.1 Introduction

This chapter presents a new Elastic Visco-Plastic model considering Swelling (EVPS) based on the classical Cam-clay model and EVPS model proposed by Yin and Tong (2011). The function and application of this model are described in detail. The results of isotropic consolidation test of sand mixed bentonite (SMB) sample are used to calibrate the 3D EVPS model. Simulation of undrained triaxial constant rate of strain tests shows good predictions of this model.

10.2 EVPS Model for 1D Isotropic Stressing

The equivalent time was defined by Yin and Graham (1989, 1994) for creep behavior and recently by Yin and Tong (2011) for both creep and swelling in 1D straining condition. In the isotropic stressing condition, the elastic strain is described by the instant time line ($\kappa - line$) as:

$$\varepsilon_{vm}^{e} = \varepsilon_{vmo}^{e} + \frac{\kappa}{V}\ln\frac{p_m^{'}}{p_u^{'}} \tag{10-1}$$

where ε_{vmo}^{e} is the volumetric strain at $p_u^{'} = p_m^{'}$; κ / V is the material parameter and V is the specific volume; $p_u^{'}$ denotes the unit stress; and the subscript 'm' stands for the isotropic stressing condition, while the superscript 'e' denotes the stress condition on the instant time line.

After the instant compression, a reference line is introduced by Yin and Graham (1999) and expressed in the following form:

$$\varepsilon_{vm}^{ep} = \varepsilon_{vmo}^{rc} + \frac{\lambda}{V}\ln\frac{p_m^{'}}{p_{mo}^{'rc}} \tag{10-2}$$

where ε_{vmo}^{rc} is the reference strain at $p_{mo}^{'rc} = p_m^{'}$; κ / V is also a material parameter; and the superscript '*ep*' denotes the stress condition on the reference line.

Following the reference time line and equivalent time line principles, the creep strain is obtained by:

$$\varepsilon_{vm}^{cp} = \frac{\psi^c}{V}\ln\frac{t_o^c + t_e^c}{t_o^c} \tag{10-3}$$

where ψ^c / V is the creep parameter, that is the slope of ε_z^c and $\ln(t_e^c)$; t_e is the equivalent time; and the superscript '^{cp}' denotes the viscoplastic behavior. Then the creep rate is:

$$\dot{\varepsilon}_{vm}^{cp} = \frac{d\varepsilon_{vm}^{cp}}{dt_e^c} = \frac{\psi^c}{V}\frac{1}{t_e^c + t_o^c} \tag{10-4}$$

If the reference time is known, based on the equivalent time t_e, the strain at any state point can be described as:

$$\varepsilon_{vm} = \varepsilon_{vm}^{ep} + \varepsilon_{vm}^{cp} = \varepsilon_{vmo}^{rc} + \frac{\lambda}{V}\ln\frac{p_m^{'}}{p_{mo}^{'rc}} + \frac{\psi^c}{V}\ln\frac{t_e^c + t_o^c}{t_o^c} \tag{10-5}$$

The "equivalent time" in equation (10-5) is rewritten as:

$$\frac{\psi^c}{V}\ln\frac{t_e^c+t_o^c}{t_o^c}=\varepsilon_{vm}-\varepsilon_{vmo}^{rc}-\frac{\lambda}{V}\ln\frac{p_m^{'}}{p_{mo}^{rc'}}$$
$$\ln\frac{t_e^c+t_o^c}{t_o^c}=(\varepsilon_{vm}-\varepsilon_{vmo}^{rc})\frac{V}{\psi^c}-\frac{\lambda}{\psi^c}\ln\frac{p_m^{'}}{p_{mo}^{'rc}} \quad (10\text{-}6)$$
$$\frac{1}{t_e^c+t_o^c}=\frac{1}{t_o^c}\exp[-(\varepsilon_{vm}-\varepsilon_{vmo}^{rc})\frac{V}{\psi^c}]\left(\frac{p_m^{'}}{p_{mo}^{'rc}}\right)^{\frac{\lambda}{\psi^c}}$$

Differentiating the total strain in equation (10-5) with the "equivalent time", we have:

$$\dot{\varepsilon}_{vm}=\dot{\varepsilon}_{vm}^{ep}+\dot{\varepsilon}_{vm}^{cp}=\frac{\kappa}{V}\frac{\dot{p}_m^{'}}{p_m^{'}}+\frac{\psi^c}{V}\frac{1}{t_o^c}\exp[-\left(\varepsilon_{vm}-\varepsilon_{vmo}^{rc}\right)\frac{V}{\psi^c}]\left(\frac{p_m^{'}}{p_{mo}^{'rc}}\right)^{\frac{\lambda}{\psi^c}} \quad (10\text{-}7)$$

Equation (10-7) is the Elastic Visco-Plastic model (1D EVP) proposed by Yin and Graham (1999) for any isotropic loading condition. More generally as illustrated in Figure 10.1, when the soil is subjected to unloading and the soil has swelling potential, the specimen will swell by increasing its volume. Similar to the creep mechanism (decreasing volume), but in opposite direction (increasing volume), the swelling strain is defined as:

$$\varepsilon_{vm}^{sp}=-\frac{\psi^s}{V}\ln\frac{t_e^s+t_o^s}{t_o^s} \quad (10\text{-}8)$$

where ψ^s/V is the viscous parameter for swelling; t_o^s is a swelling parameter; t_e^s is the "equivalent time" for swelling strain; and the "-" denotes the opposite behavior compared with creep. The swelling rate is obtained by differentiating equation (10-8) with the "equivalent" time:

$$\dot{\varepsilon}_z^{sp}=\frac{d\varepsilon_z^{sp}}{dt_e^s}=-\frac{\psi^s}{V}\frac{1}{t_e^s+t_o^s} \quad (10\text{-}9)$$

Assuming that the slope of the reference line for swelling is the same as that for creep, the total strain at any point in swelling region is considered to be the strain swelling from the reference time line to this point:

$$\varepsilon_{vm}=\varepsilon_{vm}^{ep}+\varepsilon_{vm}^{sp}=\varepsilon_{vmo}^{rs}+\frac{\lambda}{V}\ln\frac{p_m^{'}}{p_{mo}^{'rs}}-\frac{\psi^s}{V}\ln\frac{t_e^c+t_o^c}{t_o^c} \tag{10-10}$$

Then the "equivalent time" can be obtained:

$$\begin{aligned}\ln\frac{t_e^s+t_o^s}{t_o^s}&=-(\varepsilon_{vm}-\varepsilon_{vmo}^{rs})\frac{V}{\psi^s}+\frac{\lambda}{\psi^s}\ln\frac{p_m^{'}}{p_{mo}^{'rs}}\\ \frac{1}{t_e^s+t_o^s}&=\frac{1}{t_o^s}\exp[(\varepsilon_{vm}-\varepsilon_{vmo}^{rs})\frac{V}{\psi^s}]\left(\frac{p_m^{'}}{p_{mo}^{'rs}}\right)^{-\frac{\lambda}{\psi^s}}\end{aligned} \tag{10-11}$$

In the above, both the creep and swelling effects are considered in isotropic stress condition. The swelling effect can be taken into account by adding a term to equation (10-5). Thus the total strain rate is the sum of elastic strain rate, viscoplastic creep strain rate and swelling strain rate. It is noted that the compressive stress and strain are positive and the EVPS model is constructed in terms of the effective stresses. The total strain rate is expressed as:

$$\dot{\varepsilon}_{vm}=\dot{\varepsilon}_{vm}^{ep}+\dot{\varepsilon}_{vm}^{cp}+\dot{\varepsilon}_{vm}^{sp}=\frac{\kappa}{V}\frac{p_m^{'}}{p_{mo}^{'}}+\frac{\psi^c}{V}\frac{1}{t_e^c+t_o^c}-\frac{\psi^s}{V}\frac{1}{t_e^s+t_o^s} \tag{10-12}$$

Substituting equation (10-6) for $\frac{1}{t_e^c+t_o^c}$ and equation (10-11) for $\frac{1}{t_e^s+t_o^s}$ gives

$$\begin{aligned}\dot{\varepsilon}_{vm}=&\frac{\kappa}{V}\frac{\dot{p}_m^{'}}{p_m^{'}}+\frac{\psi^c}{V}\frac{1}{t_o^c}\exp[-(\varepsilon_{vm}-\varepsilon_{vmo}^{rc})\frac{V}{\psi^c}]\left(\frac{p_m^{'}}{p_{mo}^{'rc}}\right)^{\frac{\lambda}{\psi^c}}\\ &-\frac{\psi^s}{V}\frac{1}{t_o^s}\exp[(\varepsilon_{vm}-\varepsilon_{vmo}^{rs})\frac{V}{\psi^s}]\left(\frac{p_m^{'}}{p_{mo}^{'rs}}\right)^{-\frac{\lambda}{\psi^s}}\end{aligned} \tag{10-13}$$

Equation (10-13) is the general EVPS model for isotropic stressing condition. The main feature of this model is that it includes the contribution of swelling strain rate in the total strain rate. It is noted that since reference lines for creep and swelling are assumed to have the same slope, if a soil has equal properties of creep and swelling ($\psi^c / V = \psi^s / V$), the stress-strain behavior in 1D stressing condition becomes a "neutral line" in Figure 10.1.

Equation (10-13) can be integrated into EVPS models for 3D stress conditions to predict the stress-strain behavior of soils under step-changed loading, constant rate of strain loading, and unloading/reloading loops.

10.3 Basic Assumptions in the EVPS Model for Triaxial Stress Conditions

Since Bjerrum (1967) divided the total volume strain into instant volume strain and delayed (creep) volume strain, this concept has been widely adopted in both isotropic stress state and 3D stress state. Two types of assumptions are used regarding the separation of instant strain and delayed strain (Yin *et al.*, 2002). In this section, the total strain rate is equal to the sum of elastic strain rate and viscoplastic strain rate. This approach has been adopted by Desai and Zhang (1987), Kutter and Sathialingam (1992), and Yin and Graham (1999). The total strain rate is described by:

$$\dot{\varepsilon}_{ij} = \dot{\varepsilon}_{ij}^{e} + \dot{\varepsilon}_{ij}^{vp} \tag{10-14}$$

where *i*=1, 2, 3 and *j*=1, 2 3; $\dot{\varepsilon}_{ij}$ is the total strain rate; and the superscripts '*e*' and '*vp*' denote the elastic part and the viscoplastic part, respectively. The instant strain is linear, time-independent and irrecoverable. According to Yin *et al.* (2002), the relation between the elastic strain rate $\dot{\varepsilon}_{ij}^{e}$ and the effective stress $\dot{\sigma}'_{kl}$ is:

$$\dot{\varepsilon}_{ij}^{e} = C_{ijkl}\dot{\sigma}_{kl}^{'} \tag{10-15}$$

where C_{ijkl} is a fourth order compliance tensor with subindices *k*=1, 2, 3 and *l*=1, 2, 3. For isotropic soils, only two constants are independent in equation (10-15), for instance, a shear modulus G^e and a bulk modulus K^e. Nonlinear hypoelastic models may be used to describe the time-independent strain in equation (10-15). The viscoplastic strain rate is defined in equation (10-16) by a flow rule initially proposed by Perzyna (1966).

$$\dot{\varepsilon}_{ij}^{vp} = r < \phi(F) > \frac{\partial Q}{\partial \sigma_{ij}^{'}} = S\frac{\partial Q}{\partial \sigma_{ij}^{'}} \tag{10-16}$$

where S is the scaling function; Q denotes the viscoplastic potential function (termed as a plasticity potential function). F represents the difference between the dynamic loading surface and static yield surface. Once the associated flow rule is assumed, the potential is equal to the loading surface, namely $Q = F(\sigma_{ij}^{'}, k) = 0$.

Similar to the yield surface of Cam-clay model (Roscoe and Burland, 1968), the elliptic loading surface is used in this modeling (Yin and Graham, 1999).

$$F = p^{'2} + \frac{q^2}{M^2} - p^{'}p_m^{'} = 0 \tag{10-17}$$

where $p^{'} = \sigma_{ii}^{'}/3$; $q = \sqrt{3S_{ij}S_{ij}/2}$, in which $S_{ij} = \sigma_{ij}^{'} - \delta_{ij}p^{'}$ and δ_{ij} is the Kronecker delta. In a triaxial compression, $p^{'} = (\sigma_1^{'} + 2\sigma_3^{'})/3$ and $q = \sigma_1 - \sigma_3$; M

is the slope of the strength envelope in $p' - q$ plane and $M = M_c = 6\sin\phi' /(3 - \sin\phi')$ or compression; p'_m is the mean effective stress at which the loading surface F intercepts the $p' - axis$ in $p' - q$ plane; and the subscript "$_m$" denotes a mean stress of isotropic stressing. Figure 10.2(a) shows the total stress path (TSP) and the effective stress path (ESP) for an isotrocally CU compression test. Figure 10.2(b) shows the corresponding stress-strain state of A, B and C under constant strain rate; a, b and c under isotropic consolidation.

In classical plasticity, the most common laws are work hardening and strain hardening: the work hardening law assumes the plastic work on a yield surface is constant (Ladd *et al.*, 1977), while the strain hardening assumes a certain measure of plastic strain is constant on a yield surface (Roscoe and Burland, 1968). In modified Cam-Clay, the plastic volume strain determined from isotropic consolidation tests is used as the strain measure. Therefore this model is sometimes termed as volumetric hardening model (Yin and Graham, 1999).

10.4 EVPS Modeling from Triaxial Stress Condition to 3D Stress Condition

Once the associated flow rule is used and the constant viscoplastic strain rate on a flow surface is assumed, the scaling function S in equation (10-16) can be derived in triaxial states:

$$\begin{cases} \dot{\varepsilon}_v^{vp} = \dfrac{\partial F}{\partial p'} = S(2p' - p'_m) \\ \dot{\varepsilon}_s^{vp} = \dfrac{\partial F}{\partial q} = S\dfrac{2q}{M^2} \end{cases} \tag{10-18}$$

where $\dot{\varepsilon}_v^{vp}$ and $\dot{\varepsilon}_s^{vp}$ are viscoplastic volumetric strain rate and viscoplastic deviator strain rate, respectively. The deviator strain is:

$$\begin{cases} \varepsilon_s = \dfrac{2}{3}\sqrt{E_{ij}E_{ij}} \\ E_{ij} = \varepsilon_{ij} - \dfrac{1}{3}\delta_{ij}\varepsilon_v \end{cases} \tag{10-19}$$

where δ_{ij} is the Kronecker delta, and ε_v is the volumetric strain. In a triaxial state, $\varepsilon_s = 2/3(\varepsilon_1 - \varepsilon_3)$.

At a certain stress state, $p_m^{'}$ in equation (10-18) is obtained from equation (10-20) as:

$$p_m^{'} = p^{'} + \frac{q^2}{p^{'}M^2} \tag{10-20}$$

The above equation serves as a consistency condition from the viscoplasticity. It is clear that in *p'-q* space, the visco-plastic strain rate will be the same as the viscoplastic volumetric strain rate ($\dot{\varepsilon}_v^{vp} = \dot{\varepsilon}_{vm}^{vp}$) in the corresponding isotropic stressing condition.

Using the equations (10-13) and (10-16), we have:

$$\begin{cases} \dot{\varepsilon}_v^{vp} = \dfrac{\partial F}{\partial p^{'}} = S(2p^{'} - p_m^{'}) \\ \dot{\varepsilon}_{vm}^{vp} = \dfrac{\psi^c}{Vt_o^c}\exp\left[\dfrac{V}{\psi^c}\left(-(\varepsilon_{vm} - \varepsilon_{vmo}^{rc}) + \dfrac{\lambda}{V}\ln\dfrac{p_m^{'}}{p_{mo}^{'rc}}\right)\right] \\ -\dfrac{\psi^s}{Vt_o^s}\exp\left[\dfrac{V}{\psi^s}\left((\varepsilon_{vm} - \varepsilon_{vmo}^{rs}) - \dfrac{\lambda}{V}\ln\dfrac{p_m^{'}}{p_{mo}^{'rs}}\right)\right] \end{cases} \tag{10-21}$$

The scaling function *S* is thereafter can be determined as:

$$S=\frac{1}{\left|2p^{'}-p_{m}^{'}\right|}\begin{Bmatrix}\dfrac{\psi^{c}}{Vt_{o}^{c}}\exp\left[\dfrac{V}{\psi^{c}}\left(-(\varepsilon_{vm}-\varepsilon_{vmo}^{rc})+\dfrac{\lambda}{V}\ln\dfrac{p_{m}^{'}}{p_{mo}^{'rc}}\right)\right]\\ -\dfrac{\psi^{s}}{Vt_{o}^{s}}\exp\left[\dfrac{V}{\psi^{s}}\left((\varepsilon_{vm}-\varepsilon_{vmo}^{rs})-\dfrac{\lambda}{V}\ln\dfrac{p_{m}^{'}}{p_{mo}^{'rs}}\right)\right]\end{Bmatrix} \quad (10\text{-}22)$$

Assuming that the elastic proportion defined by $\kappa-line$ is isotropically elastic, the elastic strain rate in equation (10-14) can therefore be described by:

$$\dot{\varepsilon}_{ij}^{e}=\frac{1}{2G}\dot{S}_{ij}+\frac{\kappa}{3V}\frac{\dot{p}^{'}}{p^{'}}\delta_{ij} \quad (10\text{-}23)$$

where G is the shear modulus; and the nonlinear bulk modulus is determined by $K=p^{'}/(\kappa/V)$; s_{ij} is the deviator stress tensor.

Combing equations (10-16) and (10-22) gives:

$$\dot{\varepsilon}_{ij}^{vp}=\frac{1}{\left|2p^{'}-p_{m}^{'}\right|}\begin{Bmatrix}\dfrac{\psi^{c}}{Vt_{o}^{c}}\exp\left[\dfrac{V}{\psi^{c}}\left(-(\varepsilon_{vm}-\varepsilon_{vmo}^{rc})+\dfrac{\lambda}{V}\ln\dfrac{p_{m}^{'}}{p_{mo}^{'rc}}\right)\right]\\ -\dfrac{\psi^{s}}{Vt_{o}^{s}}\exp\left[\dfrac{V}{\psi^{s}}\left((\varepsilon_{vm}-\varepsilon_{vmo}^{rs})-\dfrac{\lambda}{V}\ln\dfrac{p_{m}^{'}}{p_{mo}^{'rs}}\right)\right]\end{Bmatrix}\frac{\partial F}{\partial\sigma_{ij}^{'}} \quad (10\text{-}24)$$

Substituting equations (10-23) and (10-24) into equation (10-14), a general 3D Elastic Visco-Plastic model considering Swelling (3D EVPS) is obtained:

$$\begin{aligned}\dot{\varepsilon}_{ij}&=\frac{1}{2G}\dot{S}_{ij}+\frac{\kappa}{3V}\frac{\dot{p}^{'}}{p^{'}}\delta_{ij}\\&+\frac{1}{\left|2p^{'}-p_{m}^{'}\right|}\begin{Bmatrix}\dfrac{\psi^{c}}{Vt_{o}^{c}}\exp\left[\dfrac{V}{\psi^{c}}\left(-(\varepsilon_{vm}-\varepsilon_{vmo}^{rc})+\dfrac{\lambda}{V}\ln\dfrac{p_{m}^{'}}{p_{mo}^{'rc}}\right)\right]\\ -\dfrac{\psi^{s}}{Vt_{o}^{s}}\exp\left[\dfrac{V}{\psi^{s}}\left((\varepsilon_{vm}-\varepsilon_{vmo}^{rs})-\dfrac{\lambda}{V}\ln\dfrac{p_{m}^{'}}{p_{mo}^{'rs}}\right)\right]\end{Bmatrix}\frac{\partial F}{\partial\sigma_{ij}^{'}}\end{aligned} \quad (10\text{-}25)$$

Equation (10-25) is the proposed 3D EVPS model for time-dependent stress-strain behavior of soils under general stress condition. This model will be

verified in the following by simulating the stress-strain response of step-changed undrained CRSN test in triaxial condition.

10.5 Properties of SMB and Triaxial Testing Procedure

Bentonite is a clay containing montmorillonite. A mixture consisting of silica sand and bentonite is used in laboratory tests. Mixing sand with bentonite increases the strength of the mixture. The mass fraction of silica sand in the mixture is 60% by dry weight. The silica is BS4550 Pt 5-fraction D150 μm-300 μm. The samples were prepared in slurry with 1.5 times the liquid limit of the mixtures inside containers. De-aired water was used to form the slurry. The soil slurry was pre-consolidated under 24 kPa normal pressure in large-diameter steel tanks.

When the pre-consolidation completed, specimens with 38mm-diameter and 76mm-height were prepared. The basic properties of the sample are specific gravity G_s=2.57, liquid limit w_L=106%, plastic limit w_P=29%, plasticity index I_P=77%, initial water content w=159%. Following the conventional triaxial testing procedure, each specimen was saturated, consolidated and then loaded in the Wykeham Farrance triaxial apparatus. To ensure fully saturation, a back pressure of 100 kPa was applied. The SMB specimens were isotropically consolidated to a confining pressure of 400 kpa in a multi-stage. Once the final consolidation degree exceeded 98%, undrained loading was applied. The axial load was gradually increased while the total confining pressure remained constant. The loading sequence of strain rates

was: $+1\times10^{-5}$ 1/sec, $+1\times10^{-4}$ 1/sec, $+1\times10^{-6}$ 1/sec, $+1\times10^{-7}$ 1/sec, $+1\times10^{-5}$ 1/sec, -1×10^{-5} 1/sec (unloading), $+1\times10^{-5}$ 1/sec (reloading), $+1\times10^{-4}$ 1/sec, $+1\times10^{-6}$ 1/sec, $+1\times10^{-7}$ 1/sec, $+1\times10^{-5}$ 1/sec, -1×10^{-5} 1/sec (unloading), and $+1\times10^{-5}$ 1/sec (reloading). During testing, the axial strain, axial load and porewater pressure are recorded manually.

10.6 Calibration of 3D EVPS Model by Isotropic Consolidation Test

Yin and Graham (1989, and 1994) conducted consistent studies on 1D elastic visco-plastic (1D EVP) modeling of time-dependent stress-strain behavior. A rigorous method was proposed to determine the parameters in EVP model using logarithmic functions. Yin and Tong (2011) adopted a simple method for the determination of all the parameters in 1D EVPS model. The same approach will be used in this chapter to calibrate the 3D EVPS model using the isotropic consolidation results.

a) Basic parameters

Figure 10.3(c) shows the relationship between volume change and effective pressure (in log scale). A logarithmic function with the rebounding index C_r (κ/V) is commonly used in the unloading/reloading loop to fit stress-strain data. Parameter C_r (κ/V) is related to compression in the over-consolidated stage. When loading exceeds the pre-consolidation pressure along the elastic line ($\kappa-line$), deformation

will be along the normal consolidation line with the slope C_c (the compression index). Similarly, by straight line fitting, other coefficients such as C_α (creep coefficient) and C_s (swell coefficient) can be determined.

In a conventional multi-stage isotropic consolidation test, the EOP compression and t_{EOP} can be determined by classic Casagrande's method. The 24 h and EOP $\log p_m^{'}$ - ε_v relationships allow alternative evaluation of pre-consolidation pressure and corresponding strains. Regarding the indexes in compression, it is normally considered $C_{c,24} = C_{c,EOP} = C_c$ and $C_{r,24} = C_{r,EOP} = C_r$ (Yin and Graham, 1999).

Both the compression index $C_{c\varepsilon}$, and rebounding index $C_{r\varepsilon}$ can be determined from Figure 10.3(c). The rebounding index $C_{r\varepsilon}$ is referred to the response in unloading/reloading stage and is defined as the slope of linear portion of strain against logarithmic effective stress along the unloading path. Since the slope is:

$$\begin{aligned} &\kappa / V / \log e = C_e / V = \frac{\Delta \varepsilon_v^e}{\Delta \log p_m^{'}} = C_{r\varepsilon} \\ &\frac{\kappa}{V} = \frac{\Delta \varepsilon_v^e}{\Delta \ln p_m^{'}} = 0.434 \frac{\Delta \varepsilon_v^e}{\Delta \log p_m^{'}} = 0.434 C_{r\varepsilon} \end{aligned} \tag{10-26}$$

By straight line fitting, the slope $C_{r\varepsilon} = 0.035$; and $\kappa / V = 0.015$.

In the normal consolidated stage, we have the following:

$$\begin{aligned} &C_{c\varepsilon} = \frac{\Delta \varepsilon_v^{ep}}{\Delta \log \sigma_z^{'}} \\ &\frac{\lambda}{V} = \frac{\Delta \varepsilon_v^{ep}}{\Delta \ln p_m^{'}} = 0.434 \frac{\Delta \varepsilon_v^{ep}}{\Delta \log p_m^{'}} = 0.434 C_{c\varepsilon} \end{aligned} \tag{10-27}$$

Using to the conventional 24 h loading results, the slope $C_{c\varepsilon}$ in Figure 10.3(c) is 0.272, so that λ / V is 0.118. It is assumed that the reference line for creep and the

reference line for swelling have the same slope. The $(\varepsilon_{vmo}^{rc}, p_{mo}^{'rc})$ stands for the interception point for creep, and $(\varepsilon_{vmo}^{rs}, p_{mo}^{'rs})$ for swelling. Generally we have

$$\begin{cases} \kappa / V = 0.434 C_{r\varepsilon} \\ \lambda / V = 0.434 C_{c\varepsilon} \\ \varepsilon_{vmo}^{rc} = \varepsilon_{vc,24}, p_{mo}^{'rc} = p_{c,24}^{'} \\ \varepsilon_{vmo}^{rs} = \varepsilon_{vs,24}, p_{mo}^{'rs} = p_{s,24}^{'} \end{cases} \tag{10-28}$$

Following equation (10-28), $p_{mo}^{'rc}$ is determined to be 25 kPa ($\varepsilon_{vmo}^{rc} = 0$) and $p_{mo}^{'rs} = 7$ kPa. It is noted that during calibration the reference time line is not unique and requires careful selection.

b) Viscous parameters

The viscous parameters ψ^c / V and t_o^c; ψ^s / V and t_o^s are essential in the EVPS model in that they directly influence the viscous components of strain rate. It is noted that each volume strain in Figure 10.3 is the strain at the end of 24 hour duration (1 day) under each loading (effective stress) following the standard test procedures. Large creep compression occurs in the normally consolidated stress range when stresses are larger than the pre-consolidation pressure. As recommended by Yin and Graham (1999), one load increment in the normally consolidated range should be as long as possible to obtain the ψ^c / V. Similarly, in swelling test the load decrement requires long time to obtain ψ^s / V.

In the modeling, t_o^c serves as the starting point in the reference line and can be chosen to 1440 min once the stress-strain relationship is taken under effective confining stress beyond 24 hours. This approach was adopted in Yin and Graham

(1989, 1994 and 1999). When the specimen is under 100 kPa effective stress in Figure 10.3(a), linear fitting by equation (10-3) with $t_o^c = 1440$ is conducted on creep data and ψ^c / V is determined as 0.0083.

Figure 10.3(b) presents the decrease of volume strain with time in unloading stage under an effective stress of 10 kPa. Using equation (10-8) and the data in Figure 10.3(b) with $t_o^s = 1440$ min, ψ^s / V is determined to be 0.0042. Similar to creep parameters, values of t_o^s and ψ^s / V determine a position for the swelling reference line in $(\ln p'_m, \varepsilon_v)$ space. A different set of t_o^s and ψ^s / V means a different reference time line, but they will finally produce the same swelling strain and strain rate.

Using the calibrated result above, the EVPS model will be adopted to simulate the stress-strain behavior of step-changed constant rate of strain (CRSN) tests in undrained triaxial condition. The simulated values are compared with data from the tests. In this way, the efficiency of this new model is verified.

10.7 Simulation on Undrained Triaxial CRSN Test by 3D EVPS Model

Results of consolidated undrained triaxial CRSN tests with stepped changed strain rate are presented in Figure 10.4. Figure 10.4(a) shows relationships of deviator stress against shear strain; Figure 10.4(b) shows the corresponding relationships of excess pore water pressure against shear strain; and Figure 10.4(c) shows the TSP and ESP. It is seen that both the deviator stress and excess porewater

pressure are affected by the strain rate. The larger the strain rate, the higher the deviator stress, and the higher the excess porewater pressure recorded. In the tests, each deviator stress increment was applied suddenly on the specimen and then held constant.

In this section, the proposed EVPS model in equation (10-25) is applied to undrained triaxial CRSN test. As recommended by Yin *et al.* (1994), equation (10-25) in triaxial stress condition is expressed as:

$$\begin{cases} \dot{\varepsilon}_v = \dfrac{1}{K^e}\dot{p}^{'} + \dfrac{1}{J^e}\dot{q} + S(2p^{'} - p_m^{'}) \\ \dot{\varepsilon}_s = \dfrac{1}{J^e}\dot{p}^{'} + \dfrac{1}{3G^e}\dot{q} + S\dfrac{2q}{M^2} \end{cases} \tag{10-29}$$

where the shear modulus is obtained from $G^e = \dfrac{DJ^{e2}}{J^{e2} + 3DK^e}$, in which the bulk modulus $K^e = p^{'}/(\kappa/V) = p^{'}/0.015$, D is the apparent modulus and the coupling modulus $J^e = -K^e\dfrac{dq}{dp^{'}} = -5.2K^e$.

Using the unloading/reloading data, D is determined to be 35000 kPa. The slope of Critical State Line (CSL) is computed by $M = 6\sin\phi^{'}/(3-\sin\phi^{'})$. In the extreme case, if the coupling modulus is infinite, any term related to J^e will disappear and the well known hypoelastic model (Duncan and Chang, 1970) is obtained.

In the undrained condition, $\Delta\varepsilon_v \equiv 0$. From equation (10-29), the relations for modeling $p^{'}$ versus q, q versus ε_s and variation of excess porewater pressure (Δu) are expressed as:

$$\begin{cases} \dot{p}' = -K^e[\dfrac{1}{J^e}\dot{q} + S(2p' - p_m')] \\ \dot{q} = 3G^e[\dot{\varepsilon}_s - \dfrac{1}{J^e}\dot{p}' - S\dfrac{2q}{M^2}] \\ \Delta u = p_i' + q/3 - p' \end{cases} \tag{10-30}$$

where p_i' is initial effective mean on the p'-axis.

Once the Runge-Kutta method is used, solutions are obtained numerically. In simulation of CRSN tests, new strain rate and new initial strains are used if the strain rate is changed. With varied strain rates in CRSN tests, the strain rate dependent behaviors can be simulated. The measured and predicted curves of q versus ε_s, Δu versus ε_s and effective stress path p' versus q are presented in Figure 10.5. The predicted results generally agree with the test data. The strain rate effect can be clearly seen in the prediction of q versus ε_s by the EVPS model. As pointed in Yin and Tong (2011), the simulation is sensitively dependent on the creep parameter, ψ^c/V and the swelling parameter ψ^s/V. Careful selections of viscous parameters in EVPS model are required. Compared with the EVP model in Yin and Graham (1999), the unloading/reloading loop can be reproduced. This model therefore can deal with the time-dependent effects resulting from swelling.

10.8 Summary and Conclusions

Based on "reference time" and "equivalent time" concepts, a new Elastic Visco-Plastic model considering both creep and swelling behaviors (EVPS model) is proposed. Using isotropic consolidation test results on silica sand mixed bentonite

(SMB) specimens, all the parameters in the EVPS model can be determined. This new model is then adopted to simulate the time-dependent stress-strain relations in triaxial undrained CRSN tests. The following conclusions can be made:

a. The EVPS model is an extension of the 1D EVPS model in Yin and Tong (2011) for considering the contribution of swelling rate to the total strain rate in three dimensions.

b. Eight parameters are needed to construct the model for a specific soil. Once all the parameters are determined by isotropic consolidation tests, this model can predict the time-dependent soil behaviors. Proper estimations of viscous parameters for both creep and swelling are essential to the EVPS model.

c. The EVPS model has been adopted to simulate triaxial undrained CRSN tests on different SMB specimens. The simulated results generally agree well with the test data. The unloading/reloading loop can be reproduced. This EVPS model is also valid in describing viscous soil behaviors in a wide range including stress relaxation, swelling pressure, pre-consolidation pressure, etc.

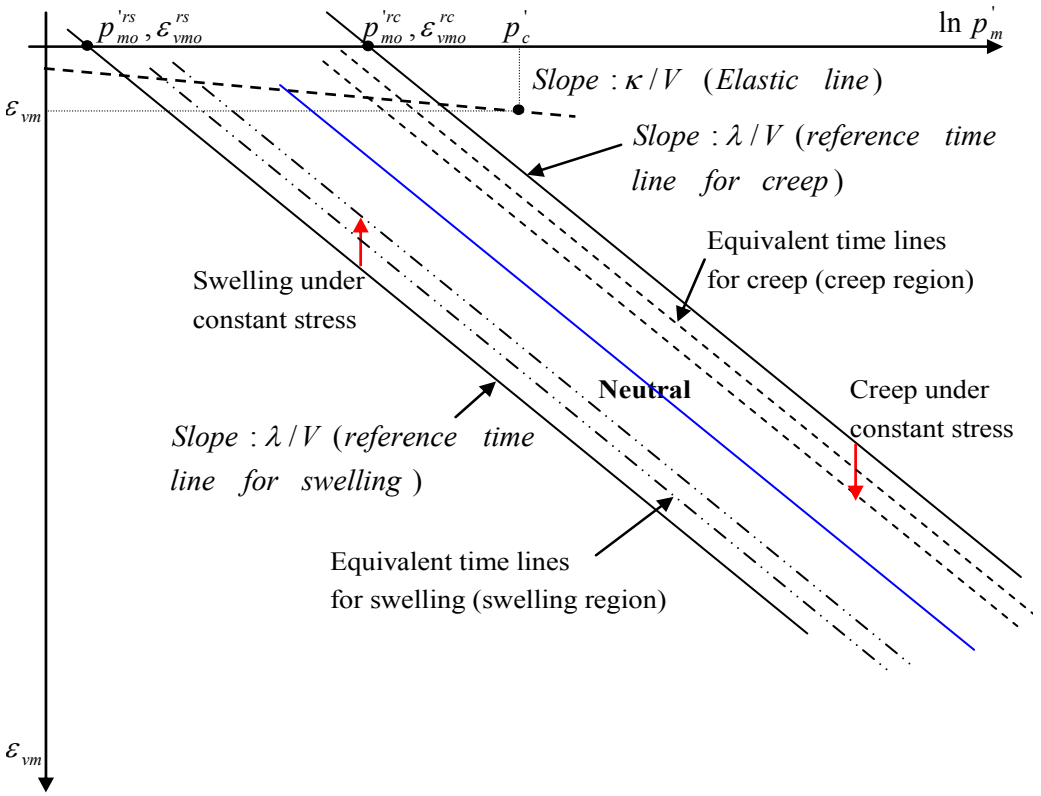

Figure 10.1 Conceptual model of creep, swelling, "reference" time line, and "equivalent" time lines for 1D stressing (extended from Yin and Tong, 2011)

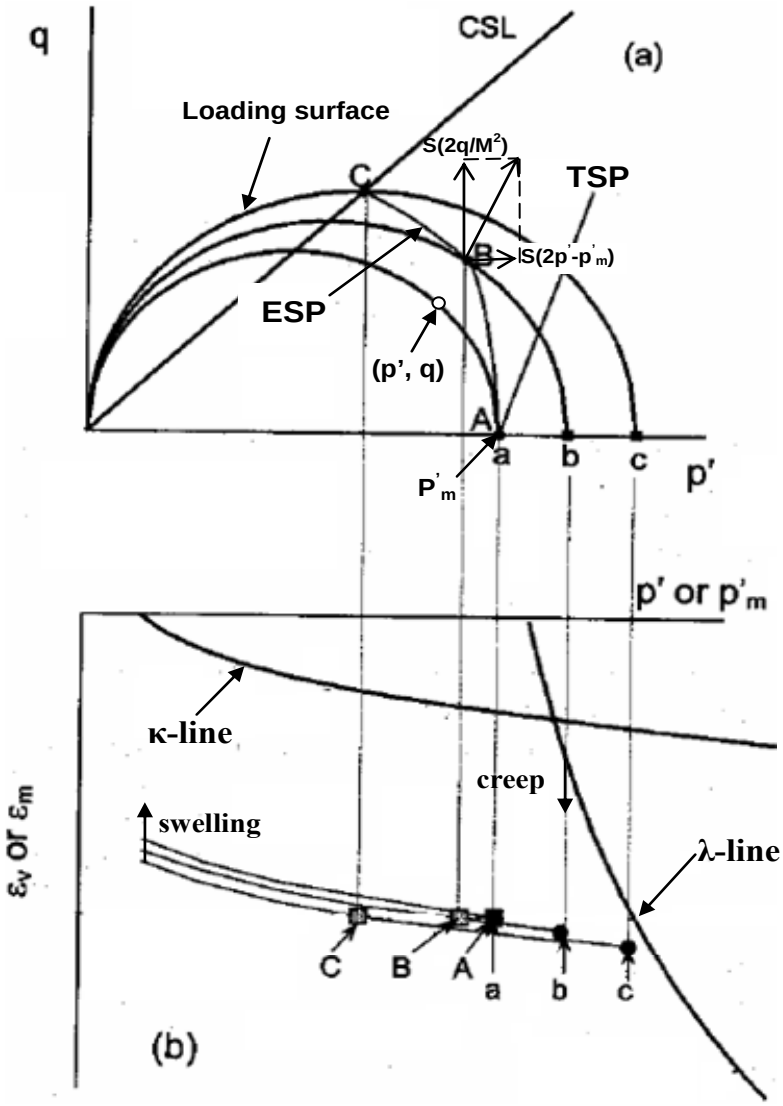

Figure 10.2 Illustration of (a) loading surfaces, total stress path (TSP), and effective stress path (ESP) in $q - p^{'}$ space and (b) corresponding ε_m (or ε_v) versus $p^{'}$, instant timeline, reference time line and limit timeline for isotropically consolidated, undrained triaxial test at constant axial strain rate (extended from Yin and Graham, 1999)

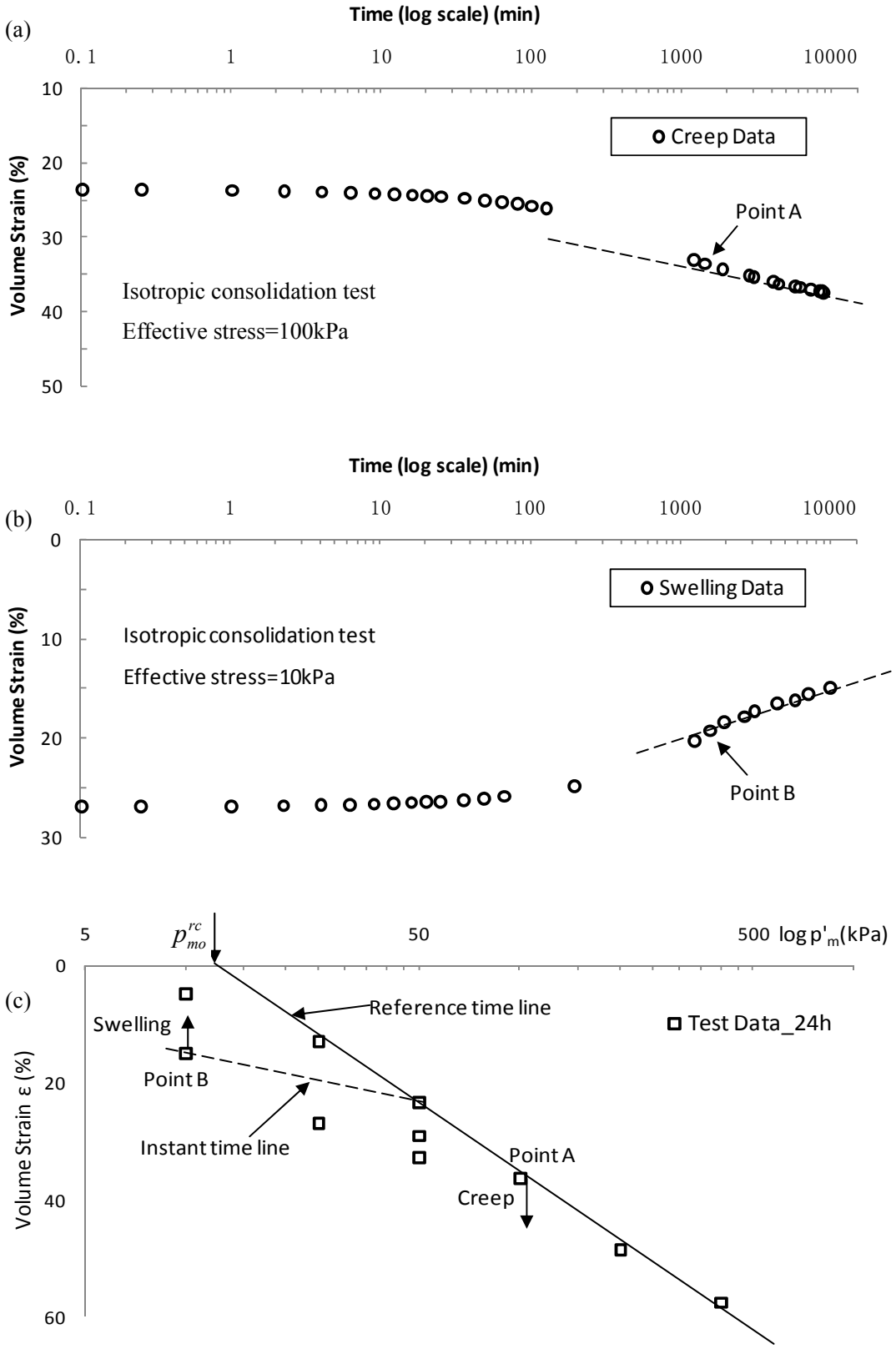

Figure 10.3 Isotropic consolidation data - (a) increase of volume strain with time, (b) decrease of volume strain with time, and (c) effective stress versus volumetric strain

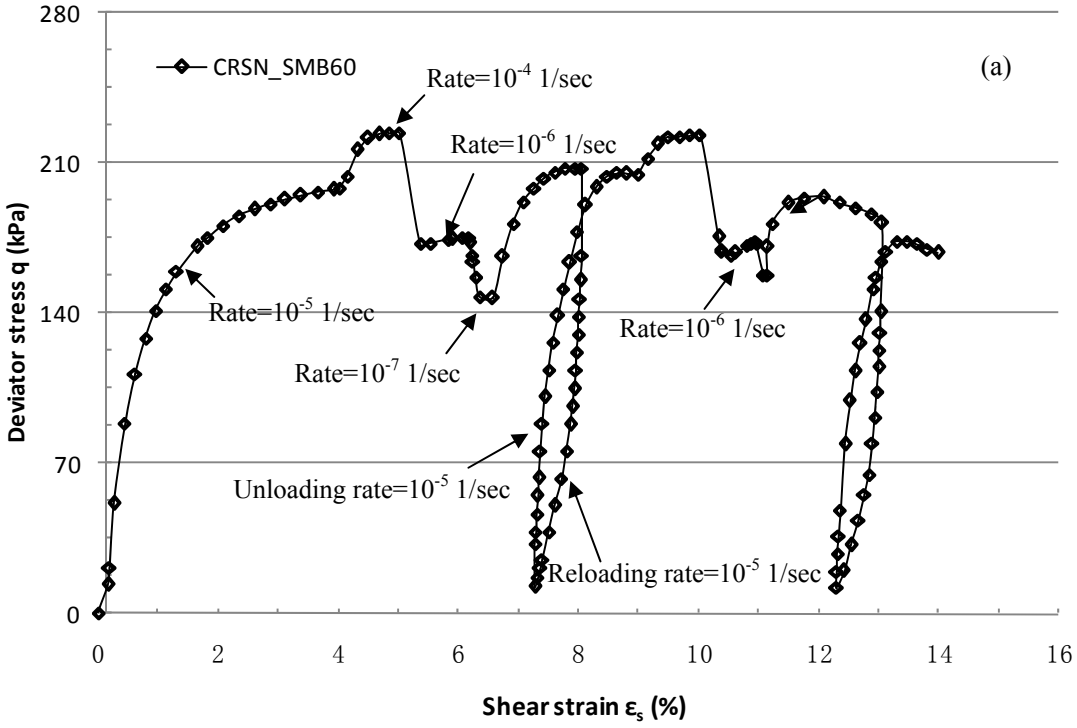
280
210
140
70
0
Deviator stress q (kPa)
CRSN_SMB60
(a)
Rate=10-4 1/sec
Rate=10-6 1/sec
Rate=10-5 1/sec
Rate=10-7 1/sec
Rate=10-6 1/sec
Unloading rate=10-5 1/sec
Reloading rate=10-5 1/sec
0
2
4
6
8
10
12
14
16
Shear strain εs (%)

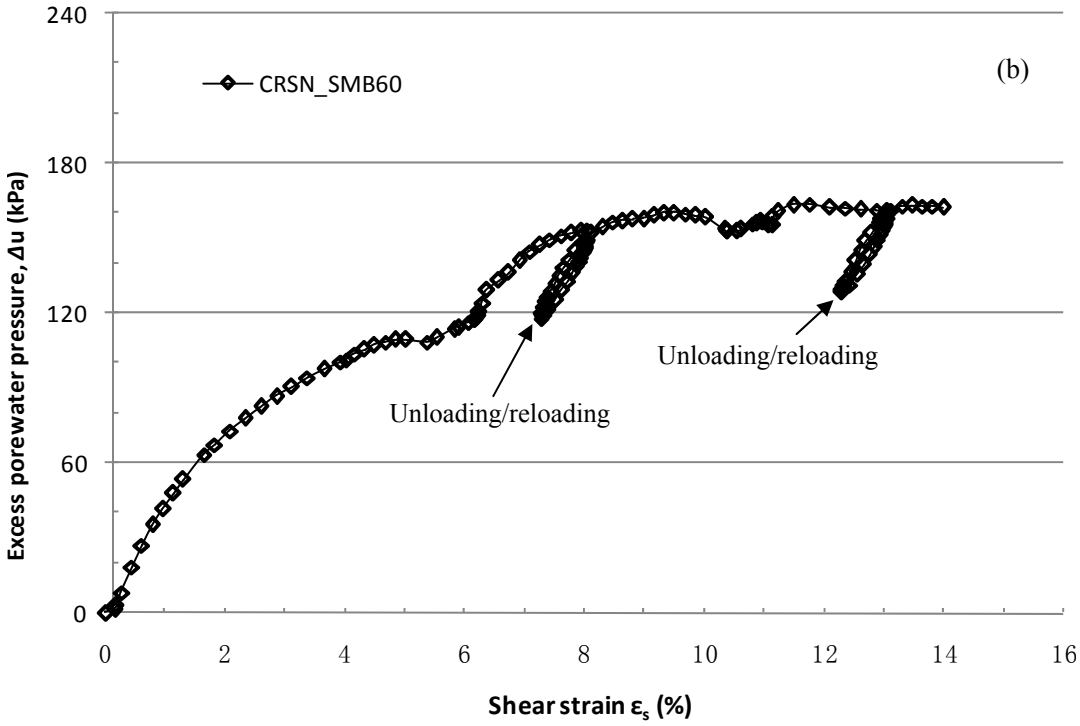
240
180
120
60
0
CRSN_SMB60
(b)
Excess porewater pressure, Δu (kPa)
Unloading/reloading
Unloading/reloading
0
2
4
6
8
10
12
14
16
Shear strain εs (%)

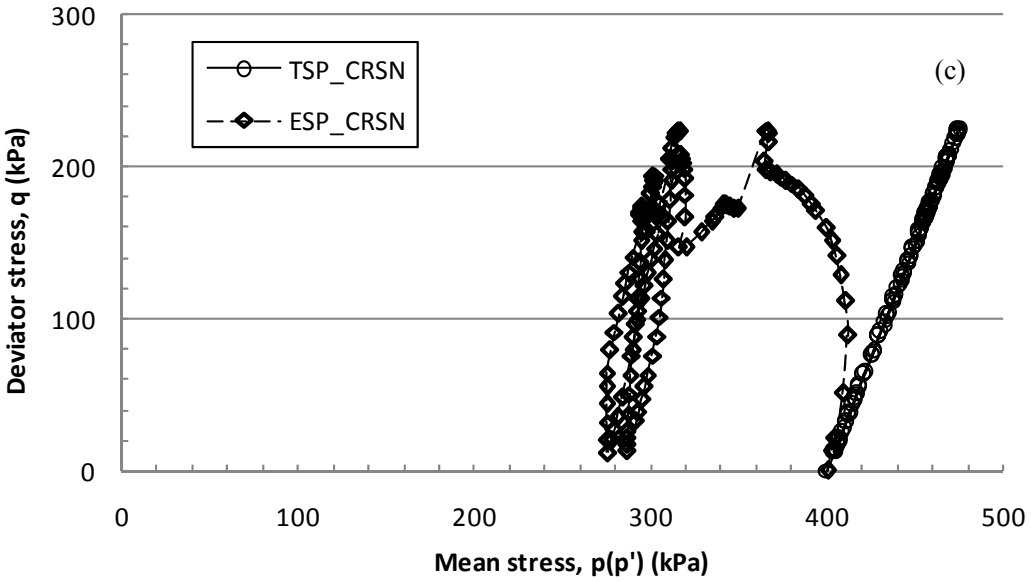

Figure 10.4 Results from the triaxial undrained CRSN test with step-changed strain rates and with unloading and reloading - (a) curve of deviator stress, q versus shear strain, ε_s, (b) curve of excess porewater pressure, Δu versus shear strain, ε_s, and (c) curve of mean stress, p (p') versus deviator stress, q

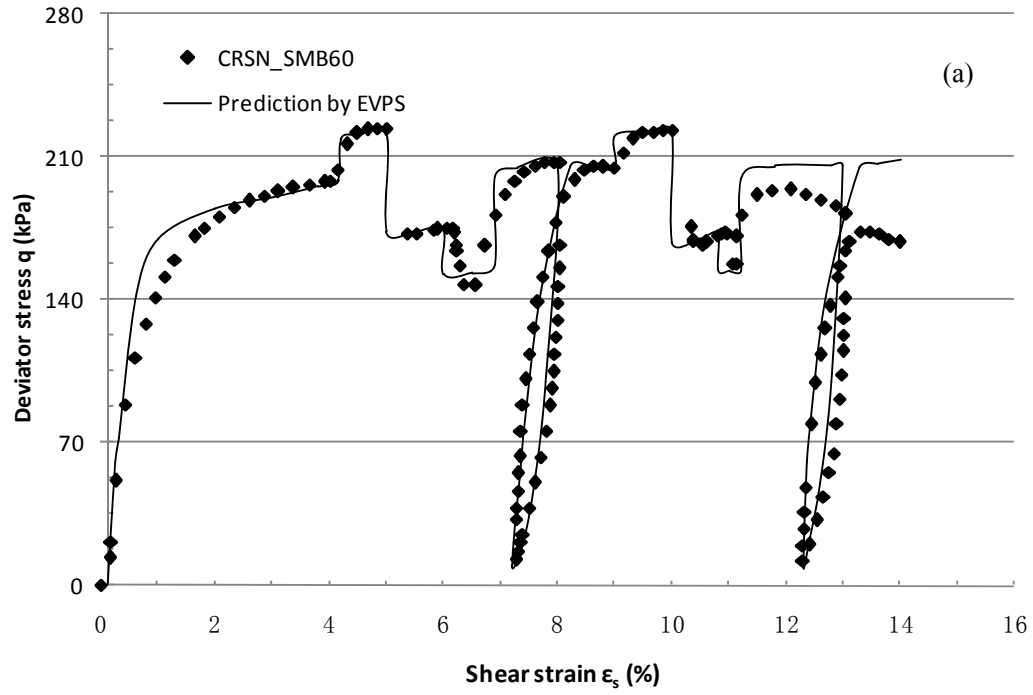
CRSN_SMB60
Prediction by EVPS
(a)
Deviator stress q (kPa)
280
210
140
70
0
0
2
4
6
8
10
12
14
16
Shear strain ε_s (%)

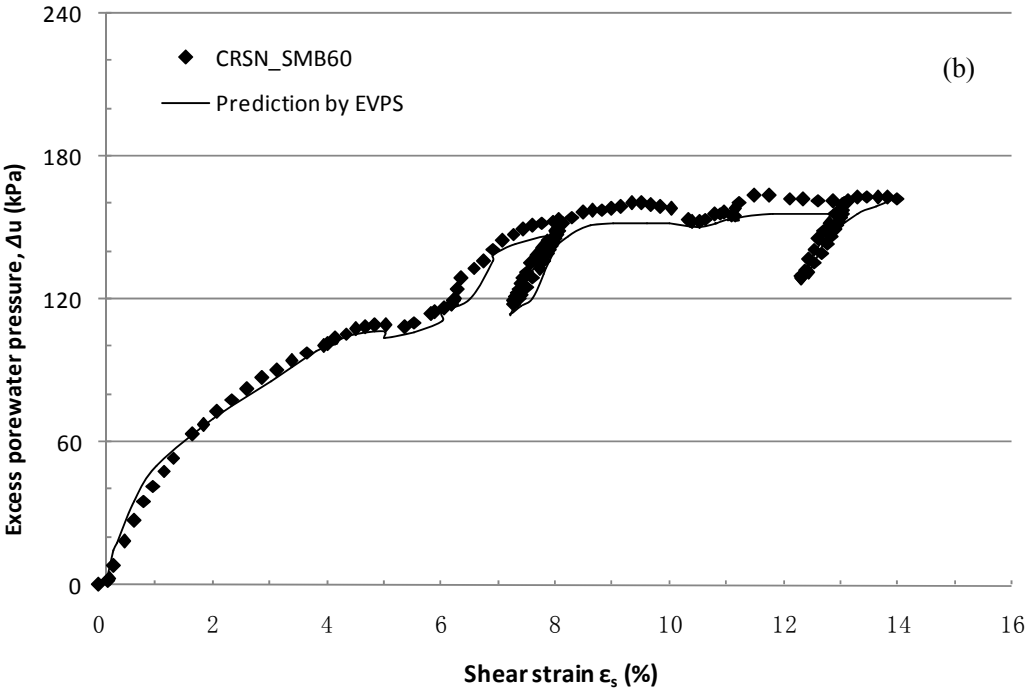
CRSN_SMB60
Prediction by EVPS
(b)
Excess porewater pressure, Δu (kPa)
240
180
120
60
0
0
2
4
6
8
10
12
14
16
Shear strain ε_s (%)

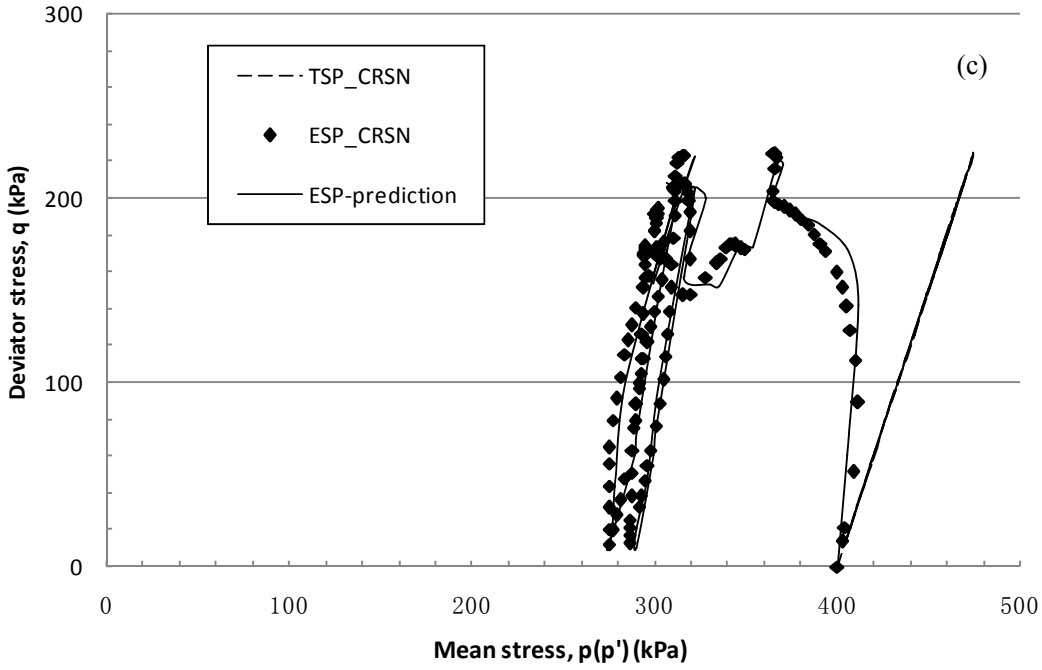

Figure 10.5 Measured and predicted curves - (a) deviator stress (q) versus shear strain (ε_s), (b) excess porewater pressure (Δu) versus shear strain (ε_s), and (c) mean stress, $p\ (p')$ versus deviator stress (q).

Chapter 11

Conclusions and Suggestions

11.1 Summary of New Works

In this thesis, the time-dependent stress-strain behaviors of clayey soils are examined. New works have been done as follows:

a. The silica sand mixed bentonite samples are tested with different sand content (50%, 60%, 70%, 80% and 90%, respectively) in different stress conditions.

b. The HKMD samples are tested in settling column condition, low stress constant rate of strain condition and oedomoter condition, in this way complete consolidation behaviors are examined.

c. Viscous behaviors of clayey soils are investigated, especially on the swelling behavior. Swellings of SMB in both oedometer condition and triaxial condition are studied. Coefficients of C_s and C_s/C_r are presented and discussed.

d. A new 1D Elastic Visco-Plastic model considering both creep and swelling behaviors (namely EVPS model) is proposed. Compared with the EVP model in Yin and Graham (1994 and 1999), the presented 1D EVPS model considers swelling so that the unloading/reloading loop can be simulated. The 1D EVPS has been verified in CRSN tests on SMBs, and then used to predict constant rate of stress tests and relaxation tests in 1D straining.

e. A 3D EVPS model is extended from the 1D EVPS model for considering the contribution of swelling rate to the total strain rate in three dimensions. The 3D

EVPS has been verified in triaxial undrained CRSN tests on SMBs. The 3D EVPS model is powerful in describing viscous soil behaviors in triaxial compression and extension conditions.

11.2 Conclusions

The SMB and HKMD samples are adopted in this thesis to conduct experimental study in different stress conditions. Based on the test results and experiment observations, following conclusions can be made:

a. Viscosity is one of the significant properties of clayey soils. Clayey soils exhibit more or less both creep and swelling behaviors in saturated condition. Non-linear creep and swelling behaviors have been observed from the 1D multi-stage oedometer tests on both SMB and HKMD specimens. Both creep and swelling behaviors appear less obvious under higher stress condition.

b. The strain rate effect is clearly observed in both CRSN oedometer tests and undrained triaxial CRSN tests on fully saturated SMB specimens. With step-changed strain rate, a unique stress-strain-strain rate relationship is obtained in compression. In undrained triaxial CRSN tests, both the deviator stress and excess porewater pressure are influenced by strain rate. The higher the strain rate, the higher the deviator stress and the excess porewater pressure. The influence of strain rate on the deviator stress is more significant than that on excess porewater pressure. Strain softening is also observed on SMB specimens.

c. Stress relaxation is a significant time-dependent behavior in clayey soils. Relaxation test is an important measure for studying the viscous properties of soils. Stress relaxations can be performed in both creep and swelling conditions. Both the HKMDs and SMBs exhibit considerable viscosity in relaxation tests. The "swelling pressure" observed in swelling relaxation test verifies that swelling occurs in saturated condition, especially for expansive soils.

d. In settling column tests, typical settling curves indicate a constant settling rate at zone settling, and then attain transition points, thereafter decreasing. Soils even exhibit viscosity in self-weight consolidation. Soil concentration has critical influence on the settling property. In final density profile, the slope of soil height over volume fraction becomes steeper once the soil concentration increases. The coefficient of consolidation C_v is found to decrease when the soil concentration increases. Combined with settling column results, MSL results and CRSN results, complete consolidation curves are obtained for HKMD samples. The basic compression index C_{bc} is determined by linear fitting for each HKMD soil.

e. The sand content exerts an indispensible impact on the behaviors of SMB soils. In MSL oedometer condition, SMB soils with higher sand content has lower compressibility, lower value of C_c, C_r, C_α, C_s, and lower ratio of C_α/C_c , C_s/C_r,; in isotropic condition, with the increase of sand content, SMB specimens exhibit lower compressibility and less viscosity; in CRSN oedometer condition at a given strain rate, the higher the sand content, the higher the vertical effective stress at a given strain. C_c and C_α/C_c decrease with the increase of sand contents; in

undrained triaxial CRSN condition at a given axial strain rate and a given confining pressure, SMB specimens with higher sand content have higher deviator stress and higher excess porewater pressure.

Based on the experimental studies, the concept of equivalent time is adopted to formulate a new Elastic Visco-Plastic model considering both creep and swelling behaviors:

a. In 1D straining condition, all the eight parameters in the 1D EVPS model are determined from MSL oedometer test results, the model can predict time-dependent behaviors of a soil element under any loading condition in 1D straining, such as constant rate of strain (CRSN) loading, constant rate of stress (CRSS) loading, relaxation, unloading/reloading, etc. Using transfer of variables and perturbation method, analytical solution is obtained for 1D EVPS model in stress relaxation condition. The simulations by the solution from the EVPS model on relaxation tests agree well with the test data.
b. The 3D EVPS model is an extension of the 1D EVPS model for considering the contribution of swelling rate to the total strain rate in three dimensions. The EVPS model has been adopted to simulate triaxial undrained CRSN tests on a SMB specimen. The simulated results agree well with the test data. This EVPS model is also valid in describing viscous soil behaviors in a wide range, such as stress relaxation, swelling pressure, pre-consolidation pressure, etc.

c. Based on reference time line and equivalent time line, both the creep parameter ψ^c / V and the swelling parameter ψ^s / V are needed in the EVPS model to predict the viscous behavior of soils. Proper estimations of viscous parameters for both creep and swelling are essential to the model. The creep parameter is more sensitive than the swelling parameter.

11.3 Suggestions for Future Research

The following works are suggested in the future research:

a. The time-dependent stress-strain behaviors of clayey soils are addressed in this thesis. For more accurate understanding and prediction of these behaviors, it is necessary to conduct experimental studies on undisturbed soil samples from field.

b. For full examination of the stress-strain behaviors of clayey soils, different soil samples beside SMBs and HKMDs are needed to carry out experimental studies and analysis in various stress conditions, such as K_o consolidated undrained/drained compression/extension tests, triaxial undrained/drained creep tests, etc. More test data are needed to describe and predict the stress-strain behaviors.

c. The small strain stiffness properties of soils, such as shear wear velocity and shear modulus play a key role in the adequate design of earth structures (Hoyos *et al.*, 2011). The small strain here denotes the strain less than 0.01%. For this purpose, some special sensor techniques are need for the measurement of local axial strain

and stiffness. The bender element technique has proved an effective approach to investigate the soil stiffness at a very small strain. On the other hand, with the application of optical-fibre sensor in geotechnical engineering projects, this powerful technique can be utilized in conventional triaxial apparatus to examine the influence of effective stress on the shear modulus and stiffness at local small strain. The installment of optical-fibre sensor incorporated with bender element in triaxial test system can be considered in future research for small strain study. This would be a very interesting research area.

d. Finite strains have become a problem in mining waste, particularly in phosphatic wastes, but are less of a problem with embankments. If finite strains are taken into account, solutions on soil behavior may encounter problem (Zhu, 1999). The present research is based on the assumption that the strain is moderately small. Most constitutive models are developed based on small strain formulations. The effect of finite strain should be considered in the future work.

e. Studies on large strain have been reviewed in Chapter 2. Behaviors in large strain condition with or without self-weight consolidation differ significantly from those in small strain condition. In consolidation analysis, the coefficient of permeability is one of the key parameters. However, this parameter is very difficult to estimate if the soil is subjected to large strain consolidation. Gibson *et al.* (1967) proposed the governing equation to describe a homogeneous material. For large strain problem, both descriptions of spatial and material are appropriate. Although some empirical relations have been obtained for determining the

coefficient of permeability, insufficient data are available for formulating a general frame-indifferent law, especially for the horizontal permeability (Al-Tabbaa and Wood, 1991). The large strain effect should be taken into consideration in analyzing the consolidation of soft soils.

f. Compared with laboratory testing, field tests are generally complex. Very few field tests were conducted satisfactorily due to many uncertain factors. However, laboratory tests and conventional constitutive models are aimed to give reliable prediction of the soil behaviors on site. Insufficient efforts are made in field study and field verification of the proposed model. More research work should be carried out in field applications.

Appendix

In equation (9-19), $Ay^{'} = By^{m} - Cy^{n}$. Assume $Z = y^{1-n}$, so that

$$\dot{y} = \frac{1}{1-n} y^{n} \cdot \dot{Z} \tag{a1}$$

and equation (9-19) can be rewritten as

$$\dot{Z} = \frac{B(1-n)}{A} - \frac{C(1-n)}{A} \cdot Z^{m-1} \tag{a3}$$

If $k = \frac{B(1-n)}{A}$ and $\varepsilon = \frac{C(1-n)}{A}$, when $|\varepsilon| < 0.01$, a perturbed solution can be obtained. Note $Z = Z_0 + \varepsilon Z_1 + \varepsilon^2 Z_2 + ...\varepsilon^n Z_n$, so that we have

$$\dot{Z} = \dot{Z}_0 + \varepsilon \dot{Z}_1 + \varepsilon^2 \dot{Z}_2 + ...\varepsilon^n \dot{Z}_n \tag{a3}$$

Moreover we assume

$$f(\varepsilon) = \varepsilon Z^{m-1} = \varepsilon(Z_0 + \varepsilon Z_1 + \varepsilon^2 Z_2 + ...\varepsilon^n Z_n) \tag{a4}$$

and apply the Taylor series expansion to ε in equation (a4):

$$\begin{aligned}
\dot{f}(\varepsilon) &= (Z_0 + \varepsilon Z_1 + \varepsilon^2 Z_2 + ...\varepsilon^n Z_n)^{m-1} + \varepsilon(m-1)(Z_1 + 2\varepsilon Z_2 + ...)^{m-1} \\
\ddot{f}(\varepsilon) &= 2(m-1)(Z_1 + 2\varepsilon Z_2 + ...)^{m-2} + \varepsilon(m-1)(m-2)(2Z_2 + 6\varepsilon Z_3 + ...)^{m-3} \\
\dddot{f}(\varepsilon) &= 3(m-1)(m-2)(2Z_2 + 6\varepsilon Z_3 + ...)^{m-3} + \varepsilon(m-1)(m-2)(m-3)(6Z_3 + ...)^{m-4}
\end{aligned} \tag{a5}$$

If truncated at the third item, $f(\varepsilon)$ can be therefore described in the following form:

$$f(\varepsilon) = \varepsilon Z^{m-1} = \varepsilon Z_0^{m-1} + \varepsilon^2 2(m-1) Z_1^{m-2} + \varepsilon^3 3(m-1)(m-2)(2Z_2)^{m-3} \tag{a6}$$

Compared with equation (a3), each item can be determined as:

$$\begin{aligned}
Z_0 &= kt \\
Z_1 &= \frac{1}{m} k^{m-1} t^{m} \\
Z_2 &= \frac{2(m-1)}{m(m+1)} k^{m-1} t^{m+1} \\
Z_3 &= \frac{6(m-1)^2(m-2)}{m(m+1)(m+2)} k^{m-1} t^{m+2}
\end{aligned} \tag{a7}$$

Finally we have the solution:

$$z = (kt)^{m-1} + \frac{\varepsilon k^{m-1} t^{m}}{m} + \frac{2\varepsilon^{2}(m-1)k^{m-1}t^{m+1}}{m(1+m)} + \frac{6\varepsilon^{3}(m-1)(m-2)k^{m-1}t^{m+2}}{m(1+m)(2+m)} \tag{a7}$$

References

Abu-Hejleh, A.N. and Znidarcic, D. (1992). Consolidation characteristics determination for phosphatic clays. Vol. 3, Publication No. 02-084-104, University of Colorado.

Abu-Hejleh, A.N., Znidarcic, D. and Barnes, B.L. (1996). Consolidation characteristics of phosphatic clays. Journal of Geotechnical Engineering, ASCE, Vol. 122(4), pp. 295-301.

Adachi, T. and Oka, F. (1982). Constitutive equations for normally consolidated clay based on elasto-viscoplasticity. Soils and Foundations, Vol. 22(4), pp. 57-70.

Adachi, T., Oka, F. and Zhang, F. (1998). An elasto-plastic constitutive model with strain softening. Soils and Foundations, Vol. 38(2), pp. 27-35.

Akai, K., Adachi, T. and Ando, N. (1975). Existence of a unique stress-strain-time relation of clays. Soils and Foundations, Vol. 15(1), pp. 1-16.

Alawaji, H.A. (1999). Swell and compressibility characteristics of sand–bentonite mixtures inundated with liquids. Applied Clay Science, Vol. 15(3-4), pp. 411-430.

Alberro, J. and Santoyo, E. (1973). Long term behaviour of Mexico city clay. Proc. of the 8th International Conference on Soil Mechanics and Foundation Engineering, Moscow, Vol. 1, pp. 1-9.

Al-Rawas, A.A. and Goosen, M.F.A. (2006). Expansive soils-recent advances in characterization and treatment. Taylor & Francis, London.

Al-Tabbaa, A. and Wood, D.M. (1991). Horizontal drainage during consolidation insight gained from analyses of a simple problem. Géotechnique, Vol. 41(4), pp. 571-585.

Arai, K. (1985). Representation of soft clay behaviour based on minimization of dissipated energy. Proc. of the 5th International Conference on Numerical Methods in Geamechanics, Nagoya, Japan, Vol. 1, pp. 277-284.

Barden, L. and Berry, P.L. (1965). Consolidation of normally consolidated clay. Journal of Soil Mechanics and Foundation Division, ASCE, Vol. 91, pp. 15-35.

Bartholomeeusen, G., Sills, G.C., Znidarcic, D., Van Kesteren, W., Merckelbach, L.M., Ryke, R., Carrier III, W.D., Lin, H., Penumadu, D., Winterwerp, H., Masala, S. and Chan, D. (2002). Numerical prediction of large-strain consolidation. Géotechnique. Vol. 52(9), pp. 639-648.

Been, K. and Sills, G.C. (1981). Self-weight consolidation of soft soils: an experimental and theoretical study. Géotechnique, Vol. 31(4), pp. 519-535.

Berlamont, J., Ockenden, M., Toorman, E. and Winterwerp, J. (1993). The characterisation of cohesive sediment properties. Journal of Coastal Engineering, Vol. 21, pp. 105-128.

Berre, T. and Iversen, K. (1972). Oedometer tests with different specimen heights on a clay exhibiting large secondary compression. Géotechnique, Vol. 22(1), pp. 53-70.

Bishop, A.W. and Lovenbury, H.T. (1969). Creep characteristics of two undisturbed clays. Proc. of the 7th International Conference on Soil Mechanics and Foundation Engineering, Mexico, Vol. 1. pp. 29-37.

Bjerrum, L. (1967). Engineering geology of Norwegian normally consolidated marine clays as related to the settlements of buildings. Géotechnique, Vol. 17(2), pp. 83-118.

Bjerrum, L. (1973). Problems of soils mechanics and construction on soft clays and structurally unstable soils (collapsible, expensive and others). Proc. of the 8th International Conference on Soil Mechanics and Foundation Engineering, Mockba, Vol. 2, pp. 109-159.

Bo, M.W., Arulrajah, A. and Choa, V. (1997). Performance verification of soil improvement work with vertical drains. Proc. of 30th Anniversary Symposium Southeast Asian Geotechnical Society, Bangkok, Thailand, pp. 191–203.

Borja, R.I. and Kavazanjian, E. (1985). A constitutive model for the stress-strain-time behaviour of 'wet' clays. Géotechnique, Vol. 35(3), pp. 283-298.

Bruun-Hansen, H.C., Raben-Lange, B., Raulund-Rasmussen, K. and Borgaard, O.K. (1994). Monosilicate adsorption by ferrhydrite and goethite at pH 3-6. Soil Science, Vol. 158 (1), pp. 40-46.

BS 1377: Part 1 to 8 (1990). British standard methods of test for soils for civil engineering purposes. British Standards Institution, London.

Buisman, A.S.K. (1936). Results of long duration settlement tests. Proc. of 1st International Conference on Soil Mechanics, Cambridge, MA, pp.103-106.

Burghignoli, A. (1979). An experimental study of the structural viscosity of soft clays by means of continuous consolidation tests. Proc. of the 7th European Conference on Soil Mechanics and Foundation Engineering, Brighton, Vol. 2, pp. 23-28.

Butterfield, R. (1979). A natural compression law for soil (an advance on e-logp'). Géotechnique, Vol. 29(4), pp. 469-480.

Cargill, K.W. (1982). Consolidation of soft layers by finite strain analysis. Miscellaneous Paper GL-82-3, US army engineer waterways experiment station, Vicksburg, US.

Carrier III, W.D. and Beckman, J.F. (1984). Correlation between index test and the properties of remoulded clays. Géotechnique, Vol. 34(2), pp. 211-228.

Casagrande, A. and Wilson, S.D. (1951). Effect of rate of loading on the strength on clays and shales at constant water content. Géotechnique, Vol. 2(3), pp. 251-263.

Chen, F.H. (1988). Foundations on expansive soils. Elsevier Applied Science Publication, London.

Cheng, C.M. and Yin J.H. (2005). Strain-Rate dependent stress-strain behavior of undisturbed Hong Kong marine deposits under oedometric and triaxial stress states. Marine Georesources & Geotechnology, Vol. 23(1-2), pp. 61-92.

Cour, F.R. (1971). Inflection point method for computing c_v. Journal of Soil Mechanics and Foundation Engineering, Vol. 5, pp. 827–831.

Craig, R. F. (2004). Soil Mechanics. 7th edition, Spon Press, London.

Crawford, C.B. (1959). The influence of rate of strain on effective stresses in a sensitive clay. American Society for Testing Materials, Vol. 254, pp. 36-61.

Crawford, C.B. (1964). Interpretation of the consolidation test. Journal of the Soil Mechanics and Foundation Division, ASCE, Vol. 90(SM5), pp. 87-102.

Crawford, C.B. (1965). The resistance on soil structure to consolidation. Canadian Geotechnical Journal, Vol. 2(2), pp. 90-97.

Dakshanamurthy, V. (1978). A new method to predict swelling using a hyperbolic equation. Journal of Geotechnical Engineering, Vol. 9, pp.79-87.

Daniel, D.E. and Wu, Y.K. (1993). Compacted clay liners and covers for arid sites. Journal of Geotechnical Engineering, ASCE, Vol. 119(2), pp. 223–237.

Den Haan, E.J. (1996). A compression model for non-brittle soft clays and peat. Géotechnique, Vol. 16(1), pp. l-l6.

Desai, C.S. and Zhang, D. (1987). Viscoplastic model for geologic materials with generalised flow rule. International Journal for Numerical and Analytical Methods in Geomechanics, Vol. 11(6), pp. 603-620.

Dixon, D.A. and Woodcock, D.R. (1986). Physical properties and standards for testing reference buffer materials. AECL Technical Record, TR352.

Duncan, J.M. and Buchignani, A.L. (1973). Failure of underwater slope in San Francisco. Journal of the Soil Mechanics and Foundations Division, ASCE, Vol. 99, (SM9), pp. 687-703.

Duncan, J.M. and Chang, C.Y. (1970). Non-linear analysis of stress and strain in soils. Journal of the Soil Mechanics and Foundation Division, ASCE, Vol. 96(SM5), pp. 1629-1654.

El-Sohby, M.A. and Mazen, O. (1983). Mineralogy and swelling of expansive clayey soils. Journal of Geotechnical Engineering, Vol. 14, pp. 79-87.

El-Sohby, M.A. and Rabba, E.A. (1981). Some factors affecting swelling of clayey soils. Journal of Geotechnical Engineering, Vol. 12, pp. 19-87.

Feda, J. (1992). Creep of soils and related phenomena. Elsevier Applied Science Publication, London.

Fitch, B. (1983). Kynch theory and compression zones. AIChE Journal. Vol. 29, pp. 940-942.

Fredlund, D.G. and Raharadjo, H. (1993). Soil mechanics for unsaturated soils. John Wiley & Sons, New York.

Garlanger, J.E. (1972). The consolidation of soils exhibiting creep under constant effective stress. Géotechnique, Vol. 22(1), pp. 71-78.

GEO (2008). Guide to soil nail design and construction, pp. 21-25 and 77-78.

Gibson, R.E., England, G.L. and Hussey, M.J.L. (1967). The theory of one-dimensional consolidation of saturated clays I. finite nonlinear consolidation of thin homogeneous layers. Géotechnique, Vol. 17(4), pp. 261-273.

Gibson, R.E. and Lo, K.Y. (1961). A theory of consolidation of soils exhibiting secondary compressions. Acta Polytechnica Scandinavica, 296, Ci 10.

Gibson, R.E., Schiffman, R.L. and Cargill, K.W. (1981). The theory of one-dimensional consolidation of saturated clays. II. finite nonlinear consolidation of thick homogeneous layers. Canadian Geotechnical Journal, Vol. 18(2), pp. 280-293.

Graham, J., Crook, J.H.A. and Bell, A.L. (1983a). Time effects on the stress-strain behavior of natural soft clays. Géotechnique, Vol. 33(3), pp. 327-340.

Graham, J., Noonan, M.L. and Lew, K.V. (1983b). Yield states and stress-strain relations in natural plastic clay. Canadian Geotechnical Journal, Vol. 20, pp. 502-516.

Graham, J., Saadat, F., Gray, M.N., Dixon, D.A. and Zhang, Q.Y. (1989). Strength and

volume change behaviour of a sand-bentonite mixture. Canadian Geotechnical Journal, Vol. 26, pp. 292-305.

Gray, H. (1936). Progress report on the consolidation of fine-grained soils. Proc. of 1st International Conference on Soil Mechanics, Cambridge, MA, pp.138-141.

Gray, M.N., Cheung, S.C.H. and Dixon, D.A. (1984). The influences of sand content on swelling pressures and structure developed by statically compacted Na-bentonite. Atomic Energy of Canada Limited Report, AECL-7825.

Hashim, R. and Muntohar, A.S. (2006). Swelling rate of expansive clay soils. Expansive soils-recent advances in characterization and treatment, edited by Al-Rawas, A.A. and Goosen, M.F.A., Taylor & Francis, London.

Hawlader, B.C., Muhunthan, B. and Imai, G. (2008). State-dependent constitutive model and numerical solution of self-weight consolidation. Géotechnique, Vol. 58(2), pp. 133-41.

Head, K.H. (1985). Manual of Soil Laboratory Testing: Effective Stress Tests. Pentech Press, London. Vol. 3, pp. 1129-1225.

Hicher, P.Y. (1988). The viscoplastic behavior of Bentonite. Proc. of the International Conference on Rheology and Soil Mechanics, edited by Keedwell, M.J., Coventry, pp. 89-107.

Holtzer, T.L., Hoeg, K. and Arulanandan, K. (1973). Excess pore pressures during undrained clay creep. Canadian Geotechnical Journal, Vol. 10(1), pp. 12-24.

Hoyos, L.R., Suescun, E.A. and Puppala, A.J. (2011). Small-strain stiffness of unsaturated soils using a suction-controlled resonant column device with bender elements. Proc. of the Geo-Frontiers 2011 Conference, ASCE, pp. 4313-4322.

Imai, G. (1980). Settling behaviour of clay suspension. Soils and Foundations, Vol. 20(2), pp. 61-77.

Imai, G. (1981). Experimental studies on sedimentation mechanism and sediment formation of clay minerals. Soils and Foundations, Vol. 21(1), pp. 7-20.

Jarrett, P.M. (1967). Time dependent consolidation of a sensitive clay. Journal of Material Research and Standards, ASTM, Vol. 7(7), pp. 300-304.

Jedinakova-Krizova, V. (1998). Migration of Radionuclides in Environment. Journal of Radioanalytical and Nuclear Chemistry, Vol. 229, pp. 3-18.

JNC (2000). Repository design and engineering technology H12: project to establish the scientific and technical basis for HLW disposal in Japan. Japan Nuclear Cycle Development Institute, Japan.

Kaliakin, V.N. and Dafalias, Y.F. (1990). Verification of the elasticplastic-visco-plastic boundaing surface model for cohesive soils. Soils and Foundations, Vol. 30(3), pp. 25-36.

Katti, R.K. and Katti, A.R. (1994). Behaviour of saturated expansive soil and control methods. Proc. of the 7th International Conference on Computer Methods and Advances in Geomechanics, Balkema, Rotterdam.

Kavazanjian, E. and Mitchell, J. K. (1980). Time-dependent deformation behaviour of clays. Journal of the Geotechnical Engineering Division, ASCE, Vol. 106(GT6), pp.

611-630.

Kelln, C., Sharma, J.S. and Hughes, D. (2008a). A finite element solution scheme for an elastic-viscoplastic soil model. Computers and Geotechnics, Vol. 35, pp. 524-536.

Kelln, C., Sharma, J.S., Hughes, D., and Graham, J. (2008b). An improved elastic-viscoplastic soil model. Canadian Geotechnical Journal, Vol. 45(21), pp. 1356-1376.

Kelln, C., Sharma, J.S., Hughes, D., and Graham, J. (2009). Finite element analysis of an embankment on a soft estuarine deposit using an elastic-viscoplastic soil model. Canadian Geotechnical Journal, Vol. 46(12), pp. 357-368.

Kim, H., Hirokane, S., Yoshikuni, H., Moriwaki, T. and Kusakabe, O. (1995). Consolidation behavior of dredged clay ground improved by horizontal drain method. Proc. of the International Symposium on Compression and Consolidation of Clayey Soils, Hiroshima, Japan, pp. 99-104.

Kim, Y.T. and Leroueil, S. (2001). Modelling the viscoplastic behavior of clays during consolidation: application to Berthierville clay in both laboratory and field conditions. Canadian Geotechnical Journal, Vol. 38, pp. 484-497.

Komine, H. (2008). Theoretical equations on hydraulic conductivities of bentonite-based buffer and backfill for underground disposal of radioactive wastes. Journal of Geotechnical and Geoenvironmental Engineering, Vol. 134(4), pp. 495-508.

Kondner, R.L. (1963). Hyperbolic stress-strain response: cohesive soils. Journal of the Soil Mechanics and Foundation Division, ASCE, Vol. 89(SM1), pp. 115-143.

Koutsoftas, D.C., Foott, R. and Handfelt, L.D. (1987). Geotechnical investigations offshore Hong Kong. Journal of Geotechnical Engineering, ASCE, Vol. 113(2), pp. 87-105.

Kutter, B.L. and Sathialingam, N. (1992). Elastic-viscoplastic modelling of the rate-dependent behaviour of clays. Géotechnique, Vol. 42(3), pp. 427-441.

Kynch, G.J. (1952). A theory of sedimentation. Transactions of the Faraday Society, Vol. 48(166), pp. 166-176.

Lacerda, W.A. and Houston, W.N. (1973). Stress relaxation in soils. Proc. of 8th International Conference on Soil Mechanics and Foundation Engineering, Moscow, Vol. 1, pp. 221-227.

Ladanyi, B. and Benyamina, M.B. (1995). Triaxial relaxation testing of a frozen sand. Canadian Geotechnical Journal, Vol. 32(3), pp. 496-511.

Ladd, C.C., Foott, R., Ishihara, K., Schlosser, F. and Poulos, H.G. (1977). Stress-deformation and strength characteristics. Proc. of the 9th International Conference on Soil Mechanics and Foundation Engineering, Tokyo, Vol. 2, pp. 421-494.

Lambe, T. (1964). Methods of estimating settlement. Journal of the Soil Mechanics and Foundations Division, ASCE, Vol. 90(SM5), pp. 181-196.

Lambe, T.W. and Whitman, R.V. (1959). The role of the effective stress in the behaviour of expansive soils. Quarterly of the Colorado School of Mines, Vol. 4(4), pp.39.

Larsson, R. (1981). Drained behaviour of Swedish clays. Swedish Geotechnical Institute Report, No. 12.

Lee, K., Choa, V., Lee, S.H. and Quek, S.H. (1993). Constant rate of strain consolidation of Singapore marine clay. Géotechnique, Vol. 43(3), pp. 471-488.

Lee, K.M. and Ng, P.C.C. (1999). A geotechnical investigation of marine deposits in a nearshore seabed for land reclamation. Canadian Geotechnical Journal, Vol. 36, pp. 981-1000.

Lee, K. and Sills, G.C. (1981). The consolidation of a soil stratum, including self-weight effect and large strains. International Journal for Numerical and Analytical Methods in Geomechanics, Vol. 5, pp. 405-428.

Lefebvre, G. and LeBoeuf, D. (1987). Rate effects and cyclic Loading of sensitive clays. Journal of Geotechnical Engineering, ASCE, Vol. 113(GT5), pp. 476-489.

Leopards, G.A. and Girault, P. (1961). A study of the one-dimensional consolidation test. Proc. of the 5th International Conference on Soil Mechanics and Foundation Engineering, Paris, Vol. 1, pp. 213-218.

Leroueil, S. (1996). Compressibility of clays: fundamental and practical aspects. Journal of Geotechnlcal Engineering, ASCE, Vol. 122(GT7), pp. 534-543.

Leroueil, S. (1988). Recent developments in consolidation of natural clays. Canadian Geotechnical Journal, Vol. 25(1), pp. 85-107.

Leroueil, S., Kabbaj, M., Tavenas, F. and Bouchard, R. (1985). Stress-strain-strain rate relation for the compressibility of sensitive natural clays. Géotechnique, Vol. 35(2), pp. 159-180.

Leroueil, S. and Marques, M.E.S. (1996). Importance of strain rate and temperature effects in geotechnical engineering. Measuring and Modeling Time Dependent Soil Behaviour, Edited by Sheahan, T.C. and Kaliakin, V.N., New York, pp.l-59.

Leroueil, S., Samson, L. and Bozozuk, M. (1983). Laboratory and field determination of preconsolidation pressures at Gloucester. Canadian Geotechnical Journal, Vol. 20, pp. 477-490.

Li, H. and Williams, D.J. (1995). Numerical modeling of combined sedimentation and self-weight consolidation of an accreting coal mine tailing slurry. Proc. of compression and consolidation of clayey soils conference, Balkema, Rotterdam, pp: 441-452.

Liu, J.C. and Znidarcic, D. (1991). Modeling one dimensional compression characteristics of soils. Journal of Geotechnlcal Engineering, Vol. 117(1), pp. 162-169.

Liu, M.D., John, P.C. and David, W.A. (2011). Sydney Soil Model. I: Theoretical Formulation. International Journal of Geomechanics, Vol. 11, pp. 211-224.

Lo Presti, D.C.F., Jamiokowski, M., Pallara, O. and Cavallaro, A. (1996). Rate and creep affect the stiffness of soils. Measuring and Modelling Time Dependent Soil Behaviour, New York, pp. 167-180.

Marcial, D., Delage, P. and Cui, Y.J. (2002). On the high stress compression of bentonites. Canadian Geotechnical Journal, Vol. 39, pp. 812-820.

Mc-Roberts, E.C. and Nixon, J.F. (1976). A theory of soil sedimentation. Canadian Geotechnical Journal, Vol. 13, pp. 294-310.

Mcvay, M., Townsend, F. and Bloomquist, D. (1986). Quiescent consolidation of phosphatic waste clays. Journal of Geotechnical Engineering, ASCE, Vol. 112, pp. 1033-1049.

Merckelbach, L. M. (2000). Consolidation and strength evolution of soft mud layers. PhD thesis, Delft University of Technology.

Merckelbach, L. M. and Kranenburg, C. (2004a). Equations for effective stress and permeability of soft mud-sand mixtures. Géotechnique, Vol. 54(4), pp. 235-243.

Merckelbach, L. M. and Kranenburg, C. (2004b). Determining effective stress and permeability equations for soft mud from simple laboratory experiments. Géotechnique, Vol. 54(9), pp. 581-591.

Mesri, G. (1973). Coefficient of secondary compression. Journal of the Soil Mechanics and Foundations Division, ASCE, Vol. 99(SM1), pp. 123-137.

Mesri, G. and Castro, A. (1987). Concept and K_o during secondary compression. Journal of Geotechnical Engineering, ASCE, Vol. 113(GT3), pp. 230-247.

Mesri, G. and Choi, Y.K. (1985). The uniqueness of end of primary (EOP) void ration effective stress relationship. Proc. of the 11th International Conference on Soil Mechanics and Foundation Engineering, San Francisco, Vol. 2, pp. 587-590.

Mesri, G., Feng, T.W. and Shahien, M. (1999). Coefficient of consolidation by inflection point method. Journal of Geotechnical and Geoenvironmental Engineering, ASCE, Vol. 125(8), pp. 716-718.

Mesri, G. and Godlewski, P.M. (1977). Time- and stress-compressibility interrelationship. Journal of Geotechnical Engineering, ASCE, Vol. 103(GT5), pp.

417-430.

Mesri, G. and Rokhsar, A. (1974). Theory of consolidation for clays. Journal of the Geotechnical Engineering Division, ASCE, Vol. 100(GT8), pp. 889-904.

Mesri, G., Rokhsar, A. and Bohar, B.F. (1975). Composition and compressibility of typical samples of Mexico City clay. Géotechnique, Vol. 25(3), pp. 527-554.

Mikasa, M. (1965). The Consolidation of soft clay, a new consolidation theory and its application. Japanese Society of Civil Engineers, pp. 21-26.

Mikasa, M. and Takada, N. (1984). Selfweight consolidation of very soft clay by centrifuge. Proc. of Symosium on Sedimentation/Consolidation Models: Prediction and Validation, ASCE, New York, pp. 121-140.

Mitachi, T. (2008). Mechanical behaviour of bentonite-sand mixtures as buffer materials. Soils and Foundations, Vol. 48(3), pp. 363-374.

Mitchell, J.K. (1993). Fundamentals of soil behaviour. 2nd Edition, John Wiley & Sons, New York.

Murakami, Y. (1979). Excess porewater pressure and preconsolidation effect developed in normally consolidated clays of some age. Soils and Foundations, Vol. 18(4), pp. 17-29.

Murayama, S., Michihiro, K. and Sakagami, T. (1984). Creep characteristics of sand. Soils and Foundations, Vol. 24(2), pp. 1-15.

Nash, D.F.T. and Ryde, S.J. (2000). Modelling the effects of surcharge to reduce long term settlement of reclamations over soft clays. Proc. of Soft Soil Engineering Conference, Japan, 2000.

Nelson, J.D. and Miller, D.J. (1992). Expansive soils: problems and practice on foundation and pavement engineering. John Wiley & Sons, New York.

Nicholson, P. G., Russell, P. W. and Fujii, C. F. (1996). Soil creep and creep testing of highly weathered tropical soils. Measuring and Modelling Time Dependent Soil Behaviour, edited by Sheahan, T.C. and Kaliakin, V.N., New York, pp. 195-312.

Niemunis, A. and Krieg, S. (1996).Viscous behaviour of soil oedometric conditions. Canadian Geotechnical Journal, Vol. 33(1), pp. 159-168.

Nishimura, A., Rodolfo, K., Koizumi, A., Gill, J. and Fujioka, K. (1992). Episodic deposition of Plio-Pleistocene pumice from the Izu-Bonin arc, Leg 126. Proc. of Ocean Drilling Program, Scientific Results, Vol. 126, pp. 3-21.

Oda, Y. and Mitachi, T. (1988). Stress relaxation characteristics of saturated clays. Soils and Foundations, Vol. 28(4), pp. 69-80.

O'Loughlin, C. (2001). Modeling the time-dependant compression of a fibrous peat using the EVP model. Proc. of the 3rd International Conference on Soft Soil Engineering, Hong Kong, pp. 362-368.

Olson, R.E. (1998). Settlement of embankments on soft clays. Journal of Geotechnical and Geoenvironmental Engineering, Vol. 124(4), pp. 278-288.

Olson, R.E. and Mesri, G. (1970). Mechanism controlling the compressibility of clay. Journal of the Soil Mechanics and Foundation Division, Vol. 96(SM6), pp. 1863-1878.

Panayiotis, D. and Athanasios, N.P. (1997). Batch analysis of slurries in zone settling regime. Journal of Environmental Engineering, Vol. 123(7), pp. 660-667.

Park, J.H., Watanabe, K. and Seguchi, M. (1992). Experimental investigation on the settling properties of mud. Bulletin in Faculty of Agriculture, Saga University, Vol. 73, pp. 129-147.

Perzyna, P. (1963). The constitutive equations for working hardening and rate sensitive plastic materials. Proc. of Vibration Problems, Warsaw, Vol. 4(3), pp. 281-290.

Perzyna, P. (1966). Fundamental problems in viscoplasticity. Advances in Applied Mechanics, Academic Press, New York, Vol. 9, pp. 244-368.

Premchitt, J., Ho, K.S. and Evans, N.C. (1995). Conventional and CRS Rowe cell consolidation test on some Hong Kong clays. GEO Report No. 55, Hong Kong: Geotechnical Engineering Office, Civil Engineering Department, pp. 16-22.

Richardson, A.M. and Whitman, R.V. (1963). Effect of strain rate upon undrained shear resistance of a saturated remoulded fat clay. Géotechnique, Vol. 13, pp. 310-324.

Robinson, R.G. (1997). Consolidation analysis by an inflection point method. Géotechnique, Vol. 47(1), pp. 199-200.

Roscoe, K.H. and Borland, J.B. (1968). On the generalised stress-strain behavior of wet clay. Engineering Plasticity, edited by Heyman, J. and Leckie, F.P., Cambridge University Press, Cambridge, pp. 535-609.

Schiffman, R.L. (1958). Consolidation of soil under time-dependent loading and varying permeability. Proc. of 37th Annual Meeting Highway Research Board, Washington, DC, pp. 584–617.

Schiffman, R.L. and Gibson, R.E. (1964). Consolidation of non-homogeneous clay layers. Journal of the Soil Mechanics and Foundations Division, ASCE, Vol. 90(SM5), pp. 1-30.

Scott, K.J. (1966). Mathematical models of mechanism of thickening. Industrial & Engineering Chemistry Fundamentals, Vol. 5, pp. 109.

Scully, R.W. (1984). Determination of consolidation properties of phosphatic clay at very high void ratios. MSc thesis, University of Colorado.

Sheahan, T.C., Ladd, C.C. and Germaine, J.T. (1994). Time-dependent triaxial relaxation behavior of a resedimented clay. Geotechnical Testing Journal, Vol. 17(4), pp. 444-452.

Sheahan, T.C., Ladd, C.C. and Germaine, J.T. (1996). Rate-dependent undrained shear behavior of saturated clay. Journal of Geotechnical Engineering, Vol. 22(2), pp. 99-108.

Sheeran, D.E. and Krizek, R.J. (1971). Preparation of homogeneous soil samples by slurry consolidation. Journal of Materials, ASTM, Vol. 6(2), pp. 356-373.

Shields, H. (1974). Discussion on session on normally consolidated and lightly overconsolidated cohesive materials. British Geotechnical Society Conference on Settlement of Structure, Cambridge, pp. 698-700.

Sills, G.C. (1995). Time dependent process in soil consolidation. Reprinted report on International Symposium on Compression and Consolidation of Clayey Soils, Hiroshima, Vol. 1, pp. 59-74.

Silva, A.J. and Brandes, H.G. (1996). Drained creep behaviour of marine clays. Measuring and modeling time dependent soil behavior, edited by Sheahan, T.C. and Kaliakin, V.N., New York, pp. 228-242.

Silva, A.J., Tian, W.M., Sadd, M.H. and Brandes, H.G. (1991). Creep behavior of fine-grained ocean sediments. Proc. of the 7th International Conference on Computer Methods and Advances in Geomechanics, Balkema, Rotterdam, Vol. 1, pp.683-688.

Silvestri, V., Rong, R.N., Soulie, M. and Gabriel, F. (1985). Controlled-strain, controlled gradient and standard consolidation testing of sensitive clays. Proc. of the Symposium on Behaviour of Soils, ASTM, Fort Lauderdale, S.T.P. 892, pp. 433-450.

Singh, A. and Mitchell, J.K. (1968). General stress-strain-time function for soils. Journal of Soil Mechanics and Foundation Divisions, ASCE, Vol. 94(SM1), pp. 21-46.

Sivapullaiah, P.V., Sridharan, A. and Stalin, V.K. (1996). Swelling behaviour of soil-bentonite mixtures. Canadian Geotechnical Journal, Vol. 33, pp. 808-814.

Skempton, A.W. (1944). Note on the Compressibility of Clays. Journal of Geological Society, Vol. 100, pp. 119-135.

Skempton, A.W. (1964). Long-term stability of clay slopes. Géotechnique, Vol. 14(2), pp. 77-101.

Skempton, A.W. and Bjerrum, L. (1957). A contribution to the settlement analysis of foundations on clay. Géotechnique, Vol. 7, pp. 168-178.

Smith, R.E. and Wahls, H.E. (1969). Consolidation constant rate of strain. Journal of the Soil Mechanics and Foundations Division, ASCE, Vol. 95(SM2), pp. 519-539.

Snethen, D.R. (1980). Characterization of expansive soils using soil suction data. Proc. of the 4th International Conference on Expansive Soils, Boulder, Colorado, pp. 54-75.

Somogyi, F. (1979). Analysis and prediction of phosphatic clay consolidation: implementation package. Technical Report, Florida Phosphatic Clay Research Project, Lakeland, Florida.

Sridharan, A. and Prakash, K. (1999). Influence of clay mineralogy and pore medium chemistry on clay sediment formation. Canadian Geotechnical Journal, Vol. 36, pp. 961-966.

Sridharan, A. and Prakash, K. (2003). Self weight consolidation: compressibility behavior of segregated and homogeneous finegrained sediments. Marine Georesources & Geotechnology, Vol. 21(2), pp. 73-80.

Sridharan, A., Prakash, K. and Asha, S.R. (1995). Consolidation behaviour of soils. Geotechnical Testing Journal, ASTM, Vol. 18(1), pp. 58-68.

Suklje, L. (1969). Rheological aspects of soil mechanics, John Wiley & Sons.

Sun, J. (1999). Rheology of geomaterials and applications (a book in Chinese). China Construction Publication House.

Tan, T.S. (1995). Sedimentation to consolidation: a geotechnical perspective. Proc. of compression and consolidation of clayey soils, Hiroshima, Japan, pp. 937–948.

Tan, T.S., Yong, K.T., Leong, E.C. and Lee, S.L. (1990). Sedimentation of clayey slurry. Journal of Geotechnical Engineering, Vol. 116(6), pp. 885-898.

Tatsuoka, F., Uchimura, T, Hayano, K., Di Benedetto, H., Koseki, J. and Siddiquee, M.S.A. (2001). Time-dependent deformation characteristics of stiff geomaterials in engineering practice. Proc. of the 2nd International Conference on Pre-failure Deformation Characteristics of Geomaterials, edited by Jamiolkowski et al., Balkema, Vol. 2, pp. 1161-1262.

Tavenas, F. and Leroueil, S. (1977). Effects of stresses and time on yielding of clay. Proc. of the 9th International Conference on Soil Mechanics and Foundation Engineering, Tokyo, Vol. 1, pp. 319-326.

Tavenas, F, Leroueil, S., Rochele, P. L. and Roy, M. (1978). Creep behaviour of an undisturbed lightly overconsolidated clay. Canadian Geotechnical Journal, Vol. 20(4), pp. 645-660.

Taylor, D.W. (1943). Cylindrical compression research program on stress-deformation and strength characteristics of soils. Proc. of the 9th Progress Report to US Army Corps of Engineering Waterways Experiment Station, Massachusetts Institute of Technology, Cambridge.

Taylor, D.W. and Merchant, W. (1940). A theory of clay consolidation accounting for secondary compressions. Journal of Mathematical Physics, Vol. 19(3), pp. 167-186.

Terzaghi, K. (1943). Theoretical soil mechanics, John Wiely & Sons, New York.

Terzaghi, K. and Peck, R.B. (1967). Soil mechanics in engineering practice. 2nd edition, John Wiely and Sons, New York.

Tian, W.M, Silva, A.J., Veyera, G.E. and Sadd, M.H. (1994). Drained creep of undisturbed cohesive marine sediments. Canadian Geotechnical Journal, Vol. 31, pp. 841-855.

Tiller, F.M. (1981). Revision of Kynch sedimentation theory. AIChE Journal, Vol. 27(5), pp. 823-829.

Umehara, Y. and Zen, K. (1982). Consolidation characteristics of dredged marine bottom sedimentswith high water. Soils and Foundations, Vol. 22(2), pp. 40-54.

Vaid, Y.P. and Campanella, R.G. (1977). Time-dependent behaviour of undisturbed clays. Journal of the Geotechnical Engineering Division, ASCE, Vol. 103(7), pp. 693-709.

Vaid, Y.P., Robertson, P.K. and Campanella, R.G. (1979). Strain rate behaviow of St. Jean Vianney clay. Canadian Geotechnical Journal, Vol. 16(1), pp. 34-42.

Vermeer, P.A. and Neher, H.P. (1999). A soft soil model that accounts for creep. Proc. of Beyond 2000 in Computational Geotechnics 10 Years of PLAXIS International, Balkema, pp. 249-261.

Vialov, S.S. and Skibitsky, A.M. (1961). Problems of the rheology of soils. Proc. of the 5th International Conference on Soil Mechanics and Foundation Engineering, Budapest, pp. 103-118.

Vyalov, S.S. (1986). Rheological fundamentals of soil mechanics. Elsevier Applied Science Publication, London.

Walker, H. E. (1969). Secondary settlement in sensitive clays. Canadian Geotechnical Journal, Vol. 6, pp. 219-222.

Wu, T.H., Douglas, A.G. and Goughnour, R.D. (1962). The friction and cohesion of saturated clays. Journal of the Soil Mechanics and Foundations Division, ASCE, Vol. 89(SM3), pp. 1-32.

Xiao, H.B., Zhang, C.S., Wang, Y.H. and Fan, Z.H. (2011). Pile-soil interaction in expansive soil foundation: analytical solution and numerical simulation. International Journal of Geomechanics, Vol. 11, pp. 159-166.

Yim, W.W.S. (1983). A sedimentological study of sea-floor sediments exposed during excavation of the East Dam site, High Island, Sai Kung. Proc. of Geology of Surficial Deposits in Hong Kong, pp. 131-142.

Yin, J.H. (1990). Constitutive modeling of time-dependent stress-strain behavior of soils. Ph.D. thesis, University of Manitoba, Winnipeg.

Yin, J.H (1999a). Properties and behaviour of Hong Kong marine deposites with different clay contents. Canadian Geotechnical Journal, Vol. 36, pp.1085-1095

Yin, J.H. (1999b). Non-linear creep of soils in oedometer tests. Géotechnique, Vol. 49(5), pp.699-707.

Yin, J.H. (2002). Stress-strain-strength characteristics of a marine soil with different clay contents. Geotechnical Testing Journal, ASTM, Vol. 25(4), pp.459-462.

Yin, J.H. (2011). From constitutive modeling to development of laboratory testing and optical fiber sensor monitoring technologies. Chinese Journal of Geotechnical Engineering, Vol. 33(1), pp. 1-16.

Yin, J.H and Cheng, C.M. (2006). Comparison of strain-rate dependent stress-strain behaviour from K_o-consolidated compression and extension tests on natural Hong

Kong marine deposits. Marine Georesources & Geotechnology, Vol. 24(2), pp. 119-147.

Yin, J.H. and Graham, J. (1989). Viscous-elastic-plastic modeling of one dimensional time -dependent behaviour of clays. Canadian Geotechnical Journal, Vol. 26(2), pp. 199-209.

Yin, J.H. and Graham, J. (1994). Equivalent times and one-dimensional elastic visco-plastic modeling of time-dependent stress-strain behavior of clays. Canadian Geotechnical Journal, Vol. 31(1), pp. 42-52.

Yin, J.H. and Graham, J. (1996) Elastic visco-plastic modeling of one-dimensional consolidation. Géotechnique, Vol. 46(3), pp. 515-527.

Yin, J.H. and Graham, J. (1999). Elastic visco-plastic modelling of the time-dependent stress-strain behavior of soils. Canadian Geotechnical Journal, Vol. 36(4), pp. 736-745.

Yin, J.H., Graham, J., Clark, J.I. and Gao, L. (1994). Modelling unanticipated porewater pressures in soft clays. Canadian Geotechnical Journal, Vol. 31, pp. 773-778.

Yin, J.H. and Tong, F. (2010). Report on settling column consolidation tests, Project No.: P09-0277, The Hong Kong Polytechnic University.

Yin, J.H. and Tong, F. (2011). Constitutive modeling of the time-dependent stress-strain behaviour of saturated soils exhibiting both creep and swelling. Canadian Geotechnical Journal, Vol. 48(12), pp. 1870-1885.

Yin, J.H., Zhu, J.G. and Graham, J. (2002). A new elastic visco-plastic model for

time-dependent behaviour of normally and overconsolidated clays-theory and verification. Canadian Geotechnical Journal, Vol. 39(1), pp. 157-173.

Yoon, G.L., Kim, B.T. and Jeon, S.S. (2004). Empirical correlations of compression index for marine clay from regression analysis. Canadian Geotechnical Journal, Vol. 41(6), pp. 1213–1221.

Yoshikuni, H., Kisakabe, O., Okada, M. and Tajima, S. (1995a). Mechanism of one-dimensional consolidation. Proc. of the International Symposium on Compression and Consolidation on Clayey Soils, Hiroshima, Vol. 1, pp. 497-504.

Yoshikuni, H. and Nakanodo, H. (1974). Consolidation of soils by vertical drain wells with finite permeability. Soils and Foundations, Vol. 14(2), pp. 35-46.

Yoshikuni, H., Nishiumi, H., Ikegami, S. and Seto, K. (1994). The creep and effective stress-relaxation behaviour on one-dimensional consolidation. Proc. of the 29th Japan National Conference on Soil Mechanics and Foundation Engineering, Vol. 29, pp. 269-270.

Yoshikuni, H., Okada, M. and Ikegami, S. (1995b). One-dimensional consolidation analysis based on an elasto-viscous liquid model. Proc. of the International Symposium on Compression and Consolidation of Clayey Soils, Hiroshima, Japan, Vol.1, pp. 505-512.

Zhu, G.F. (1999). Numerical and analytical solutions for consolidation analysis of soils without and with vertical drains. Ph.D. thesis, the Hong Kong Polytechnic University.

Zhu, J.G. (2000). Experimental study and elastic visco-plastic modeling of the

time-dependent stress-strain behavior of Hong Kong marine deposits. Ph.D. thesis, the Hong Kong Polytechnic University.

Zhu, J.G. and Yin, J.H. (2000). Strain-rate dependent stress-strain behaviour of overconsolidated Hong Kong marine deposits. Canadian Geotechnical Journal, Vol. 37(6), pp. 1272-1282.

Zhu, J.G. and Yin, J.H. (2001). Drained creep behaviour of soft Hong Kong marine deposits. Géotechnique, Vol. 51(5), pp. 471-474.

Zhu, J.G., Yin, J.H. and Luk, S.T. (1999). Time-dependent stress-strain behaviour of soft Hong Kong marine deposits. Geotechnical Testing Journal, ASTM, Vol. 22(2), pp.112-120.

Zienkiewicz, O.C. and Cormeau, I.C. (1974). Visco-plasticity, plasticity and creep in elastic solids: a unified numerical solution approach. International Journal of Analytical and Numerical Methods in Geomechanics, Vol. 8(2), pp. 821-845.

Znidarcic, D. and Liu, J.C. (1989). Consolidation characteristics determination for dredged materials. Proc. of the 22nd Annual Dredging Seminar, Center for dredged Studies, Texas A&M Univ, College Station, pp. 45–65.